UNIVERSITA' DI PAVIA

Dipartimento di Scienze della Terra e dell'Ambiente

PhD PROGRAM IN EARTH AND ENVIRONMENTAL SCIENCES
33rd SERIES

Improve Source Rock Evaluation using Inorganic Geochemistry (ISRIG)

PhD thesis of
Greta Bonacina

Tutors
Prof. Alessio Sanfilippo (Unipv),
Dott.ssa Elisabetta Previde Massara (Eni),
Dott. Paolo Scotti (Eni)

Coordinator
Prof. Roberto Sacchi

Academic year: 2019/2020

RINGRAZIAMENTI

Giunta alla conclusione di questo percorso triennale, desidero ringraziare una lunga lista di persone. Innanzitutto, un grazie speciale va ai miei tutor, Alessio, Elisabetta e Paolo, che mi hanno dato l'opportunità di intraprendere questi anni di crescita, non solo professionale, ma anche personale. Le loro diverse vite professionali, accomunate dallo stesso interesse per la ricerca, hanno permesso di dare vita ad un progetto di dottorato in cui la vera ricchezza si è dimostrata essere la sinergia tra il mondo universitario e quello dell'industria. Li ringrazio per aver creduto nelle mie capacità e per essere sempre stati disponibili ad un sano e proficuo confronto e perché mi hanno permesso di fare nuove esperienze che altrimenti sarebbero rimaste "il mio sogno nel cassetto".

Grazie di cuore a tutti i "colleghi" Eni per avermi accolta fin dal principio e per avermi fatta sentire parte della loro grande "famiglia". In particolare, un ringraziamento va a Pier, Tiziano, Flavio, Lorenzo e Cesare: i migliori compagni di laboratorio che potessi mai sperare. Infine, un grazie anche a Simone e Claudio, miei insostituibili compagni di pause caffè. Grazie a tutta l'azienda Eni, dove ho lavorato in un clima amichevole, informale e sereno, e che mi ha permesso di migliorarmi professionalmente traendo il meglio da questa esperienza.

Desidero ringraziare anche tutta la mia "famiglia" universitaria, in particolare Marta, Roberta, Alberto ed Elisa, che hanno condiviso con me questo lungo percorso e i momenti di gioia e di frustrazione.

Infine, ultimo ma non meno importante, un ringraziamento a tutta la mia famiglia; i miei fratelli, i miei genitori e i miei nonni. Grazie per avermi sostenuta durante questo lungo percorso iniziato ancor prima del dottorato, per avermi dato una spinta nei momenti in cui avrei voluto mollare e per non aver mai dubitato che sarei arrivata al traguardo.

ABSTRACT

The following dissertation constitutes a part of an Eni's project called "Improved Source Rock Evaluation using Inorganic Geochemistry" (ISRIG), focused on the evaluation of source rocks. The target of the PhD is to identify inorganic proxies (elements or mineralogical phases) that can help to evaluate source rocks and in particular to trace the original organic parameters (Total Organic Carbon and Hydrogen Index, TOC and HI respectively) that are depleted compared to the original ones in the mature source rocks.

The PhD has been divided mainly in three phases: (i) bibliographic research; (ii) evaluation of immature source rocks and (iii) evaluation of mature source rocks.

The bibliographic research was aimed to identify some inorganic proxies to evaluate the depositional conditions of the rocks. In particular, we focused on proxies that can give us information about the redox conditions of the depositional environment (i.e. water column, sediment-water interface, pore waters). The latter are of fundamental importance for the accumulations and preservation of the organic matter that is at the base of the hydrocarbons' generation. Specifically, the main goal is to find some proxies and univocal correlations between the proxies and the organic content that do not change with age, lithology, depositional environment and maturity. However, it is very unlikely that a proxy will be able to respect all these parameters. That is why a multi-proxy approach is very useful and highly recommend to reach the target. In addition, one of the fundamental requirements was to identify proxies of elements that could be acquired with classical analytical techniques owned by Eni, such as X-ray diffraction (XRD) and X-ray fluorescence (XRF). However, due to the fact that the Laser Ablation ICP-MS is available in Pavia, we were able to acquire also Trace Elements (TEs) and Rare Earth Elements (REEs) concentrations.

Eni played a fundamental role in providing the samples of the cases of study. In particular, Eni provided:

- Cretaceous (immature): a case of study from Southern Italy and 7 from the Central Atlantic. Of the latter, 4 cases are related to a proximal depositional environment, while 3 are related to a distal depositional environment together with the one from Southern Italy;
- Triassic (immature): 2 cases of study from Northern Italy;
- Devonian (mature): 2 cases of study from Northern Africa.

The bibliographic research has led to the identification of four three of inorganic redox proxies:

1. Redox sensitive elements (RSEs): this class of proxies is represented by Mo, V, U, Ni and Cu that show enrichments under reducing conditions and generally correlates positively with the organic matter content (TOC);
2. Elements not related to the organic matter: these are represented by Th, Al, Zr and Mn. In particular, Th, Al and Zr are related to the detrital fraction, while Mn show enrichments under oxic conditions and play a fundamental role in transport the RSEs from the water column to the sediments;
3. Unconventional proxies: this class of proxies includes iron speciation, sulfur and thallium isotopes. These proxies cannot be acquired with classical techniques but requires special sample treatments and specifical analytical instruments. However, being a research project, we were able to deepen also this typology of proxies and to acquire new knowledges in analytical techniques. Specifically, this was able thought a period abroad (November 2019 – February 2020) at the University of California (Riverside) and MagLab (Tallahassee – Florida).

Thus, we were able to apply the aforementioned proxies to our cases of study. The results of these PhD are very successful, firstly, because this is one of the first work in which so many different source rocks are compared in order to identify some proxies to trace the organic content and to identify a series of proxies that can be applied on each type of source rock. Secondly, this work demonstrates that the inorganic geochemistry and its integration with the organic parameters can be very useful to evaluate the source rocks and the conditions at the depositional time. In addition, many analytical techniques have been applied during the PhD, leading to a deeper knowledge of these and to a greater awareness of the analytical data. In particular, the Laser Ablation ICP-MS allowed to discover that patterns in trace elements (TEs) and Rare Earth Elements (REEs) can be very useful to investigate the depositional conditions of source rocks.

Specifically, the data processing on the immature and mature source rocks has led to the following results:

- A multi-proxy approach (trace elements, mineralogy and organic parameters) in necessary and successful in the data processing of different rocks, in order to reconstruct the depositional conditions of a source rock;
- Maturity is firstly observed in a depletion in the HI values, whereas TOC shows weaker impoverishments. In addition, the degree of maturity determines the degree of depletion of TOC and HI;

- Redox Sensitive Elements (V, Mo and U) always show positive correlations with the organic matter content and are not dependent on the age and maturity of the source rocks studied. This allow to use their concentrations to reconstruct the original naphtogenic parameters (TOC_0 and HI_0) when they are depleted because of maturity;
- Lithology can affect the distribution of some elements. For instance, V and U can show some relationships with the mineralogical content (clays and carbonates, respectively) leading to the idea that these elements can be reliable only if rocks with the same lithology are compared. Differently, Mo depends only on the OM, allowing to use this element to compare also very different rocks in terms of lithology;
- Ni and Cu are not always reliable redox proxies, but they can give information about the OM flux toward the sediments;
- Th, Zr and Al reflect the detrital fraction of the rock (aluminosilicates and clastic sediments) and are not related to the OM content. However, these elements can give information about the depositional environment, and in particular about the dilution degree of the OM and RSEs when rocks of different depositional environments (e.g. distal and proximal) are compared;
- Mn concentrations can give information about the redox conditions. However, it is not reliable due to its high mobility after diagenesis. Thus, its use as redox proxy needs to be coupled with other more reliable elements as V, Mo and U;
- Anomalies allow to trace the presence of the organic matter even if the organic data is not present. In fact, as explained for the Cretaceous and Triassic cases of study, V and Mo (and with a lesser extent U) are always enriched in presence of OM, allowing to use them to trace the TOC content or to understand that organic matter was present, even if its concentration in the rock is depleted due to a maturation process. In addition, TEs and REEs pattern allow to trace the provenance of the sediments, the rock composition and the depositional environment.

Also, we were able to apply the inorganic geochemistry to a scientific case of study (Fontana Valloneto Section), represented by an immature case from Southern Italy (SI1). The samples and the organic parameters have been collected by Sabato et al. (2007), whereas XRD (mineralogy) and XRF (TEs) analysis have been carried out during this PhD. The target was to study the depositional environment of SI1, that represent a sedimentary succession that intersect an equivalent of the Bonarelli Level (Cenomanian – Turonian boundary; ~94Ma). This work has led to the paper "Geochemical evidence for local variability in redox and depositional

conditions in a deep-water Bonarelli equivalent section from Southern Tethys (Fontana Valloneto section, southern Italy)" published in 2020 on Ofioliti (vol. 46, No.1).

Finally, the period abroad has led to the study of one the immature case of study from the Central Atlantic Ocean (CA1) with unconventional proxies, and in particular with iron speciation, sulfur and thallium isotopes in order to study the local and global oxygenation during the Cretaceous. Specifically, this section intersects four Oceanic Anoxic Events (OAE 1c, OAE 1d, OAE 2 and OAE 3). Importantly, this work represents the first long-term study of the Cretaceous that allow to study how the redox conditions changed in the Central Atlantic Ocean moving in and out each of the aforementioned OAE. Likely, the collaboration with the American institutions will lead to a paper on a scientific journal with impact factor during 2021.

SUMMARY

CHAPTER 1

Introduction

The following PhD dissertation constitutes a part of the internal Eni's project "Improved Source Rock Evaluation using Inorganic Geochemistry" (ISRIG), focused on the evaluation of source rocks in order to reduce the uncertainty in the definition of the original organic properties of the rock by combining well-known organic with inorganic geochemical parameters.
Eni played a crucial role in providing the samples and cases of study on which apply the methodologies and procedure developed during the PhD. Also, it had an important role in providing the samples preparation and analysis.
Importantly, all the data discussed here are owned by Eni. Due to the confidentiality of the data, it was not possible to publish in this dissertation the dataset. To consult it, it is necessary to submit a request to the oil company.

The Improved Source Rock Evaluation using Inorganic Geochemistry (ISRIG) project is aimed to evaluate source rocks using inorganic geochemistry through a classical data analysis approach in order to reduce the uncertainty in the definition of the original organic properties of a source rock by combining well-known organic parameters with inorganic geochemical tools, such as minor and trace element compositions of the source rock and/or the mineral constituents. A correct evaluation of the source rock parameters is of paramount importance for the success of any exploration initiative.

Once the source rock was subjected to the hydrocarbons generation and expulsion processes, the measured naphtogenic data as Total Organic Carbon (TOC) and Petroleum Potential (S2 value - measured with Rock-Eval pyrolysis) turn out to be more or less depauperated compared to the original values. The same happens to the derived parameter Hydrogen Index (HI=S2/TOC *100), that only in case of immature kerogen expresses the effective original kerogen quality. Input parameters for basin modelling are original TOC and original Hydrogen Index (original Petroleum Potential is consequent to the choice of them). These naphthogenic parameters together with the definition of the source rock thickness are fundamental for the final result of basin modelling as they have repercussions on the quantity of generated, expelled, migrated and entrapped hydrocarbons. A formula for the assessment of the original naphthogenic parameters, starting from measured data, was applied in Eni since 1998 (Scotti, 2004, internal report) in order to get rid of both subjective choices and choices not in line with

the measured residual data. Mosci (2014) observed that quite similar results in original TOC assessment can be obtained using both Eni's formula (simplified, not considering S1 value) and Jarvie's formula (deduced from his paper Jarvie, 2012). TOC will undergo a depletion as greater as the production of hydrocarbons per organic carbon unit will be. All of them depend on the assumption of the most probable original Hydrogen Index value (HI_O - mg HC/g TOC). If we are able to estimate the original Hydrogen Index value (considering type of organic matter and sedimentary environment, so from the kerogen quality), starting from residual TOC (TOC_R)and from Rock-Eval pyrolysis data (S1 and S2 values), it is simple to assess the depletion of the TOC. So, the original HI (original kerogen quality) has carefully to be assessed taking into account organic matter type and its preservation.

Summarizing, for source rocks so called "mature", TOC and HI parameters cannot be considered fully representative of the original potential and do not expresses the effective original kerogen quality. They represent residual values (TOC_R and HI_R), depauperated compared to the original ones (TOC_O and HI_O). Contrarily, in an immature source rock, the organic parameters measured are representative of the original values (TOC_O and HI_O).
Thus, in this work we seek to synthesize the peculiarities of immature and mature source rocks, highlighting analogies and differences. In light of this, 12 cases of study have been selected by Eni. These comprise 10 immature source rocks of Cretaceous and Triassic age, and 2 mature/weak mature source rocks of Devonian age. In particular, differences and similarities in age, lithology, organic content and paleogeographical setting have been emphasized.

A classical approach has been applied to the cases of study, together with classical analytical techniques (XRD, XRF and TOC, Rock – Eval analysis). However, we had the possibility to apply also some unconventional and innovative techniques (Laser ablation ICP – MS, iron speciation, thallium isotopes, sulfur isotopes) in a novel approach in collaboration with CNR of Pavia, the University of California – Riverside (CA, USA) and MagLab (Tallahassee – FL, USA).

To reach our target, a methodology of data processing has been developed starting by some inorganic geochemical proxies. Many of those are useful to characterize the redox conditions in the water column and, in turn, in the depositional environment. Redox conditions are one the most important parameter to characterize for the source rock evaluation because they are fundamental for the organic matter accumulation, preservation and, in turn, for the hydrocarbon

production. This means that the depositional environment is what more affect the quality of the source in terms of amount of hydrocarbons produced and typology. Most of these information can be extrapolated by using inorganic proxies widely used and discussed in literature, that is why redox conditions are, partially, the focus of our research.
In light of this, the goal of the project is to combine organic parameters and inorganic parameters to trace the organic matter content and quality in source rocks. The target is also to find univocal and always valid correlations that do not change with the source rock maturity, composition, geological context and age. This has allowed to develop a methodology to characterize different source rocks, independently from their composition, geological provenance and history.

The dissertation is articulated as follow:

- Source rocks: synthesis of the petroleum system and results obtained by the study of immature and mature source rocks and their comparison;
- Geochemical proxies: the state of art about the most useful geochemical proxies to apply to the source rock evaluation, in particular regarding the environmental conditions;
- Sample typology;
- Methodology: a synthesis of which samples have been used, how they have been prepared, which analytical techniques have been used to analyze the samples;
- Data processing procedure: a brief synthesis of how we selected our samples and how we decided to process our data;
- Cases of study: description of our cases of study, in particular the depositional setting, mineralogy and organic features have been described;
- Results and discussions divided in age;
- Comparison between immature and mature cases of study;
- Conclusions on the immature and mature cases of study;
- Paper "Geochemical evidence for local variability in redox and depositional conditions in a deep-water Bonarelli equivalent section from Southern Tethys (Fontana Valloneto section, southern Italy)" published in 2020 on Ofioliti (vol. 46, No.1);
- "Long-term de-oxygenation throughout the mid-Cretaceous: local and global implications": project regarding the collaboration with professors Timothy W. Lyons (University of California – Riverside) and Jeremy Owens (MagLab & Florida State University – Tallahassee) in which we applied novel geochemical proxies to a section from the Central Atlantic.

CHAPTER 2

Source rocks

In this section, a brief synthesis of the petroleum system and the role of source rocks in it is proposed first (based on the book of Novelli et al., (2004), "*Hydrocarbons: Origin, exploration and production*" printed by Eni).

The hydrocarbons formation and accumulation follow six steps:

1. Deposition and preservation of the organic matter under reducing conditions;
2. Sediments and organic matter burial with kerogen formation;
3. Increasing of temperature that leads to the transformation of kerogen into hydrocarbons into the source rock;
4. Primary migration;
5. Secondary migration toward the reservoir;
6. Interruption of migration to the surface with the encounter of a trap and hydrocarbons accumulation.

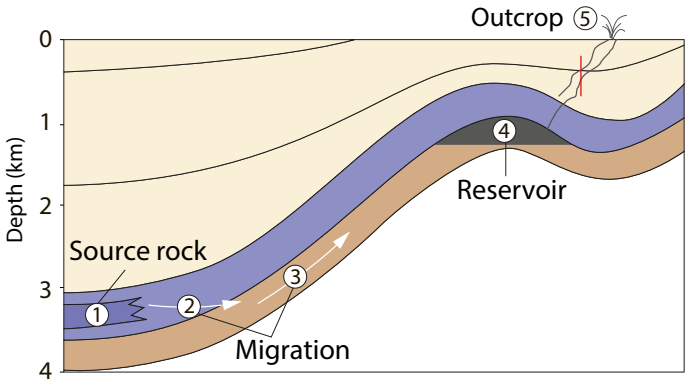

Figure 2.1 (from Leythaeuser D., 2005): (1) petroleum genesis in the source rock; (2) primary migration, (3) secondary migration; (3) accumulation in a trap and reservoir formation; (4) outcrop of the petroleum thank to the fracturing of the cap rocks.

The sum of the source rocks, the layers and rocks that in which the hydrocarbons move, and the trap constitute the so-called petroleum system represented in figure 2.1. The first step is related to the carbon cycle: C is exchanged between geosphere, hydrosphere, biosphere and atmosphere as indicated in figure 2.2.

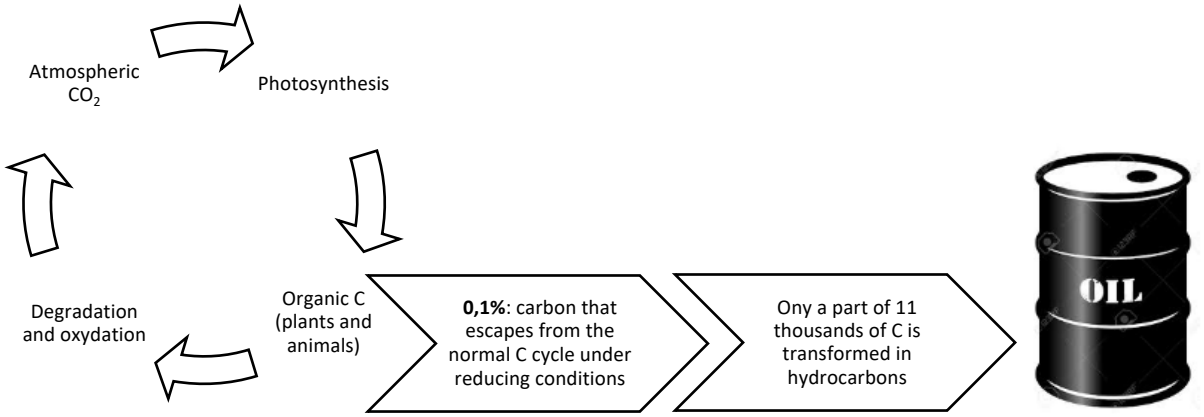

Figure 2.2: scheme of the carbon cycle.

The carbon related to hydrocarbons escapes from the normal C cycle through burial under reducing conditions. These are fundamental for the organic matter preservation.

There are several types of anoxic basins in which OM can accumulate and preserved, here we list them (figure 2.3). It is our intention describe briefly the hydrocarbons genesis.

1. Large anoxic lakes;
2. Anoxic seawater under the photic zone in correspondence of upwelling zones, these regions are also called Oxygen Minimum Zone (OMZ).
3. Silled basins characterized by weak restriction;
4. Silled basins characterized by strong restriction.

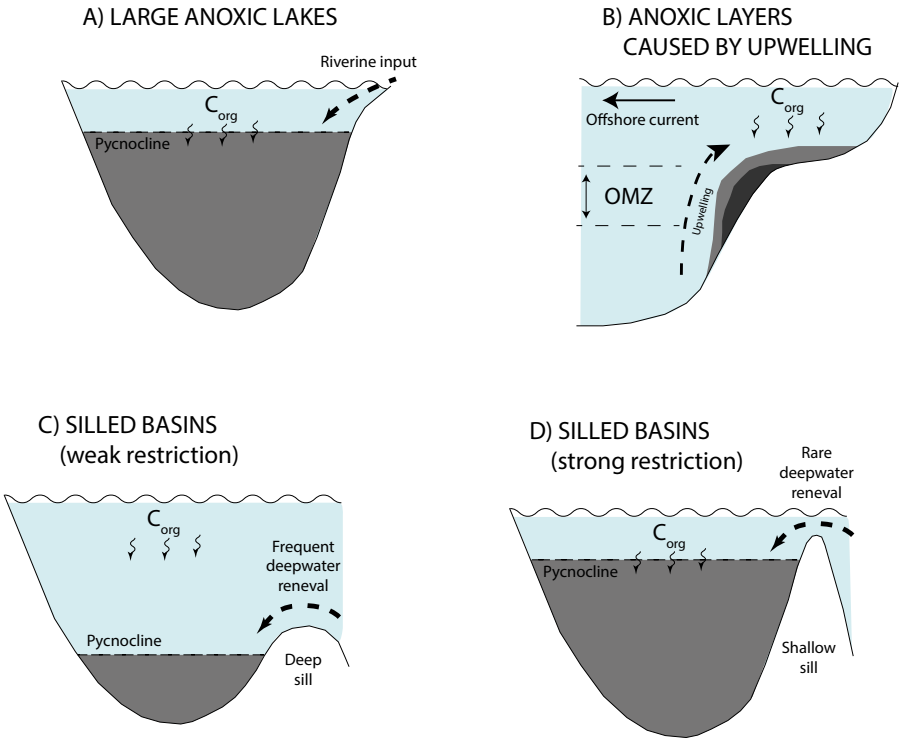

Figure 2.3 (modified by Algeo and Rowe, 2012): different depositional settings: (A) large anoxic lake, (B) continental shelf upwelling zone, (C) anoxic basin with deep sill, and (D) anoxic basin with shallow sill. These settings represent a continuum with respect to deepwater restriction.

The paper of Demaison and Moore (1980) is focused on the anoxic environments and the oil source beds genesis. The latter are OM-rich sediments containing kerogen type that is sufficiently H-rich to convert to oil during thermal maturation. Usually rocks with TOC between 1 and 20 wt% are oil prone. There are many factors that influence OM accumulation in aquatic environment:

1. Biological: related to primary productivity and biogeochemical degradation of OM;
2. Physical: related to the transit of OM toward the water – sediment interface.

Primary productivity is related to the phytoplankton production in the euphotic zone and to the terrestrial OM supply by rivers. Once in the oceans, OM is degraded mainly by bacteria. The main oxidants are, in order of oxygen availability, O_2, NO_3 and SO_4. The biochemical degradation slows down a lot or is even arrested when SO_4 is present in very low concentrations. Moreover, the absence of bioturbation does not allow the re-supply of the oxidants from the water column, leading to laminated layers in the sediments.
Also, the transit of OM to the depositional environment influence its accumulation; a long residence time of OM in the oxygenated water column affect its preservation. The particle size plays a fundamental role: fine grained sediments tend to have lower levels of bacterial activity then coarse-grained sediments because diffusivity of oxidizing agents is restrained. Finally, also the sedimentation rate (SR) influence OM accumulation and preservation: in general TOC increases with SR but when the latter is too high a dilution is observed. So, the positive correlation between TOC and SR is maintained from slow to medium SR. However, in general, SR in anoxic environments are higher than oxic environments.

After the depositional process, the organic matter is transformed into kerogen by bacterial activity. Kerogen is defined as complex organic matter insoluble in organic solvents. It is composed by C, O, H and minor S and N. There are several types of kerogen:

1. Type I: it derives from algae that lives in warm weather. This is the richest kerogen in H and the poorer in O. Usually it forms liquid hydrocarbons;
2. Type II: it derives from algae, spores and pollen. It is the most common kerogen and is very rich in H giving liquid hydrocarbons:
3. Type III: it derives from terrestrial vegetation. It is poor in H and it gives gaseous hydrocarbons.

Source rocks are sedimentary rocks composed by an inorganic portion (minerals) and organic matter (kerogen) in enough amount to generate hydrocarbons.

1. Bituminous shales are the most prolific in type I kerogen;
2. Source rocks that contains type II kerogen are the most prolific in oil;
3. Source rocks that contains type III kerogen are the most prolific in condensed gas.

The Total Organic Carbon (TOC) concentration is an approximate measure of the content of organic material in a rock. The source rock must have high concentrations of TOC to produce hydrocarbons.

After the depositional processes and burial, the diagenesis plays a fundamental role in hydrocarbons genesis. Indeed, the thermal history (temperature and time) is important to determine what kind of hydrocarbons are produced.
The increase of temperature leads to the cracking of the organic particles and to the hydrocarbons' generation. This process can be divided into three phases based on temperature as indicated in the figure 2.4: diagenesis, catagenesis and metagenesis.

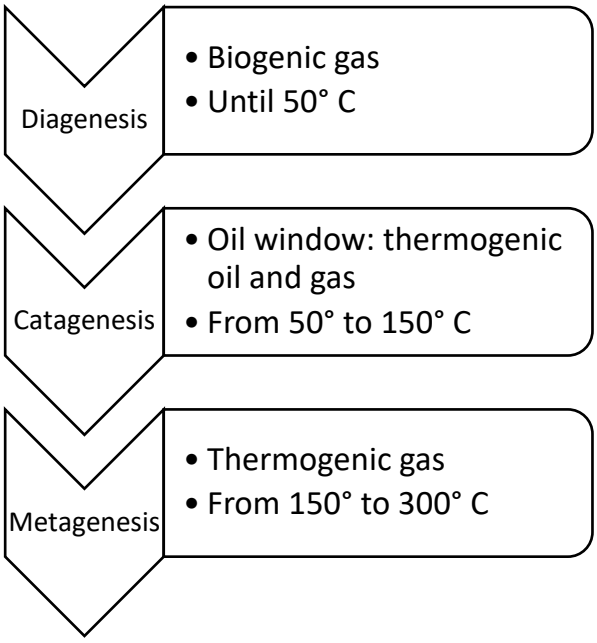

Figure 2.4: scheme of the maturation process and main characteristic of each phase.

This distinction is fundamental in order to estimate the **maturity** of the source rock (figure 2.5):

1. **Diagenesis**: biogenic gas is produces (methane) thanks to bacteria degradation of the organic matter. With the increase of temperature, the organic matter is transformed into complex compounds (geopolymers). This is the **immature zone** because no hydrocarbons are generated. The products of this step are H_2O, CO_2 and kerogen.
2. **Catagenesis**: in this steps liquid and gaseous hydrocarbons are produced with the thermal decomposition of kerogen. With the increasing of temperature, kerogen forms petroleum through cracking of organic molecules. First, heavy oils are generated which gradually become lighter because of the cracking. If the temperature increases more, humid gasses are generated (thermogenic gasses) due to thermal cracking (100-200°C). This phase includes the oil window: in this depth – temperature interval more liquid hydrocarbons than gasses are generated. This is the **mature zone** in which hydrocarbons production culminates.
3. **Metagenesis**: kerogen has lost his capacity to produce hydrocarbons and the gas produced derives from the thermal attack of the hydrocarbons already produced. In this phase the dry gas is produced (99% methane). This phase is called **over-mature zone**.
4. **Metamorphism**: above 300°C the organic matter is transformed into graphite losing the hydrocarbons.

Other ways to study the thermal maturity are:

1. **Vitrinite reflectance**: this is on organic particle that increasingly reflects light based on the temperature to which it was subjected (maturity is comprised between 0.5 and 2% of vitrinite reflectance);
2. **Spores color**: darkness of the spores increases with temperature;
3. **Kerogen pyrolysis temperature and evaluation of the Hydrogen Index (HI)**: temperature at which there is the maximum production of hydrocarbons.

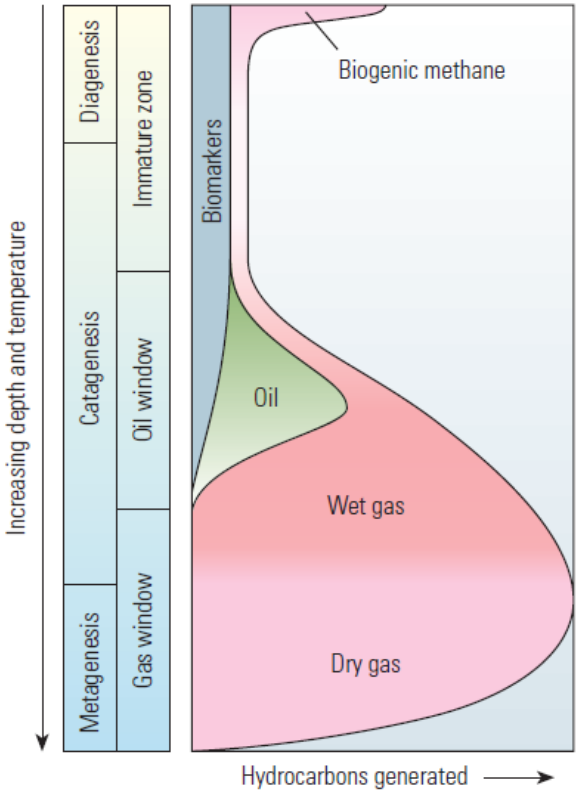

Figure 2.5 (from McCarthy et al., 2011): scheme of the maturation process with main characteristic of each phase and hydrocarbon genesis.

After the hydrocarbons' generation, in a conventional way, they need to migrate toward the carrier. This is a porous and fractured means that links the source rock with the trap (reservoir rock). The primary migration is controlled by: (i) pressure gradients, (ii) compaction pressure, (iii) capillary pressure and (iv) fracturing and increase of permeability.

The secondary migration is related to the movement of the hydrocarbons from the carrier to the reservoir rock. Hydrocarbons move like a discontinuous phase under the action of (i) driving forces (floating boost), (ii) resistant strength (capillary pressure) and (iii) hydrodynamic forces (e.g. presence of a water current). A good reservoir rocks needs to be characterized by a good porosity and permeability parameters because they increase the amount of hydrocarbons that can be trapped and the migration efficiency. Once in the reservoir rock, hydrocarbons generate a reservoir. The latter is confined above by a cap rock: an impermeable rock that do not allow the rising of the hydrocarbon forward the surface. A common type of cap rocks are fine grained rocks as shales. The petroleum can crop out on the surface when the cap rock is fractured by tectonic stress or, in the case of a carbonaceous cap rock, when dolomitization processes occur.

The sum of the reservoir rock, cap rock and the geometric configuration of the system is called trap.

CHAPTER 3

Inorganic geochemistry of OM-rich rocks with variable redox conditions

The quantity of oxygen presents in the diagenetic environment is of fundamental importance for a source rocks because anoxic conditions allow organic matter accumulation and preservation, not possible with oxygen. The amount of oxygen affects the quantity and the quality of the preserved sedimentary organic matter. Studying the redox conditions in marine depositional settings means tracking distributions of oxygen in the environment and the biogeochemical and physical processes that control these distributions.

In literature, four redox conditions can be identified (i.e., Tyson and Pearson, 1991; Tribovillard et al., 2006; Algeo and Rowe, 2012; Algeo and Li, 2020), subdivided mainly according to the concentration of oxygen in the environment, represented in table 3.1. Oxidizing conditions are divided in oxic and suboxic; the latter is characterized by very low oxygen concentrations in the water column, while H_2S is limited to pore waters below the sediment – water interface. Reducing conditions may be anoxic or euxinic (also called sulfidic); the latter is characterized by the presence of hydrogen sulfide within the water column. H_2S is a catabolic product of sulfate-reducing bacteria (BSR).

REDOX CLASSES	O_2 CONCENTRATIONS IN BOTTOM WATERS
Oxic conditions	8.0 – 2.0 ml O_2/l H_2O
Suboxic conditions	2.0 – 0.2 ml O_2/l H_2O
Anoxic conditions	<0.2 ml O_2/l H_2O
Euxinic conditions	0 ml O_2/l H_2O with free H_2S

Table 3.1 (from Tribovillard et al., 2006): redox classification of the depositional environments. The values for O_2 concentrations in bottom waters are valid for present – day oceans.

Aerobic organisms use oxidant sources to their metabolism, first of all O_2. Organic Matter (OM in following) degradation occurs via organisms using secondary oxidant sources; in order of consumption (depends on free energy gain stemming from each microbial process) we have: (i) oxygen, (ii) nitrate, (iii) manganese and iron oxides and oxyhydroxides, (iv) sulfate. When all these oxidants are exhausted, methanogenic bacteria begin to decompose organic matter via an oxidative-reductive disproportionation of carbon. This classical early diagenesis sequence can be illustrated by the sequence of equations illustrated in table 3.2.

At the sediment–water interface oxygen depleted conditions may develop when there is no enough oxygen supply compared to its consumption. Anoxia can occur in stagnant or confined water masses (e.g. figure 2.3) where insufficient circulation prevents O_2 renewal or in places where intense OM degradation consumes O_2 faster than it is replenished (even in open-marine conditions). In sediments can occur the same but O_2 supply is also related to their composition (clay vs. sands), texture (fine- vs. coarse-grained) and the intensity of bioturbation.

In the presence of free O_2:

Aerobic respiration

$$(CH_2O)_{106}(NH_3)_{16}H_3PO_4 + 138O_2 \rightarrow H_3PO_4 + 16HNO_3 + 106CO_2 + 122H_2O$$

In the absence of free O_2:

Denitrification

$$(CH_2O)_{106}(NH_3)_{16}H_3PO_4 + 94.4HNO_3 \rightarrow H_3PO_4 + 55.2N_2 + 106CO_2 + 177.2H_2O$$

Manganese reduction

$$(CH_2O)_{106}(NH_3)_{16}H_3PO_4 + 236MnO_2 + 472H^+ \rightarrow H_3PO_4 + 236Mn^{2+} + 16NH_3 + 106CO_2 + 366H_2O$$

Iron reduction

$$(CH_2O)_{106}(NH_3)_{16}H_3PO_4 + 212Fe_2O_3 + 848H^+ \rightarrow H_3PO_4 + 424Fe^{2+} + 16NH_3 + 106CO_2 + 530H_2O$$

Sulfate reduction

$$(CH_2O)_{106}(NH_3)_{16}H_3PO_4 + 53SO_4^{2-} \rightarrow H_3PO_4 + 53S^{2-} + 16NH_3 + 106CO_2 + 106H_2O$$

Absence of free and linked oxygen:

Disproportionation

$$(CH_2O)_{106}(NH_3)_{16}H_3PO_4 \rightarrow H_3PO_4 + 16NH_3 + 53CO_2 + 53CH_4$$

Table 3.2 (from Tribovillard et al., 2006): the classical sequence of equations illustrating how heterotrophic bacterial activity consumes OM, using various electron acceptor.

The state of art (e.g. Jones and Manning, 1994; Lyons et al., 2003; Rimmer, 2004; Algeo and Maynard, 2004; Algeo, 2004; Tribovillard et al., 2004a, 2005, 2006; Gallego - Torres et al., 2007; Pattan and Pierce, 2009; Pi et al., 2014; Baioumy and Lehmann, 2017; Owens et al., 2013; Ostrander et al., 2017; Owens et al., 2017a) on inorganic geochemical proxies for redox conditions has led to the selection of a series of proxies that allow to trace the redox conditions of the diagenetic environment. The papers analyzed show trace elements (e.g. redox – sensitive elements, RSEs), ratios of trace elements, major elements (e.g. speciation of iron), isotopic compositions which allow to identify the redox conditions of the depositional environment. The behavior of these proxies is very useful: their concentrations are the results of several environmental changes like temperature, seawater level, oceanic circulation, volcanic activity, riverine inputs, etc.

To behave as an effective measure of bottom water paleo-oxygenation a parameter should be sensitive to the bottom water oxygen concentration alone and should be independent of any variation in the compositional and textural properties of the host sediment (e.g., clay mineral type and abundance, grain size, surface area), and to other environmental factors such as

sedimentation rate. If ancient sediments are to be interpreted using such indices, they must also be independent of the post-depositional burial history to which the host sediment has been subjected. Obviously, it is unlikely that any parameter will be perfect in every aspect (Jones and Manning, 1994).

That is why a multi proxy approach is the best way procedure that allow to trace several global changes occurred during the depositional time. This multi proxy approach is also very useful also because TEs respond in predictable ways to redox changes and so, the analysis of environmental redox conditions is best studied using a suite of proxies.

In this work we focused mainly on five typologies of proxies:

1. Common redox – sensitive elements (RSEs)
2. Elements not correlated to OM
3. Anomalies in trace elements (TEs) and rare earth elements (REEs)
4. Unconventional redox proxies

Actually, in literature a large part of redox proxies is represented by ratios between elements as indicated in table 3.3. Indeed, many authors use them to assess the redox conditions in their cases of study (references indicated in table 3.3).

	OXIC	SUBOXIC	ANOXIC	EUXINIC	COMMENTS	REFERENCES
V/Ni	<1.9	1.9-3	>3 (Ni <90 ppm)	>3 (Ni >90 ppm)	Generally, in anoxic conditions V is very enriched respect to Ni. In particular, V concentrates more easily in silicate minerals, while Ni in sulfur. Ni and V are often present in petroleum because they form many stable porphyrin complexes.	Adegoke et al. (2014)
V/(Ni+V)	/	0.46 – 0.60	0.54 – 0.82	>0.84		Adegoke et al. (2014)
V/Cr	<2	2 – 4.25	>4.25	/	/	Rimmer (2004)
V/(Cr+V)	/			>0.6	/	Baioumy and Lehmann (2017)
V/Mo	10.0 - 60.0	2.0 - 10.0	<2	/	The positive correlation between Mo and V suggests anoxic conditions, in particular for	Baioumy and Lehmann (2017)
Ni/Co	<5	5 – 7	>7		Diagenetic pyrite usually has Ni/Co > 1.	Rimmer (2004)
Authigenic U (UO_2, U_3O_7, U_3O_8)	≤4 ppm	4 – 10 ppm	>10 ppm		(Authigenic U) = (Total U) - Th/3 because detrital materials has Th/U = 3.8 ±1.1.	Pattan and Pierce (2009)
(U+V)/(U+V+Mo) vs. Mo	/	High ratio (>0.85) but low Mo (<1ppm)		Low ratio (0.7 - 0.85) but high Mo (>1ppm)	/	Pi et al. (2014)
U/Th	<0.75	0.75 – 1.25	>1.25		The relation between U and Th exists because U is very soluble and moble with the changing of oxygenation while Th is relatively immoble.	Adegoke et al. (2014)
Th/U	Between 2 and 7		<2			Baioumy and Lehmann (2017)

Table 3.3: redox proxies based on elements ratios and their reference.

Even if they are widely used in this field, we could not find a study on their reliability. In the first year of PhD, we applied these proxies as in literature, but we found out that they are not reliable: if they are applied on the same section, often they give very different redox conditions.

That is why we decide to abandon this typology of redox proxies and, instead, focus on the five categories explained above.
Indeed, in a recent study of Algeo and Liu (2020), the authors suggest that bimetal proxies are known to be rather poor in their ability to discriminate redox variations. In particular, their use has fallen out of favor among experienced sedimentary geochemists, who generally prefer trace metal enrichments factors (EFs) or trace metal absolute values. This is due to the fact that, all metals are enriched authigenically (in different degrees) under reducing conditions and therefore the ratio of two of them is not as efficient as a ratio between a metal and a redox-insensitive, detritally hosted element such as Al (as in metal EFs).

In the next pages we seek to describe how those elements behave by varying redox conditions and which elements are most useful to describe the geochemical composition of the shales. The section is divided into five sections following the redox typologies listed above.

3.1 REDOX-SENSITIVE ELEMENTS

In general, the most used proxies are the so called redox – sensitive elements (RSEs) that correlates positively with TOC. They are U, V, Mo, Cr, Ni, Co, P, Ba, Cu, Zn, Cd. In the work of Tribovillard et al. (2006) an attempt was made to summarize the characteristics for each of them, specifying which elements to use and in which cases, also on the basis of which mineralogical/organic phases are more correlated.

Before considering which processes occur after deposition, we have to take in account that the degree of restriction of the deep water mass (subpycnoclinal) of the basin can affect environmental conditions and biogeochemical cycles, in particular it can influence TEs concentrations in seawater. From the study of Algeo and Maynard (2008) we can identify three typology of marine basin (B. C and D in figure 2.3): unrestricted circulation as in B allows continuous resupply of trace metals, resulting in a dominant redox control where trace-metal uptake is proportional to the intensity of reducing conditions and hydrographic effects are limited. Strongly restricted circulation as in D results in limited resupply of trace metals, favoring a hydrographic control where sediment TM concentrations are proportional to the rate of deep-water renewal and redox effects are secondary.

Generally, RSEs are present in seawater either in soluble form or adsorbed onto particles. Abiotic processes can remove dissolved trace elements from the water column and concentrate

them in the sediments. These processes are very efficient under reducing conditions and include: (i) diffusion of dissolved trace elements from the water column across the sediment–water interface (ii) remobilization and repartitioning along redox gradients within the sediments, (iii) redox cycling of manganese and iron, (iv) adsorption of metallic ions or ionic species onto organic or mineral substrates, (v) formation of organometallic complexes and (vi) precipitation of (iron-) sulfides and/or insoluble oxyhydroxides.
All these processes result in some enrichment that mirror the specific redox conditions present in the depositional environment and early diagenesis. Consequently, trace-element abundances in sediments and sedimentary rocks allow us to reconstruct paleodepositional conditions (as summarized in some recent papers like Lyons et al., 2003; Rimmer, 2004; Algeo and Maynard, 2004; Algeo, 2004; Tribovillard et al., 2004a, 2005, 2006).
Trace elements (TEs) usually show good enrichment in laminated, organic- rich facies, especially the euxinic ones, and little in organic-poor sediments.

In order to use RSEs, the need to assess if one is depleted or enriched born. Generally, the degree of enrichment/depletion of an element is evaluated relative to its concentration in a reference sink, like the average crustal rocks (Upper Continental Crust – UCC) or average shale (Post Archean Australian Shales – PAAS) (McLennan, 2001; Wedepohl, 1971, 1991; respectively). In this work, we used UCC values to assess if in our cases of study trace elements are enriched/depleted.

In summary, enrichments in RSEs can be used to assess bottom water redox conditions. Generally, these elements are soluble under oxidizing conditions. Under reducing conditions, they are removed and enriched though authigenic minerals formation and or uptake by organic matter. OM-rich shales formed under anoxic and euxinic conditions can be really enriched in RSEs, especially Mo.

Many elements suffer of mobilization during diagenesis that can led to elemental distributions that do not mirror the primary distribution (e.g. reoxygenation). That is why we focused on those elements less vulnerable to primary and secondary mobilization (i.e. Mo, V, U, Ni and Cu).

In our case we focused on the redox - sensitive elements that mostly correlate with TOC and HI, i.e. Mo, V and U and to a lesser extent Ni and Cu. These are more soluble in oxidizing

conditions and less soluble in reducing conditions, leading to an enrichment in the oxygen-poor sediments. Some of these metals (e.g. Ni and Cu) are brought into the sediment by organic matter and then sequestered in sediments in association with pyrite after the decay of organic matter.

Follow a brief review (from Tribovillard et al., 2006 and references therein) of the main elements discussed in this dissertation.

Molybdenum (^{98}Mo)

Molybdenum is one of the most abundant transition metals in seawater and is present mainly in the form of molybdate (MoO_4^{2-}; Broecker and Peng, 1982). Under oxidizing conditions, Mo displays little affinity for the surfaces of clay minerals, $CaCO_3$ and Fe-oxyhydroxides at marine pH values (Brumsack, 1989; Goldberg et al., 1998). In addition, molybdenum is easily captured by Mn-oxyhydroxides (Bertine and Turekian, 1973; Calvert and Pedersen, 1993; Crusius et al., 1996; Erickson and Helz, 2000; Zheng et al., 2000). Subsequent reduction of these phases liberates adsorbed Mo to pore waters (Crusius et al., 1996). This phenomenon can enhance Mo enrichment in the shallow burial environment: dissolved Mn refluxing from the sediment has the potential to absorb and concentrate molybdate at or near the sediment–water interface, when the oxic–anoxic interface is encountered (Berrang and Grill, 1974; Adelson et al., 2001). Although this process can concentrate Mo in surficial sediments, a reduction step is necessary to explain the mechanism of Mo fixation within the sediment: (i) Mo can be scavenged directly from the water column or (ii) it can be captured from pore waters supplied with Mo from the water column (François, 1988; Emerson and Huested, 1991; Huerta-Diaz and Morse, 1992; Calvert and Pedersen, 1993; Crusius et al., 1996, Zheng et al., 2000). Other models favour a direct role played by sulfide: Helz et al. (1996) and Vorlicek et al. (2004) suggested that fixation in the presence of dissolved sulfide result in a mineralization that occurs through organic thiomolybdates and inorganic Fe–Mo–S cluster. Helz et al. (1996) introduced the concept of a geochemical switch, through which hydrogen sulfide transforms Mo from a conservative element to particle-reactive species, in marine depositional environments. Thus, the reaction MoO_4^{2-}→thiomolybdates (MoO_xS_{4-x}, x=0–3) represent the geochemical switch in which the products are particle-reactive and prone to scavenging (Erickson and Helz, 2000). In the sediments, the transformation reactions are catalysed by proton donors or in the presence of some active surface minerals such as kaolinite (Erickson and Helz, 2000; Vorlicek and Helz, 2002).After the reaction, Mo is scavenged by forming bonds with metal-rich (notably Fe)

particles, sulfur-rich organic molecules (Helz et al., 1996; Tribovillard et al., 2004b) and iron sulfide (Vorlicek et al., 2004).

Organic detritus can also scavenge Mo. One role of OM is simply as a carrier for Fe and other trace metals. The second role is more direct: organic O–S groups attached to macromolecular detritus may insert directly into the MoO_4^{2-}, resulting in covalent bonding between Mo and the macromolecule (Tribovillard et al., 2006).

Owing to generally strong enrichment in organic-rich marine facies deposited under anoxic conditions, sedimentary Mo concentrations have been widely used as a proxy for benthic redox potential (e.g., Meyers et al., 2005; Pattan and Pierce, 2009; Pi et al., 2014; Baioumy and Lehmann, 2017). However, recent investigations revisited the use of Mo as a paleoredox and paleoenvironmental proxy.

For instance, Algeo (2004) suggests that Mo concentrations in sediments can trace ancient anoxia in the ocean due to the fact that large quantities of Mo (but also V and U) can become sequestered in organic-rich deposits during marine anoxic events, potentially leading to a substantial drawdown of their seawater concentrations compared with those of a well-oxygenated ocean. This is the case of the Oceanic Anoxic Event 2 (OAE 2 - 94 Ma ca., Cenomanian – Turonian boundary; Schlanger and Jenkyns, 1976): in many localities around the world a drawdown of the redox-sensitive elements has been observed due to an expansion of the anoxic and euxinic seafloor. During this period, 40 - 50% by volume of the global ocean was anoxic (Monteiro et al., 2012; Ostrander et al., 2017) while euxinia was restricted to a maximum of 7% of the seafloor (Owens et al., 2013; Owenset al., 2018; Dickson et al., 2016 a, b).

Moreover, Algeo and Lyons (2006) and Algeo and Rowe (2012) suggest a possible use of Mo/TOC ratio to provide insight into the degree of water mass restriction and estimates of deep-water renewal times. The amount of Mo taken up by sediments in anoxic marine systems depends on both the aqueous concentration of Mo (i.e., source-ion availability) and the concentration of sedimentary organic matter (i.e., host-phase availability). Normalization of [Mo]s to organic carbon is necessary because of the role that OM has as a substrate for Mo uptake by the sediment, allowing comparison of levels of sediment Mo enrichment among marine systems containing variable amounts of organic matter. Thus, increasing restriction results in lower deep-water aqueous Mo concentrations, owing to rates of Mo removal to the sediment in excess of resupply (low Mo/TOC), whereas under unrestricted conditions Mo/TOC will be high. The key factor is the degree of water mass restriction environments that causes different relationships between sedimentary Mo enrichments and declining benthic redox

potential. Ultimately, deep-water renewal and aqueous [Mo] depend on basin geometry: the subpycnoclinal water mass is renewed less readily in larger basins with shallower sills (e.g., Black Sea), than in smaller basins with deeper sills (e.g., Saanich Inlet) (figure 2.3; Algeo and Lyons, 2006).

Vanadium (^{51}V)

In oxic waters, vanadium is present as V(V) in the form of vanadate oxyanions (HVO_4^{2-} and H_2VO^{4-}) (Tribovillard et al., 2006). In pelagic and hemipelagic sediments, vanadate can be adsorbed onto both Mn- and Fe-oxyhydroxides (Calvert and Piper, 1984; Wehrly and Stumm, 1989) and clays (Breit and Wanty, 1991). Under mildly reducing conditions, V(V) is reduced to V(IV) and forms vanadyl ions (VO^{2-}), related hydroxyl species $VO(OH)^{3-}$ and insoluble hydroxides VO(OH)2. This reaction is favoured by the presence of organic acids. In marine environment, the V(IV) ionic species may be removed to the sediment by surface adsorption processes or by formation of organometallic ligands (Emerson and Huested, 1991; Morford and Emerson,1999) or by the so called "Vanadyl Organic Complexes" (Glikson et al., 1985; Alberdi-Genolet and Tocco, 1999). Under euxinic conditions, the presence of free H_2S causes the reduction of V(IV) in V(III), which can be taken up by geoporphyrins or be precipitated as the solid oxide V_2O_3 or hydroxide $V(OH)_3$ phase (Breit and Wanty, 1991; Wanty and Goldhaber, 1992). The two-step reduction process of V may lead to the formation of separate V carrier phases of contrasting solubilities under anoxic versus euxinic conditions (Calvert and Pedersen,1993; Algeo and Maynard, 2004).
Vanadium is thus probably not trapped in solid solution by Fe-sulfides (Algeo and Maynard, 2004) and may be removed from pore waters below the level of Mn–Fe-oxyhydroxides reduction (Hastings et al., 1996; Morford and Emerson, 1999). In the diagenetic environment, V(III) readily substitutes for aluminum in the octahedral sites of authigenic/diagenetic clay minerals (Breit and Wanty, 1991).

Algeo and Maynard (2004) show that under anoxic conditions, V is contained mainly in organic fractions and to a lesser extent in sulphidic fractions. Therefore, in this type of sediments TOC has a good correlation with V. Under euxinic conditions, instead, V seems to reside mainly in sulphidic phases and exhibits good correlations with Mo and Pb, although unlike these it is not in solid solution with Fe sulfides but more likely as an insoluble oxyhydroxide.

Uranium (^{238}U)

Uranium in seawater is present mainly as U(VI) in the form of uranyl ions that bind to carbonate ions, forming $UO_2(CO_3)_3^{4-}$. In particular, some studies show that U(VI) is more easily incorporated into aragonite over calcite: Reeder et al. (2000) found that $UO_2(CO_3)_3^{4-}$ is directly incorporated in aragonite without coordination change; contrarily, the coordination of $UO_2(CO_3)_3^{4-}$ is altered during incorporation into calcite (Reeder et al., 2000, 2001). Similarly, studies of natural calcite samples have suggested that uranyl can substitute Ca with an equatorial coordination number of 4 (Kelly et al., 2003, 2006).

Reduction of soluble U(VI) to insoluble U(IV) occurs under conditions near of those for conversion of Fe^{3+} to Fe^{2+} through microbial mediation (Klinkhammer and Palmer, 1991; Crusius et al., 1996; Zheng et al., 2000; Morford et al., 2001; Chaillou et al., 2002; McManus et al., 2005). Authigenic U(VI) enrichment is considered to take place primarily in the sediment thank to the presence of free H_2S (Algeo and Maynard, 2004; McManus et al., 2005).

Consequently, in the sediments, the main U-enrichment process is $UO_2(CO_3)_3^{4-}$ diffusion from the water column, reduction reactions and adsorption or precipitation as UO_2 (uraninite, the most frequent form), U_3O_7 or U_3O_8 (e.g., Klinkhammer and Palmer, 1991; Crusius et al., 1996; Zheng et al., 2000; Morford et al., 2001; Chaillou et al., 2002; McManus et al., 2005) or adsorption onto the sediment or clay mineral surfaces (Pattan and Pierce, 2009 and references therein). Since the enrichment takes place within the sediment and not in the water column, the oxygen penetration depth and the sedimentation rate may play a role (Crusius and Thomson, 2000). In the reduced state, removal of U from the water column to the sediment may be accelerated by the formation of organometallic ligands in humic acids (Klinkhammer and Palmer, 1991; Zheng et al., 2002a, b; McManus et al., 2005). The accumulation of U is at least partly mediated by bacterial sulfate reduction (BSR) reactions, because without bacterial activity, the reduction process would be very slow (Zheng et al., 2002a, b; Sundby et al., 2004; McManus et al., 2005). As the intensity of sulfate reduction activity is linked to the abundance of reactive organic matter, U abundance usually shows a good correlation with the organic carbon rain rate (McManus et al., 2005) and with the organic-carbon content in anoxic (non-sulfidic) facies (Algeo and Maynard, 2004).

U can be remobilized within the sediments if oxygen penetrates to a depth where authigenic U has accumulated (Morford et al., 2001; Zheng et al., 2002a, b; McManus et al., 2005). This re-oxidation process can either erase a primary U signal (e.g., through loss of U from the sediments to the overlying water column) or result in the vertical migration of the initial U peak to another location in the sediments where conditions favouring reprecipitation are met (McManus et al.,

2005). A way to identify a post-depositional reoxygenation is to observe V and Mo, which are not affected by this issue: when an enrichment of V and Mo with less evident enrichment of U is observed, it is possible that there has been an event of this type.

Nickel (^{58}Ni) and copper (^{63}Cu)

Nickel. Under oxic conditions nickel is a macronutrient and is present as Ni^{2+} or $NiCl^{+}$ ions, although it is more present in solution as a carbonate complex ($NiCO_3$) or adsorbed on fulvic and humic acids (Calvert and Pedersen, 1993; Whitfield, 2002; Algeo and Maynard, 2004). The removal of Ni in the sediment can be accelerated by the complexation and sedimentation with organic matter that transports Ni towards the water – sediment interface (Piper and Perkins, 2004; Nameroff et al., 2004; Naimo et al., 2005). The organic matter re-mineralizes, below the water – sediment interface, releasing Ni in pore waters. Under anoxic conditions Ni forms insoluble NiS which can go into solid solution with the syngenetic pyrite. However, the take up of Ni is cinematically slow (Huerta-Diaz and Morse, 1990, 1992; Morse and Luther, 1999), so it leans towards to limit its concentration in hydrogenous sulfides. It is probable, therefore, that under anoxic conditions Ni is hosted by the organic such as tetrapyrrole complexes and Nigeoporphyrins (correlating with the TOC; Lewan and Maynard, 1982; Grosjean et al., 2004) and detrital phases, while under euxinic conditions it resides mostly in the sulphidic phase (correlating with S).

Copper. Under oxic environment, copper is more present as Cu^{2+}, as an organometallic ligand and to a lesser extent as a $CuCl^{+}$ ion present in solution (Calvert and Pedersen, 1993; Whitfield, 2002; Achterberg et al., 2003; Algeo and Maynard, 2004). The complexation of copper with organic matter, as well as the adsorption on the particulate of Fe and Mn oxy – hydroxides accelerates its removal from water and the enrichment of sediments (Fernex et al., 1992; Sun and Püttmann, 2000; Nameroff et al., 2004; Naimo et al., 2005). Following the decay of organic matter and the dissolution under reducing environment of Fe and Mn oxides - hydroxides, copper can diffuse in pore waters. Here, under reducing conditions, Cu(II) is reduced to Cu(I) which can be incorporated in solid solution with pyrite or form copper sulfides (CuS and CuS2) (Huerta-Diaz and Morse, 1990, 1992; Morse and Luther, 1999). In pelagic sediments with slow sedimentation it can be fixed diagenetically on smectites or syngenetic nontronites (Pedersen et al, 1986).

This suite of RSEs can show different sensitivities to the variation of redox conditions (from oxic to euxinic), as shown in figure 3.1 (from Tribovillard et al., 2006, modified after Algeo and Maynard, 2004). Basically, under anoxic conditions U and V can accumulate, while Ni, Cu and Mo are enriched mainly under sulfidic conditions. Using the different behaviour between these elements and a multi-element approach, it is possible to trace redox conditions in the depositional environment (figure 3.1). For example, an enrichment of U and V without Mo can point to reducing conditions without free H_2S. Or, samples enriched in U, V and Mo point toward euxinic conditions (Tribovillard et al., 2006). Or, finally, the two-step reduction of some elements (e.g., V(V)→V(IV)→V(III)) give other information about small redox variations at the sediment water-interface or in the water column.

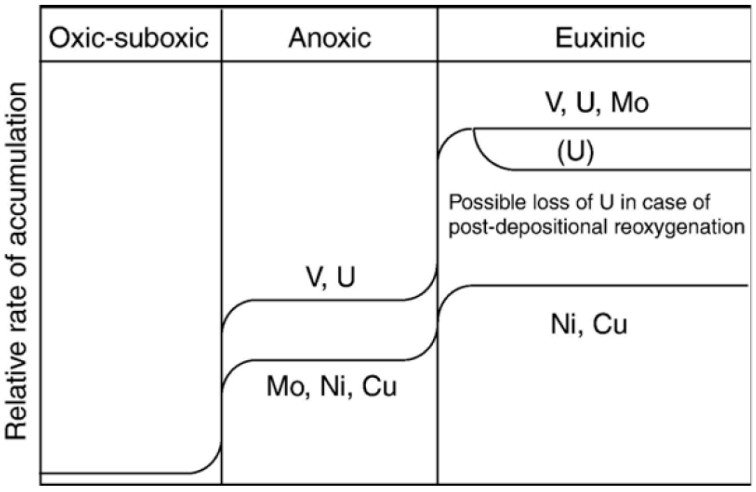

Figure 3.1 (from Tribovillard et al., 2006): schematic behavior of Ni, Cu, Mo, U and Vas a function of the redox conditions of the depositional environment.

Of course, this is not always true and could be a simplification in some complex environment. For example, several authors (e.g. Goldberg et al., 2016; Ostrander et al., 2017) found out that during OAE 2 (~94 Ma) global euxinic conditions occurred associated to a drawdown of Mo, V and U concentrations in seawater.

In addition, we should consider the relationship of the RSEs with OM. For example, Ni and Cu arrive most often in the sediment associated with organic matter. These two elements are not particularly enriched in sediments, even if anoxic conditions develop rapidly. They can accumulate when OM decays and releases them; they can concentrate in phases such as pyrite (while OM is remineralized by bacterial activity) , under sulfidic conditions. Consequently, a high content in Ni and Cu indicates that a high flux of organic matter brought these elements to the sediments in great abundance and that reducing conditions were met, allowing Ni and Cu fixation within the sediments. Therefore, Ni and Cu are the main indicators of organic matter flux toward the sediments and can give information about OM presence even if this has been lost during after deposition (Tribovillard et al., 2006).

3.2 ELEMENTS NOT CORRELATED TO THE ORGANIC MATTER

This group includes immobile elements (Th), the elements that give information on detrital fraction (Al, Zr) and elements that are enriched in oxidizing but not in reducing conditions (Mn). Usually, we expect to observe negative correlations or no correlations between these elements and the organic matter content (TOC) because they are enriched under oxic conditions (Mn) or in the detrital fraction (Th, Al and Zr) that dilute the organic fraction.

Thorium (^{232}Th)

Thorium is relatively immobile with low temperatures and redox conditions. It is often concentrated during weathering in the most resistant minerals (Jones and Manning, 1994). In fine – grained sediments, such as mudstones, it is often detected in the detrital fraction associated with heavy minerals or clays (aluminosilicates).

Aluminum (^{27}Al) and zirconium (^{90}Zr)

These elements are used for the normalization of trace elements, mainly in the cases with variable content of carbonates and opal (Tribovillard et al., 2006). In fact, usually, sedimentary rocks may have variable proportions of mineral phases, often of biogenic origin, that dilute the trace-element abundance of a sample (e.g. calcium carbonate and opal). Thus, in order to be able to compare trace-element proportions in samples with variable carbonate and opal contents, normalize to Al or Zr can be useful (Calvert and Pedersen, 1993; Tribovillard et al., 2006). Aluminum and zirconium (the latter is concentrated mainly in heavy minerals) are often used as indicators of the aluminosilicate and detrital fraction in sediments and they have low mobility during diagenesis. However, there are exceptions where aluminum cannot be used, and titanium and zirconium are preferable. This occurs in the case of marine sediments with a detrital content of less than 5 wt% and a relative excess of aluminum with respect to other detrital elements (e.g. Ti).

Manganese (^{55}Mn)

Manganese has only limited utility as a redox proxy (e.g., Calvert and Pedersen, 1993), but its peculiar geochemical behaviour makes it play a prominent role in the transfer of trace metals from the water column to the sediment and their subsequent uptake by authigenic phases.
The main manganese species in anoxic seawater are Mn^{2+} and $MnCl^{+}$, whereas in oxygenated waters it is oxidized to insoluble Mn(III) and Mn(IV) oxides (Calvert and Pedersen, 1993,

1996). The Mn(IV) solid phases, referred to as Mn-oxyhydroxides, are mainly MnO_2 and MnOOH. Below the oxic–anoxic interface, the reductive dissolution of oxyhydroxide particles releases soluble Mn(II) that may diffuse upward and downward within the sediment (Brumsack, 1986; Middelburg et al., 1987; Brumsack, 1989; Rajendran et al., 1992), partly because dissolved Mn is not taken up significantly by any organic or sulfide phase (Huerta-Diaz and Morse, 1992; Algeo and Maynard, 2004). The diffusion of Mn^{2+} can lead to $MnCO_3$ precipitation under oxic conditions (Pedersen and Price, 1982; Calvert and Pedersen, 1993; Caplan and Bustin, 1999, 2001; Morford et al., 2001), to Mn^{2+} escape from the water column (particularly in anoxic basins) or oxidation and precipitation of Mn oxides oxygen is encountered (Cruse and Lyons, 2004 and references herein). Due to this mobility in reducing sediments, Mn cannot be used as a redox proxy, even if negative correlations often observed with TOC.

However, due to the difference in solubility of Mn(II) and Mn (IV) species, Mn displays an active biogeochemical cycle across redox boundaries (Canfield et al., 1993), in particular Mn plays a fundamental role in transport TEs from the water column to the sediments and their uptake by hydrogenous phases (Tribovillard et al., 2006). Thus, dissolved Mn concentrations are usually relatively high in stratified water columns immediately below the chemocline (i.e., O_2–H_2S interface). This is due to the rain of particulate oxyhydroxides that are dissolved under the chemocline (encountering reducing condition) (Calvert and Pedersen, 1996). Owing to rapid settling, some fraction of particulate Mn-oxyhydroxides reaches the sediment–water interface even under anoxic water columns. The trace metals adsorbed onto Mn-oxyhydroxides are then released upon reductive dissolution of the host particles and become available for new reactions (e.g., capture in solid solutions by authigenic sulphides, such as pyrite).This process is very important for the enrichment of trace metals because the Mn (but also Fe) oxyhydroxides accelerate TEs export from the water to the sediment – water interface (e.g., Morford et al., 2005 and references therein). Mn and Fe phases take both bivalent cations (Ni^{2+}, Cu^{2+}, Zn^{2+}, Pb^{2+} and Co^{2+}) and ionic species (e.g., MoO_4^{2-}, $Cr(OH)^{2+}$ e VO^{2+}).

3.3 ANOMALIES OF TRACE ELEMENTS AND REEs

The elements analyzed with the LA – ICP – MS (CNR – Pavia) comprise trace elements analyzed with XRF and, in addition, REEs. The values of trace elements and rare earth elements for the study cases normalized to those of the Upper Continental Crust (McLennan, 2001) to understand how much the composition of the source rocks differs from the average value of the composition of the continental crust. The calculation of anomalies and their relationship with

other elements, mineralogical or organic phases allow to recognize the host phases of the elements, if they are enriched/depleted in presence of OM or detrital fraction or a particular mineralogical phase (e.g. carbonates). Anomalies have been calculated as follow:

V* = V'/radq (Sc' x Cr')

Mo* = Mo'/radq (Cr' x Ni')

U* = U'/radq (Th' x Ba')

Sr* = Sr'/radq (Pb' x Pr')

Tm* = Tm'/radq (Er' x Yb')

Ti* = Ti'/radq (Tb' x Dy')

Zr* = Zr'/radq (Nd' x Hf')

Y* = Y'/radq (Ho' x Er')

Rb* = Rb'/radq (Cs' x Th')

Eu* = Eu'/radq (Sm' x Gd')

Hf* = Hf'/radq (Zr' x Sm')

Ta* = Ta'/radq (Nb' x La')

Pb* = Pb'/radq (Ce' x Sr')

Ba* = Ba'/radq (U' x Nb')

Where «'» stands for the values normalized to the UCC value (McLennan, 2001). Basically, the anomaly is defined as the difference between the concentration of the element X compared to the two elements immediately more compatible and more incompatible. Thus, the value of the anomaly calculated with the aforementioned equations does not indicate if the anomaly is positive or negative, but how much its width is.

3.4 UNCONVENTIONAL INORGANIC REDOX PROXIES

These chapter is focused on some novel redox proxies, very useful for distinguish between the redox conditions. Unfortunately to have the concentrations of these proxies, a particular treatment of the samples with several acidification steps is needed. It is a very long procedure and it requires a special laboratory. We were not able to analyse all our samples to measure these proxies, but with a collaboration with the professor Timothy W. Lyons (University of California, Riverside – USA) and Jeremy Owens (MagLab and University of Florida, Tallahassee – USA) we were able to measure these proxies on CA1. The methodology and results are exposed in chapters 12.

Iron speciation

Iron based proxies are used to distinguish between redox conditions in the water column. The analysis aims to define highly reactive iron (Fe_{HR}) as a sum of iron in pyrite (Fe_{PY}), iron in oxides (Fe_{OX}), iron in magnetite (Fe_{MAG}) and iron in carbonates (Fe_{CARB}). All these phases should be highly reactive in presence of H_2S.

To understand how Fe behaves changing redox conditions, the relationship between the Fe_{HR}/Fe_T ratio and the Fe_{PY}/Fe_{HR} ratio (measure of the fraction of the reactive of the reactive pool that has been pyritized through exposure to H_2S) should be observed.

As shown in figure 3.2, oxic conditions occurred with Fe_{HR}/Fe_T below 0.38. Above this limit reducing conditions occurred (Poulton and Canfield, 2011). These can be divided in ferruginous and euxinic conditions by the limit in the Fe_{PY}/Fe_{HR} ratio of 0.7 (figure 3.2; Poulton and Canfield, 2011). Another parameter that point to anoxic conditions is Fe_T/Al ratio above 0.51 (± 0.1, Phanerozoic mudstones and shales value from Raiswell and Canfield, 1998 and Raiswell et al., 2008).

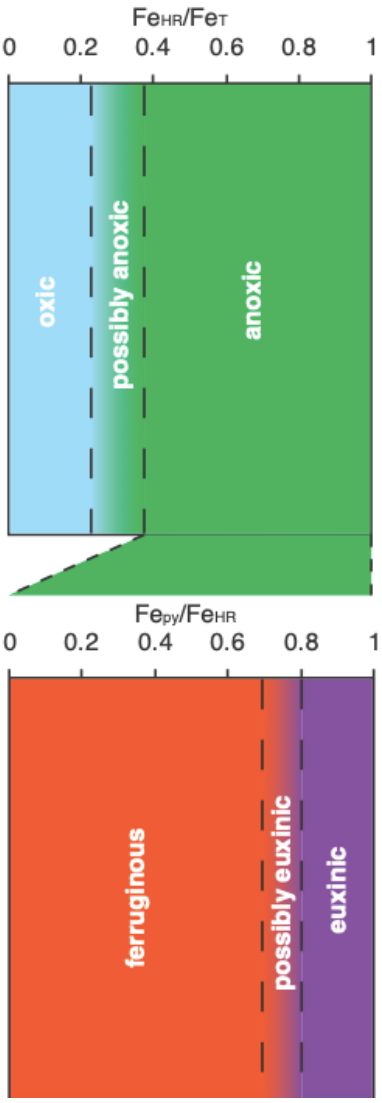

Figure 3.2 (from Poulton and Canfield, 2011): conceptualization of the iron speciation parameters for evaluation ocean redox conditions.

The ratio between Fe_{PY} and reactive iron (Fe_{REA} = Fe_{PY} + HCl soluble Fe) is called DOP (Raiswell and Berner, 1985) and is controlled by (a) Fe delivered with detrital sediments and (b) Fe present as a fraction that is decoupled from the local detrital flux. The latter represents scavenging of dissolved Fe during pyrite formation in the sulfidic water column (syngenetic pyrite). This kind of pyrite (in contrast to diagenetic pyrite formed within the sediments) yields high DOP values in addition to elevated ratios of highly reactive Fe (Fe_{HR}) to total Fe (Fe_T) and Fe_T to Al (Lyons et al. 2009). Iron enrichment occurs thanks to the export of iron remobilized from shallow oxic waters to deep basins (euxinic), where its consumption though pyrite formation is nearly quantitative (figure 3.3, from Lyons et al., 2009). In light of this, high Fe_{PY}/Fe_{HR}, Fe_{HR}/Fe_T and Fe_T/Al values can be explained only by syngenetic pyrite formation under euxinic conditions (Lyons et al., 2009). Syngenetic pyrite forms when the chemocline

lies above the sediment – water interface and consists of fine – grained, euhedral crystals and iron is its principal limiting factor (Tribovillard et al., 2006). Elevated ratios of Fe_{HR}/Fe_T and Fe_T/Al but with low degrees of pyritization finger anoxic settings that were iron-rich (ferruginous) rather than sulfidic.

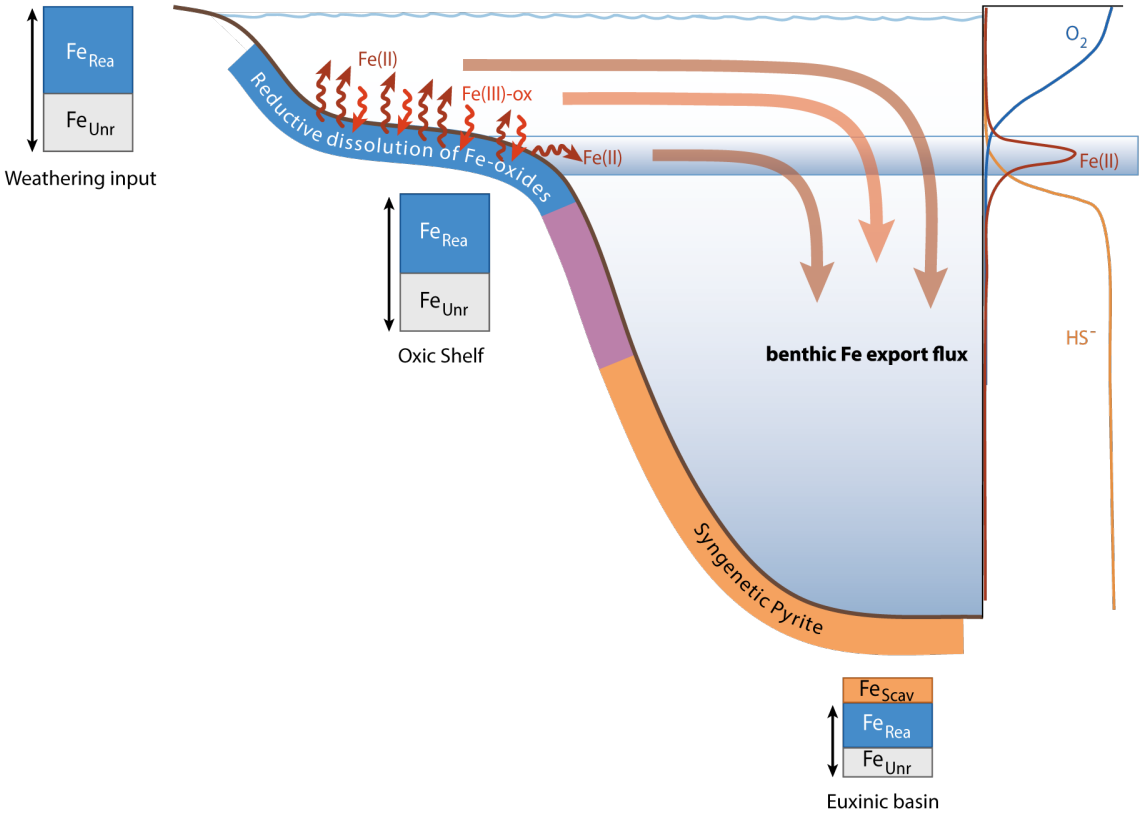

Figure 3.3 (from Lyons et al., 2009): Scheme of the shelf-to-basin shuttle that results in iron enrichment in sediments deposited under euxinic conditions. Colored shading indicates oxic deposition on the shelf (blue), high siliciclastic accumulation (or suboxic bottom waters) on the upper slope (purple), and euxinic deposition with low siliciclastic contributions in the deep part of the basin (orange). Columns depic idealized Fe speciation along a depth transect and corresponding oxic-to-euxinic redox transition. Shown are the relative proportions of detritally delivered, dominantly oxide iron with strong potential to react with H_2S (FeRea); unreactive detrital, dominantly silicate Fe (FeUnr); and additional reactive Fe that is scavenged from shuttled Fe during syngenetic pyrite formation (FeScav = FePY used in the text). (FeRea ± FeScav = FeHR as used in text.) The changing column height reflects a decreasing detrital Fe flux with increasing distance from land.

Sulfur isotopes ($\delta^{34}S$)

Also, sulfur provides a variety of both direct and indirect information about redox conditions (figure 3.4). The main sources of sulfur are sulfide- and sulfate-bearing minerals from continental rocks and emissions from volcanic/hydrothermal systems (Owens et al., 2013). The

isotopic signature of these varies between a range of 0–8‰ ($\delta^{34}S$). The main outputs of sulfur from the ocean are through the precipitation and burial of gypsum, organic-S compounds (which may be particularly important during OAEs), and pyrite in sediments (Owens et al., 2013). However, pyrite burial has a large impact on the isotopic composition of the marine sulfite reservoir.

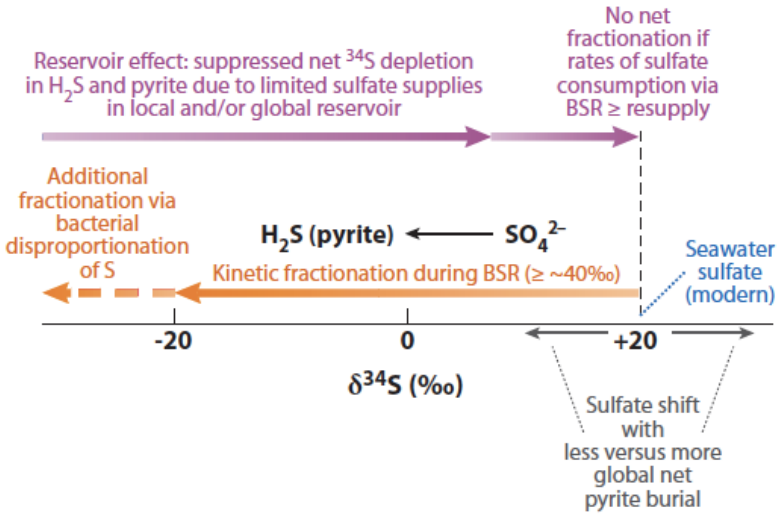

Figure 3.4 (from Lyons et al., 2009): sulfur isotope schematic highlighting the fractionations associated with bacterial sulfate reduction (and disproportionation) and the impact of reservoir properties (sulfate transport/availability) on net isotope fractionation.

Sulfate reduction can be represented by the following reaction (Lyons et al., 2009):

$$8SO_2 + 2Fe_2O_3(\text{hematite}) + 15CH_2O + 16H^+ \rightarrow 4FeS_2(\text{pyrite}) + 15CO_2 + 23H_2O$$

in which sulfate reducing bacteria (BSR) under reducing conditions consume sulfate and organic compounds forming pyrite and H_2S. It is well known that pyrite is enriched in ^{32}S (lighter isotope) relative to the sulfate, that became enriched in ^{34}S (heavier isotope). In turn, pyrite burial enriches the ocean in ^{34}S (Lyons et al., 2009). Some reservoir controls reflect the extent of diagenetic versus syngenetic pyrite formation, with the former resupply of sulfate. The rate of sedimentation and the activities of organisms in the sediments can enhance the transport of sulfate into the sediment affecting the isotopic values of pyrite because they impact the openness of the system: diagenetic pyrite can be heavier (more enriched in ^{34}S with higher $\delta^{34}S$) and more isotopically variable than syngenetic forms, although exceptions are common (Lyons et al., 2009). In general, positive shifts in sulfur isotopes point through euxinic conditions in which large amount of organic C and pyrite are buried. Meanwhile negative shifts indicate and increase into input fluxes (Owens et al., 2013).

Thallium Isotopes ($\varepsilon^{205}Tl$)

Thallium isotopes in organic matter-rich mudstones provide a novel window to secular variations in the oceanic oxygen inventory. The application of Tl isotopes as an ancient paleoceanographic tool is relatively recent and several papers illustrate its use during OAEs or under reducing conditions (Ostrander et al., 2017; Owens et al., 2017b; Them et al., 2018;

Owens, 2019). Here, we present a synthesis of Thallium as a paleoredox proxies based on literature studies. The modern open ocean seawater Tl isotope composition (residence time of ca. 20 ka) is homogenous. Thallium sources are represented by rivers, high-temperature hydrothermal fluids, volcanic emissions, mineral aerosols, and pore-water fluxes from continental margin sediments (figure 3.5 from Owens et al., 2017b).

These have Tl isotopic signature of $\varepsilon^{205}Tl \approx -2$, which reflects minimal isotope fractionation during continental weathering and high temperature mobilization of Tl. The main outputs of Tl are adsorption onto manganese (Mn) oxides and, low-temperature (<100 °C) alteration of oceanic crust (AOC), the only processes that fractionate Tl.

In particular, Mn oxides have a heavier signature compared to seawater because the isotopic fractionation during the oxidation of Tl when it sorbed to Mn oxides. While the fractionation during incorporation into AOC cause an enrichment of this in the lighter isotope. The average of the samples of AOC is close to $\varepsilon^{205}Tl \approx -7$. $\varepsilon^{205}Tl$ can be used to trace rapid global changes in Mn oxide burial due to the short residence time of Tl. It is well known that Mn oxides are buried only under oxic conditions at the sediment-water interface, while under reducing conditions these oxides are dissolved. Consequently, Mn oxides can trace the extent of bottom water anoxia, and so also Thallium isotopic composition.

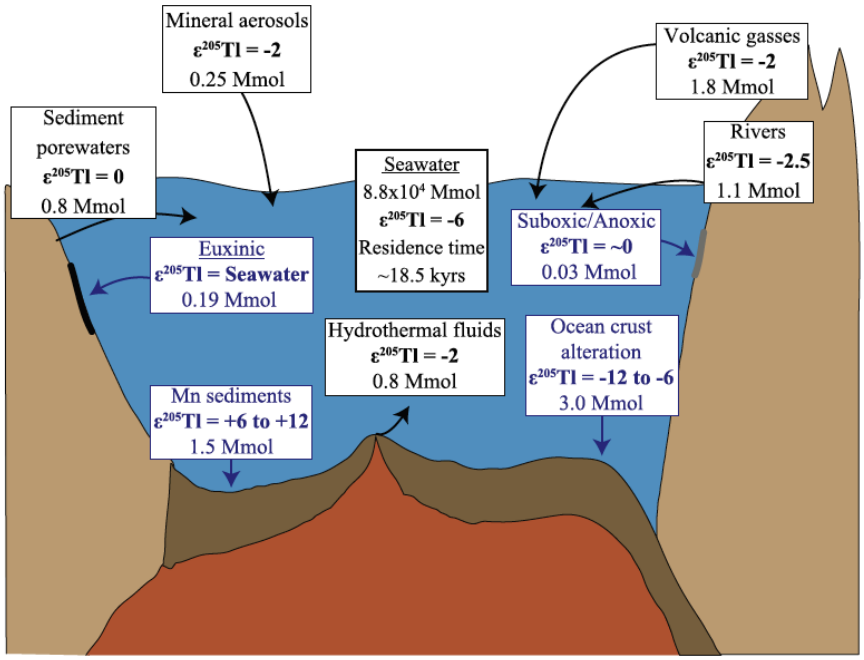

Figure 3.5: Updated mass balance modified of Thallium isotopes from Owens et al. (2017b). Purple boxes represent the output fluxes which largely dictate the Tl isotope value of seawater. All fluxes are given in mega moles per year.

CHAPTER 4

Sample typology

Mainly we were able to work on three types of samples represented in figure 4.1:

1. Cuttings: the most common samples coming from Eni's well;
2. Cores: rare samples coming from Eni's well;
3. Outcrops/surface samples: samples collected on the field.

Cuttings (figure 4.1A) represent the most common typology of samples because they are cheaper compared to the cores. In addition, cuttings are always collected during the drilling process, while cores are collected in particular cases only (e.g. on request). Usually, a cutting is a sort of coarse-grained sand that represent 5 or 10 meters of depth. In this way, you can have the average of the sampled interval in terms of element concentrations and lithology (e.g. you can't distinguish between a marl and carbonates interbedded to black shales). The main disadvantage they present is that usually they are polluted with drilling muds (mostly high content of barite, vaterite and portlandite are detected), falsifying many trace elements concentrations. Sometimes washing them with water is enough to solve the problem, other times it is not. The oil-based muds can also pollute the organic fraction of the rock leading to a falsified value of TOC and HI.
So, during the data processing is important to check if they are polluted and be careful during the data processing.

Cores (figure 4.1B) represent the ideal typology of sample but they are becoming unusual because of their cost. They do not present pollution and the sampling can be made very tight. In this way, you can also see how lithology changes along the well and how element concentrations vary in every single layer sampled. Because of their cost and the way they are collected, compared to cuttings, cores show another disadvantage: they cannot cover a long interval, usually they are long no more than a hundred meters. Vice versa, cuttings can cover the entire length of a well that can be km long.

Surface samples (figure 4.1C) represent, as the core, the ideal typology of samples because they are pollution-free. They requires much time for being collected and a carful treatment during the sample preparation. For examples, they need to be cleaned from every alteration crust that can falsify the chemical and mineralogical results, especially.

Figure 4.1: (A) cutting; (B) core; (C) surface sample.

CHAPTER 5

Methodology

Eni's target is to add more information about the source rocks to the Petroleum System Modeling (PSM) leading to a better knowledge of underground and decreasing the explorations risk. So, Eni is willing to add the geochemical study of source rocks to his routine procedures. That is why it was important for the oil company to focus on analytical techniques it already has is its laboratories (San Donato Milanese, Italy).

So, internally, it was possible to use classical analytical techniques like X-ray fluorescence (XRF), X-ray diffraction (XRD), Total Organic Carbon (TOC) and Rock-Eval analysis provided by Eni (San Donato Milanese, Italy). These allowed to use a classical approach during the data processing, e.g. looking for enrichments/depletions and/or correlations between data. This approach proved successful to the project purpose. These classical techniques are able to give us much information about the formation environment of the source rock with a reasonable expense.

However, being a research project it has been possible to use also some unconventional analytical techniques like Laser Ablation ICP – MS (CNR, Pavia), extraction of iron for iron speciation (University of California, Riverside, CA, USA), ICP – MS for thallium (MagLab, Tallahassee, FL, USA) and sulfur isotopes (University of California, Riverside, CA, USA).

The techniques requires a specialized laboratory and often they need a long and with many reaction steps samples preparation. So, the analysis are very expansive and they require long times that makes it tough to add these procedures to the daily routine of a source rock evaluation in the oil company.

Nevertheless, they presents some advantages:

- Data are clear and mostly they do not need to be interpreted;
- Mostly, they are precise and unequivocal;
- Mostly, Tl and S isotopes and iron speciation do not suffer of post depositional remobilization.

Using these techniques was an opportunity to test the results obtained with the classical approach. This was fundamental to understand that also the classical approach can give almost the same information about the source rock of these innovative proxies but in a cheaper way. Obviously, there is the need of a specialized figure that can interpret the geochemical data, that can understand the relationships between organic and inorganic parameters with a good

geochemical background on source rocks (low temperature anoxic environments). The data processing and interpretation is a heavy duty that requires a good knowledge of which processes act in the depositional environment of a source rock and how they can influence the inorganic and organic parameters.

5.1 CLASSICAL ANALYTICAL TECHNIQUES

The rock samples have been finely ground with a W-Cr mortar. Afterwards, fused beams using $Li_2B_4O_7$ and two types of pressed pellets were obtained from the powder (one for XRD and one for XRF). The latter are obtained by compressing the powder with a press (for XRF the powdered sample is mixed with wax).

Major elements were obtained by X-ray fluorescence analysis (XRF) (figure 5.1A) on fused beams (figure 5.1C), while trace elements were obtained on pressed pellets (figure 5.1D) using the same analytical technique. Mineralogy was acquired by X-ray diffraction (XRD) (figure 5.1B) on pressed pellets (figure 5.1E). The organic parameters (TOC and HI) were measured on powder using TOC and Rock Eval techniques (figure 5.2). Data were obtained at the Geolab of Eni S.p.a. in San Donato Milanese (IT). The total pattern of trace elements and REEs were analyzed through a mass spectrometer with laser ablation (LA - ICP - MS) on fused beams at CNR of Pavia. Biostratigraphic analysis were also performed for some wells at Eni S.p.a. (SPES). Therefore, for more information about each case of study refer to the internal reports of Eni Spa.

Mineralogy was carried out by X-ray Powder Diffraction (XRD) using a Panalytical Cubi'X (figure 5.1B) instrument equipped with a CuKα (λ =1.54178 Å) radiation source and a Fast detector. The data have been collected in the spectral interval $3° \leq 2\theta \leq 70°$ with steps of 0.02° 2θ and accumulation times of 10s/step. The phase identification was made by a search-match procedure comparing the position and the relative intensity of the reflections with the data contained in a reference database. The quantitative bulk analysis was carried out by means of a full-profile fitting procedures based on the Rietveld method using the SIROQUANT software. This method consists of a least-square refinement carried out until the best fit is obtained between the experimental spectrum and the one calculated from the structure data of all the crystal phases identify in the sample.
Chemistry (major and trace elements) was obtained using a Wavelength Dispersive X-Ray Fluorescence system (Panalytical Magix Pro) (figure 5.1A). Several calibration curves using

standards were carried out in order to obtain quantitative elemental analysis for both majors and trace elements. X-Ray fluorescence is particularly well suited for investigations that involve:

1. Bulk chemical analyses of major elements (i.e. Si, Ti, Al, Fe, Mg, Ca, Na, K) generally converted in the most common oxides: SiO_2, TiO_2, Al_2O_3, Fe_2O_3 or FeO, MgO, Na_2O, K_2O) and normalized to 100% taking into account also the calculated LOI (Loss Of Ignition that mainly includes CO_2 and water molecules);
2. Bulk chemical analyses of trace elements (in abundances > 1 ppm; i.e. Sc, V, Cr, Mn, Co, Ni, Cu, Zn, Ga, Ge, As, Se, Br, Rb, Sr, Y, Zr, Nb, Mo, Sb, I, Cs, Ba, REE) - the Lower Limit of Detection (LLD) for trace elements are typically on the order of a few parts per million (ppm) and, for each elements and each samples, were carried out.

The chemical data on major elements is routinely used to check the quality of the mineralogical data by XRD and then support the mineralogical model. For each trace elements measured and for each samples the Lower Limit of Detection (LLD) was calculated, and only the elements in quantity more than LLD were considered.

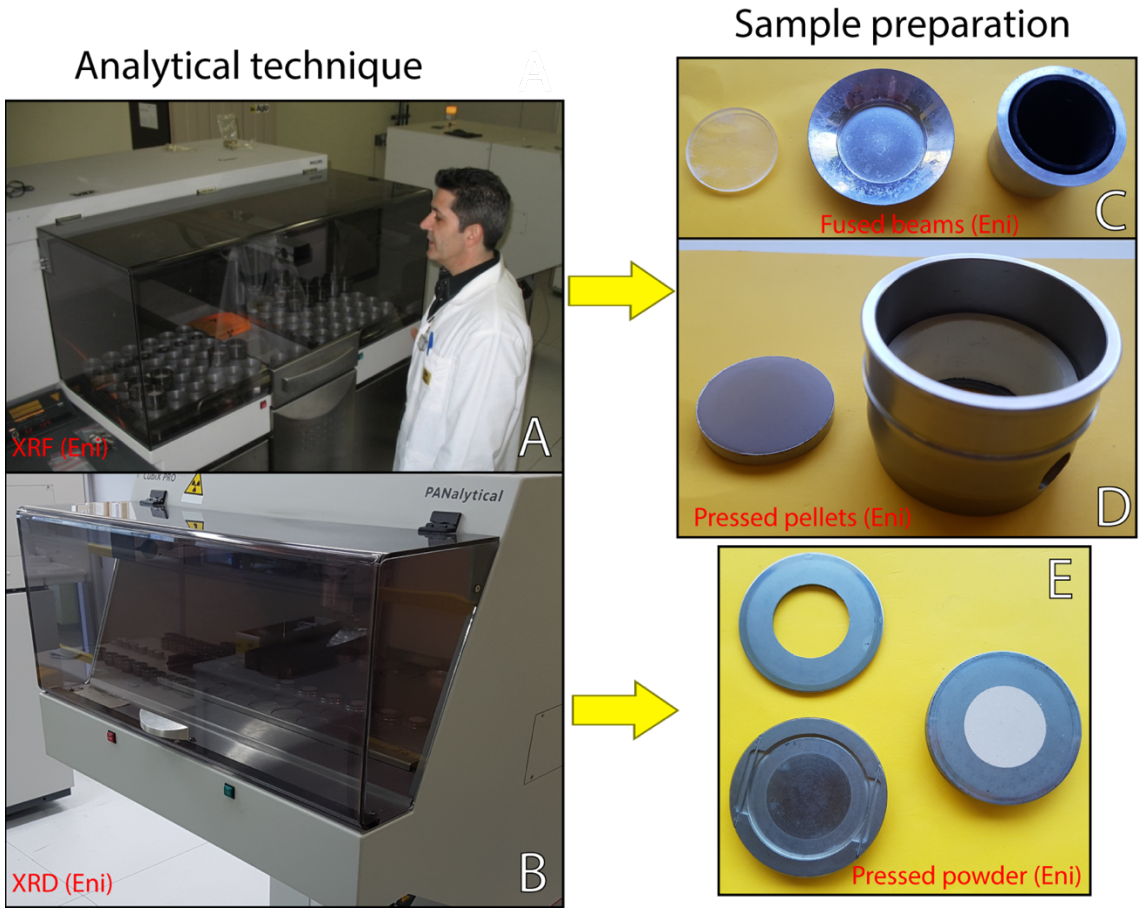

Figure 5.1: (A) X-ray fluorescence (XRF) at the Geolab (Eni) in San Donato Milanese; (B) X-ray diffraction (XRD) at the Geolab (Eni) in San Donato Milanese; (C) from the left, fused beam, platinum plate, crucible; (D) from the left, pressed pellet and sample holder for XRF; (E) pressed powder for XRD.

Total Organic Carbon (TOC) analysis were carried out using a 150-200 mg ground rock sample treated with HCl (9%) to remove carbonate minerals. The so obtained residue is washed with distilled water and the percentage of TOC in the sample is measured using a LECO CS-200 (figure 5.2A) carbon and sulphur analyzer, heating the sample at high-temperature in an oxygen stream (combustion) (figure 5.2B).

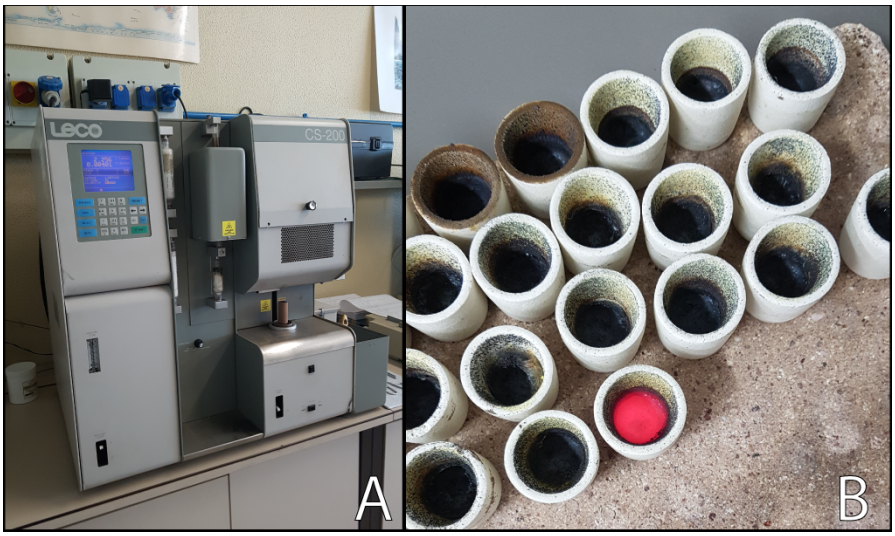

Figure 5.2: (A) LECO CS-200 for TOC analysis at Geolab (Eni) in San Donato Milanese; (B) analyzed samples in crucibles after the TOC analysis (the red one is still hot after the combustion).

Rock-Eval analysis are aimed to quantify (Kg/Ton of rock) free hydrocarbons (S1) and1hydrocarbons that can be produced by thermal cracking of the kerogen (S2), to obtain information about1the kerogen1maturity (Tmax) and quality (Hydrogen Index or HI) cross-checking TOC data (HI=S2*100/TOC).

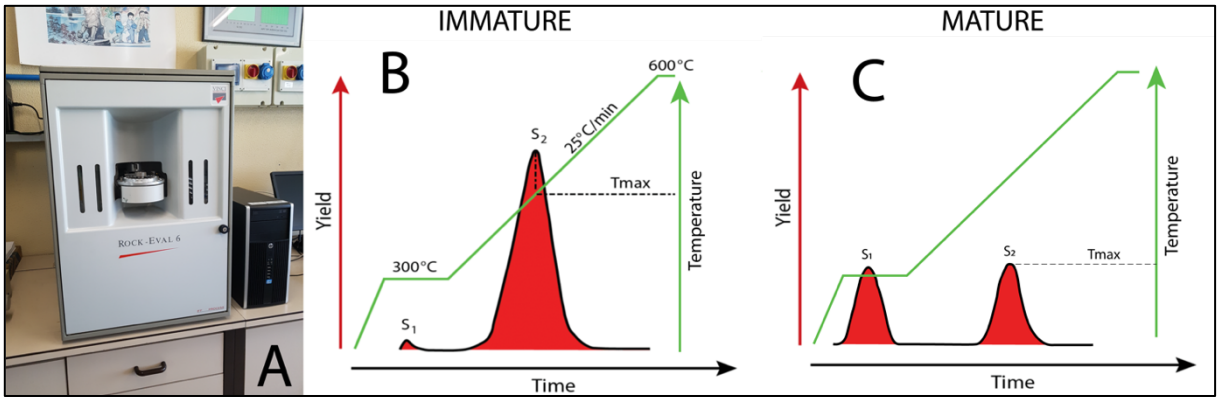

Figure 5.A: (A) Rock-Eval 6 instrument at Geolab (Eni) in San Donato Milanese; (B) Rock-Eval cycle for an immature sample; (C) Rock-Eval cycle for a mature sample.

In a Rock-Eval 6 instrument (figure 5.3A), about 70-100-mg sample of ground rock is heated in a nitrogen atmosphere at 300°C for 3 minutes followed by a programmed pyrolysis, increasing the oven temperature at 25°C/min to a final temperature of 550°C.
The Rock-Eval analytical technique has been developed by Espitalié et al. (1977). The analysis lasts 20 minutes for each sample and a cycle consists in heating the sample up to 600°C (as shown in figure 5.3B and C). With the increasing of the temperature, the thermal cracking of the kerogen progressively occurs with the generation of hydrocarbons not yet produced in a natural way by the sample. S1 represents the free hydrocarbons (mg HC/g of rock) already generated by the source rock and not yet expelled; S2 represent the residual petroleum potential (mg HC/g of rock) produced by thermal degradation of kerogen. Tmax is the temperature at which the maximum of residual petroleum potential (after kerogen pyrolysis) occurs. With the increasing of maturity S1 and Tmax increase, while S2 decreases (figure 5.3C). This is due to the fact that the free hydrocarbons (S1) are already present in a mature samples because the rock has already generated them. So the residual petroleum potential (S2) in lower than in an immature sample that have not yet generated hydrocarbons. Thus, for a mature samples, higher temperatures (Tmax) are needed to expel the hydrocarbons still present.

5.2 INNOVATIVE ANALYTICAL TECHNIQUES

Laser ablation

Laser Ablation (LA)-ICP-MS analysis were carried out at the CNR-IGG-U.O. of Pavia (Istituto di Geoscienze e Georisorse, Consiglio Nazionale delle Ricerche; figure 5.4A). The laser probe consisted of a Q-switched Nd:YAG laser, model Quantel (Brilliant), whose fundamental emission in the near-IR region (1064 nm) was converted into 266 nm wavelength using three harmonic generators (Jeffries et al. 1998). Spot diameter was typically ~ 100 μm for the samples and ~ 50 μm for the standards. The ablated material was analyzed using an Elan DRC-e quadrupole mass spectrometer. Helium was utilized as carrier gas and mixed with Ar downstream of the ablation cell. NIST SRM 610 was used as external standard, while CaO was used as internal standard. Precision and accuracy were assessed from repeated analyses of the BCR2-g and NIST612 standards and are estimated to be better than 10% at ppm concentration level. A particular sample preparation was carried out in order to minimize the analytical times, following the procedure suggested by Eggins (2003). Indeed, the fused beam discs have flat surfaces that are suitable for LA-ICP-MS analysis but, because of their large diameters (> 30 mm), could only be analyzed one at a time due to limitations of the laser ablation sample cell geometry (figure 5.4B). To enable LA-ICP-MS analysis of multiple samples following XRF

analysis, the glass discs were bonded in stacks of 5 discs using epoxy resin (figure 5.4C). These stacks were then cut with a diamond saw to expose the discs as a sandwich in cross-section (figure 5.4D) and bonded with epoxy resin to a slide for thin sections. The samples were then ground flatted using progressively finer abrasives (wet paper). The resultant flat surface was polished to be scratch-free using 0.5 µm diamond on a felt lap (figure 5.4E). The data resulting from the laser ablation analysis were then processed with Glitter (http://www.glitter-gemoc.com) in order to obtain the concentrations for the analyzed elements.

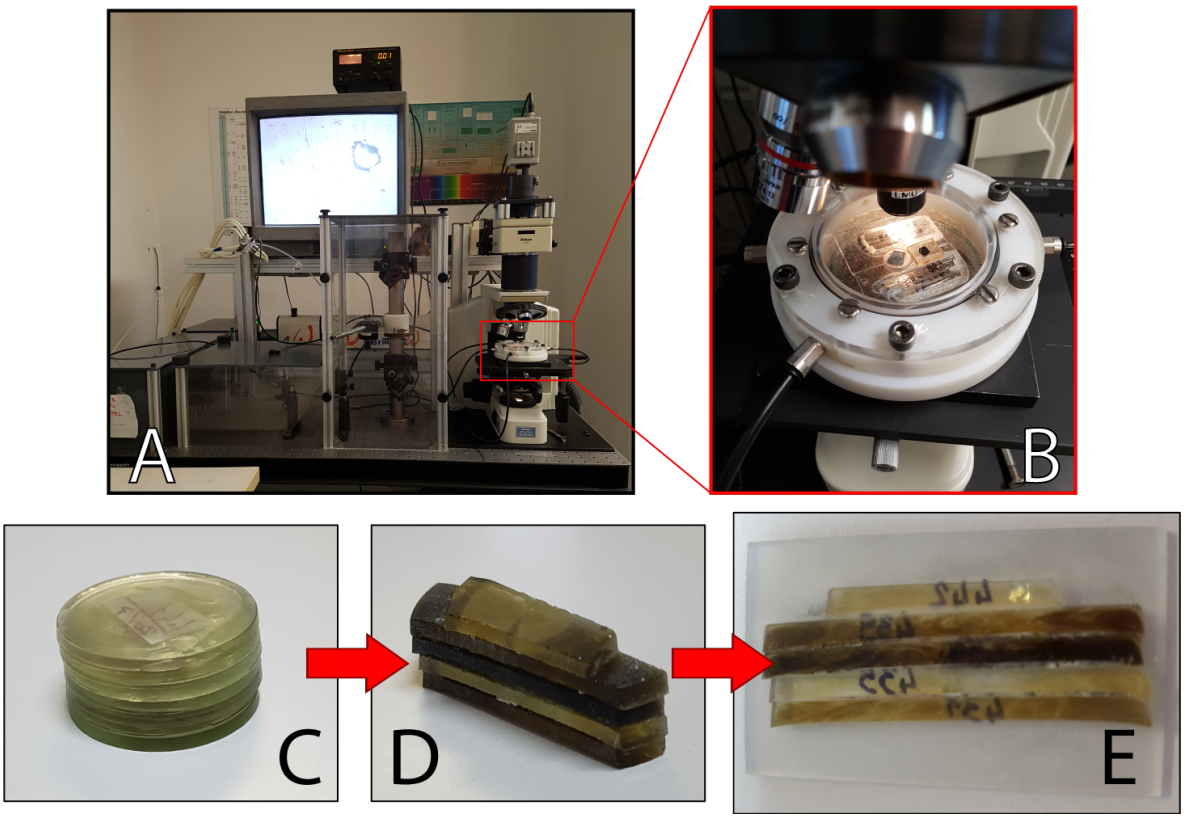

Figure 5.4: (A) Lser ablation ICP-MS at the Istituto di Geoscienze e Georisorse, Consiglio Nazionale delle Ricerche in Pavia; (B) laser ablation sample cell with the samples and standards during the analysis; (C)glass discs bonded in stacks; (D) discs in cross-section; (E) flat surface of the 5 samples bonded to a slide for thin sections.

CHAPTER 6

Data processing procedure

The goal of the project is to find univocal correlations between organic parameters and inorganic parameters that allow to trace the organic matter content and quality in source rocks. This means trying to find out correlations (negative or positive) with TOC in our study cases. To reach this target, it is necessary to focus on those elements that are related to the organic matter such as the redox – sensitive elements (RSEs). The arrangement of all the samples along a positive correlation line between the metals and TOC allow to trace the organic matter content using the concentration of the metals. When there is a variation from the general trend it is important to understand the causes, to be found often in the differences in mineralogy and/or in the phases in which the metals concentrate.

In literature, many authors tried to generalize the relationships between OM content and TEs concentrations, using TOC values as thresholds for redox conditions as shown in figure 6.1 and 6.2 (Algeo and Maynard, 2004; Tribovillard et al., 2006).

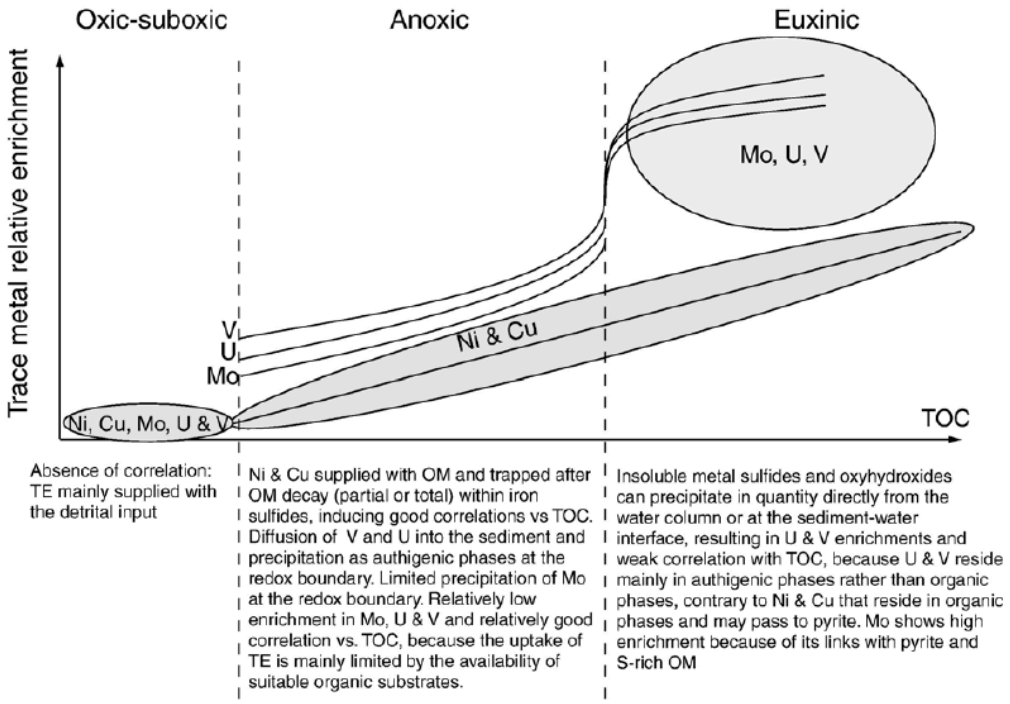

Figure 6.1 (from Tribovillard et al., 2006): Schematic diagram illustrating the relative enrichment of Ni, Cu, Mo, U and V versus total organic carbon (TOC). TE stands for trace elements and OM stands for organic matter.

The second target is also to find out if the depositional paleo-environment leads to some differences in RSEs – TOC correlations and if it is possible to distinguish between, for example, distal and proximal environments.

This means, for example, check correlations between mineralogy and major elements or between mineralogy and TOC to understand the dilution organic matter degree. For example, it is well known that usually in distal environment illite is dominant over kaolinite and vice versa in proximal environment (Parkinson, 1996).

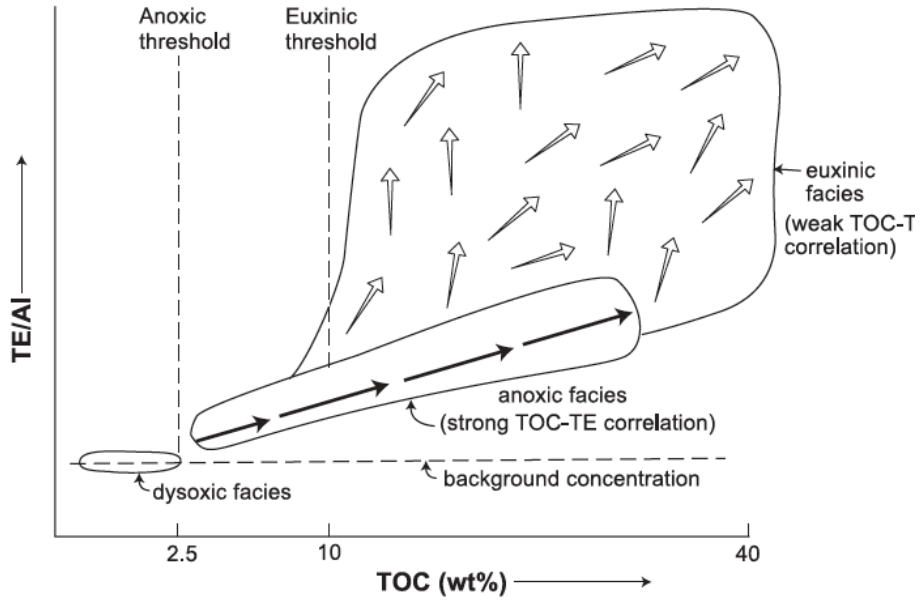

Figure 6.2 (from Algeo and Maynard, 2004): theoretical model of TE enrichment: samples characterized by low and invariant TE concentrations owing to TE residence primarily in detrital phases; samples deposited under nonsulfidic anoxic conditions exhibit modest TE enrichment and strong TOC–TE covariation owing to TE residence primarily in organic phases; and samples deposited under euxinic conditions exhibit strong TE enrichment and, at most, weak TOC–TE covariation owing to TE residence primarily in authigenic sulfide or oxyhydroxide phases.

A paper from shows that the depositional environment has some influence on TOC preservation and dilution. In particular, the author showed the relationships between sedimentation rates and TOC values (e.g. figure 6.3 for oxic environments). The author shows that with high sedimentation rate (SR) (above 35 cm/ka) there are no differences in TOC regardless of whether the sediment – water interface is anoxic or not. However, with very high SR (45 cm/s) in oxic environment a dilution occurs if carbon supply is held constant. With low SR (< 10 cm/ka) redox conditions play a fundamental role on TOC preservation. In these cases, TOC is strongly influenced by the burial efficiency, which in turn depends on redox conditions. In these environments, strong preservation is due to anoxia that could be a result of an increased carbon delivery flux and circulation regime or, with high sedimentation rates, more rapid incorporation

of sediment OM into the sediments or reduced water column oxygen levels. With low SR, dilution has a positive effect on TOC. In shelf waters, anoxia is often due to the carbon delivery flux under stratified conditions and when associated to slow SR and low dilution, very high TOC values are observed.

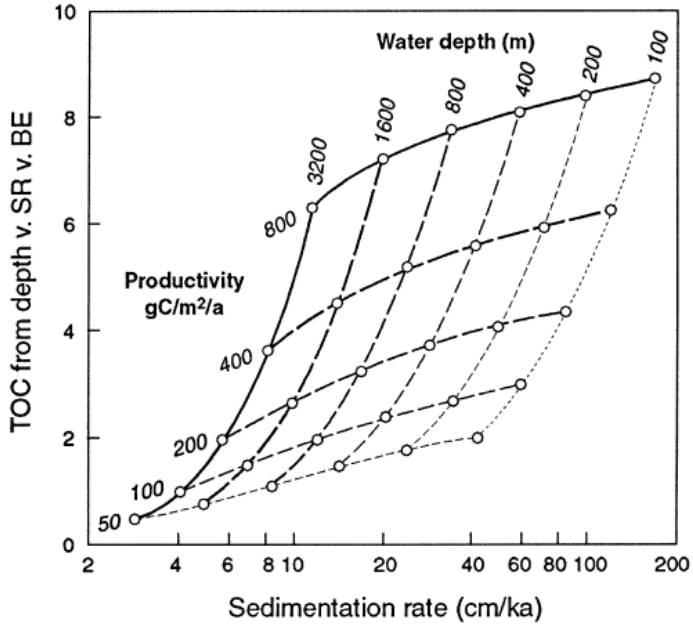

Figure 6.3 (from Tyson et al., 2001): relationship between TOC, sedimentation rate (SR), water depth and primary productivity for oxic settings. The SR here is determined by regression with depth and productivity, and is the used to derive the BE, and hence a TOC value.

Finally, the target is also to compare mature and immature source rocks to be sure that the relationships between TOC and TEs or mineralogy do not change with temperature. Only two cases of mature rock have been analyzed (NA1 and NA2). In particular, NA2 is at the beginning of the oil window but it is possible to see some differences in HI values compared to immature source rocks as explained in the relative chapter 8.3. As said above, a mature rocks shows HI (and minor TOC) values lower compared to its original values. If the RSEs values do not decrease together with HI (and TOC) but keep maintaining their values, it is possible to trace the original HI and TOC values from RSEs concentration. This also allow to make some consideration about the redox conditions under which the source rock has formed.

CHAPTER 7

Cases of study

We chose some cases of study characterized by differences in:

- Age (figure 7.1);
- Depositional environment (table 7.1);
- Samples availability: we had to consider this point in term of availability of a continuous interval and pollution;
- Possibility to compare immature and mature rocks with similar age and depositional environment.

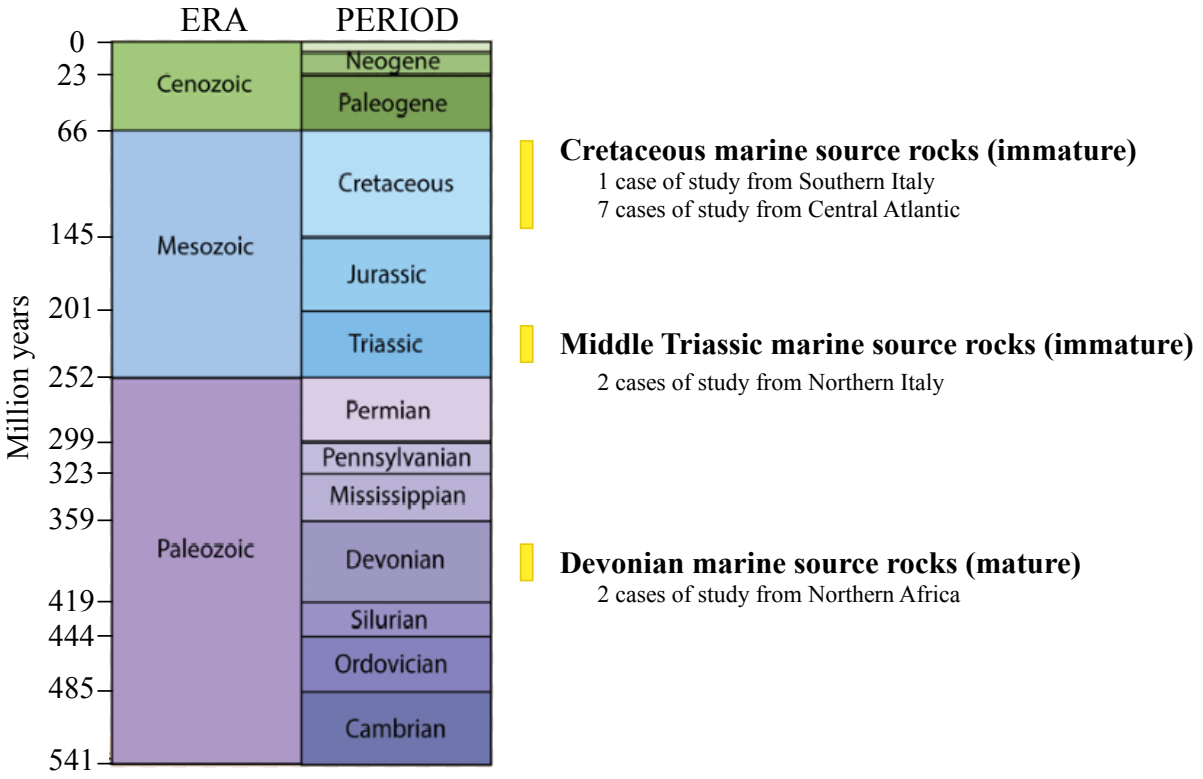

Figure 7.1: representation of the cases of study in relation with the age.

We started studying immature source rocks because TOC and HI measured on these samples are not depleted and reflect the original organic content of the rock at the depositional moment. This means that hydrocarbons have not migrated from the source rock to the reservoir and TEs concentrations in the rock should be the original ones, with the exception of post depositional re-mobilization. In fact, one of the crucial point of the comparison between mature and immature rocks was to verify if the maturation process affects our proxies. But before doing this, it is necessary to identify some robust proxy that always works with immature rocks and

then test it on mature rocks. So we selected several immature cases of study with different age and depositional environment and characterized by a mature analogue. The purpose is to compare mature and immature cases looking mainly at two aspects: (i) does the proxy change with maturity? If not, can it trace the original values of TOC and HI?; (ii) do TOC and HI change with maturity and how much?

	Proximal Environment (Shelf)	**Distal Environment (Pelagic)**	
	IMMATURE	*IMMATURE*	*MATURE*
CRETACEOUS	4 cases from Central Atlantic (CA2, CA3, CA4, CA5)	• 3 cases of study from Central Atlantic (CA1, CA6, CA7) • 1 case of study from Southern Italy (SI1)	
TRIASSIC	2 cases of study from Northern Italy (NI1, NI1)		
DEVONIAN			2 cases of study from Northern Africa (NA1, NA2)

Table 7.1: representation of the cases of study in relation with the age, maturity and depositional environment.

In table 7.1 are indicated all the cases studied in this dissertation, divided based on age, paleo-depositional environment and maturity. We will discuss immature and mature source rock separately in order to identify which geochemical proxies describe better the redox conditions during the depositional process, when it is necessary to be careful in applying some proxies and to highlight analogies and differences between source rocks having the same age, a similar depositional contest but different maturity.

During the data processing an impact of the depositional environment and age on elements concentrations and mineralogy has been observed. So, we seek to distinguish and compare the cases based on geological time and depositional environment in order to classify the proxies according to this distinction.

Specifically, this section is focused on describing the mineralogical and naphtogenic (TOC and HI) features and the depositional environment of each case of study.

7.1 CRETACEOUS MARINE SOURCE ROCKS

As shown in table 7.1.1, Cretaceous immature source rocks from the Central Atlantic are represented by CA1, CA6 and CA7 for distal environments and by CA2, CA3, CA4, CA5 for proximal environments. SI1 represents a distal immature case of study from the Tethys. The environments data are provided by Eni's biostratigraphic studies.

Name	*Thickness*	*Sample type*	*Number of samples*
CA1	1885.21 m	Cuttings	193
CA2	275 m	Cuttings	36
CA3	365 m	Cuttings	25
CA4	380 m	Cuttings	12
CA5	1995 m	Cuttings	11
CA6	792.48 m	Cuttings	156
CA7	2447 m	Cuttings and side well cores	143
SI1	41.75 m	Surface samples	39 (sampled in 2007)

Table 7.1.1: Cretaceous cases of study in relation with the location, sample type and number of samples analyzed.

CA1

CA1 is a ~1.8 km-long sedimentary section spanning from Early Aptian to Early Campanian (~115-80 Ma) drilled within a sedimentary succession in the Central Atlantic. The section is composed of 194 cutting samples collected each ~5m. The continuous recovery allowed intersecting four anoxic events namely the OAE 1c OAE 1d, OAE 2 and OAE 3, identified thank to the biostratigraphic data (provided by Eni and briefly described below).

Depositional environment

The section represents an interval of ~35 Ma in which a deepening trend is observed accordingly to the biostratigraphic data. In Aptian the section is located in a proximal marine setting consistent with the terrestrial OM input, pollen and spores. From Late Albian more a decreasing of continental organic matter, pollen and spores is observed pointing toward more open marine settings. OAE 1c and OAE 1d are intersected and recognized thanks to an abundance of amorphous organic matter and peaks in TOC and HI (within the distribution of the planktonic marker *Biticinella breggiensis* and *Ticinella* spp.). During OAE 1c the section

is located in shallow waters. The basin progressively deepens until OAE 1d, where an environment characterized by a slope and upwelling start to develop. From Cenomanian, conditions become more and more eutrophic with a pervasive occurrence of amorphous organic matter. At the boundary Cenomanian – Turonian, OAE 2 is intersected with peaks in TOC and HI and a high marine organic matter content. The Oxygen Minimum Zone (OMZ) develops under the photic zone where high production of organic matter occurred thank to the nutrient supply from riverine input and upwelling. The OAE 2 is characterized by and expansion of the OMZ and anoxia during this period is testified also by the lack of benthic fauna. During Turonian age eutrophic conditions in open marine setting still persist with presence of amorphous OM. From Coniacian – Santonian bathyal conditions are observed (deep marine environment) with eutrophication pulses in which OAE 3 is located (HI and TOC peaks). The latter is characterized by peaks in accumulation and preservation of continental OM. Finally in Early Campanian a mid – outer shelf environment is observed with a reworking of proximal material into basinal conditions (high amount of continental palynomorph and sand).

Organic content and Hydrogen Index

In most of the sediments TOC does not exceed 2 wt%, local enrichments occur ranging from ~2 to ~9 wt%, concentrated in the central part of the section. The greatest TOC enrichment occurs in a thickness of about 28m relative to Cenomanian – Turonian age, where TOC reaches values between ~5 and ~9 wt%. These levels are related to OAE2.

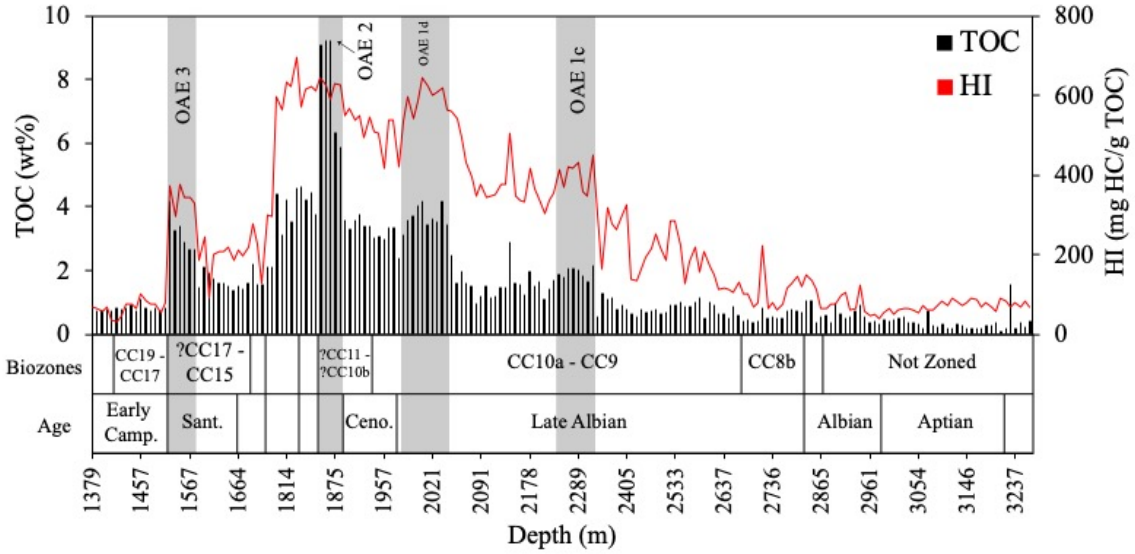

Figure 7.1.1: TOC (wt%) content, HI (mg HC/g TOC) values and biozones for CA1.

Hydrogen Index shows values from ~100 to ~600 mg HC/g TOC along the section and it mirrors TOC trend as shown in figure 7.1.1: to low values of TOC correspond low values of HI and vice versa. The only exception is represented by the values after OAE 2 (from Turonian to

Late Coniacian) in which TOC decreases while HI values remain high (~600 mg HC/g TOC). From OAE 1d to OAE 2, HI shows values higher than 400 mg HC/g TOC pointing toward a marine organic matter (algae and bacteria) with a type II kerogen.

Mineralogy

Lithological reconstructions provided by Eni based on the mineralogical content (figure 7.1.2) show that the upper part of the sedimentary record consists mainly of shales, predominantly micas and illite, interbedded with thin layers of carbonates, mostly calcite.

The central part of the section is formed by an intercalation of shales and sandstones. Moving in towards the older part of the section, the carbonaceous content increases with an intercalation

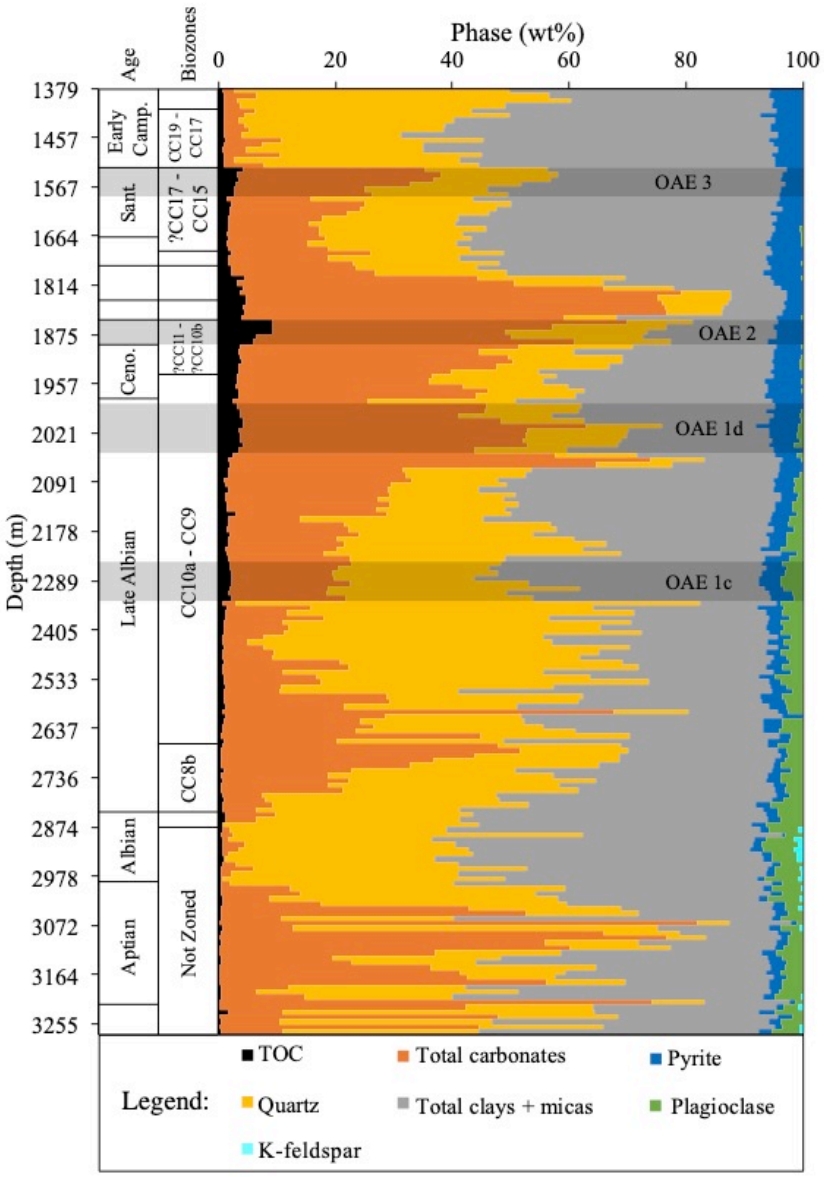

Figure 7.1.2: mineralogical (wt%) and TOC (wt%) content of CA1.

of argillaceous limestones, shales and sandstones. Despite the samples are cuttings, the advantage of this well is that it shows a few traces of pollution due to drilling processes.
The section shows that the richest samples in organic matter are also those richer in carbonates. These are related to Cenomanian – Turonian age, the carbonates values reach up to 60 wt%. On the contrary, micas and clays increase where organic matter is low (TOC <2 wt%). As for micas and clays, they are mainly muscovite and illite. Finally, pyrite increases from the bottom to the top of the section with values ranging from ~1.5 to ~6 wt%; plagioclase has concentrations of ~3 wt% from Early Aptian to OAE 1c (Late Albian) and after this it start decreasing reaching negligible values after OAE 1d.

CA2, CA3, CA4, CA5

CA2, CA3, CA4 and CA5 are wells from Central Atlantic. In table 7.1.2 are summarized: (i) thickness, (ii) age and (iii) type of samples and (iv) number of samples analyzed. Their TOC content are rarely are higher than 2.5 wt% but, based on the age, they should intersect OAE 2. For this reason they represent a good comparative example with CA1 but related to a proximal environment.

Name	*Thickness*	*Age*	*Samples type*	*Number of samples*
CA2	275 m	Turonian/Cenomanian – Lower Santonian	Cuttings	36
CA3	365 m	Late Turonian – Early Campanian	Cuttings	25
CA4	380 m	Lower Coniacian – Lower Campanian	Cuttings	12
CA5	1995 m	Albian - Danian	Cuttings	11

Table 7.1.2: CA2, CA3, CA4 and CA5 wells related to their thickness, age, sample type and number of samples analyzed.

These wells suffer of pollution due to drilling processes. For this reason it was necessary, before the data processing, to identify the polluted samples and eliminate them from our considerations. An indicator of pollution is Ba, linked to barite, a mineral added to the drilling muds.
The Post – Archean average Australian Shale (PAAS), Ba has a concentration of about 650 ppm (Taylor and McLennan, 1985). The wells, however, show that the concentrations are much

higher. This may be due to the fact that in a reducing environment Ba is much more concentrated than in an anoxic environment. However, we can observe that there are really anomalous barium values, reaching concentrations of almost 80'000 ppm. In CA2, CA3 and CA4, Ba values often exceed 10'000 ppm, indicating greater pollution of the samples. Furthermore, the correlation of Ba content with some metals, such as Cu, Mo, V, and Ni shows that where Ba peaks are present, peaks in the concentration of these metals are observed. The most obvious case is that of copper in the well of CA2.

Consequently, all samples of CA2 with values of Ba higher than 3000 ppm were eliminated from the analysis, for CA3 and CA4 the value rise to 3500 ppm. The remaining samples of CA2, CA3 and CA4 present values of the metals that do not seem to vary with Ba, so they do not seem to be polluted. For CA5, Ba average is 2266 ppm, Ba values never exceed 4600 ppm. The samples with Ba values above 3000 ppm were eliminated from the data processing. The following data is the result of this cleaning work.

Depositional environment

The paleoenvironmental history of these wells, based on biostratigraphy data provided by Eni, can be resumed as follow. The depositional environment during Albian is located in a land – locked marine basin that progressively opens towards Cenomanian. In this period there is a high fluvial discharge and abundant supply of pollen, spores and freshwater algae. OAE 2 (Cenomanian – Turonian boundary) is recorded by the absence of benthic taxa and a drop in the palynomorph groups. This is a strong eutrophication pulse characterized by high TOC values (>2 wt%), enhanced seafloor dysoxia and poor ventilation of the water – sediments interface. A late drift stage characterize Turonian until Early Senonian. This period is characterized by massive dissolution of calcareous shells. The basin opened into a middle outer shelf setting. Sedimentation is characterized by pollen and spores of continental origin, freshwater algae and enhanced fluvial discharge. Due to the volcanic activity of the Caribbean – Colombian area (~90Ma) two different alternated pulses are recorded: (i) high OM preservation and (ii) high degree of carbonate availability. In these levels TOC correlate positively with the carbonate content. High greenhouse gasses concentrations in this period led to the acidification of water masses with a shallower CCD. Moreover, an increase of precipitation and runoff is observed. In Early Senonian eutrophication pulses are recorded by peculiar assemblages of planktonic foraminifera and calcareous nannoplankton. These pulses are characterized by freshwater pulses testified by high organic matter preservation and carbonate dissolution. One of these events seems to be consistent with OAE 3 based on age

(Coniacian – Santonian transition). Late Senonian is still characterized by an active spreading rate with a moderate reprise of the tectonic activity (Campanian) consistent with the opening of the Southern Central Atlantic. Enhanced sediment erosion and runoff are recorded. The location is compatible with an outer shelf – upper slope depositional environment with still eutrophic and reducing conditions. Finally, Maastrichtian is characterized by an oceanization stage in which the basin has opened and become fully marine and more distal from coastline. Carbonate dissolution is observed due to connection with polar waters that are more prone to carbonate dissolution.

Organic content and Hydrogen Index

CA2, CA3, CA4 and CA5 are very similar regarding the TOC content (figure 7.1.3). This shows constant values in the wells with an average of1.87 wt% for CA2, 1.68 wt% for CA3, 1.57 wt% for CA4, 1.22 wt% for CA5. In CA2 and CA3 TOC peaks do not correspond to OAE 2 while in CA4, OAE 2 is related to the highest TOC values in the section (~1.75 wt%). Generally, HI mirrors TOC values even if for similar TOC values not always correspond similar HI values. This could be due to the HI calculation: HI is the result of (S2/TOC) x 100 in which S2 is the amount of hydrocarbons generated through thermal cracking of nonvolatile organic matter in mg/g of rock and TOC is total organic carbon in wt%. S2 could be the very different even if the organic content is similar between two samples: S2 in fact is a parameter that depends on the organic matter typology. In the cases of study HI rarely exceeds 300 mg HC/g TOC indicating that the organic matter is mainly marine (algae and bacteria). HI is also linked to the depositional environment: with HI values <200 mg HC/g TOC the organic matter is generally related to coastal plains, deltaic and turbiditic environments (the principal biomass is lignin) pointing toward a proximal environments with terrestrial and detrital inputs from, for example, rivers.

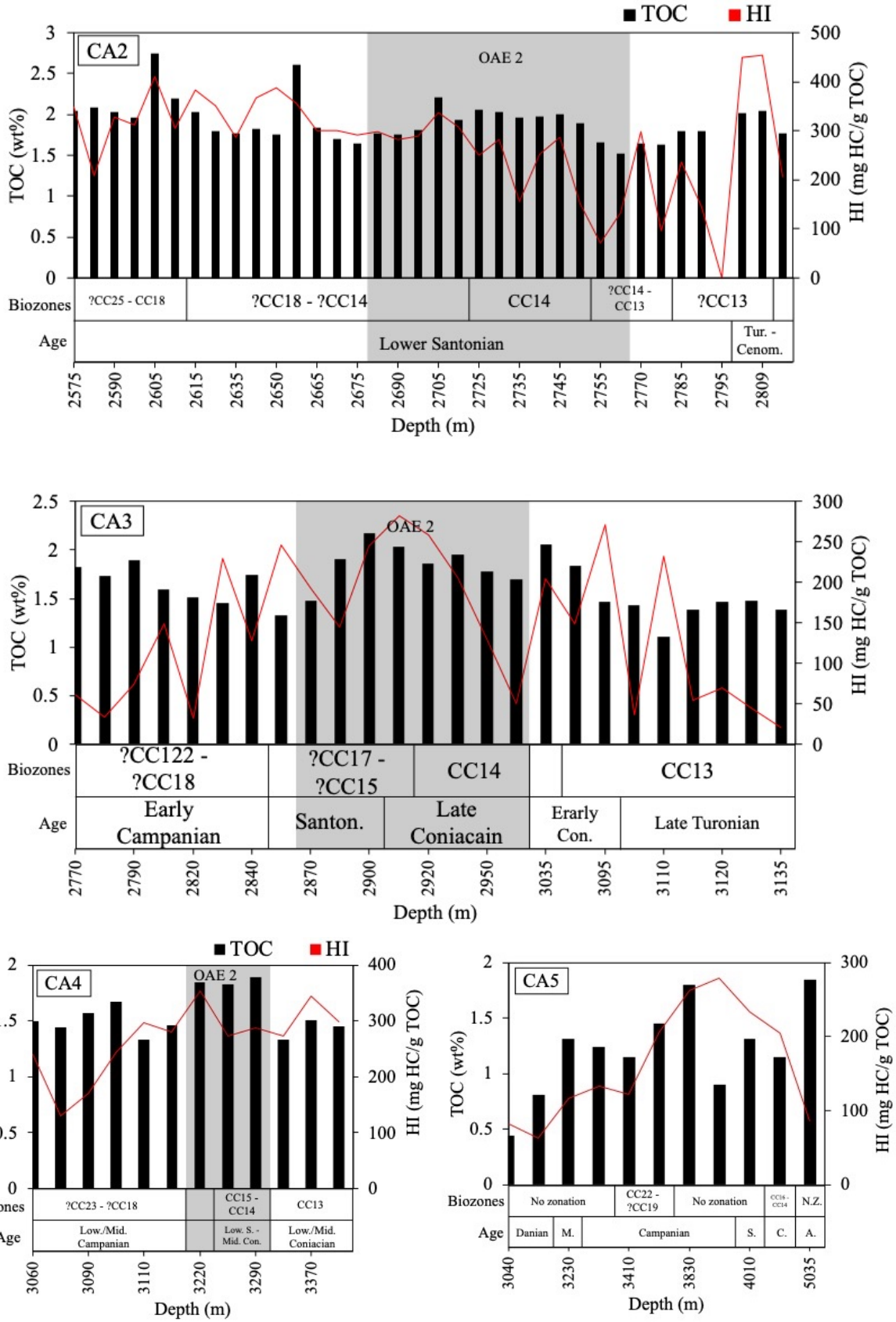

Figure 7.1.3: TOC (wt%) content, HI (mg HC/g TOC) values and biozones for CA2, CA3, CA4, CA5.

Mineralogy

CA2, CA3 and CA4 wells are very similar to each other in mineralogy (figure 7.1.4). The samples are shales, with carbonate content (mainly calcite and siderite) rarely higher than 20 wt%. Micas and clays are mainly muscovite and kaolinite. The content in pyrite is constant in all the wells and varies between a minimum of ~2 and a maximum of ~7 wt%. Finally, as regards the contaminants, they are mainly barite and halite and generally they do not exceed 2 wt%.

From the mineralogical point of view (figure 7.1.4), CA5 is composed mainly by shales, very poor in carbonates that do not exceed 8 wt%, except for the sample relating to the Albian where the carbonates (mainly calcite) reach ~36 wt%. Micas and clays are mainly muscovite and kaolinite which together with chlorite have values around ~45-50 wt%. Pyrite content is around ~7 wt%. Finally, as regards the contaminants, they include barite, halite, C4AF and gypsum and generally they do not exceed 2 wt%.

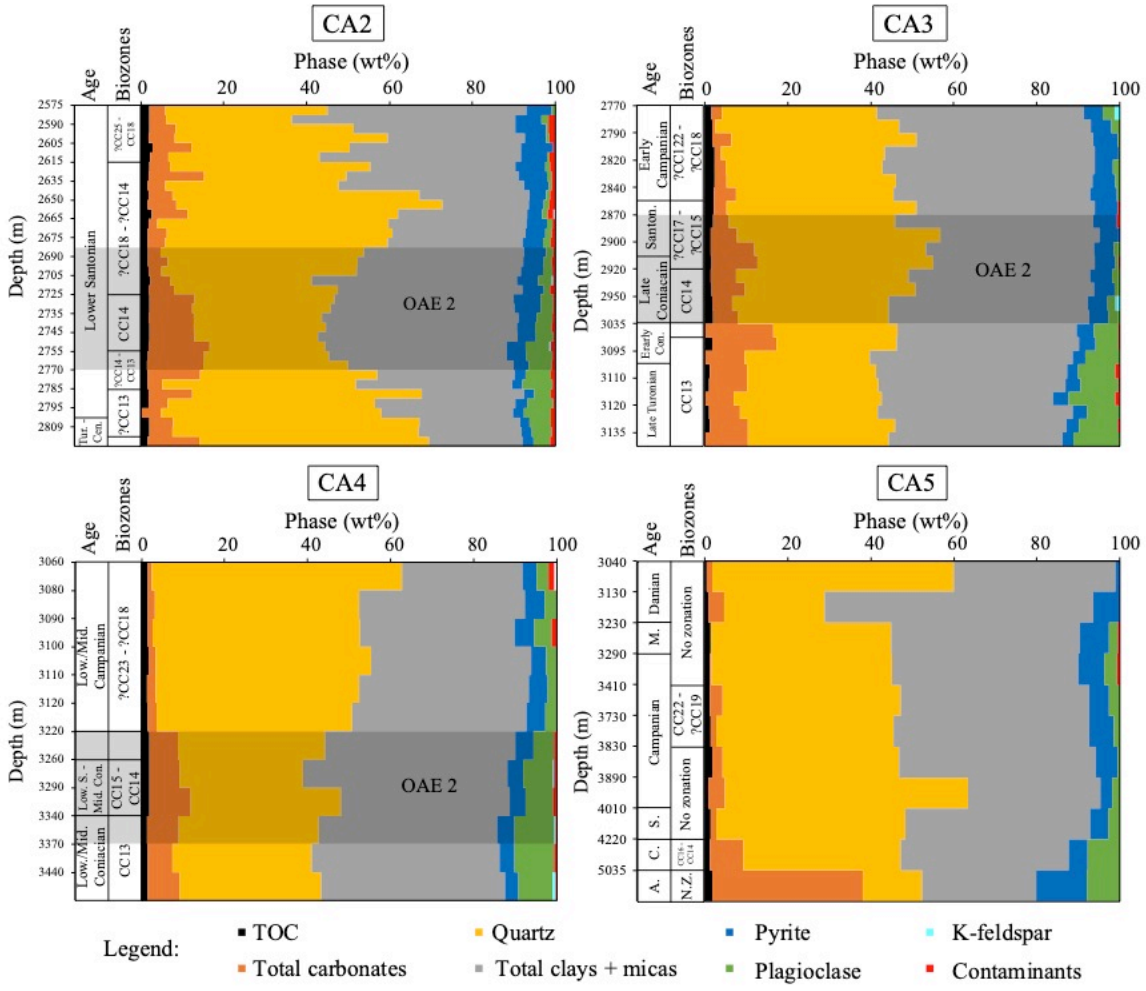

Figure 7.1.4: mineralogical (wt%9 and TOC (wt%) content for CA2, CA3, CA4, CA5.

CA6

CA6 is a ~800 m-long sedimentary section of Late Albian – Late Santonian age (~103-83 Ma) drilled within a sedimentary succession in the Central Atlantic. The section is composed of 156 cutting samples. Biostratigraphic data are not available for this well, not allowing to define a paleoenvironmental history. However, based on its geochemical features are similar to those of CA1 (distal environment) we can suggest a similar paleoenvironmental history.

Organic content and Hydrogen Index

TOC content in CA6 ranges between a minimum of 0.55 wt% and a maximum of 5.44 wt% with an average of ~2.5 wt%, as shown in figure 7.1.5. TOC shows 3 main peaks:

- 3310.12m depth: TOC reaches 5.44 wt%;
- 3304.95m depth: TOC reaches 3.60 wt%;
- 2983.99m depth: TOC reaches 3.81 wt%.

Along the section, HI varies between 44.85 and 536.45 mg HC/g TOC, with an average of ~322.65 mg HC/g TOC. Mostly, HI mirrors TOC trend, especially from the top of the section to ~3060m depth. Under this depth, to lower values of TOC (~2 wt%) correspond higher values of HI (~ 400 mg HC/g TOC). To the peak of TOC of 5.44 wt% at 3310.12m is not related a peak in HI, that reaches its maximum (536.45 mg HC/g TOC) slightly above this depth.

From the bottom of the section to ~3060m depth HI has an average of ~400 mg HC/g TOC pointing towards a marine environment with marine organic matter (algae and bacteria). From ~3060m to the top of the section, HI shows 2 peaks (~400 mg HC/g TOC) related to TOC peaks and then decreases reaching values even <100 mg HC/g TOC indicating a decreasing in TOC but also an increase of terrestrial organic matter (lignin).

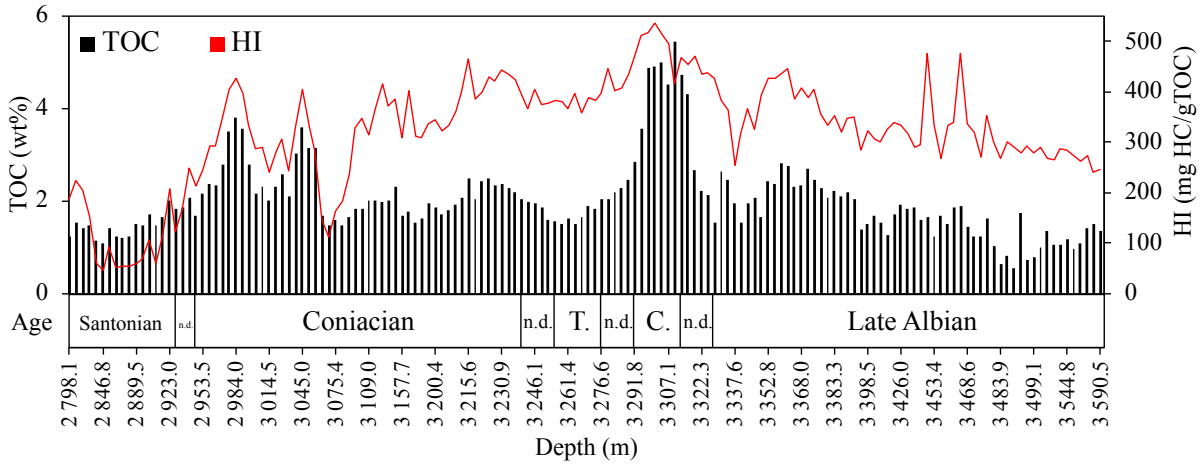

Figure 7.1.5: TOC (wt%) content and HI (mg HC/g TOC) values for CA6.

Mineralogy

CA6 (figure 7.1.6) is composed mainly by shales except in the lower part of the section where there in an increase of the carbonates content and plagioclase reaching ~60 wt% and ~24.5 wt% respectively. Quartz is very abundant along the entire section, especially in the central and upper part where it reaches ~80.5 wt%. TOC content has an average of ~2 wt% and shows two peaks, one of Cenomanian age and one of Coniacian age, in which it increases reaching a maximum of ~5.5 wt%. These two peaks are probably related to OAE1d and OAE2

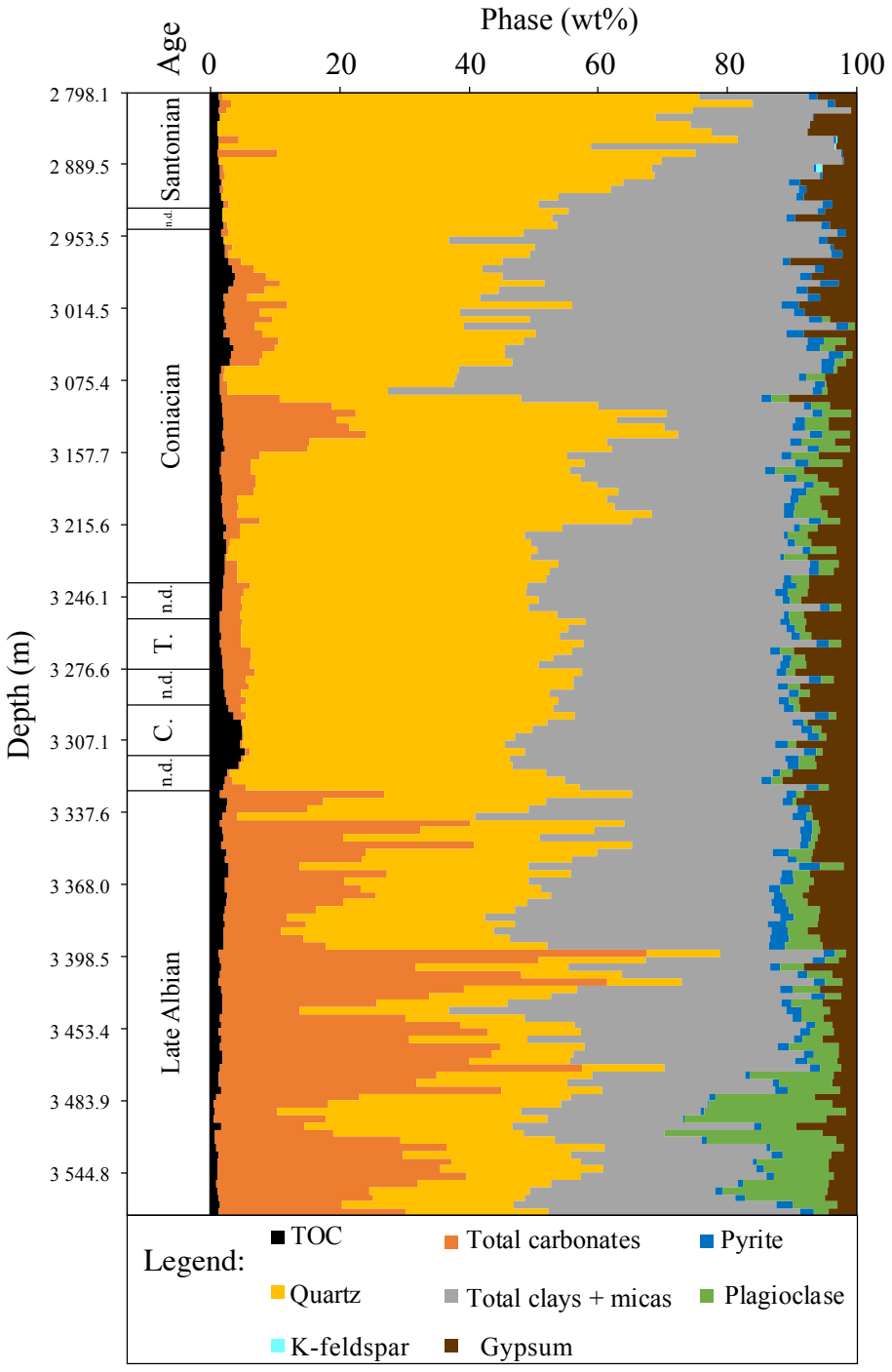

Figure 7.1.6: mineralogical (wt%) and TOC (wt%) content for CA6.

(Cenomanian) and OAE3 (Coniacian). Contrary to CA1, TOC does not show correlations (positive or negative) with any mineralogical phase. Pyrite content is low in the lower part of the section, where the carbonate content is higher. The average of pyrite content along the section is ~1.5 wt%. Vaterite is due to pollution and its content is pretty stable along the entire section with an average of ~5.0 wt%. There are no biostratigraphic data available for this section. Despite this, knowing the location of the well we can associate a story similar to that of CA1 in which a deepening of the section is observed. This is consistent with the mineralogy: the carbonate content decreases from the bottom to the top of the section indicating, maybe, an approaching to the CCD.

CA7

CA7 is a ~2.4 km-long well of Barremian – Ypresian age (~129 – 49 Ma) from Central Atlantic. It is divided in two section: the oldest is of Barremian – Aptian age and it is ~800 m-long, the youngest is of Upper Albian – Ypresian age and it is ~500 m-long. There is a lack of data between the two portion of the well of ~350 m relative to Albian. The data are very fragmented: first of all the samples are both cuttings and side well cores (as indicated in figure 7.1.8), secondly the chemical data have been acquired only for the source rock levels. Moreover, the naphtogenic parameters have been acquired for the source rock levels but not for all the samples. Finally, the geological reconstruction have been made just for the Barremian – Aptian portion of the well. CA7 is characterized by two source rocks horizons, the first one is from Cenomanian to Upper Coniacian, the second one is deeper and it of Barremian age (figures 7.1.7 and 7.1.8).

Depositional environment

The depositional environment and geological evolution of CA7 has been provided for the lower part of the section, from Barremian to Aptian. CA7 is located in the Central Atlantic Ocean and its depositional basin developed during the opening of the Central Atlantic Ocean. The evolution of the depositional environment is given by Eni. We can summarize here some main phases:

1. The pre-rift phase (Late Jurassic) is characterized by the development of subsiding basins that were filled by fluvio-lacustrine sediments;
2. The rift phase (Neocomian) is characterizes by extension with the formation of extensional faults and grabens;

3. The sag phase (Barremian to lowermost Aptian) is characterized by the filling of the grabens, in a period of attenuated extension and deactivation of the normal faults. In this interval the Source Level 2 (figure 7.1.7) is deposited.

Organic content and Hydrogen Index

Organic parameters have been acquired just for some samples along the section, and in particular in the source rock levels as shown in figure 7.1.7. In the Source Level 2 (Barremian) TOC has constant values with an average of 0.67 wt% and HI mirrors TOC trend with an average value of 184.80 mg HC/g TOC. In the Source Level 1 (Cenomanian – Coniacian) TOC reaches a value of ~8 wt% then decreases with an average value of13.06 wt%. Again, HI follow TOC trend but with values between 56 and 495.20 mg HC/g TOC (average of 301.59 mg HC/g TOC). In these level HI point toward a marine environment with marine organic matter (algae and bacteria) and kerogen type of II – III.

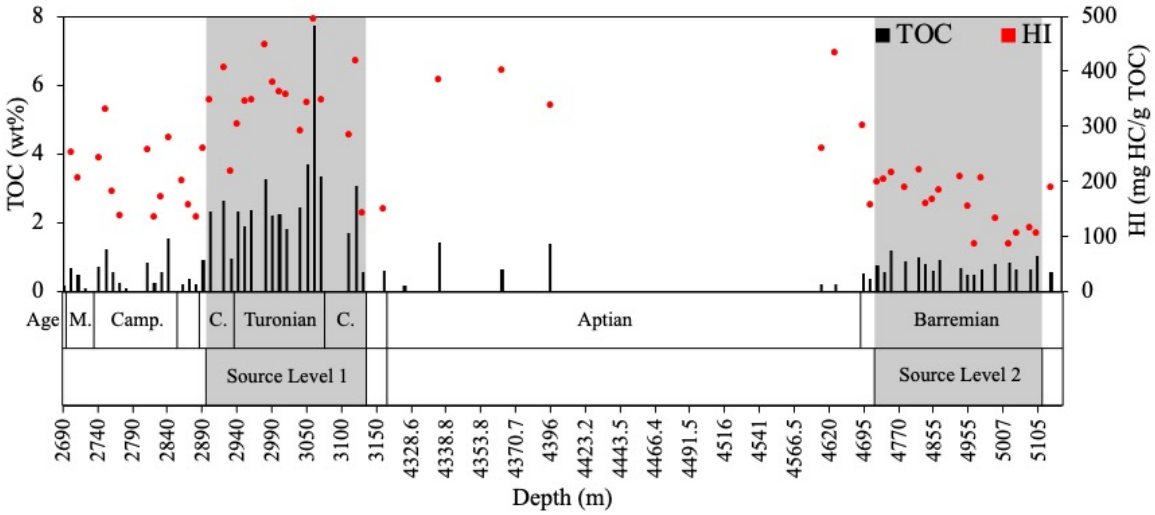

Figure 7.1.7: TOC (wt%) content, HI (mg HC/g TOC) values for CA7.

Mineralogy

The mineralogical content of CA7 is represented in figure 7.1.8. The source rock levels are very similar in fact of mineralogical content: they are rich in micas and clays (average of ~20 wt %) and carbonates (from a minimum of ~15 to a maximum of ~60 wt%). Moreover, these levels are richer also in Plagioclase and K-feldspar that are present only in the source rocks level and the upper part of the section with an average of ~4 and ~2.5 wt%, respectively. In the source rock levels and the upper part of the section are present also halite, hematite, clinoptilolite, cristobalite, fluorite, gypsum and barite. Especially, the latter is related to pollution due to drilling processes and it is present mainly in the younger source rock level (Cenomanian –

Coniacian). The presence of these phases is probably due to the fact that the samples are cuttings, more affected to pollution that the side well cores. Quartz content is quite constant along the section with an average of ~12 wt%. The central portion of the well is sterile and it is composed mainly by carbonates (average of ~85 wt%) and quartz.

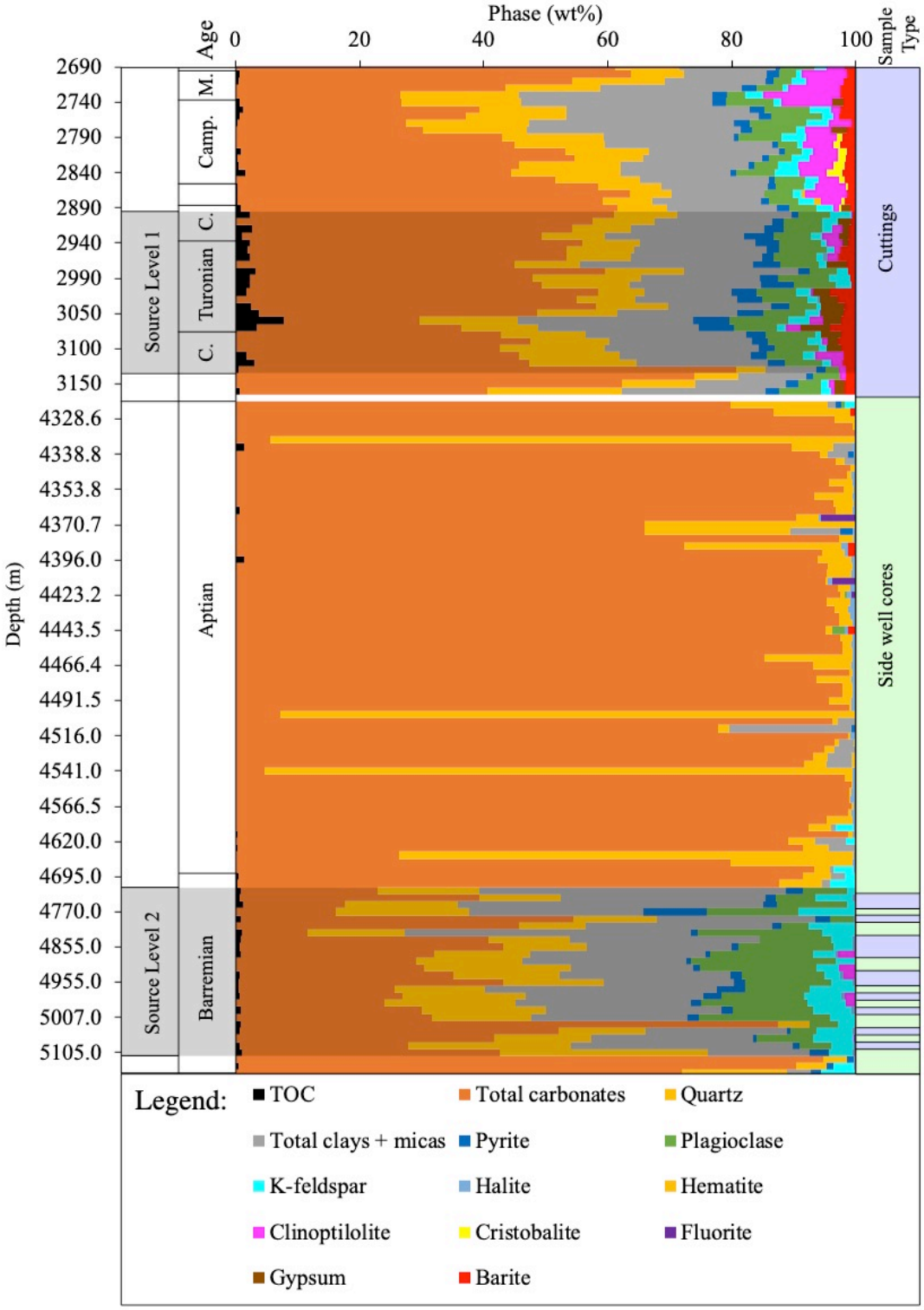

Figure 7.1.8: mineralogical (wt%) and TOC (wt%) content for CA7.

SI1

The section of SI1 has been studied previously by Sabato et al. (2007) that analyzed the organic features and biostratigraphy. The section covers an age that goes from Lower Albian to Turonian (~ 100 – 90 Ma) and includes the sediments deposited previously, during and subsequently to an Anoxic Event equivalent to the Bonarelli Level (also called OAE 2; Schlanger and Jenkyns 1976). In the samples that precede the Bonarelli Horizon (from Lower Albian to Lower Cenomanian) there is a gap of samples relating the Late Albian up to the beginning of the Cenomanian due to a vegetation cover of 15m. We analyzed 39 samples selected for the collection of Sabato et al. (2007) from this section as shown in figures 7.1.9 and 7.1.10. In particular, we analyzed the mineralogical content and major and trace elements, while the organic geochemistry (TOC and HI values) is from Sabato et al. (2007).

Depositional environment

Due to the lack of carbonates along the entire section, the depositional environment of SI1 has been related by Sabato et al. (2007) to a deep basin, under the CCD. In addition, Bonacina et al. (2020) studied the inorganic geochemical features of the section, in comparison with other Italian sections that intersect the Bonarelli Level (e.g. Bottaccione and Calabianca sections; Scopelliti et al., 2004, 2006). The authors suggest that the depositional environment of SI1 is a deep distal basin in which a fluctuation of the redox conditions occurred. In particular, the OM-rich layers (black shales) deposited under euxinic conditions, in a period of stagnant conditions, while the radiolarites, less rich in OM, deposited under suboxic-anoxic conditions in a period of enhanced bottom water currents activity. This is suggested by the mineralogical composition and by the variations in Ti, Ti/Al, K/Al and Rb/Al ratios.

Organic content and Hydrogen Index

The organic characteristic of the Fontana Valloneto section have been already discussed by Sabato et al. (2007), where can be found an in-depth discussion of the data. Here, we used the TOC values collected by Sabato et al. (2007), that are represented in figure 7.1.9 together with the mineralogy. HI values has been calculated only for the sample with TOC > 0.5 wt% with an average value of ~441 mg HC/g TOC. The black shales in the Bonarelli Horizon have high TOC content (>10 wt%) and the values from Rock – Eval pyrolysis suggest that these rocks are "immature", thus having HI and TOC comparable to the original values. Some samples from other lithofacies (i.e., dark siliceous claystone and black siliceous mudstone – samples SI1/23A, SI1/29B, SI1/31B and SI1/36A) from the Bonarelli Horizon have high organic matter content

(TOC between 1 and 10 wt%). The Bonarelli Horizon – equivalent is characterized by a large amount of organic matter for the black shales (the maximum is 29.19 wt%).

Prior to and after the Bonarelli Horizon, TOC never exceeds 0.5 wt%, except for the samples SI1/13A that represents a local anoxic event (AE1).

HI is always above 500 mg HC/g TOC for the samples with TOC > 1 wt% indicating a marine source of the organic matter (mainly algae and bacteria).

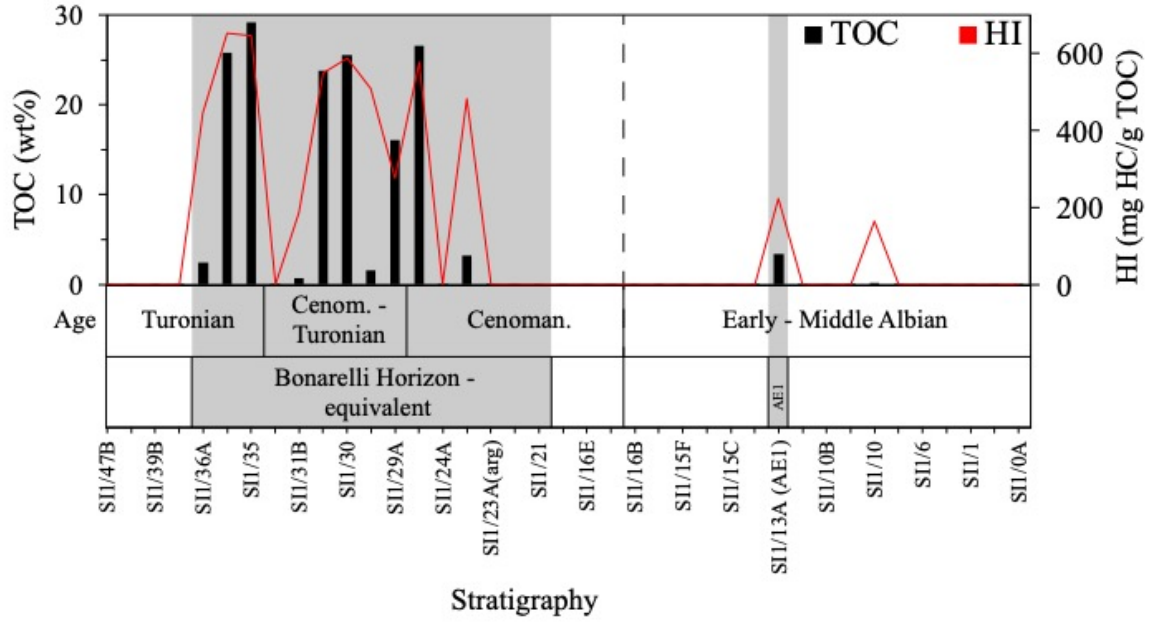

Figure 7.1.9: TOC (wt%) content, HI (mg HC/g TOC) values for SI1.

Mineralogy

The mineralogical composition of the selected samples is shown in figure 7.1.10. Along the entire section the mineralogy is rather homogeneous: the quartz content is about 50 wt% (in the Cenomanian it reaches almost 90 wt%), micas and clays are about 35 wt% and the other minerals (Fe oxy – hydroxides, gypsum, fluorapatite, pyrite, plagioclase) do not exceed ~15 wt%.

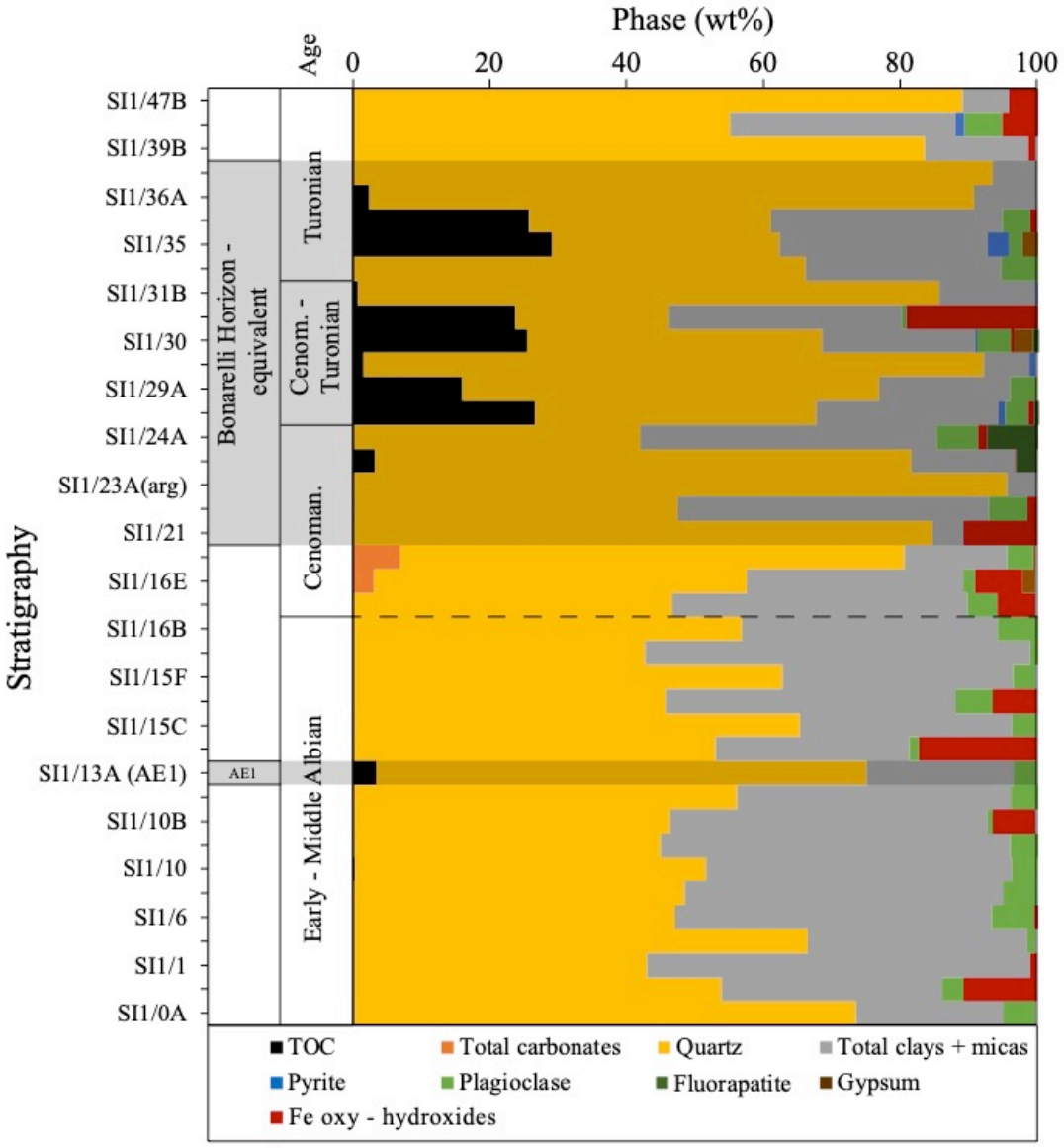

Figure 7.1.10: mineralogical (wt%) and TOC (wt%) content for SI1.

7.2. MIDDLE TRIASSIC MARINE SOURCE ROCKS

As shown in table 7.2.1, Middle Triassic immature rocks are represented by NI1 and NI2 (figure 7.1). Both are immature and are related to an intraplatform basins with restricted circulation. The samples for both NI1 and NI2 have been collected on the field by Eni.

Name	*Stratigraphy*	*Age*	*Samples type*	*Number of samples*
NI1	From sample NI1/1 to NI1/50	Ladinian	Surface samples	49
NI2	From sample NI2/0 to NI0/11	Anisian - Ladinian	Surface samples	9

Table 7.2.1: stratigraphy, age, sample type and number of samples analyzed for NI1 and NI2.

NI1

In NI1 the main lithofacies observed are limestones, grey and dark grey laminated limestones and marlstones.

Organic content and Hydrogen Index

Naphtogenic parameters in NI1 are shown in figure 7.2.1. TOC in NI1 shows very variable contents: at the base of the stratigraphy (from sample NI1/1 to NI1/5, except for sample NI1/2C) TOC reaches its maximum value of 6.71 wt%. From the sample NI1/6, the organic content decreases to ~1 wt%. TOC increases again between the sample NI1/15 and NI1/27 with values between 0.24 and 4.02 wt%. Upwards, TOC shows constant values with an average of 0.49 wt%. A last peak is observed in the samples NI1/48 with a value of 2.37 wt%. HI follow the TOC but the highest values is observed in the sample NI1/48 where it reaches 639.66 mg HC/g TOC. In the rest of the section HI shows values between 102.86 and 591.04 mg HC/g TOC, with an average of 336.60 mg HC/g TOC. HI indicate a marine environment with a kerogen type of II-III. Organic matter is concentrated mainly in the marlstone that constitute thin intercalations (rarely more than 10cm-thick) and minor into laminated limestones.

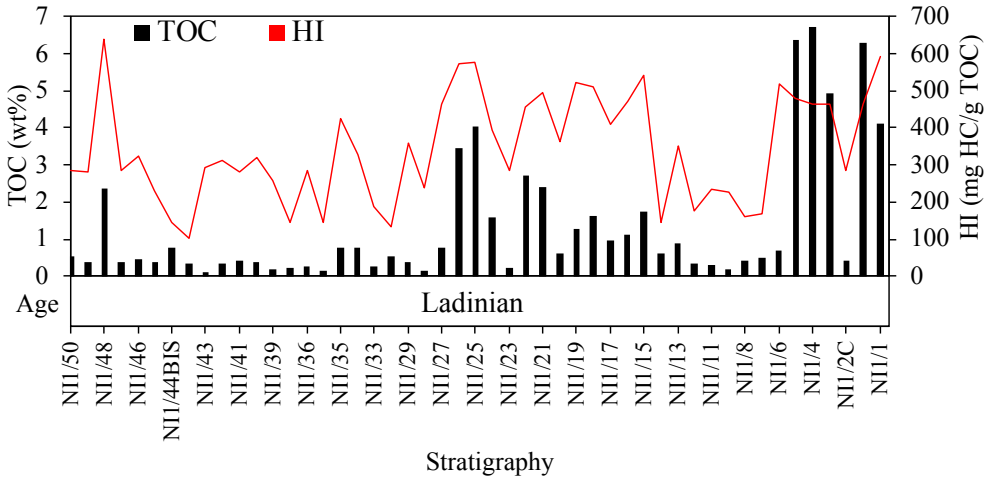

Figure 7.2.1: TOC (wt%) content, HI (mg HC/g TOC) values for NI1.

Mineralogy

NI1 (figure 7.2.2) is mainly composed of carbonates (mainly calcite) which reach up 98 wt%. Samples with higher contents of micas and clays are also those with higher contents of organic matter. These are at the base of the NI1 stratigraphy and TOC reaches values of about 7 wt%. TOC decreases going upward in the section, reaching values lower than 1 wt%.

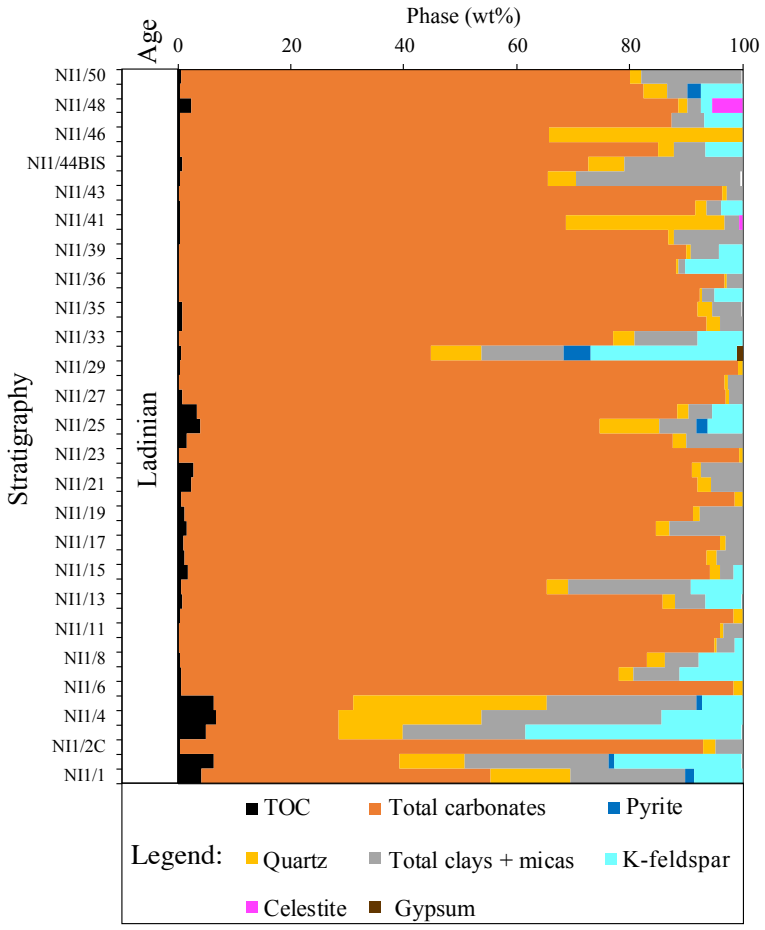

Figure 7.2.2: mineralogical (wt%) and TOC (wt%) content for NI1.

NI2

In NI2 the main lithofacies observed are grey and dark grey laminated limestones, marlstones and black shales.

Organic content and Hydrogen Index

TOC content is very high in NI2, in fact the average values is 21.21 wt% (figure 7.2.3). Only the sample NI2/11 show a low value of TOC (1.08 wt%) in contrast with a high values of HI, the highest of the section (392.85 mg HC/g TOC) as shown in figure 7.2.3. The other samples shows a HI values of ~400 mg HC/g TOC. HI values point toward a marine environment with the deposition of marine organic matter (algae and bacteria) and a kerogen type II S (the samples are S rich). Organic matter is concentrated mainly in marlstones and black shales levels.

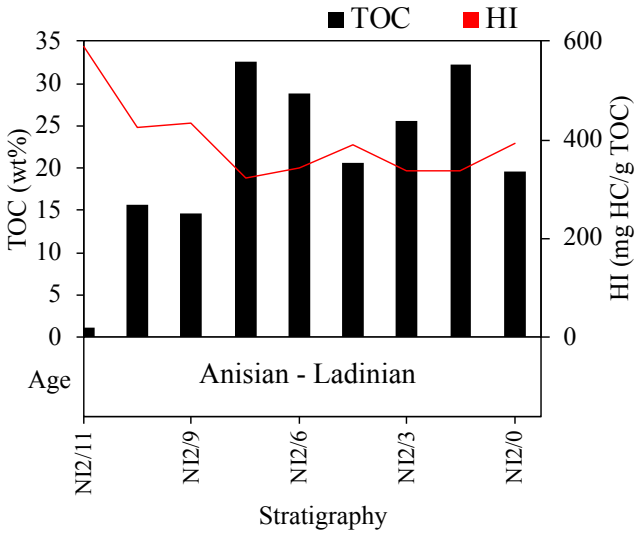

Figure 7.2.3: TOC (wt%) content, HI (mg HC/g TOC) values for NI2.

Mineralogy

9 samples for NI2 (figure 7.2.4) are available, everyone very different from each other. Starting from the bottom, there is an absent content of dolomite and ankerite, which increase upwards, reaching 97 wt% in the samples BE/11, while micas and clays (mainly muscovite and illite) represent 75 wt% in the lower sample of the stratigraphy. With the exception of the first (BE/0) and the last sample (BE/11), there is a variable content of quartz (between 5 and 30 wt% approx.). Orthoclase varies between 5 and 20 wt%, while pyrite varies between 3 and 10 wt%. As regards organic matter, with the exception of the sample BE/0, in which it is around 1 wt%, it has values between 15 and 32 wt%.

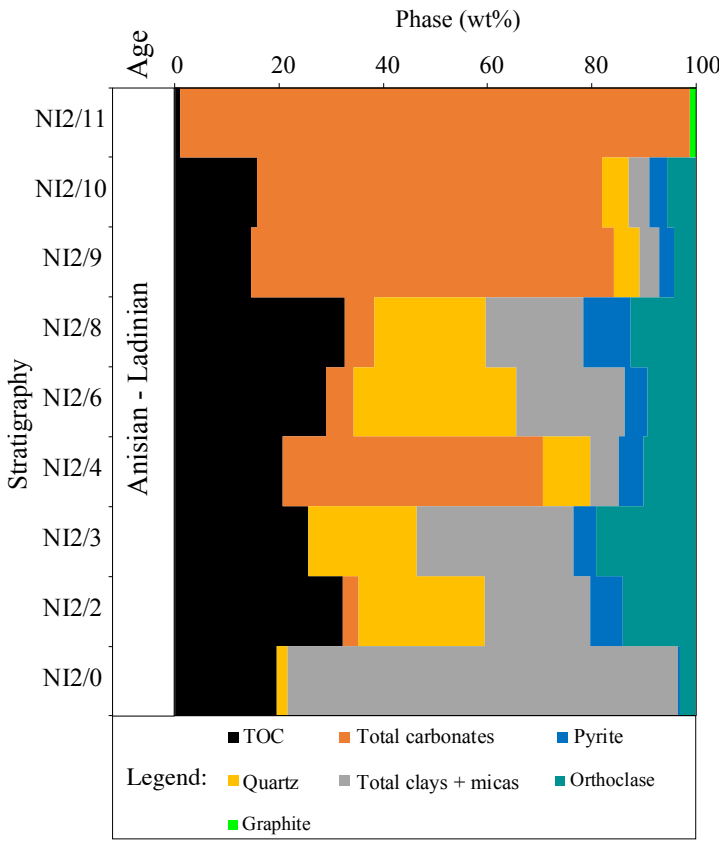

Figure 7.2.4: mineralogical (wt%) and TOC (wt%) content for NI2.

7.3 DEVONIAN MATURE MARINE SOURCE ROCKS

As shown in table 7.3.1, Devonian mature source rocks are represented by NA1 and NA2 from North Africa. NA1 represents a weak mature source rock while NA2 is mature (oil window). Being mature means that TOC and HI are depauperated compared to the original values (TOC_o and HI_o).

Name	*Thickness*	*Age*	*Samples type*	*Number of samples*
NA1	277.56 m	Givetian – Frasnian	Cores	15
NA2	94 m	Frasnian	Cuttings	21

Table 7.3.1: thickness, age, sample type and number of samples analyzed for NA1 and NA2.

NA1

The samples of this section are collected by cores so they are not affected by pollution by drilling muds. The core is composed by two portion of different age:

- Givetian: 4 samples from 3456.9 to 3448.8m depth;
- Frasnian: 11 samples from 3183.1 to 3179.34m depth.

Organic content and Hydrogen Index

Naphtogenic parameters of NA1 are represented in figure 7.3.1. Samples from Givetian are TOC and HI poor with an average of ~0.25 wt% and1~68, respectively. These samples are sterile. Frasnian samples are richer in TOC; the values are quite constant close to an average values of 8.77 wt%. Also HI is quite constant and its average values is 438.47 mg HC/g TOC. This section has been classified as slightly mature, so it is possible that both TOC and HI are slightly depauperated compared to the original values (TOC_o and HI_o). Original values could be depauperated of ~10% compared to the originals one. This means that the HI_o is >350 mg HC/g TOC indicating a marine environment with the deposition of marine organic matter (algae and bacteria).

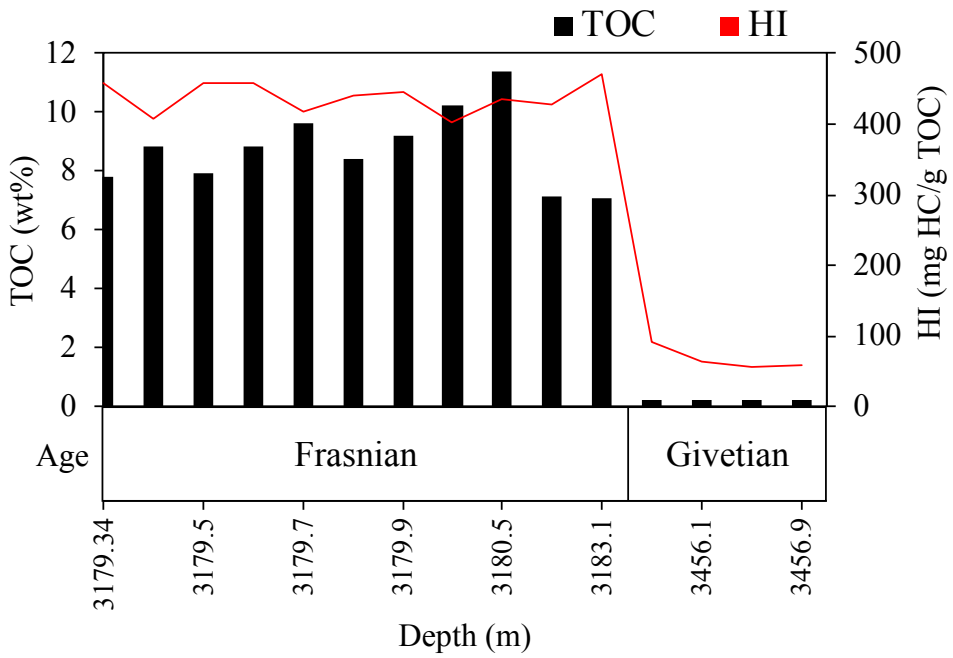

Figure 7.3.1: TOC (wt%) content, HI (mg HC/g TOC) values for NA1.

Mineralogy

Mineralogy is quite homogeneous from the bottom to the top of the NA1 core (figure 7.3.2). The samples of Givetian age are composed mainly by clays and micas that reach ~75.0 wt% and quartz (~20.0 wt%). Clays and micas are the sum of illite type (~55.0 wt%), kaolinite (~15.0 wt%) and chlorite (~2.0 wt%). The samples of Frasnian age are composed mainly by clays and micas (around ~50.0 wt%), quartz (~14.0 wt%), carbonates (~10.0 wt%) and pyrite (from a minimum of ~5.0 wt% to a maximum of ~10.0 wt%). Clays and micas represent the amount of illite type (~35.0 wt%), kaolinite (~18.0 wt%) and chlorite (~1.5 wt%).

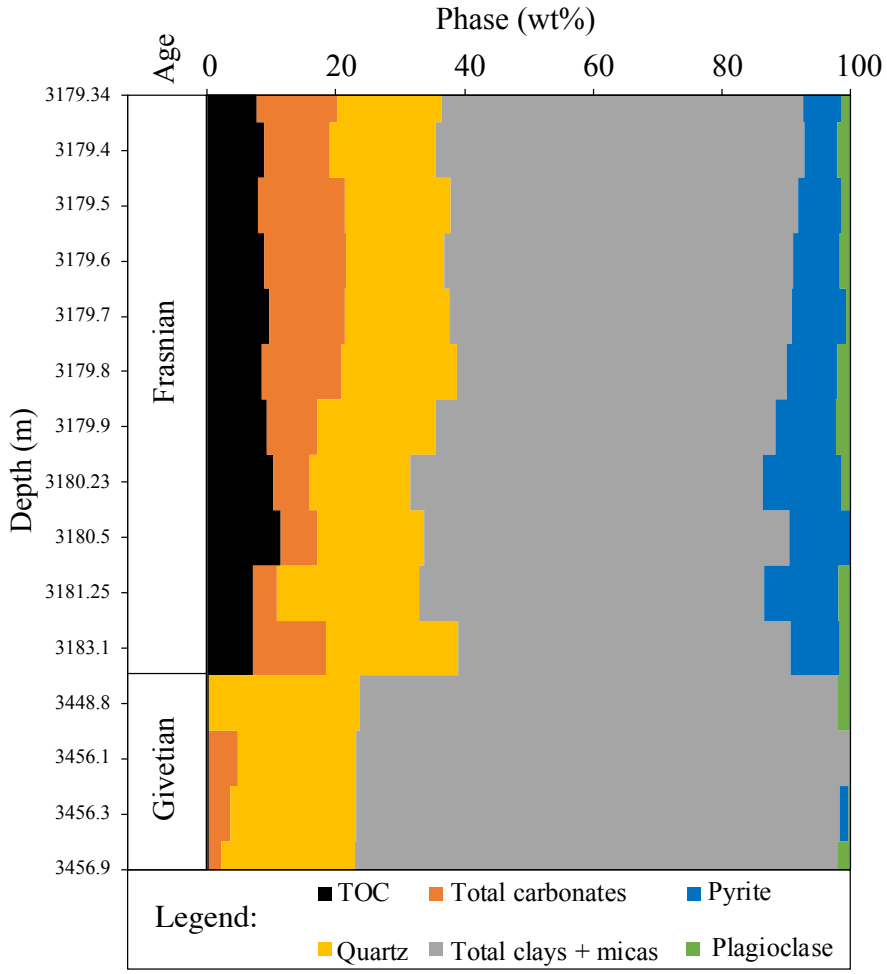

Figure 7.3.2: mineralogical (wt%) and TOC (wt%) content for NA1.

NA2

NA2 is a mature source rock from North Africa. The samples are cutting.

Depositional environment

The depositional environment is characterized by fine-grained facies, suggesting a low energy setting in which macrofossils are abundant and well preserved. These characteristics are typical of a middle ramp depositional environment. The macrofossils assemblages was fundamental to reconstruct the depositional environments because each facies was characterized by a different fossil content, related to a specific depth. In particular an outer neritic depositional environment is suggested by the presence of *Planolites* and *Chondrites*. Subsequently, high pyrite and organic matter contents suggest the development of reducing conditions at the sediment – water interface. Here in this period, bottom water currents developed reorganizing the sediments. The fist burial phases are characterized by carbonates dissolution and deposition (dissolution of shells) of organic matter or pyrite as filler.

Organic content and Hydrogen Index

TOC in NA2 shows very variable contents between 1.46 and 11.80 wt% (figure 7.3.3). The richer samples are located in the upper part of the section, from 3902m to 3870m depth. Generally, also HI mirrors TOC behavior even if for similar TOC content, very different HI values are observed. HI varies between a minimum of 39.53 and a maximum of 160.70 mg HC/g TOC, with an average values of 95.10 mg HC/g TOC (figure 7.3.3). The higher value is 160.70 mg HC/g TOC observed in a sample with TOC of 3.41 wt%.

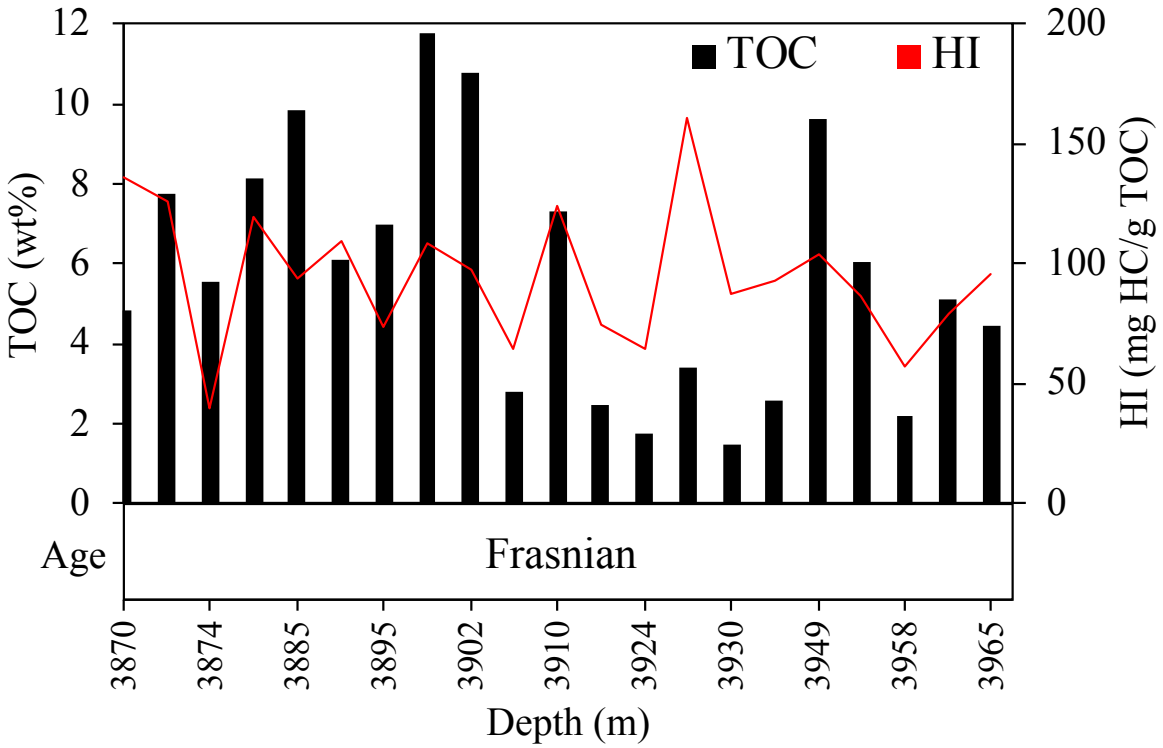

Figure 7.3.3: TOC (wt%) content, HI (mg HC/g TOC) values for NA2.

Mineralogy

The sequence is an alternation of clayey (up to 60 wt% of total clays) and carbonates (up to 80 wt% of calcite and dolomite) levels. In fact, the main mineralogical phases are clays and carbonates and, because of the dominant reducing conditions, high content of pyrite (~15 wt%) and preserved organic matter were detected (figure 7.3.4).

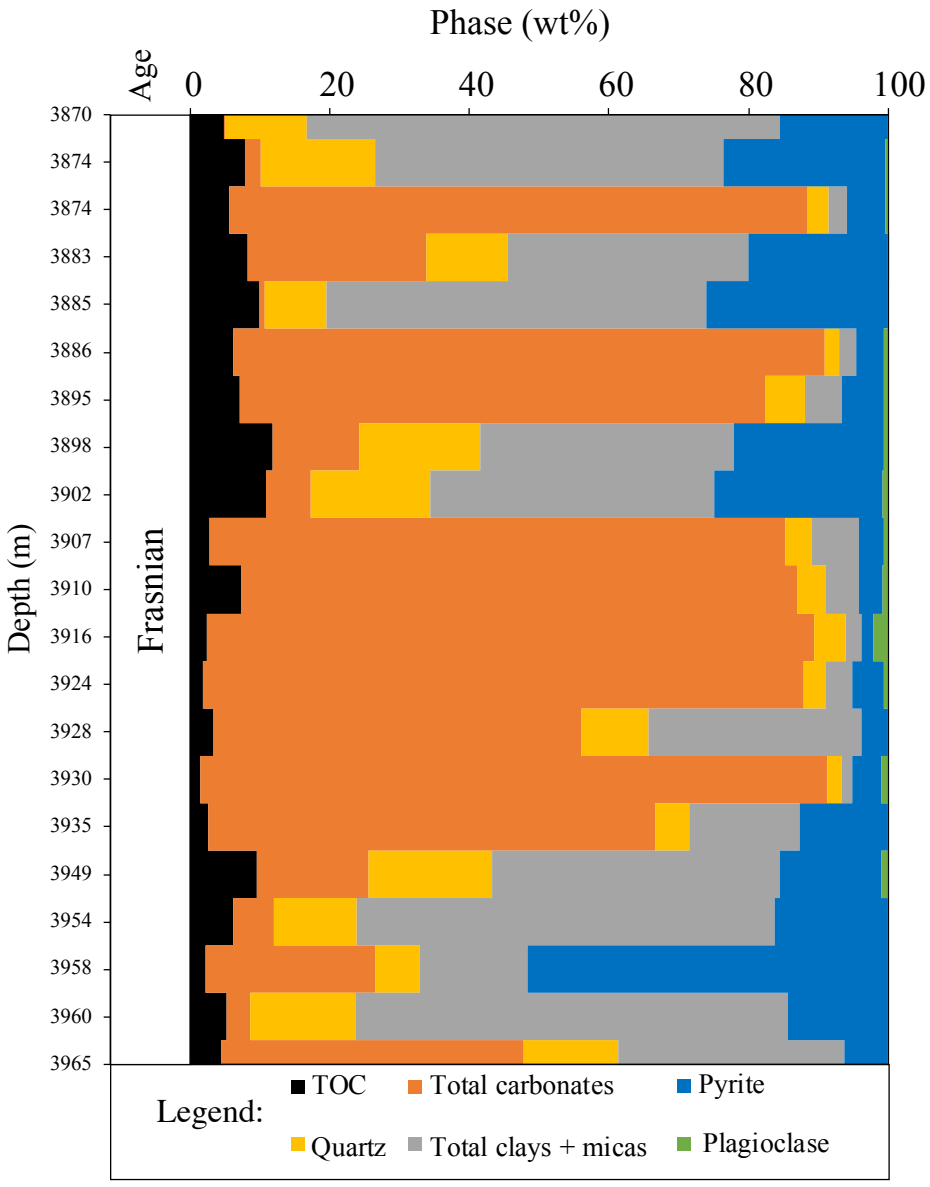

Figure 7.3.4: mineralogical (wt%) and TOC (wt%) content for NA2.

CHAPTER 8

Results and Discussions

In this chapter are presented the main results obtained after the data processing. Immature cases of study (Cretaceous and Triassic) are widely discussed in this section. In particular, we seek to highlight the main features, the links between organic and inorganic parameters and their significance. Finally, some food for thought is presented for mature rocks (Devonian).

The discussion of the results is divided into three parts regarding:

- Cretaceous immature source rocks;
- Triassic immature source rocks;
- Frasnian source rocks.

In each section are shown the results regarding the relations between TOC, HI and mineralogy with:

- Elements related to the organic matter: V, Mo, U, Ni, Cu
- Elements that not correlated with organic matter: Th, Al, Zr, Mn
- Anomalies in trace elements and REEs.

Where it is possible, we seek to highlight the differences and the analogies between distal and proximal environments for each group of elements.

Finally, a discussion combining all the cases of study is presented in order to trace different features related to variabilities in organic matter content, age and depositional environment.

8.1 CRETACEOUS IMMATURE SOURCE ROCK

8.1.1 Results

Elements related to the organic matter: V, Mo, U

In the distal cases of study, V varies between ~10 and ~1800 ppm, with an average of ~237 ppm; in proximal environments, it varies between ~60 and ~400 ppm, with an average of ~165 ppm. Mo concentrations are between ~2 and ~200 ppm (average of ~ 20 ppm) in distal environments, while I proximal environments Mo varies between ~3 and ~20 ppm, with an average of ~7 ppm. Finally, U values are between ~0.2 and ~20 ppm with an average value of ~5 ppm in distal cases; in proximal cases U varies between ~0.6 and ~8 ppm, with an average of ~3 ppm.

Generally, V shows concentrations above the UCC value (107 ppm; McLennan, 2001) (figures 8.1.1A and 8.1.1B). Some samples of the distal cases of study show values below the UCC: mainly, these show TOC <1wt% and are not source levels. Mo values are above 1.5 ppm for all the Cretaceous cases of study (figures 8.1.1C and 8.1.1D), that is the concentration in the UCC (McLennan, 2001). Finally, U show values that are below the UCC value (2.8 ppm; McLennan, 2001) when TOC < ~1.5 wt% for distal environments and when TOC < ~1.9 wt% for proximal environments (figures 8.1.1E and 8.1.1F). However, usually the source levels show values close to or higher than the UCC value. Except for CA7, the source levels are the most enriched in TOC and TEs in both distal and proximal cases of studied. Indeed, in CA7 the source levels are divided into two groups, the first show TOC >1 wt% and is more enriched in TEs and the second shows TOC < 1wt% and lower enrichments in TEs (figures 8.1.1A, 8.1.1C and 8.1.1E). The first group is related to the source level of Cenomanian – Turonian - Coniacian age, while the second is related to the older source level of Barremian age (as shown in figures 7.1.7 and 7.1.8).

In CA1, the samples with TOC > 5wt% show a decreasing of V and Mo or a not linear increasing for U compared to the general trend between the TEs and TOC indicated by the black lines in figures 8.1.1A, 8.1.1C and 8.1.1E. These samples are source levels of Late Cenomanian, corresponding to OAE 2.
The same behavior is observed for 7 samples in CA6; these has the same age (Late Cenomanian) and are probably related to OAE 2 (circled in figures 8.1.1A, 8.1.1C and 8.1.1E). A similar trend is observed in CA1, for the samples related to OAE 3 when Mo is plotted against TOC (figure 8.1.1C).

Generally a positive correlation is observed between Mo, V, U and the naphthogenic parameters (TOC and HI) for the distal Cretaceous Source Rocks, as indicated by the trend lines (black lines in the figures 8.1.1A, 8.1.1C, 8.1.1E and 8.1.2A, 8.1.2C and 8.1.2E) along which all the samples are arranged. Proximal cases of study show weak positive correlations between TEs and TOC as indicated by the black trend lines in figures 8.1.1B, 8.1.1D and 8.1.1F, but no correlations with HI (figures 8.1.2B, 8.1.2D and 8.1.2F).
With negligible percentages of TOC (<0.5 wt%) the correlations between TOC and TEs become weaker and the trend lines tend towards the composition of the Upper Continental Crust (dashed lines in figure 8.1.1; McLennan, 2001). This trend is very clear for the cases of study located in a distal paleoenvironment (CA1, CA6, CA7 and SI1; figures 8.1.1A, 8.1.1C and 8.1.1E),

while it is less visible for the cases characterized by a proximal paleoenvironment (CA2, CA3, CA4 and CA5; figures 8.1.1B, 8.1.1D and 8.1.1F). Instead, the latter show a more vertical trend in which for a narrow range of TOC (mostly from ~0.5 to ~2.0 wt%), large variations in V, Mo and U are observed. Notably, in figures 8.1.1E some samples of CA7 scatter from the general trend of CA1 and CA6 between U and the organic matter content when TOC is < 1wt%.

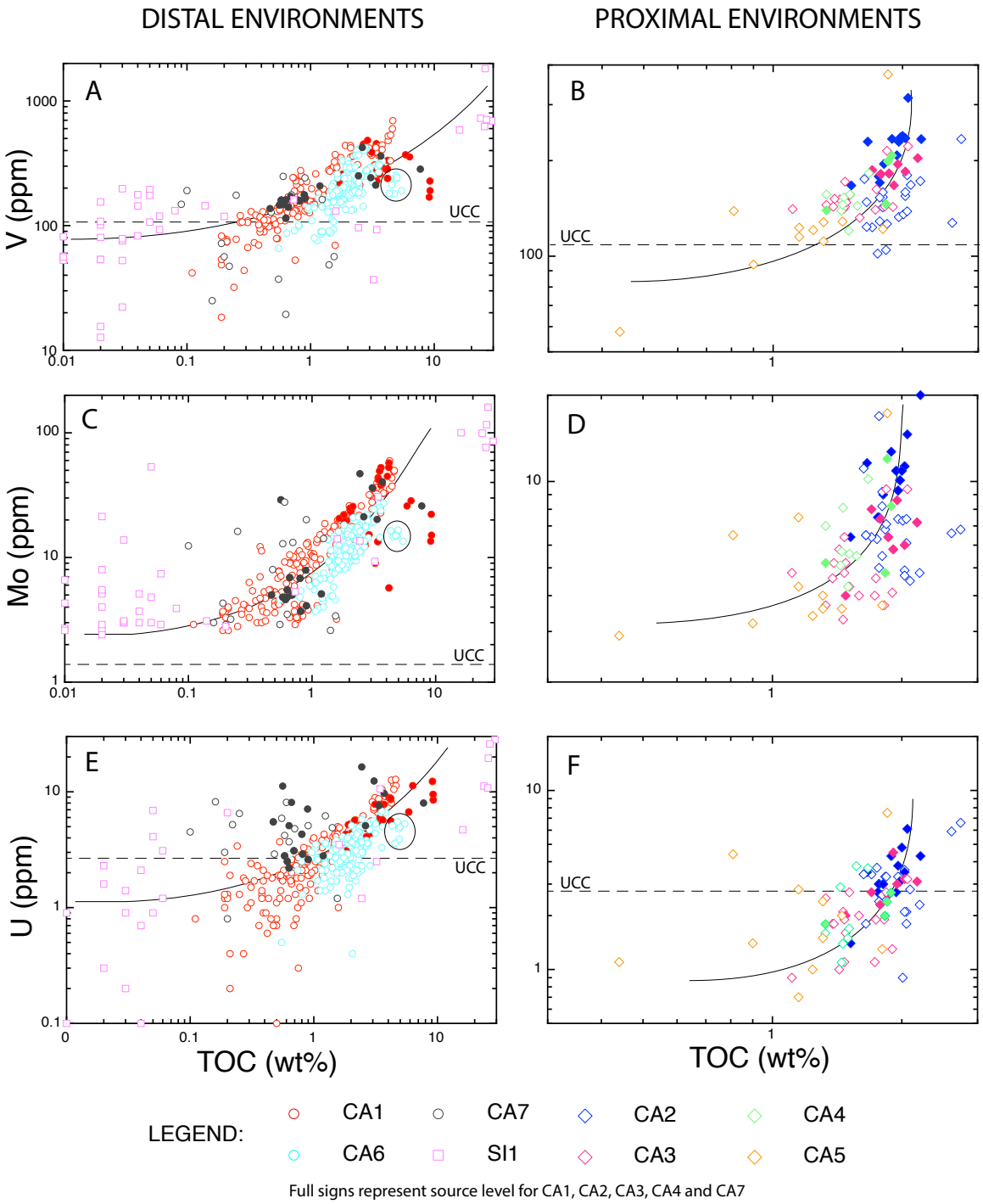

Figure 8.1.1: cross plots of V, Mo and U (ppm) with TOC (wt%) for the Cretaceous cases of study divided according to the environmental typology (distal and proximal).

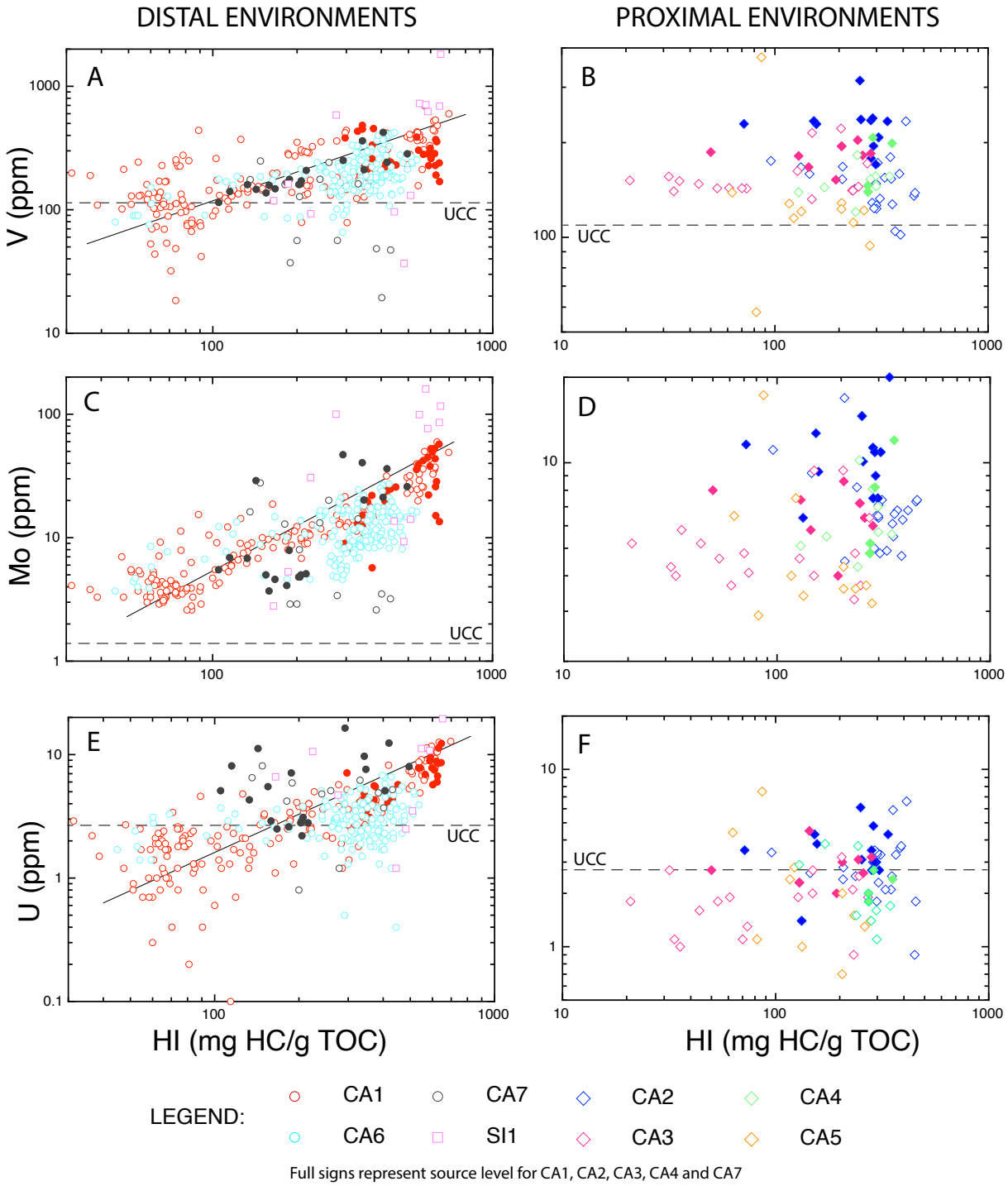

Figure 8.1.2: cross plots of V, Mo and U (ppm) with HI (mg HC/g TOC) for the Cretaceous cases of study divided according to the environmental typology (distal and proximal).

Elements related to the organic matter: Ni and Cu

Ni varies between ~2 ppm and ~1000 ppm for distal environments, with an average of ~54.5 ppm. In proximal environments, Ni varies between ~30 and ~100 ppm, with an average of ~44 ppm. The average concentrations show that in both environments, the values are close or above the Ni UCC value (44 ppm; McLennan, 2001). Specifically, source samples for CA1 show Ni values close or above the UCC value, while source sample from CA7 show values between ~20

and ~100 ppm. Source samples of the proximal environments show Ni values always very close or higher than the UCC value.
Cu shows values between ~30 and ~400 ppm, with an average of ~38.5 ppm in distal environments. Instead, in proximal environments, it shows an average of ~26.5 ppm and varies between ~15 and ~80 ppm. As for Ni, the averages are close or above the Cu UCC values (25 ppm; McLennan, 2001). In particular, CA1's source samples show Cu values from ~15 to ~30 ppm, while CA7's source sample show Cu concentrations always higher than the UCC values. Finally, CA2 shows source sample with Cu concentrations always higher than 25ppm, CA3's source samples show values always slightly lower than the UCC value, while the source samples of CA4 show Cu concentrations between ~15 and ~35ppm.

Positive correlations between Ni and TOC are observed for both distal and proximal environments (figures 8.1.3A and 8.1.3B). However, for distal environments the correlation is weaker than in proximal environments. In particular, the trend is marked mainly by the cases from the Atlantic Ocean, while SI1 show no correlations between TOC and Ni. Specifically, the samples with TOC<1 wt% are widespread, while the samples with TOC > 10 wt% show a wide range of Ni concentrations for a narrow range of TOC. Finally, the samples with TOC between 1 and 10 wt% are mostly overlapped to the trend drawn by the Central Atlantic cases. Contrarily, no correlations are observed between Cu and TOC for both distal and proximal environments (figures 8.1.3C and 8.1.3D). However, source samples from CA1 and CA7 seems to drawn a positive trend, together with CA6.

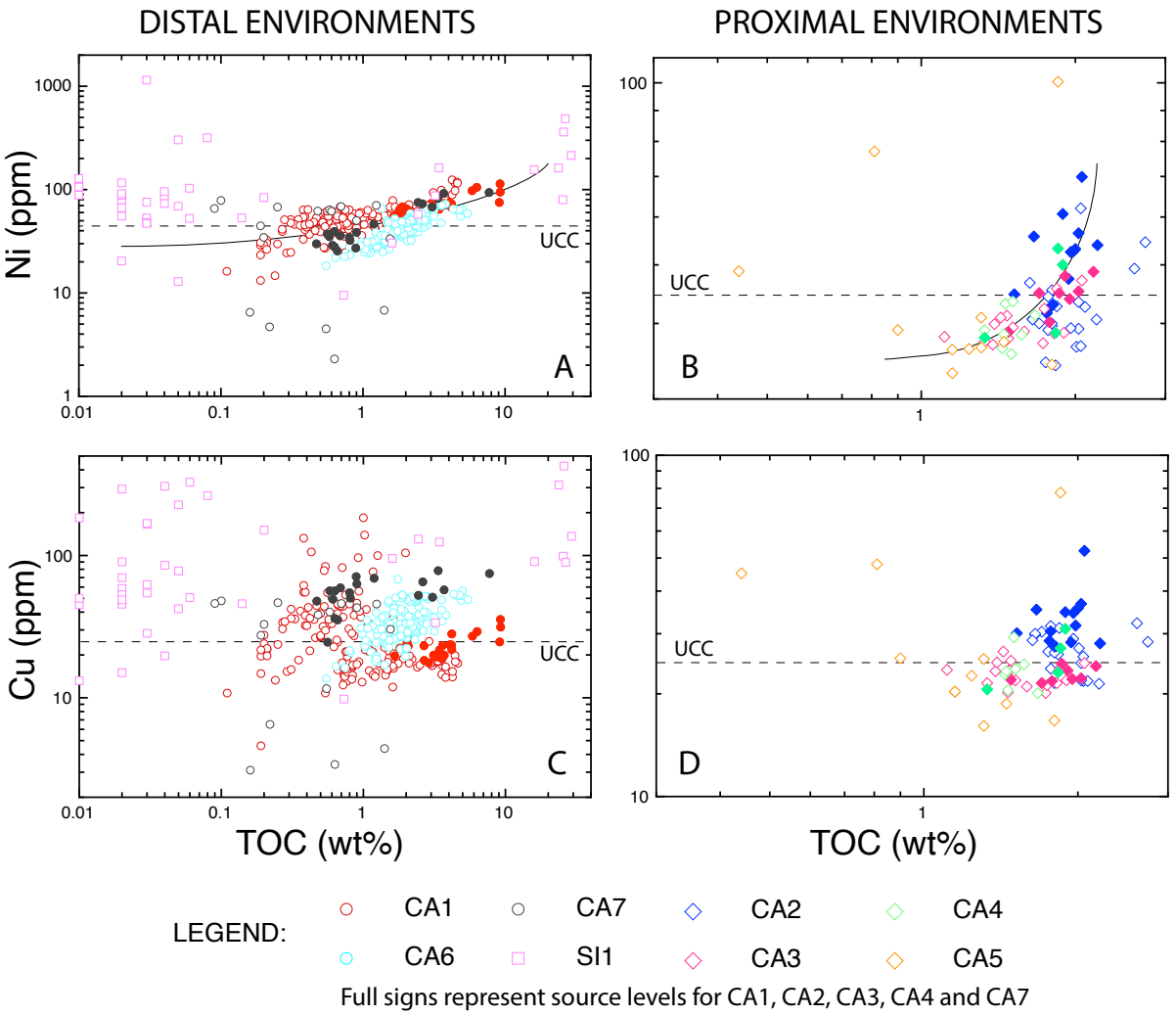

Figure 8.1.3: cross plots of Ni and Cu (ppm) with TOC (wt%) for the Cretaceous cases of study divided according to the environmental typology (distal and proximal).

No correlations between Ni, Cu and HI are observed (figure 8.1.4) for both proximal and distal environments. In particular, the samples are arranged horizontally, especially for Ni.

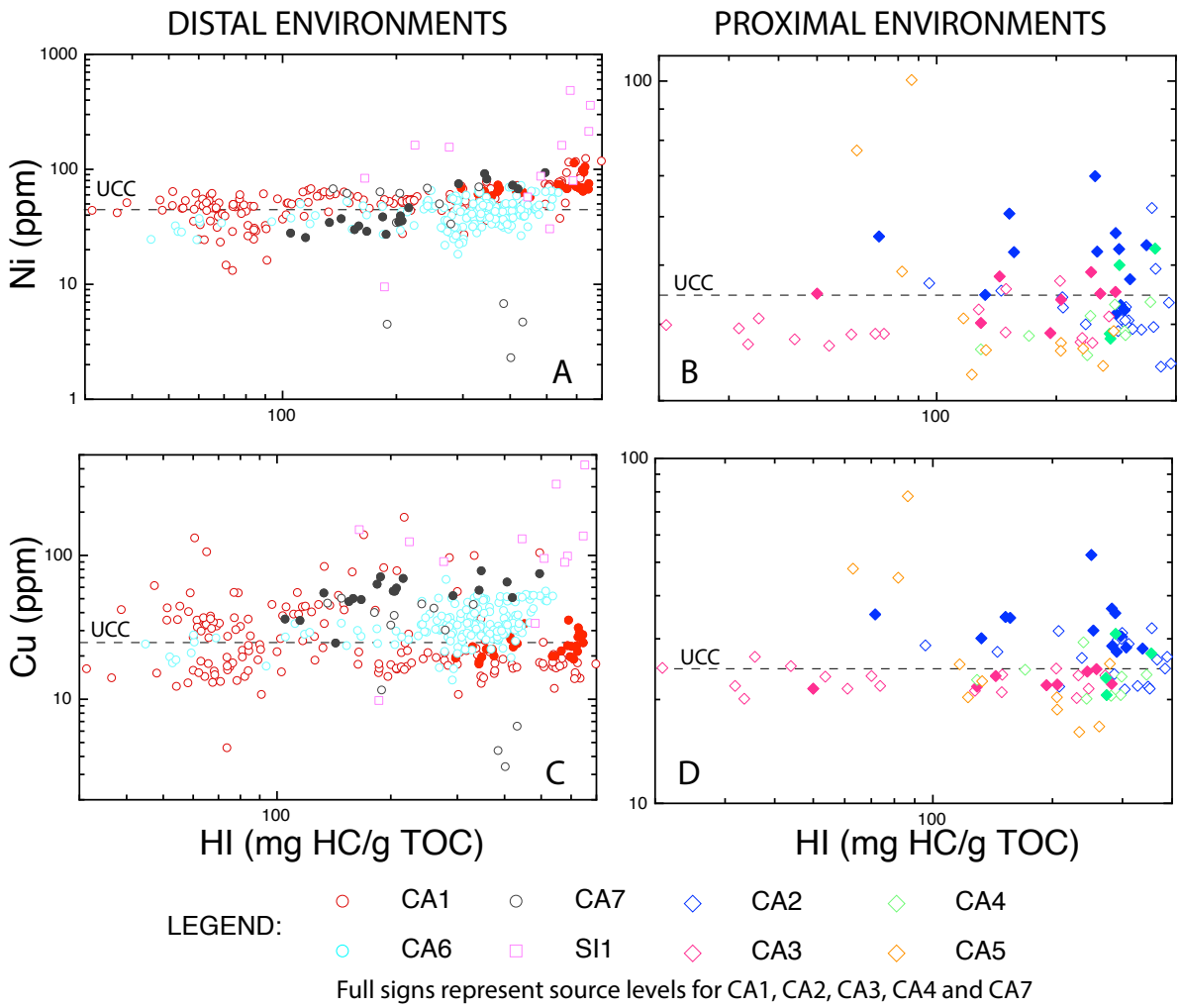

Figure 8.1.4: cross plots of Ni and Cu (ppm) with HI (mg HC/g TOC) for the Cretaceous cases of study divided according to the environmental typology (distal and proximal).

Elements not related to the organic matter: Th, Zr, Al, Mn

Thorium in distal environments shows an average of ~3 ppm, with values between ~10 and ~0.1 ppm.

In proximal environment, Th show concentrations between ~8 and ~1 ppm, with an average of ~4 ppm. Generally, in all the cases of study Th concentrations are below the UCC value (10.7 ppm; McLennan, 2001).

This element shows weak correlations with TOC. In particular, for TOC < 1.5 wt%, no correlations between the organic content and Th are observed for both distal and proximal environments (figures 8.1.5A and 8.1.5B). A weak exponential negative correlation with organic carbon > 1.5wt% (figure 8.1.5A), marked mostly by CA1 and CA6 for the distal environments and CA2 for proximal environments. Regarding the source samples, only the

ones of CA1 show a clear negative correlation between Th and TOC. Finally, CA7, CA2, CA3 and CA4 do not show correlations whit TOC.

Moreover, in our cases of study a positive correlation is observed between Th, Zr and clays and micas (figures 8.1.5C and 8.1.5F), in both distal and proximal environments. CA6 is the only case that slightly slip from the correlation marked by the black line in figure 8.1.5C. Especially, CA6 shows lower contents of Th for similar contents of total clays and micas compared to the other distal cases of study.

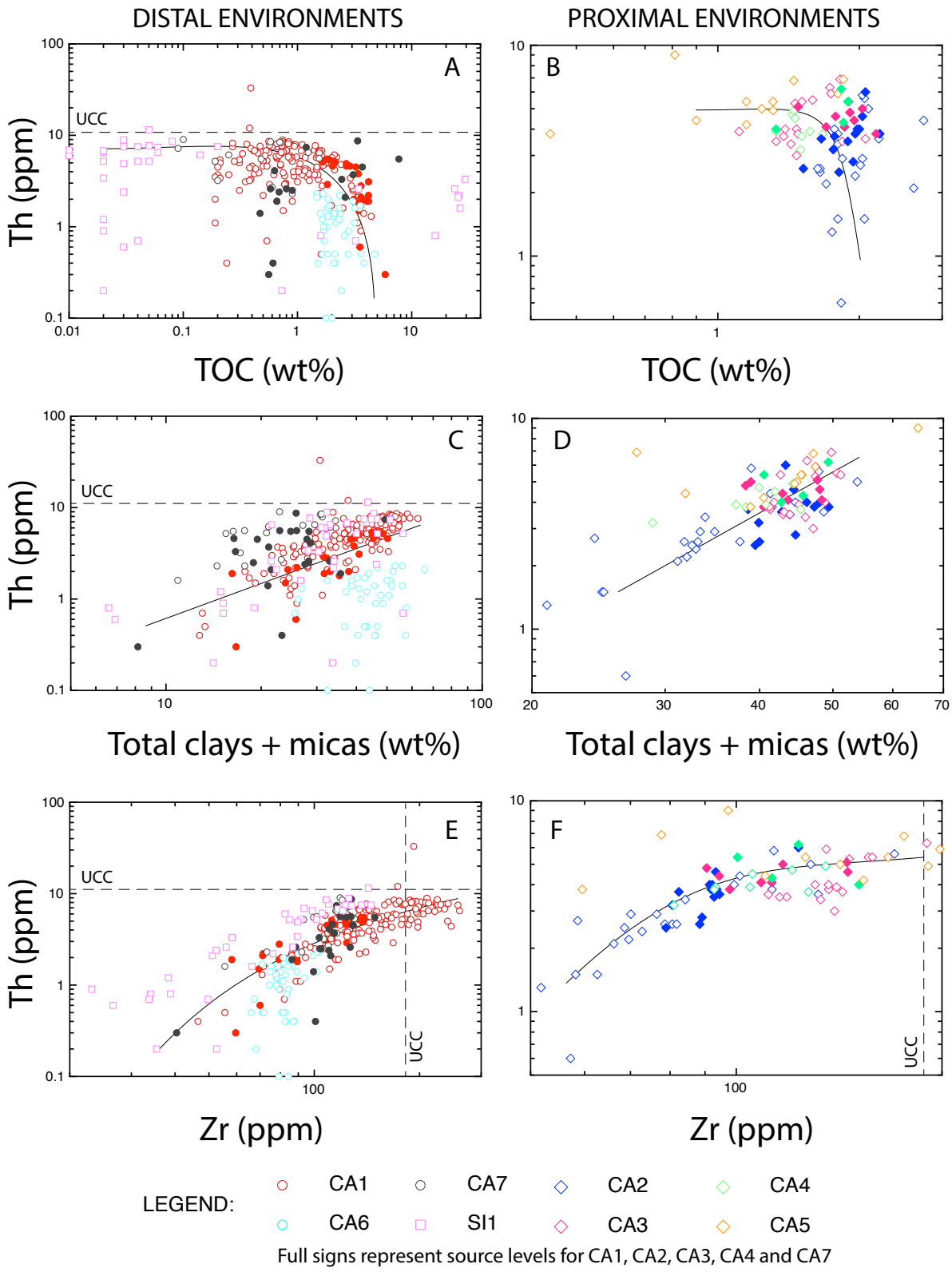

Figure 8.1.5: cross plots of Th (ppm) with TOC (wt%), total clays and micas (wt%) and Zr (ppm) for the Cretaceous cases of study divided according to the environmental typology (distal and proximal).

In distal environments, zirconium shows concentrations between a maximum of ~300 ppm and a minimum of ~ 20 ppm, with an average of ~ 103 ppm; whereas in proximal environments it shows between ~200 and ~50 ppm, with an average of ~112 ppm. The values are mainly above the UCC value of 190 ppm (McLennan, 2001). Aluminum shows values between ~10 x 10^4 and ~2 x 10^4 ppm in distal environments, with an average of ~5.2 x 10^4 ppm. In proximal environments, concentrations of Al between ~10 x 10^4 and ~4 x 10^4 ppm, with an average of ~7.9 x 10^4 ppm. The Al averages are below the UCC value (8.0 x 10^4 ppm; McLennan, 2001).
Zr show a negative correlation with TOC in distal environments (figure 8.1.6A), marked mainly by CA1. Especially, the source samples of CA1 draw a well-marked negative relationship for TOC >1~2 wt%. Whereas, very weak negative correlations between TOC and Zr are observed for SI1 and CA6.
Finally, CA7 shows no correlations between Zr and TOC, even if the source samples draw a positive relationship. However, all the cases are generally aligned along a single trend (black line in figure 8.1.6A) and are partially overlapped to CA1, drawing a negative correlation between Zr and TOC.
Instead, for proximal case of study, and in particular for CA2, CA3 and CA4, Zr shows a wide range of values with similar TOC values (figure 8.1.6B), resulting in a negative correlations with a very high slope (almost vertical). Contrarily, CA5 shows a positive correlation between Zr and TOC.
In figures 8.1.6C and 8.1.6D, the correlation between Zr and total clays + micas for distal and proximal environments is shown. In both cases, all the samples are aligned along a single trend (black line in figures 8.1.6C and 8.1.6D) that draw a well-marked positive correlation between Zr and total clays + micas, also marked by the source samples.

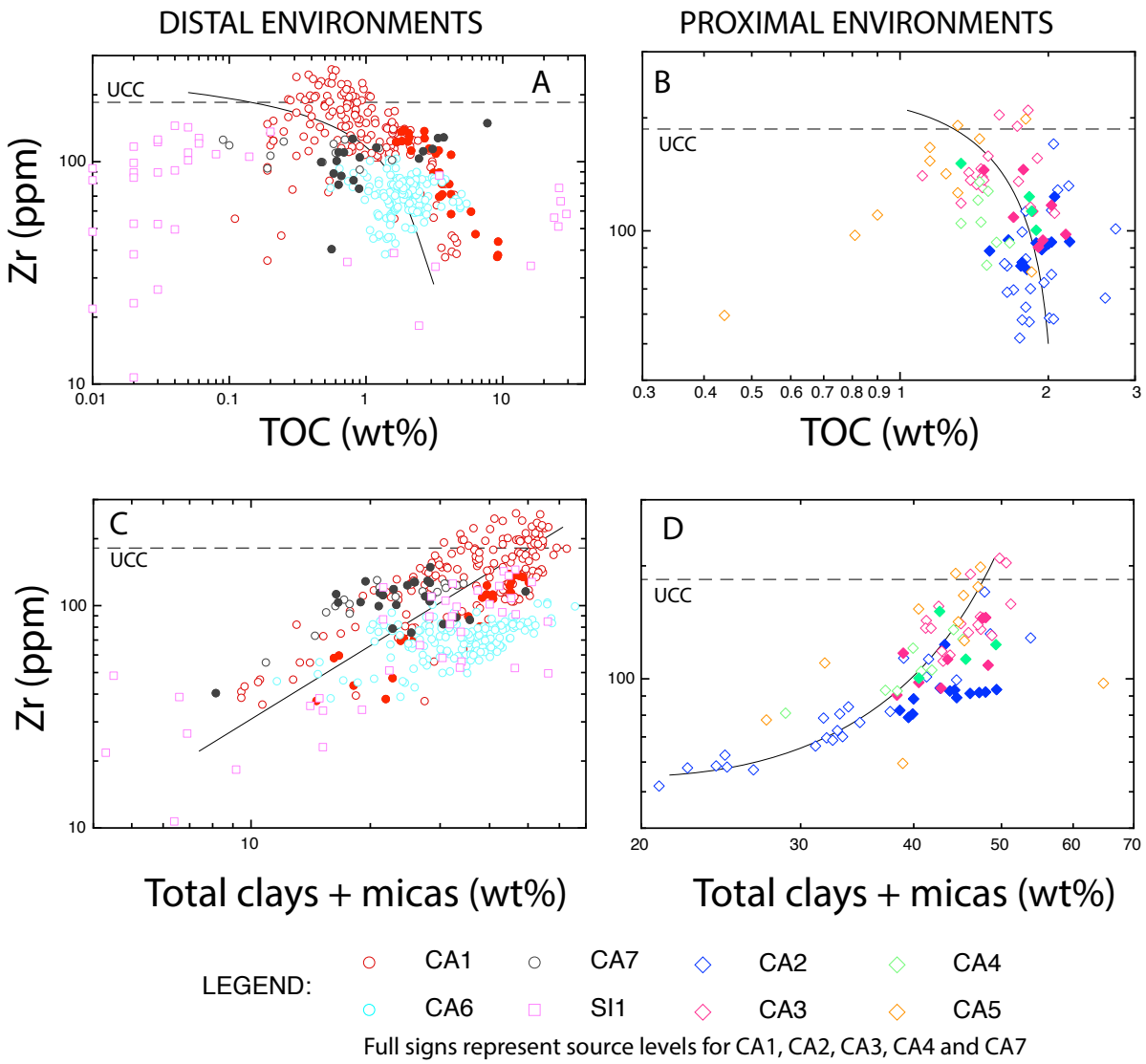

Figure 8.1.6: cross plots of Zr (ppm) with TOC (wt%) and total clays and micas (wt%) and Zr (ppm) for the Cretaceous cases of study divided according to the environmental typology (distal and proximal).

Aluminum show a very weak negative correlation with TOC for the distal cases of study (figures 8.1.7A); importantly, the source levels of CA1 draw a negative relationship between Al and TOC. For the proximal cases of study a negative correlation between Al and TOC is observed (figure 8.1.7B).

A well-marked positive correlation is observed between Al and total clays + micas for all the Cretaceous cases of study (figures 8.1.7C and 8.1.7D).1

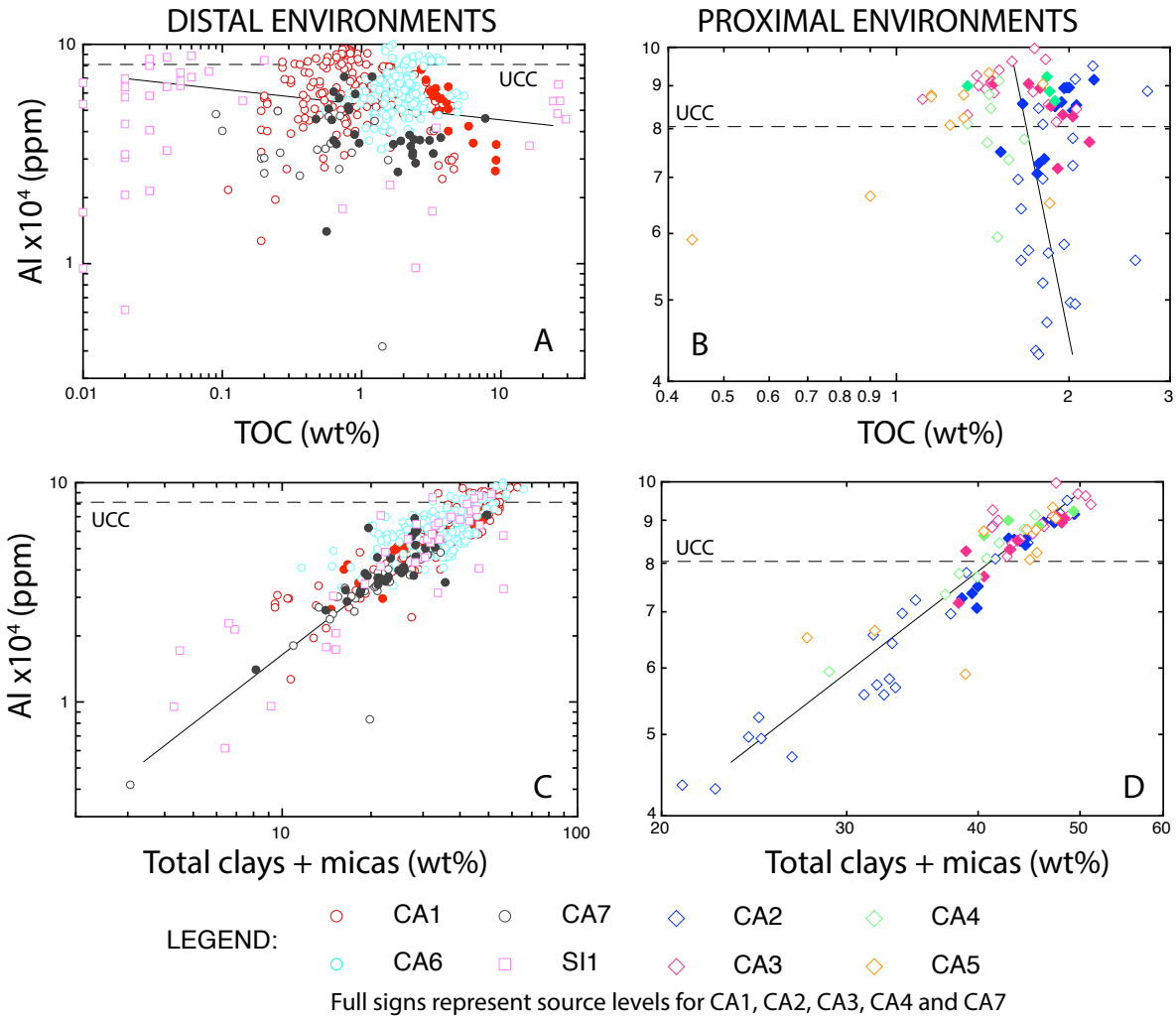

Figure 8.1.7: cross plots of Al (ppm) with TOC (wt%) and total clays and micas (wt%) for the Cretaceous cases of study divided according to the environmental typology (distal and proximal).

Manganese shows concentrations between ~3 x10^3 and ~30 ppm, with an average of ~365 ppm for CA1, CA6 and CA7. For SI1, Mn concentrations are between ~10^6 and ~100 ppm, with an average of 6.4 x 10^4 ppm. In proximal environments, it varies between ~40 and ~50 pm with an average of ~78 ppm.

Generally, in distal cases of study a weak negative correlation with TOC is observed (figure 8.1.8A), especially marked by CA1, CA7 and SI1. Proximal environments do not show correlations between Mn and TOC (figure 8.1.8B) and are depleted in Mn compared to the distal cases.

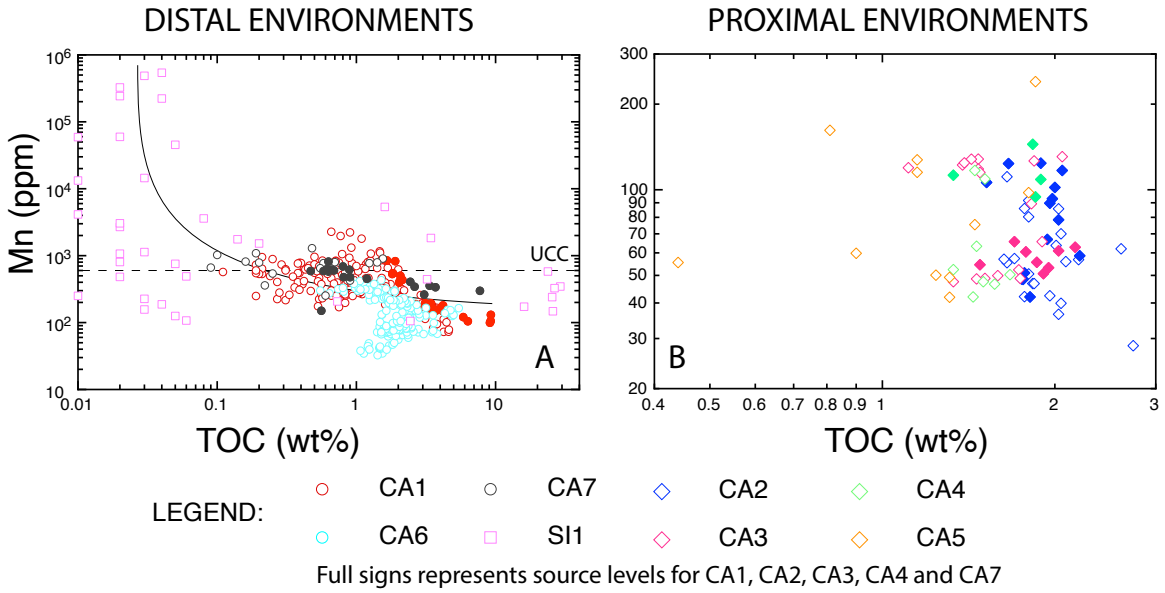

Figure 8.1.8: cross plots of Mn (ppm) with TOC (wt%) for the Cretaceous cases of study divided according to the environmental typology (distal and proximal).

Anomalies of trace and Rare Earth Elements (REEs)

The values of trace elements and rare earth elements were obtained only CA1 and CA5 for 38 and 6 samples, respectively. The values have been normalized to UCC (McLennan, 2001) to understand how much the composition of the source rocks differs from the average value of the composition of the upper continental crust represented by the horizontal dashed line with value 1 in figure 8.1.9.

The samples have been divided into 3 classes for CA1 and 2 classes for CA5, divided based on TOC, as shown in figure 8.1.9. Subsequently the average for each group have been plotted in figure 8.1.9 that shows the values of REEs and TEs for both CA1 and CA%. For CA1, the patterns progressively move away from the UCC line with value 1 (dashed line in figures 8.1.9B and 8.1.9D) as the TOC decreases. Contrarily, for CA5, the pattern closer to the UCC line is the one with TOC < 1.2 wt%, while the one characterized by TOC > 1.2 wt% is the farer from the UCC line (figures 8.1.9A and 8.1.9C).

REEs values are generally depleted compared to the UCC, especially the incompatible ones (on the left side of the graphs in figures 8.1.9A and 8.1.9B). For both CA1 and CA5 a positive anomaly in Eu is observed, that is higher than 1 for the class with TOC > 4wt% in CA1. In addition, CA5 show a positive anomaly in Tm, especially for the class of samples with TOC > 1.2 wt%.

In CA1, trace elements shows positive anomalies in U, Sr, V (except if TOC < 1 wt%) and Mo. Negative anomalies are observed for Ta, Zr, Hf and Ti (figure 8.1.9D). In CA5 positive anomalies are related to Ba and Mo, while negative correlations are related to Rb, Sr, and Y (figure 8.1.9C).

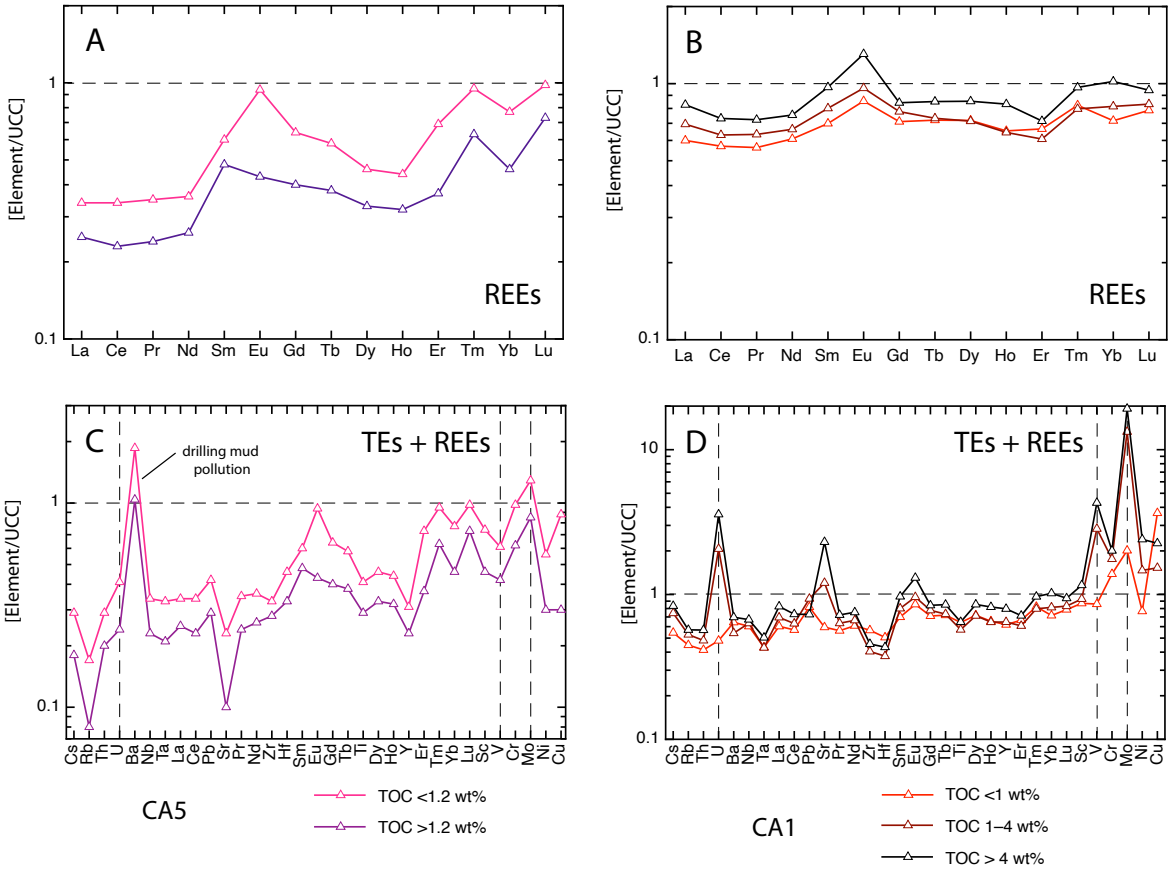

Figure 8.1.9: cross plots of REEs and TEs concentrations (normalized to UCC) for CA1 and CA5.

8.1.2 Discussion

In this chapter analogies and differences between distal and proximal cases of study are shown. Firstly the two typology of environment are discussed separately, then we seek to compare then based on the inorganic and organic features. Follow a discussion and interpretation of the results.

Elements related to the organic matter: V, Mo, U

- Distal environments

Generally, the positive relationship between V, Mo and U and the naphtogenic parameters (TOC and HI) suggests that these elements are hosted by the organic matter and indicates that the increasing of OM was due to the development of reducing conditions leading to enrichments in TEs. Considering the relationships between TEs and the naphtogenic parameters, all the samples follow the same trend, indicating that V, Mo and U depends mainly by the organic matter (figures 8.1.1A, 8.1.1C and 8.1.1E and 8.1.2A, 8.1.2C and 8.1.2E) and are not affected by age, location and mineralogy.

The trend between TEs and TOC is characterized by an exponential growth, in particular with TOC < 0.5 wt% for V, < 0.3 wt% for Mo and <1 wt% for U, the trends (black lines in figures 8.1.1A, 8.1.1C and 8.1.1E) tend to horizontalize with a values close to the UCC value. In addition, with negligible TOC contents (<0.1 wt%), the correlation between organic matter and RSEs disappears (i.e. SI1). This is consistent with the fact that with low organic matter content, no enrichments in redox sensitive elements compared to the UCC occur due to the lack of reducing conditions and organic matter (that is the main host phase for V, Mo and U).

However, some differences in each case of study are observed. CA1 intersects four Cretaceous Oceanic Anoxic Events (OAEs; Schlanger and Jenkyns, 1976): OAE 1c (Late Albian), OAE 1d (Late Albian), OAE 2 (Late Cenomanian) and OAE 3 (Santonian); details in chapter 7). In particular, trace elements and TOC highlight that the enrichment in TOC not always is related to an enrichment in TEs. The OAE 1c is the only that always shows a positive relationship between TOC and TEs (figures 8.1.10A, 8.1.10D and 8.1.10G); OAE 1d shows a positive correlation between TOC and Mo and U (figures 8.1.10D and 8.1.10G) but a negative correlation between TOC and V (figure 8.1.10A); OAE 2 shows negative correlations between TOC and V and Mo (figures 8.1.10A and 8.1.10D), and a weaker positive correlation between TOC and U compared to the general trend of the section (figure 8.1.10G); finally, OAE 3 shows a negative relationship between TOC and V and Mo (figures 8.1.10A and 8.1.10D) but a positive relationship between TOC and U (figure 8.1.10G). However, the negative relationships between TOC and TEs are not related to oxygenated conditions or to the fact that these elements are not hosted by the organic matter. Indeed, Algeo (2004) explained that periods of intense reducing conditions (e.g. euxinia) can drawdown the global metals inventory in the oceans due to the abundance of anoxic sinks compared to the metals supply. Especially, for global events like OAE 2, the drawdown of TEs (especially Mo) has been observed in many localities around the world in both Atlantic Ocean (ODP sites; Hetzel et al., 2009; Westermann et al., 2014;

Wang et al., 2016; Ostrander et al., 2017) and Tethys (Scopelliti et al., 2004 and 2006; Tribovillard et al., 2012; Westermann et al., 2014; Owens et al., 2017a). The other anoxic events are not very known from this point of view, but it is probable that a similar process to OAE 2 has triggered the drawdown of trace elements, especially during OAE 1d when the Central Atlantic was not completely open and the basin may have been restricted. Also, CA6 show 7 samples of Late Cenomanian age that differ from the general trend because of their depletion of TEs (figures 8.1.10B, 8.1.10E and 8.1.10H). It is probable that these samples are related to OAE 2, due to their geochemical characteristic and age.

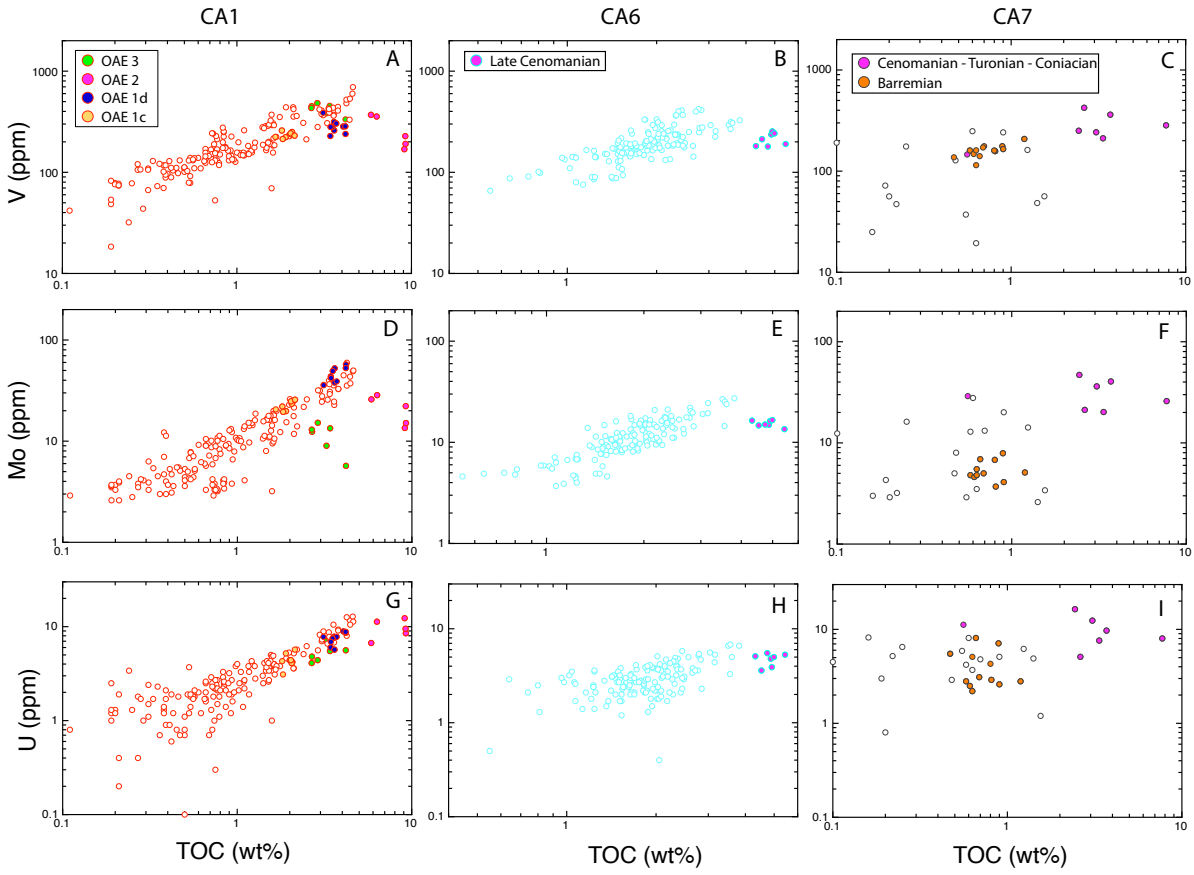

Figure 8.1.10: cross plots of V, Mo and U (ppm) with TOC (wt%) for CA1, CA6 and CA7.

Also, in figures 8.1.10C, 8.1.10F and 8.1.10I, CA7 shows that its source levels are divided into two groups: (i) Cenomanian – Turonian – Coniacian age (TOC >1 wt%) and (ii) Barremian age (TOC < 1wt%). The first group shows negative relationship between V, Mo and TOC and no correlations between TOC and U. Again, due to the age of the first group together with its geochemical characteristics it is possible that these sample may represent the OAE 2 in CA7. The second group, instead show positive relationships between TEs (V, Mo and U) and TOC and in figures 8.1.1A, 8.1.1C, 8.1.1D it is overlapped to the general trend represented by the

black trendlines indicating that for these samples an increase of TOC was due to the development of reducing conditions leading the enrichments of TEs hosted by the OM.

In addition, for the distal cases of study, the relationship between U and TOC is weaker than the one between V, Mo and TOC. Indeed, in figure 8.1.1E, the samples are more scattered, especially the ones of CA7. This is due to the fact that U can be hosted not only by OM but with by others mineralogical phases, mainly carbonates. However, no relationships between U and carbonates or any other elements (except other RSEs) or mineralogical phases have been observed. It is probable that U is distributed in not significant amount in carbonates or that it forms its own phase (e.g. uraninite). In the first case the amount of U in carbonates may be enough to decrease the relationship between TOC and U but not enough to draw a relationship with carbonates. In the second case, uraninite may be present in very little amounts (<0.5 wt%) or it may be microcrystalline, not allowing to be detected by XRD.

Finally, regarding HI (defined as HI = S2/TOC*100, where S2 is the residual petroleum potential produced by thermal degradation of kerogen that depends on the organic matter typology), distal environments show a linear co-variation with RSEs (figures 8.1.2A, 8.1.2C and 8.1.2E), indicating that the RSEs depend on the amount of OM.
Again, some differences between the cases of study can be observed. CA6 show HI values between 250 and 550 mg HC/g TOC mainly (typical values of marine organic matter produced by algae). However, there are some samples linearly aligned along the trendline with HI between 45 and 250 mg HC/g TOC. These samples are of Santonian age and are characterized by TOC ~ 1.5 wt% (figures 8.1.2A, 8.1.2C and 8.1.2E). It is probable that these samples are characterized by an increase of the terrestrial organic matter (lignin) that, compared to the samples with the same organic matter content, show lower values than the marine OM.
CA7 samples, as for TOC, are more scattered compared to the other distal cases of study, especially if U is considered (figure 8.1.2E), indicating that U is not hosted only by the OM, but it probably forms its own microcrystalline phases.

- Proximal environments

For proximal cases of study, a weak relationship between TEs and TOC has been observed (figures 8.1.1B, 8.1.1D and 8.1.1F). However, these cases present a narrow range of TOC (between ~0.5 and ~2 wt%) compared to the distal cases of study (between ~0.01 and ~30 wt%) that does not allow to see a clear correlation. Nevertheless, positive correlations between TOC

and RSEs point toward the idea that these elements are enriched due to the development of reducing conditions under which the OM has been preserved.

Nevertheless, it is clear that CA2, CA3, CA4 and CA5 show correlations with TEs with a higher slope than the distal cases of study. In fact, for a narrow range of TOC, the proximal cases of study show a wider range of TEs. This is maybe due to the dilution of the organic matter by the detrital fraction in this environments (see discussion in "comparison between distal and proximal environments").

Regarding HI, no relationships with RSEs for these environments have been observed (figures 8.1.2B, 8.1.2D and 8.1.2F). It is probable that when HI is calculated, S2 play a fundamental role compared to TOC. Since RSEs show no preferences on the organic matter typology this leads to the disappearing of the correlations.

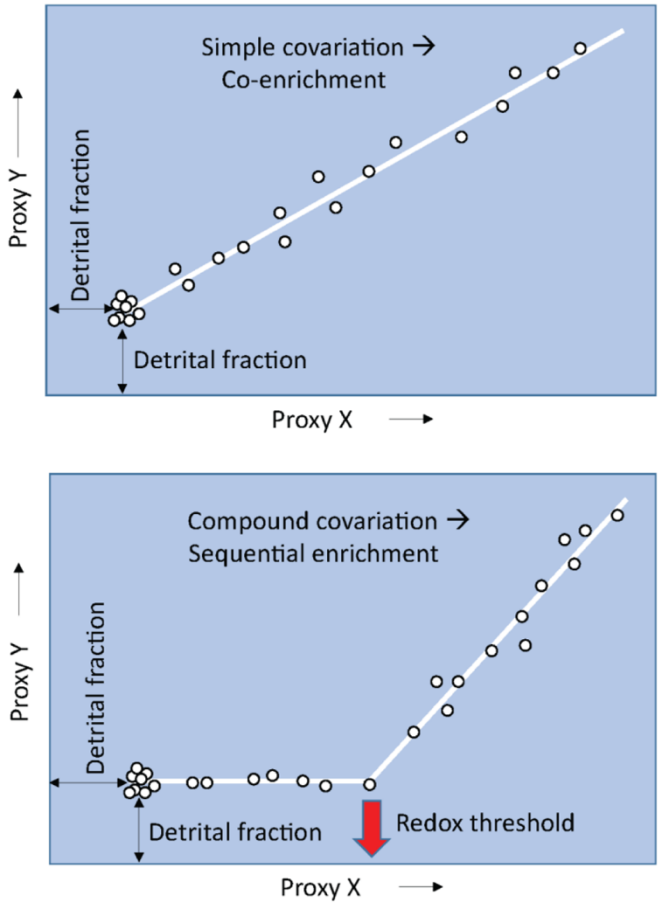

Figure 8.1.11 (from Algeo and Li, 2020): Conceptual relationships among two redox proxies X and Y. (A) Simple covariation of proxies X and Y, reflecting simultaneous co-enrichment in response to reducing depositional conditions. (B) Compound covariation of proxies X and Y, reflecting sequential enrichment, i.e., initial enrichment of X at a higher redox threshold than Y, with the sharp bend (red arrow) representing the redox threshold at which enrichment of Y began. The concentrations of X and Y in the detrital fraction are shown as a cluster of points close to the graph origin, representing an absence of authigenic enrichment of both X and Y under relatively oxidizing conditions.

- Comparison between distal and proximal environments

Two distinct trend are observed for proximal and distal environments between TOC and RSEs (figure 8.1.12): the distal ones show a trend defined by a two-line segment connected by a sharp bend at TOC ~0.5 wt%, under which the trend horizontalizes. Instead, proximal environments

show a simple covariation between TOC and the trace metal (i.e. V, Mo, U) characterized by a linear covariation with a positive slope.

In distal cases of study, the trend suggest that there is an early increase in TOC, that have begun to accumulate at higher redox threshold (i.e. under less reducing conditions) than V, Mo or U. Instead, in proximal environments the linear relationship suggests a co-enrichment of TOC and V, Mo or U. Algeo and Li (2020) suggest that the sharp bend shape of a trend represents a redox threshold (figure 8.1.11).

Following this idea, and considering the low content of TOC, the immaturity of the rock and low TEs enrichments compared to the UCC, we can assume that the sharp bend for the distal cases of study represents a redox threshold (figures 8.1.12A, 8.1.12D and 8.1.12G). Below this threshold, we can speculate that the conditions in the depositional environment were not in favor of accumulation and preservation of the OM leading to no enrichments in TEs. Instead, above the threshold, a co-enrichment of TOC and TEs began, indicating the development of more reducing conditions in the depositional environment together with an increase of the organic matter preservation and TEs enrichments.

Instead, in proximal environments, the linear relationship suggests that the enrichments of TOC and TE has started in the same time (i.e., same redox conditions) (figure 8.1.11; Algeo and Li, 2020). In addition, for TOC <2wt%, proximal environments show lower values of V, Mo and U than the distal environments; in other words, for the same TOC values proximal cases of study show an intercept for the TEs that is lower than the one observed for distal cases of study (e.g. for TOC = 1.5 wt%, V distal environment's intercept ~190 ppm while for proximal environments it is of ~85 ppm; Mo distal environment's intercept ~12 ppm while for proximal environments it is of ~3.5 ppm; U distal environment's intercept ~2.9 ppm while for proximal environments it is of ~ 1.2 ppm ; figures 8.1.12B, 8.1.12E and 8.1.12H). This is may be due to the major detrital supply presents in this kind of environments that dilute the trace metals that precipitate from the water column under reducing conditions causing a decreasing the TEs concentrations that is faster than in the distal environments.

In addition, for the same V, Mo or U value, TOC are higher in proximal environments than distal ones (e.g. for V = 180 ppm, TOC for distal environments is ~0.8 wt%, while for proximal environments it is of ~1.8 wt%; for Mo = 10 ppm, TOC for distal environments it is of ~1.3 wt%, while for proximal environments it is of~1.9 wt%; for U = 2 ppm, TOC for distal environments it is of ~0.7 wt%, while for proximal environments it is of ~1.8 wt%; figures

8.1.12C, 8.1.12F and 8.1.12I). This is in agreement with the idea of Algeo and Li (2020) that represent the concentrations of the two proxy X and Y in the detrital fraction as a cluster of points close to the origin in the graphs in figure 8.1.11, meaning an absence of authigenic enrichment of both X and Y under relatively oxidizing conditions. The higher values of1TOC for similar values of TEs (figures 8.1.12C, 8.1.12F and 8.1.12I) indicates that for similar redox conditions, suggested by similar V, Mo and U concentrations, in proximal environments the organic matter accumulated was higher than in distal environments under the same redox condition (e.g. for V = 180 ppm, in distal environments TOC is ~0.8 wt%, while for proximal environments is ~1.8 wt%; figure 8.1.12C). This idea is consistent with the idea that eutrophication is higher in proximal environments (Brumsak, 2006; Soua, 2011) and with the idea that in proximal environments a dilution of the OM can occur thanks to the detrital supply coming from the land (e.g. riverine runoff).

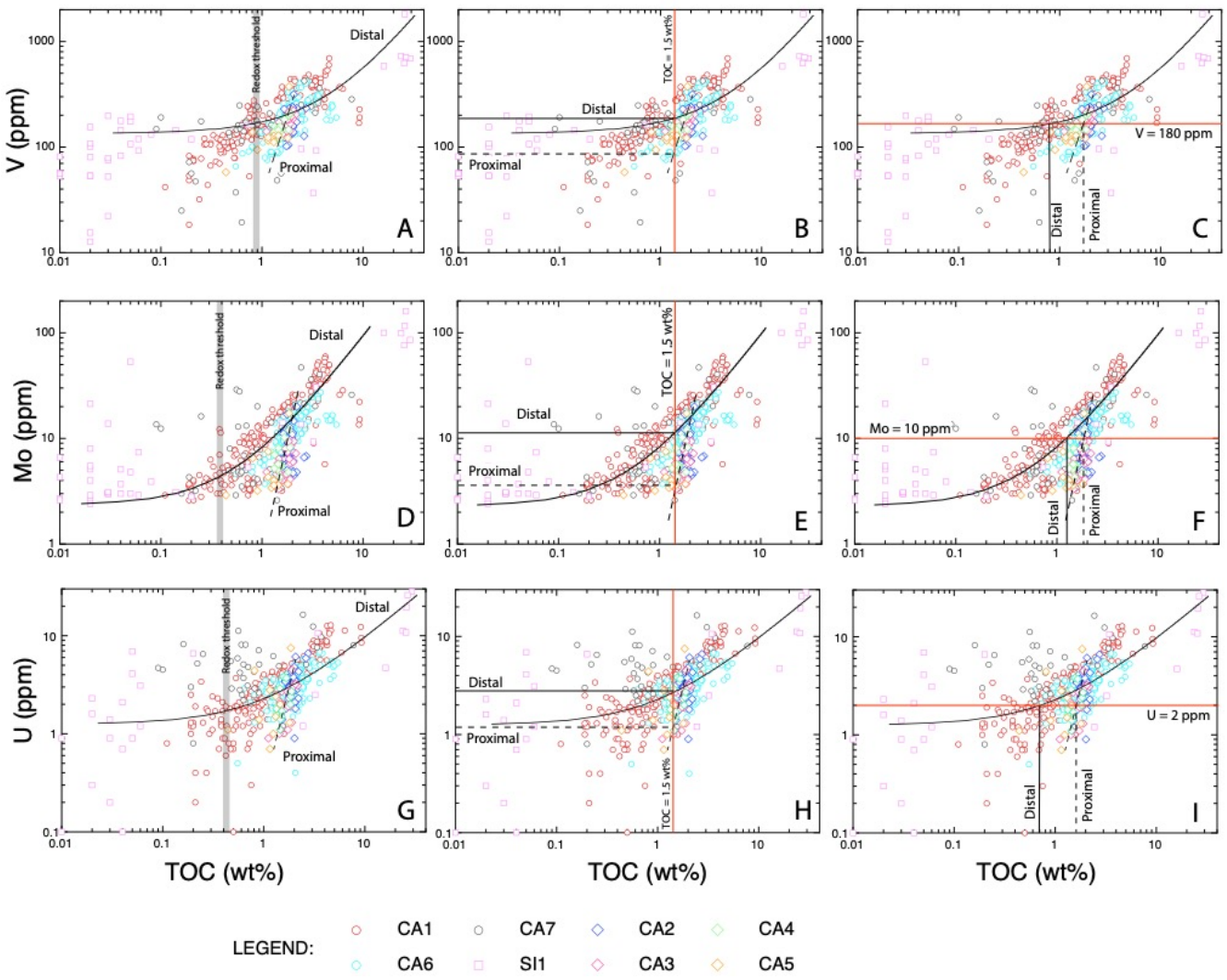

Figure 8.1.12: cross plots of V, Mo and U (ppm) with TOC (wt%) all the Cretaceous cases of study. The differences between distal and proximal environments are highlighted.

Regarding HI, the trends of proximal and distal environments are mostly overlapped for TEs, indicating no differences between the two typologies of depositional environments (figures 8.1.13A, 8.1.13B and 8.1.13C). The differences in HI between the cases of study are marked by differences in the organic matter typology. Indeed, distal environments show HI values related to marine organic matter (marine algae, bacteria - HI between 200 and 650 mg HC/g TOC), while proximal environments show HI values rarely above 350 mg HC/g TOC indicating a major continental supply of the organic matter (marine algae and lignin). Specifically, CA3 show HI values between ~20 and ~275 mg HC/g TOC with TOC between ~1 and ~2 wt% indicating that the organic matter is mainly lignin deposited coastal plains, delta environments or through turbiditic fluxes. TOC is one of the main parameters to calculate HI, this means that HI is not only related to the organic matter typology but also on the TOC. Indeed, HI is calculated with the following formula HI=S2*100/TOC, where S2 is the Residual Petroleum Potential (measured with Rock-Eval pyrolysis) produced by thermal degradation of kerogen. In turn, samples with low TOC (< 1 wt%) can show low HI (<200 mg HC/g TOC) values, but this does not mean necessarily that the organic matter is not marine. Consequently, a multi proxy approach and a comparison between TOC and HI is necessary to assess the organic matter typology and the depositional environment.

Moreover, the relationship between the HI and the OM typology means that to different HI values could correspond similar values of V, Mo or U, that are related to the redox conditions. That is why an horizontalization compared to TOC vs TEs trend is observed. In fact, the redox conditions do not determine which type of OM is deposited but only the amount of the organic matter preserved, leading to a decreasing of the slope of the correlation line (black line in figure 8.1.13).

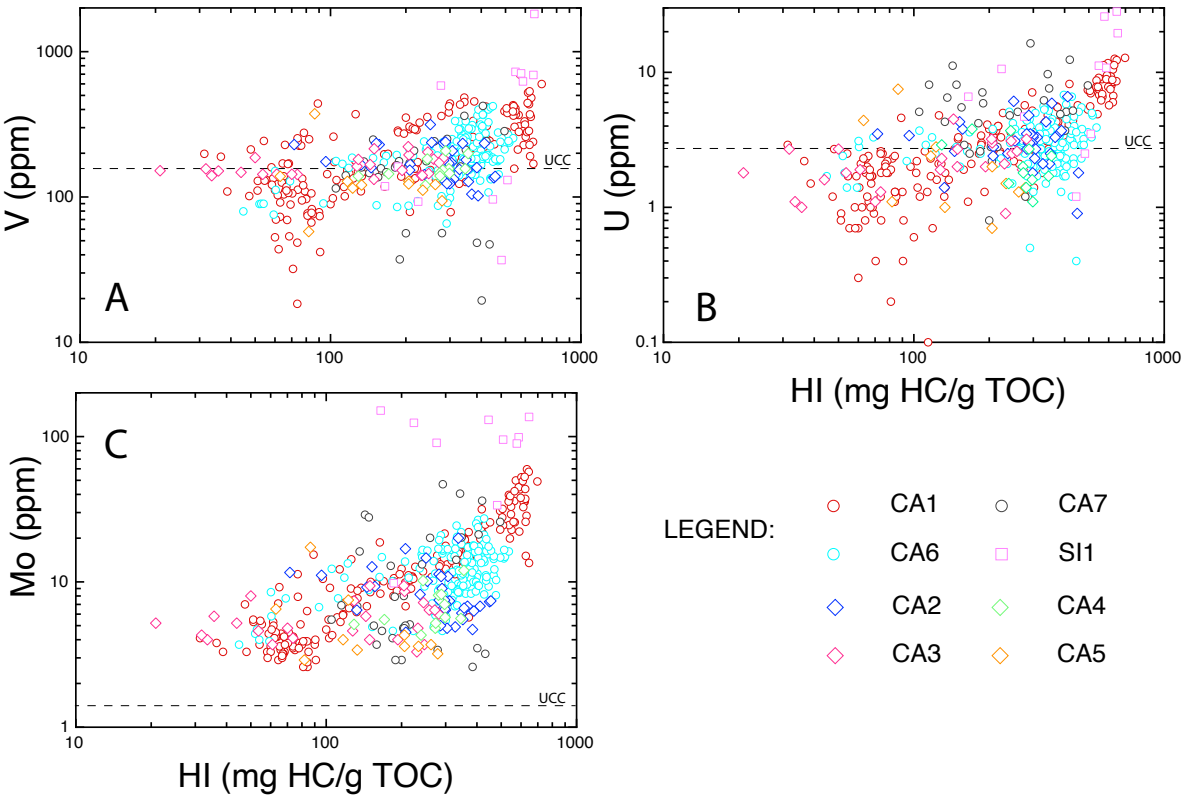

Figure 8.1.13: cross plots of V, Mo and U (ppm) with HI (mg HC/g TOC) for all the Cretaceous cases of study.

In conclusion, in the Cretaceous cases of study, the positive relationship between the organic parameters and TEs can be used to trace both redox conditions and organic matter content into a sedimentary marine rock. This is possible because of the positive relationship of V, Mo and U with TOC and HI. In particular, on the basis of the trend lines in figures 8.1.12, it can be assumed that to a given content of V, Mo or U corresponds a specific content in organic carbon (TOC) allowing to trace the OM content. In addition, HI can give us indications about the OM typology and, in turn, on the depositional environment. However, the relationships between TOC and TEs can give us indications about the detrital supply in a depositional environment that can led to lower enrichments in trace metals for similar TOC values. Thus, the dilution of the TEs caused by the higher detrital supply in the proximal environments has to be taken in account.

Elements related to the organic matter: Ni and Cu

The weak correlation between Ni, Cu and the naphtogenic parameters indicates that the organic matter is not the principal host phase for these two metals. This is also highlighted by the lack of correlations with HI. Despite these elements are delivered to the sediments with organic

matter bounded to organometallic complexes (Tribovillard et al., 2006), once the organic matter is degraded, Ni and Cu are released and trapped into authigenic phases. In particular, Ni is mainly taken up by the organic matter and the detrital fraction under anoxic conditions and by pyrite or authigenic sulphides under euxinic conditions; whereas Cu can be fixed in nontronite or smectite minerals under anoxic conditions or can be taken up by pyrite or forms its authigenic sulphides (CuS or CuS_2) under reducing conditions (notably bacterial sulfate reduction conditions) (see cap. 3 and references therein).
This means that if they are not transported by organic particles, they do not show significant enrichments, even if anoxia develops rapidly. Thus, if accompanied by discrete values of TOC, enrichments in Ni and Cu indicates high OM fluxes towards the sediments and reducing conditions that allowed Ni and Cu fixation within the sediments (Tribovillard et al., 2006). Therefore, low enrichments of Ni and Cu compared to the UCC values may indicate (i) not reducing conditions; (ii) low organic matter flux toward the sediments or (iii) dilution by the detrital flux toward the sediments.

The combination of these two last processes could be inferred for our cases from the Central Atlantic (both proximal and distal), due to the fact that oxygenated conditions for the samples with TOC > 1wt% are excluded, as testified by enrichments in V, Mo and U. In particular, for proximal environments the dilution process may have played a fundamental role (see discussion below about the detrital proxies) in diluting both the organic matter and the trace metals.
Contrarily, SI1 show enrichments in Ni and Cu, especially with high contents of TOC (>10 wt%). In the paper of Bonacina et al. (2020), has been demonstrated that the deposition of the OM-rich layers (black shales) is related to periods of high organic matter productivity, sluggish oceanic circulation, low terrigenous input, fine-grained sedimentation (mainly illite and aeolian dust) for decantation and euxinic conditions. Thereby, enrichments in Ni and Cu are due to both reducing conditions that led to high preservation of an abundant flux of OM.

In conclusion, Ni and Cu are not reliable redox conditions proxies but they can give information about the organic matter flux towards the sediments. In addition, under reducing conditions, the OM is not their main host phase.
All these considerations indicate that care should be taken in the use of Ni and Cu as redox conditions. Therefore, a multi proxy approach is the most useful and successful to trace ancient redox conditions of a depositional environment and organic matter input.

No differences are visible for proximal and distal environments; indeed the samples are overlapped drawing a single trend (black line in figure 8.1.14). This could be related to the fact that the proximal environment are characterized by dilution of a high amount of organic matter by the detrital fraction leading to a trend that is more similar to the distal cases, in which there is a lower organic matter flux toward the sediments but the dilution is minimal compared to the preservation. This idea is supported also by the differences in the correlations between V, Mo and U with TOC (see above, figure 8.1.12).

This aspect highlights once again the importance of using a multi proxy approach to reconstruct the depositional conditions of a rock.

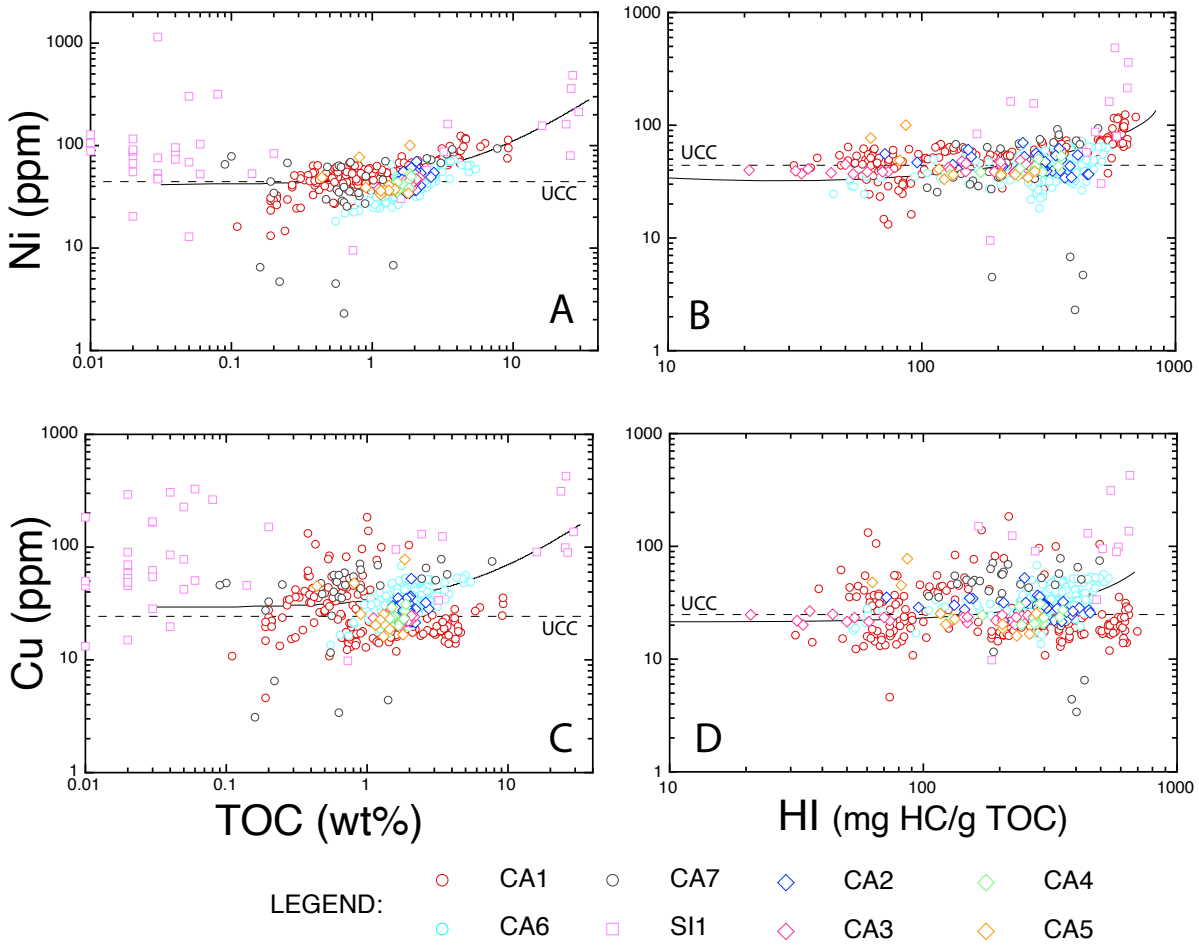

Figure 8.1.14: cross plots of Ni and Cu (ppm) with TOC (wt%) and HI (mg HC/g TOC) for all the Cretaceous cases of study.

Elements not related to the organic matter: Th, Zr, Al, Mn

- Distal environments

The negative relationship or the lack of it between Th, Zr, Al and TOC (figures 8.1.5A, 8.1.6A and 8.1.7A) in the distal cases of study indicate that the OM is not the host phase for these elements. Differently, the negative relationship between Mn and TOC (figure 8.1.8A), marked especially by SI1 is related to the behavior of Mn under with variable redox conditions. In particular, Mn show enrichments under oxidizing conditions due to the accumulation of Mn oxyhydroxides, while under reducing conditions, and in turn, with high OM contents Mn is dissolved in the water. Thus, the negative relationship of Mn and TOC is not related to the host phase of Mn but to the redox conditions.

Negative correlations between Th, Zr, Al and TOC are always observed for the source sample of CA1, indicating a decrease in the clays and micas content together with an increase of the carbonates content. In addition, in CA6 Th and Zr show lower contents compared to the other distal cases of study and show weaker correlations with total clays + micas.

Contrarily, the positive relationship between Th, Zr, Al and total clays + micas indicate that these minerals are the main host phases for these elements. Moreover, Zr and Al show a well-marked correlation (figure 8.1.15A). This may indicate that they are hosted by the same minerals (clays and micas).

Finally, a very weak negative correlation has been observed between total clays and micas and TOC for the distal cases of studies (figure 8.1.16A), indicating that the deposition of the organic matter is not accompanied by high detrital supply or that the organic rich-layers are not constituted by mainly by clayey material (e.g. black shales).

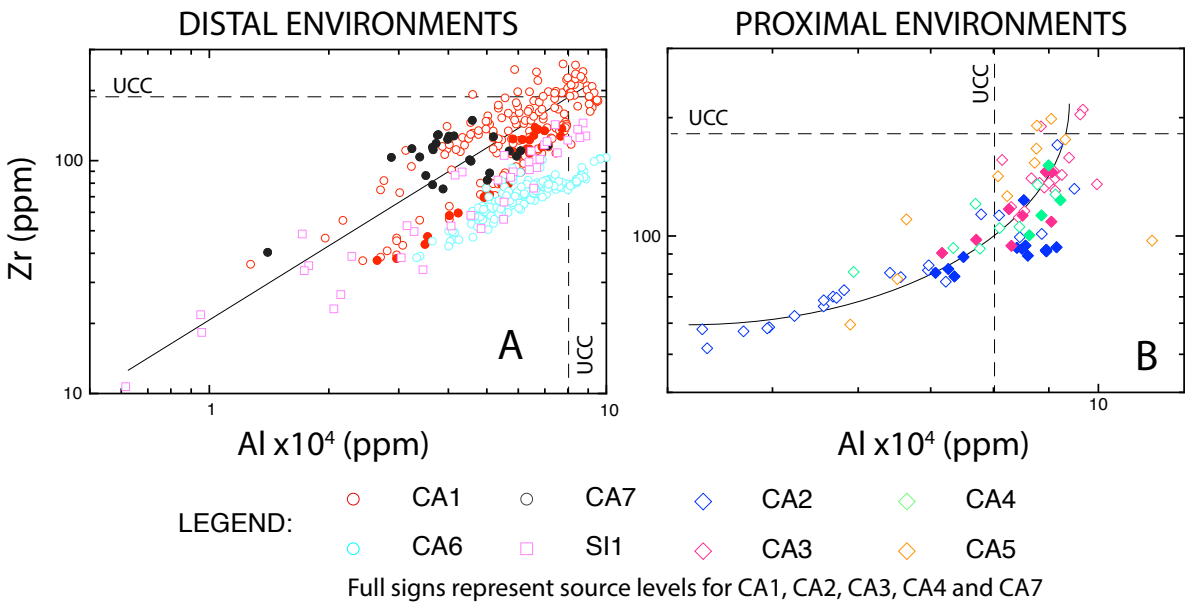

Figure 8.1.15: cross plots of Zr (ppm) and Al (ppm) for distal and proximal Cretaceous cases of study.

- Proximal environments

As for the distal cases of study, the negative relationship between Th, Zr, Al, Mn and TOC (figures 8.1.5B, 8.1.6B, 8.1.7B and 8.1.8B) in the proximal cases of study indicate that the OM is not the host phase for these elements. Again, well-marked positive relationship between Th, Zr, Al and total clays + micas indicate that these minerals are the main host phases for these elements. Also, Zr and Al show a positive correlation (figure 8.1.15B), confirming that they are hosted by the same mineralogical phases (clays and micas). Finally, no correlations has been observed between TOC and total clays + micas (figure 8.1.16B) indicating that the mineralogical content cannot help us to distinguish between different OM contents.

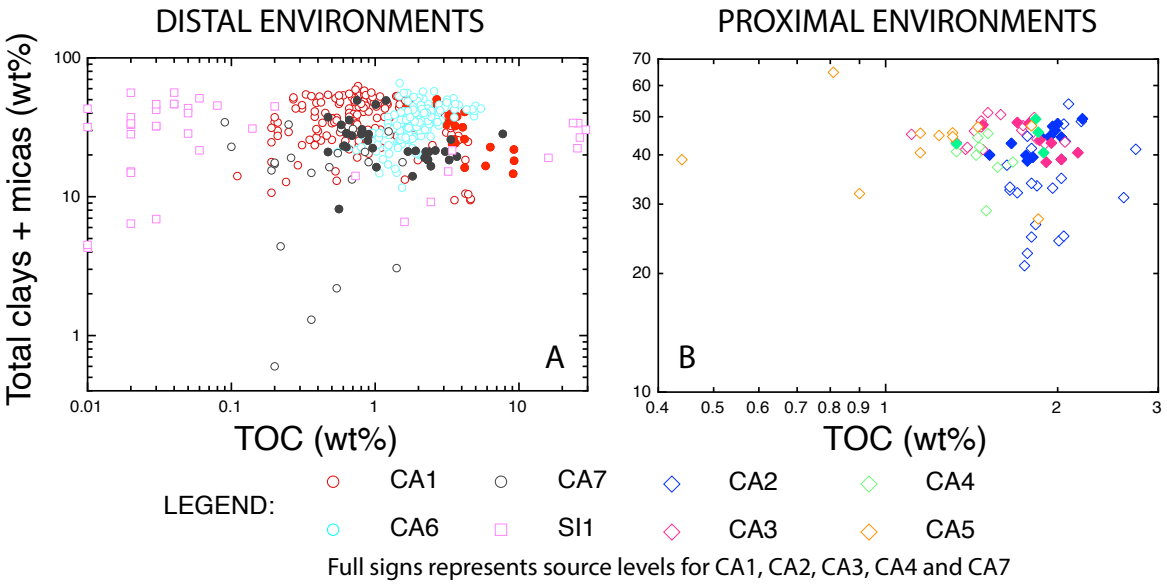

Figure 8.1.16: cross plots of total clays + micas (wt%) and TOC (wt%) for the Cretaceous cases of study divided according to the environmental typology (distal and proximal).

- Comparison between distal and proximal environments

Thorium, zirconium and aluminum are not related to the organic matter content in both proximal and distal environments but to the detrital fraction, represented mainly by clays and micas. In particular:

- The positive relationship of Th with total clays + micas and Zr (figures 8.1.5E and 8.1.5F) indicates that Th is hosted mainly by the detrital fraction or by the same phases that host Zr. Actually, Jones and Manning (1994) suggest that Th is an immobile elements that resides mainly in the detrital fraction (clays, aluminosilicates, resistant minerals);
- Proximal environments show an Al average of ~7.9 x 10^4 ppm, that is closer to the UCC value (8.0 x 10^4 ppm; McLennan, 2001) compared to the distal environments (average of ~5.2 x 10^4 ppm). This indicate that composition of the samples of the proximal environments is closer to the UCC composition. Thereby, a higher detrital influx can be inferred for these samples that obfuscates the enrichments in organic matter and RSEs thank to a dilution process. In fact, it is probable that those samples have deposited under reducing conditions under which enrichments in TOC and RSEs should occur. However, the dilution due to a higher detrital supply led to a damping of the values of these redox proxies (see discussion above);

- The stronger negative correlation observed between Th, Zr, Al and TOC in the proximal environments compared to the distal ones is likely related to the fact that the increase of these elements, and thus of the detrital fraction (clays, aluminosilicates, resistant minerals), obfuscates the OM content, thus resulting in a narrow range of TOC for a wide range of TEs (V, Mo and U) in proximal environments;
- Zr and Al correlate with illite type in the distal environments while they correlate with kaolinite in proximal environments (figure 8.1.17). This variability in clay distribution is consistent with the depositional environment: illite type is a fine-grained clays that can deposit under stagnant conditions for decantation, whereas kaolinite is related to a more energetic environment with a higher contribution of the riverine supply (Parkinson, 1996). In figures 8.1.17A and 8.1.17C, SI1 seems to not show correlations between Al or Zr and illite type despite its environment is distal. However, in Bonacina et al. (2020) it is demonstrated that also in this section illite increases with the development of reducing and stagnant conditions. These considerations indicates that the differences in the depositional environments are mirrored by differences in the typology of clays deposited and not by their total amount: proximal environments show a predominance of kaolinite over illite, vice versa for the distal environments;

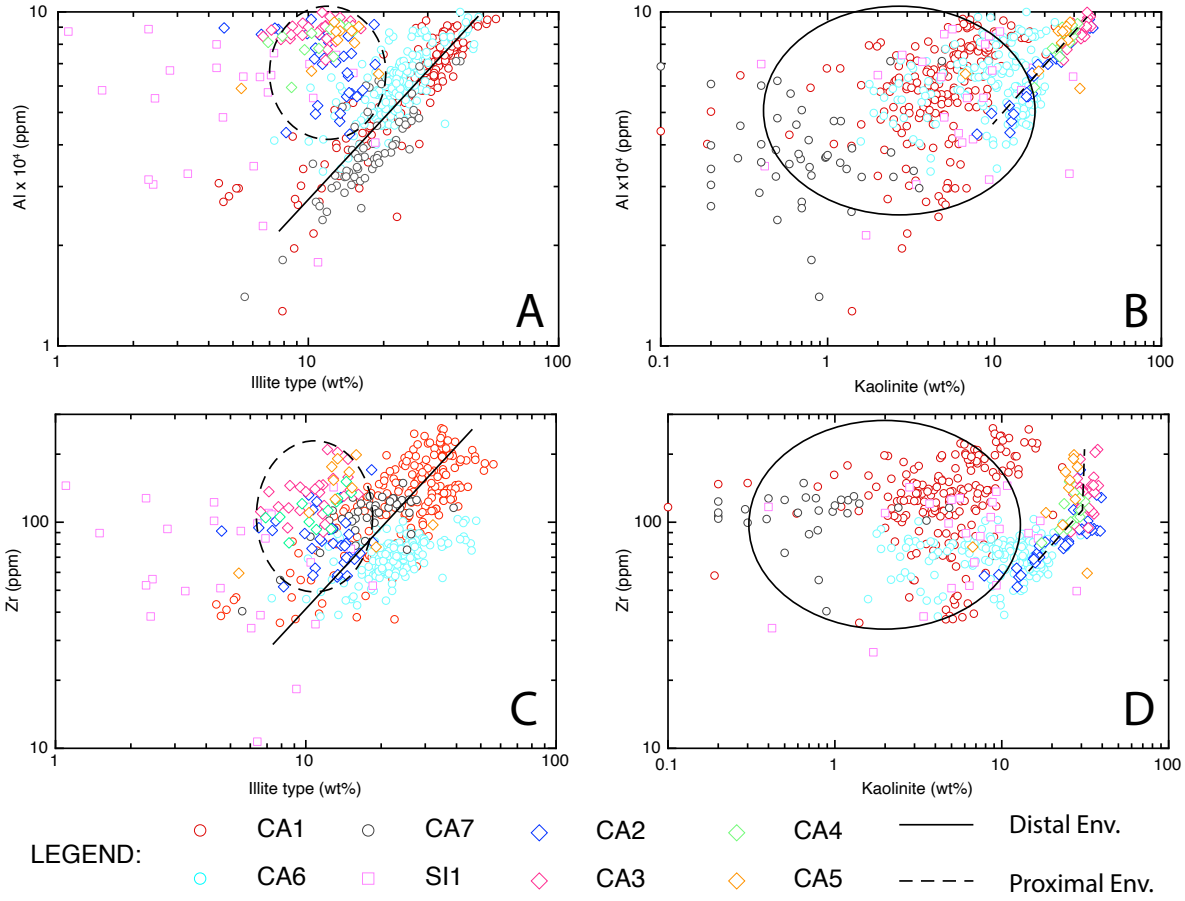

Figure 8.1.17: cross plots of Zr (ppm) and Al (ppm) with illite type (wt%) and kaolinite (wt%) for both distal and proximal Cretaceous cases of study. The differences between the two environmental typologies are highlighted.

- The negative relationship between Mn and TOC for all the cases of study indicates the development of reducing conditions in the depositional environments. However, proximal cases and some samples of CA6 (younger than the Cenomanian) show a different trend compared to the distal environments (figure 8.1.18). Looking at the mineralogical features of the first samples, we can notice that a carbonate content below ~15 wt% is related to low manganese contents as for the proximal cases of study. This could be related to a deepening of the depositional environment that led to a less carbonaceous and oxygen supply leading to a decrease in Mn content. All these considerations about Mn could be not possible without a comparison with other elements' behavior. Again, the importance of a multi-proxy approach is remarked in a study of this type. Regarding SI1 (Fontana Valloneto), the samples preceding the Bonarelli Horizon, relating to the Late Albian and Cenomanian, are very rich in Mn. Probably in these samples Mn forms microcrystalline phases (e.g. oxy - hydroxides) or

amorphous phases. Indeed, they are visible in the samples by hand but they are not detected by XRD, although there is a large amount of manganese. In these samples they form well-marked black levels, probably incrustations formed during oxygenation events of the water-sediment interface. This has also been discussed in the paper of Bonacina et al. (2020).

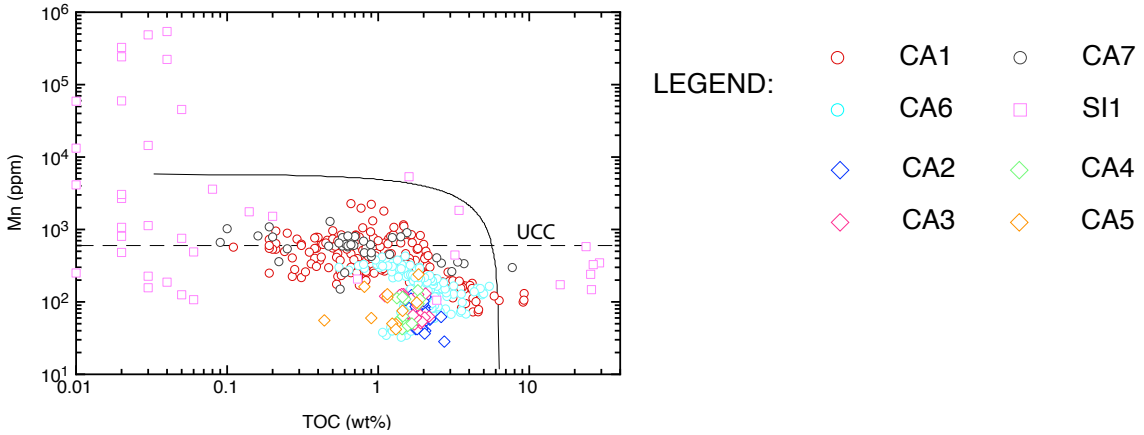

Figure 8.1.18: cross plot of Mn (ppm) and TOC (wt%) for both distal and proximal Cretaceous cases of study.

- Mineralogical considerations

In distal environments, different relationships have been observed between the carbonates content, clays and micas content and TOC (figures 8.1.19A, 8.1.19C and 8.1.19E). The source samples of CA1 show a positive correlation between TOC and the carbonates content and a negative correlation with total clays + micas, indicating an increase of the carbonate content in these samples at increasing organic matter content. Viaggi et al. (2019) suggest that the increase of the carbonates in these samples is related to an increase in the foraminifera shell production in a period of eutrophication during the OAEs intersected by the well. On the contrary, CA6 shows a weak negative relationship between carbonates and TOC and a weak positive correlation with total clays and micas, indicating that the deposition of the OM is accompanied by the deposition of clays and micas and not by carbonates, as expected in an anoxic environment. Indeed, the most common source rocks are represented by shales because they are constituted by fine-grain size that can deposit, for instance, under stagnant conditions (Novelli et al., 2004). The latter are very common during the OAEs deposition and are caused by an increase of the atmosphere and seawater temperature, eutrophication and anoxic condition at the sediment-water interface (Takashima et al. 2006; Jenkyns, 2010). In addition, the fine grain size does not easily allow fluids to pass through them. Indeed, the oxygen contained in the water present in the pores is rapidly used up during the initial oxidation of any

organic matter contained and as they do not allow replacement with other water, a highly anoxic environment is created inside these sediments and the remaining organic matter can be preserved against further alteration (Novelli, 2004). Moreover, as CA6, very weak correlations have been observed between carbonates, clays and micas and TOC for CA7.

For proximal environments no relationship has been observed between the carbonates content, clays and micas content and TOC (figures 8.1.19B, 8.1.19D and 8.1.19F) due to the fact that mostly the amount of these phases is constant in the samples.

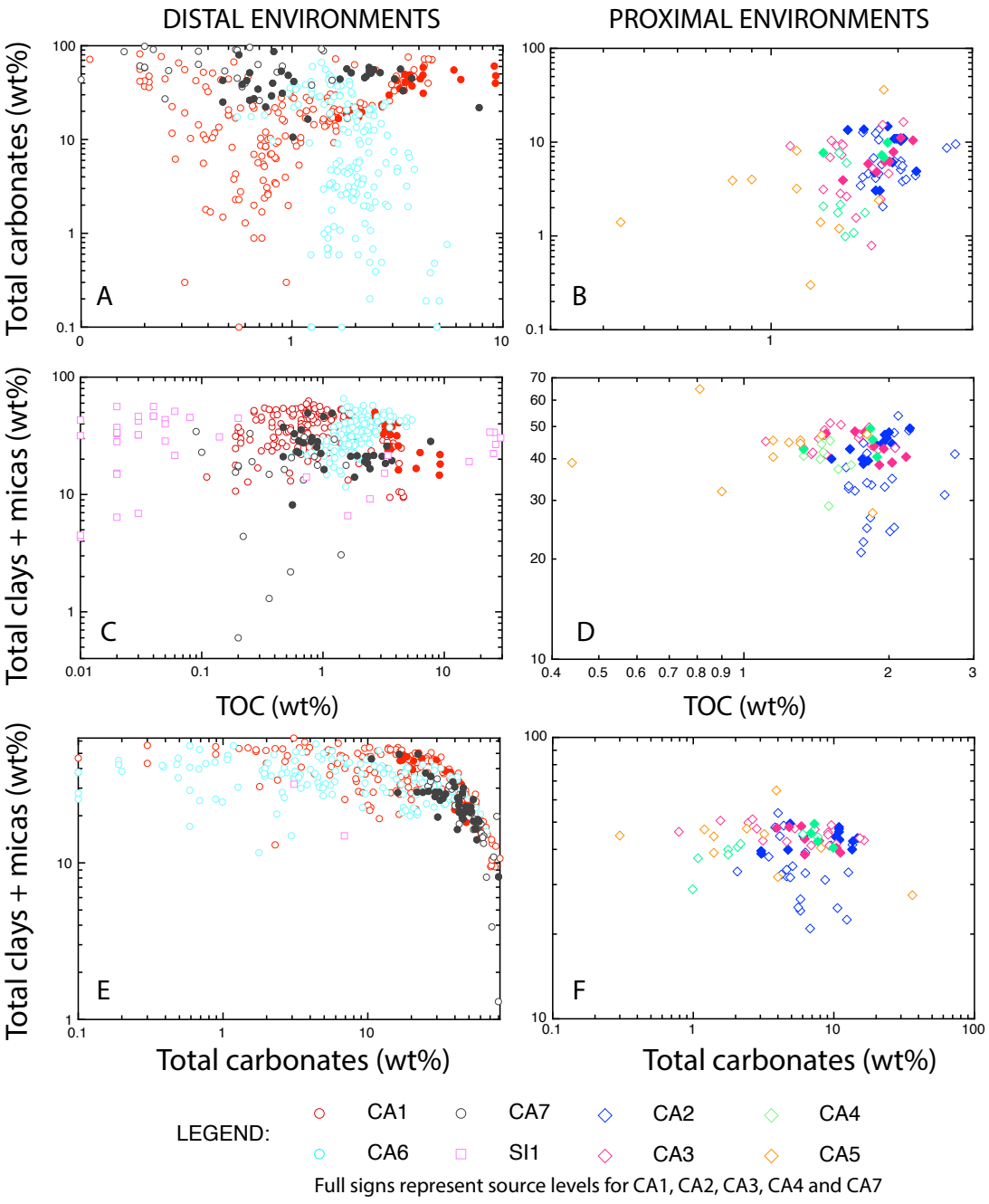

Figure 8.1.19: cross plots of total carbonates (wt%), total clays + micas (wt%) and TOC (wt%) for the Cretaceous cases of study divided according to the environmental typology (distal and proximal).

Anomalies of trace and Rare Earth Elements (REEs)

Anomalies in V, Mo, U, Pb, Sr and Ba have been calculated and are defined as in chapter 3.3. The general shape of REEs patterns has been interpreted has related to the provenance of the sediments that form the rock and to the mineralogical content. This is confirmed also by the values of the elements (both REEs and TEs) that do not differ much from 1, i.e. the value of the Upper Continental Crust, especially for CA1. This is maybe due to the fact that McLennan (2001) used a mix of terrigenous sediments to calculate the UCC values. In particular, the author used both "fine-grained" lithologies (i.e. shales, muds and silts) and "coarse-grained" lithologies (e.g. sand, sandstones and tillites) that are maybe closer to CA1 composition than CA5. CA5 (proximal environment) shows values in the incompatible elements (left side of the graph in figure 8.1.9A) that are farer from the UCC value compared to CA1 (distal). This could be due to the fact that the REEs pattern of CA5 could be affected by the terrigenous flux that brought materials from the continent, modifying the pattern based on the provenance of the sediments.

Regarding TEs, the composition is very different for each case of study. CA5 shows positive anomalies in Ba independently from the TOC class and any mineralogical phase; these are most likely related to the pollution due to drilling mud. Also, Mo* shows positive correlation with TOC highlighting its relationship with the content of organic matter and its preservation under anoxic redox conditions (figure 8.1.20A). Thus, the positive anomaly in Mo can be related to the presence of organic matter (figure 8.1.20C) and its values depends on the amount of OM present in the samples. The weak negative anomaly in V is related to the environment typology. In fact, V* show negative correlations with kaolinite (figure 8.1.20C), indicating that the increasing of kaolinite (mostly related to terrigenous fluxes toward the basin) led to a depletion of V.

The anomaly in Eu (Eu*) is related to the presence of plagioclase since it correlates positively with this mineralogical phase (figure 8.1.20E) and it is linked to the provenance of the plagioclase. Also, Tm* show a very weak positive correlation with kaolinite (figure 8.1.20B). Thus, the positive anomalies in Tm can be related to an increase of this element with kaolinite. that is mainly related to the terrigenous input. Contrarily, negative anomalies are observed for Zr and Ti (figure 8.1.20C). In particular, Ti* and Zr* correlate positively with illite (figures 8.1.20D and 8.1.20F). Thus, the impoverishment of these sample in illite (compared to kaolinite that is more abundant) causes negative anomalies in Zr and Ti.

Sr* is positively correlated to the total carbonates content indicating that the increase of these mineralogical phases cause an increase of the anomaly (figure 8.1.20G). Thus, the negative anomaly in Sr in figure 8.1.20C is related to the low carbonate content in the samples. In addition, the negative anomaly is more prominent in the class with TOC > 1.2 wt% indicating a decrease of carbonates in these samples. Finally, no significant correlations have been observed between Y* and Rb* and any mineralogical or organic phase indicating that maybe the negative anomalies (figures 8.1.20A and 8.1.20C) are inherited by the provenance of the sediments or that they are distributed in more than a mineralogical phase.

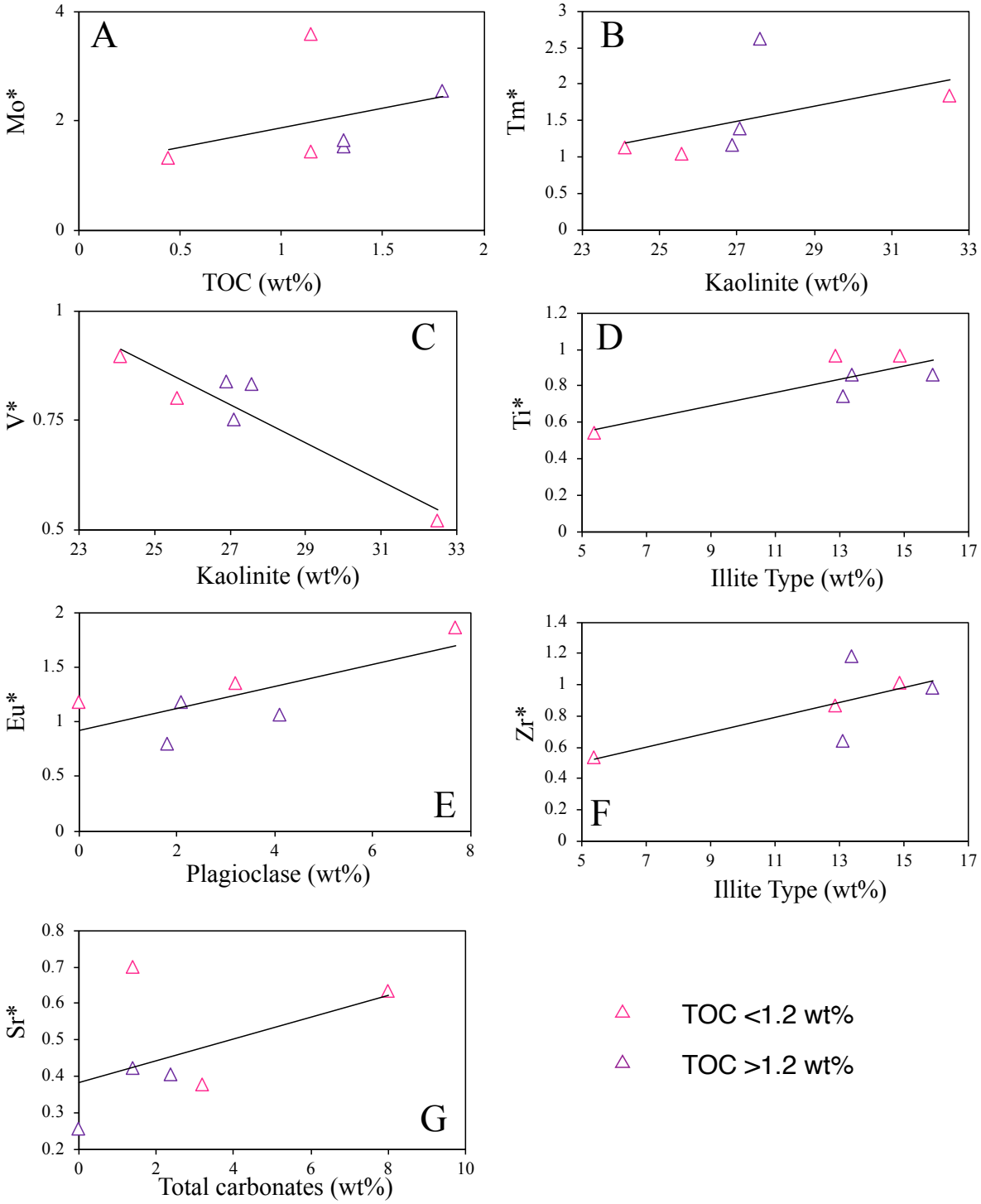

Figure 8.1.20: correlations between (a) Mo* and TOC (wt%); (B) Tm* and kaolinite (wt%); (C) V* and kaolinite (wt%); (D) Ti* and illite type (wt%); (E) Eu* and plagioclase (wt%); (F) Zr* and illite type (wt%); (G) Sr* and total carbonates (wt%) for CA1. * indicates the anomaly as explained in chapter 3.3.

Regarding CA1, positive anomalies in redox sensitive elements (V, Mo and U) appear increasing the TOC content (figure 8.1.21D): they are not visible for TOC less than 1wt%, above they appear and become well-marked with TOC > 4wt% indicating the OM content. This

is confirmed by the positive correlations of V*, Mo* and U* with TOC (figures 8.1.21A, 8.1.21D and 8.1.21G). However, for the source samples that own to the OAE 1d, OAE 2 and OAE 3 a negative correlation between V*, Mo*, U* and TOC can occur. This negative covariation, as explained above, is and is related to periods of intense reducing conditions (e.g. euxinia) that can drawdown the global metals inventory in the oceans due to the abundance of anoxic sinks compared to the metals supply (Algeo, 2004).

Contrary to CA5, CA1 shows positive anomalies in Sr (figure 8.1.21D), especially with TOC > 4 wt%, in agreement with the positive covariation of TOC and carbonate content and highlighted by the positive correlation of Sr* and the carbonate content (figure 8.1.21B).

Negative anomalies in Ti and Zr are also observed, consistent with the environment typology (distal, low terrigenous supply). In particular, Ti* shows a positive covariation with plagioclase (weak), quartz and total clays + micas (figures 8.1.21E, 8.1.21H and 8.1.21C), thus the low content of these phases in this typology of environment cause a negative anomaly. Zr* shows a negative correlation with TOC (figure 8.1.21F). This means that the increase of TOC results in a negative anomaly in Zr (figure 8.1.21D); contrarily, as for Ti, low concentrations of quartz, plagioclase, clays and micas can cause negative anomalies. Finally, Hf*, Ta* and Eu* do not correlate with any mineralogical phases indicating that they do not have a single host phase and likely the anomalies in these elements are inherited from the provenance of the sediments.

Importantly, the negative anomalies for the detrital elements (Ti and Zr) are more prominent increasing the TOC content, indicating that the development of reducing conditions in this environment is related to a decrease of the detrital supply (mainly clays, micas and quartz). This is in agreement with the idea that during the OAEs a slowdown of the ocean circulation occur, leading to a decreasing of the terrigenous supply.

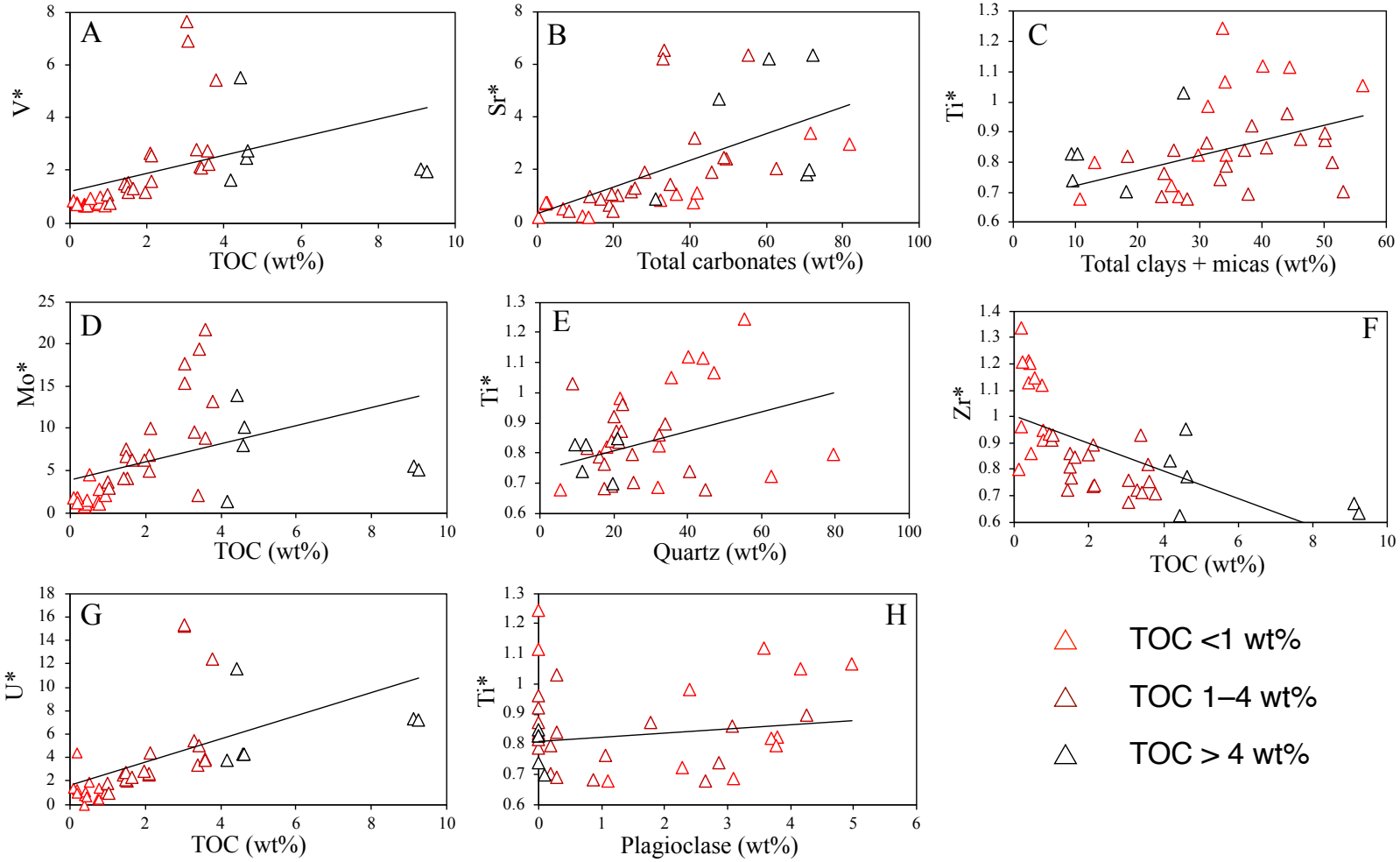

Figure 8.1. 21: correlations between (A) V* and TOC (wt%); (B) Sr* and total carbonates (wt%); (C) Ti* and total clays + micas (wt%); (D) Mo* and TOC (wt%); (E) Ti* and quartz (wt%); (F) Zr* and TOC (wt%); (G) U* and TOC (wt%); (H) Ti* and plagioclase for CA5. * indicates the anomaly as explained in chapter 3.3.

Summarizing:

- Some elements can give information about the organic matter content and, in turn, on the redox conditions (e.g. V, Mo and U). However, a cautious approach needs to be maintained in the interpretation of the anomalies of these elements, especially in proximal environments (e.g. V and U in CA5);
- Sr always give information about the carbonate content;
- Several elements can give information about the terrigenous supply. Especially, Ti and Zr can give information about the terrigenous influx. However, these elements are not always related to the same mineralogical phase; in CA1 they are positively related to quartz, plagioclase, clays and micas (Ti), whereas negatively related to TOC (Zr), resulting in negative anomalies since kaolinite content is low and TOC is high; while in CA5 they are related by illite causing negative anomalies since illite content is low compared to kaolinite. Thereby, a cautious approach needs to be adopted when these elements are interpreted.

In conclusion, anomalies can give us direct information about both organic matter content, carbonate content and detrital supply. Indirectly, we can relate anomalies in RSEs (i.e. V, Mo and U) to redox conditions, Sr and Ti-Zr anomalies to the carbonate content and detrital supply, respectively.

8.2 TRIASSIC IMMATURE SOURCE ROCKS

8.2.1 Results

Elements related to the organic matter: V, Mo, U, Ni and Cu

In NI1, V varies between ~4.5 and ~800 ppm, with an average of ~102 ppm; in NI2 it varies between ~155 and ~3900 ppm with an average of ~2450 ppm. Mo shows values between ~3 and ~134 ppm with an average of ~19 ppm in NI1, while in NI2 it shows values between ~50 and ~335 ppm, with an average of ~175 ppm. U shows concentrations between a minimum of ~2 and a maximum of ~30 ppm, with an average of ~8.5 in NI1, whereas it varies between ~5 and ~67 ppm in NI2, with an average of ~35 ppm. Finally, in NI1 Ni and Cu varies between ~2.5 and ~155 ppm and between ~1 and ~220 ppm, respectively. The averages are1~18.5 ppm for Ni and ~18.7 ppm for Cu. In NI2, Ni and Cu show concentrations between1~13 and ~280 ppm and between ~3.5 and ~600 ppm, respectively. The average values are ~170 ppm for Ni and ~320 ppm for Cu.

A linear positive well-marked correlation is observed between V, Mo, U, Ni, Cu and TOC (figures 8.2.1A, 8.2.1C, 8.2.1E, 8.2.2A and 8.2.2B) for the Triassic Source Rocks, as indicated by the trend lines (black lines in the figures 8.2.1A, 8.2.1C, 8.2.1E, 8.2.1A and 8.2.2B) along which all the samples are arranged.

With TOC < 1 wt% for V and < 3 wt% for Ni and Cu, NI1 shows concentrations below the UCC value (107 ppm, 44 ppm and 25 ppm, respectively; McLennan, 2001), above these TOC values, both NI1 and NI2 show concentrations above the UCC value for these trace metals. On the contrary, with any value of TOC, both NI1 and NI2 show values of Mo and U above UCC concentration (1.5 ppm and 2.8 ppm, respectively; McLennan, 2001).

In addition, a positive linear correlation has been observed between Ni, Cu and S (figures 8.2.2E and 8.2.2F). S varies between a minimum of ~170 ppm and a maximum of ~ 6.8 x $10^3$1ppm, with an average of ~2 x 10^3 ppm for NI1, while it shows values between ~1.9 x 10^3 ppm and ~37 x 10^3 ppm and an average of ~22.2 x 10^3 ppm for NI2. The group of samples of NI1 circled in figures 8.2.2A, 8.2.2B, 8.2.2E and 8.2.2F, represents the samples with TOC > 6wt%, with Ni and Cu values higher than UCC and that in relation with S draw a separate trend compared to linear one that connects NI1 to NI2 (black lines in figures 8.2.2A, 8.2.2B, 8.2.2E and 8.2.2F).

On the contrary, no correlations are observed between V, Mo, U, Ni, Cu and HI if all the samples are considered. If NI1 and NI2 are considered separately, two trends are observed. NI1

shows a "U" relationship (figures 8.2.1B, 8.2.1D, 8.2.1F, 8.2.2B and 8.2.2C): with HI increasing from ~100 to ~300 mg HC/g TOC a decreasing of the RSEs content is observed, with HI increasing from ~300 to ~700 mg HC/g TOC a positive relationship with the trace metals occur. HI values for NI1 indicate that the organic matter is produced mainly in a marine environment and it is constituted mainly by marine algae, bacteria and lignin. Contrarily, NI2 shows a negative correlation between HI and RSEs. HI values together with high S contents for NI2 indicate that the organic matter formed in a marine/carbonaceous environment and it is constituted mainly by marine algae and bacteria.

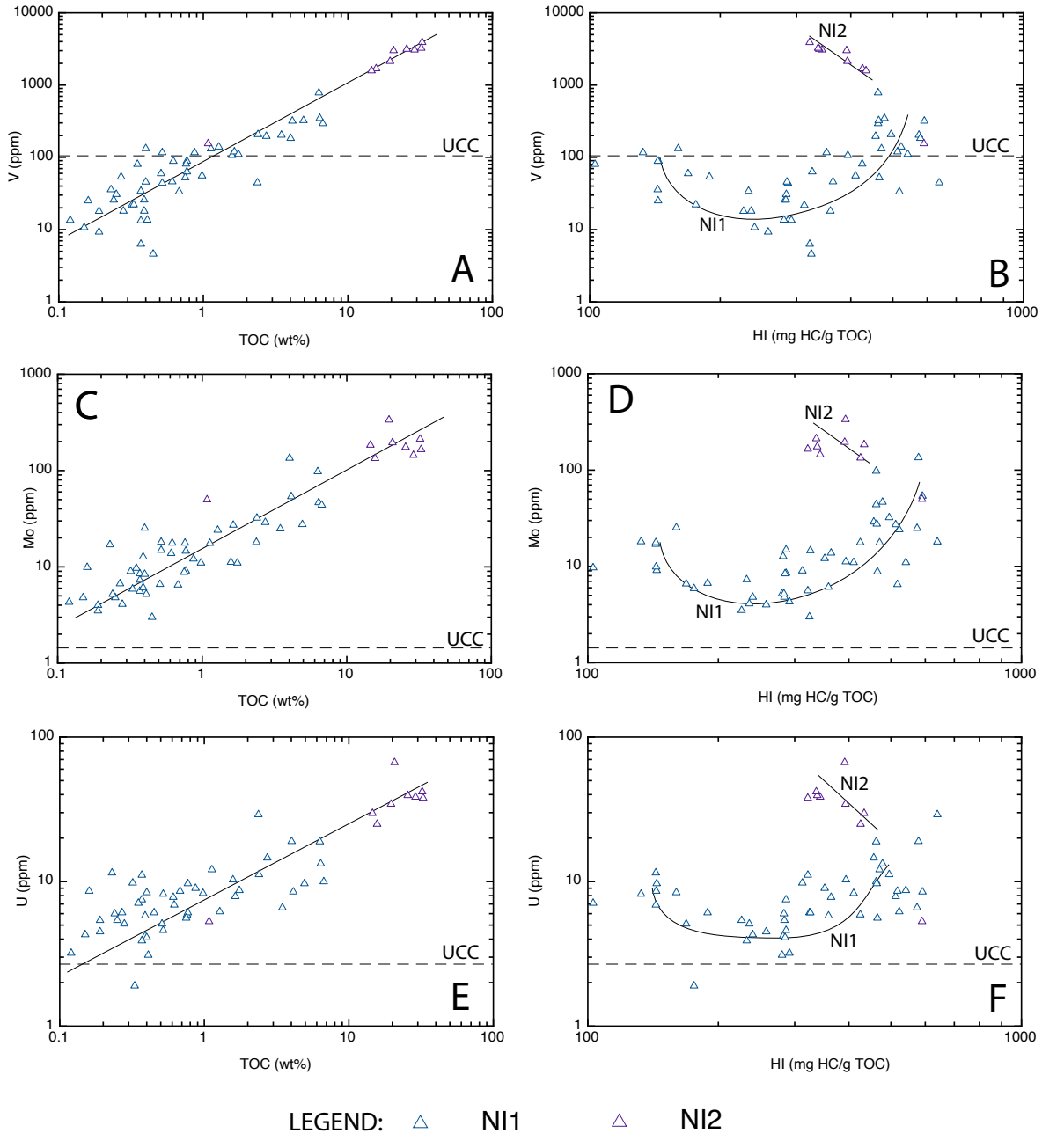

Figure 8.2.1: cross plots of V, Mo and U (ppm) with TOC (wt%) and HI (mg HC/ g TOC) for the Triassic cases of study.

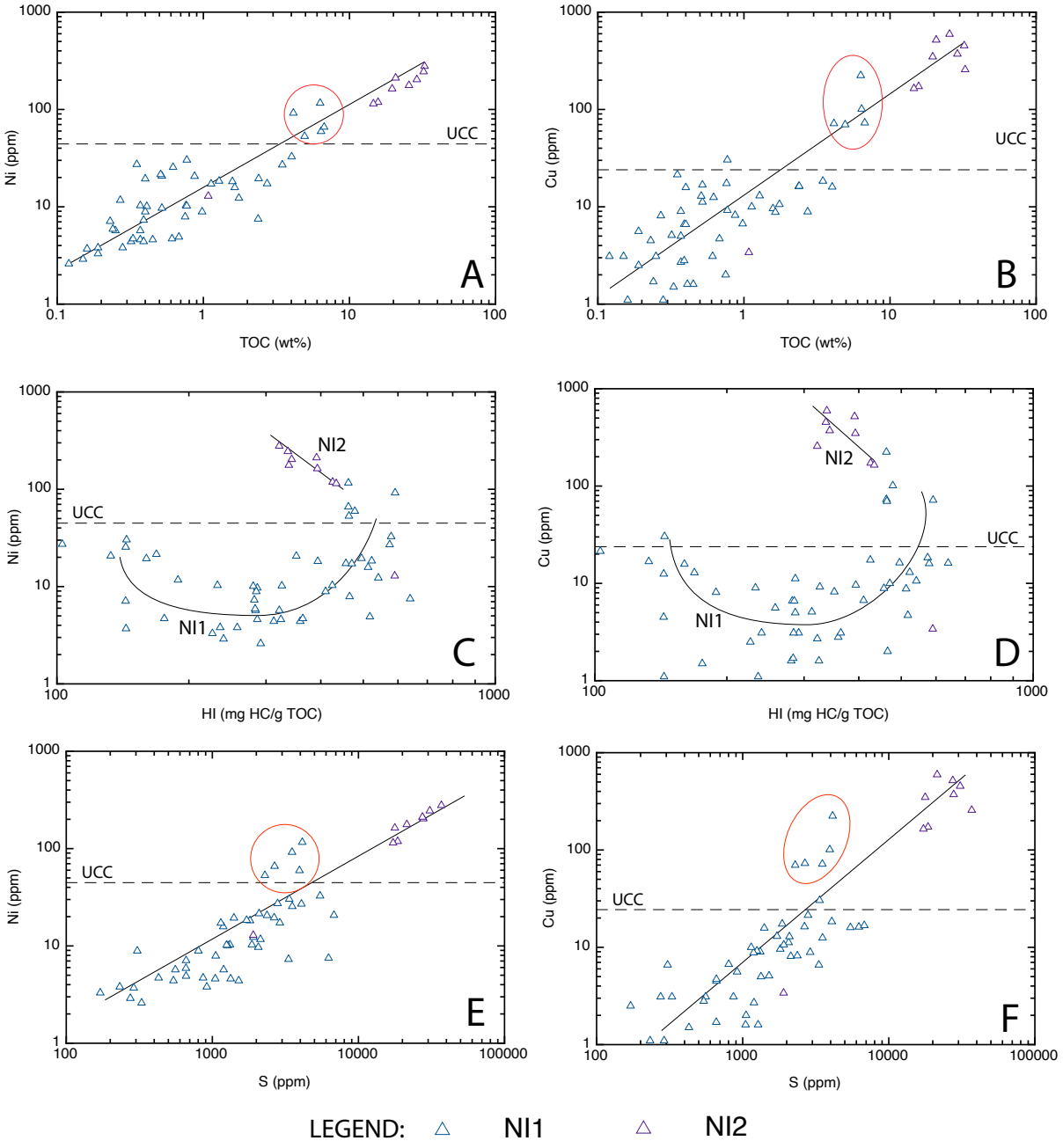

Figure 8.2.2: cross plots of Ni and Cu (ppm) with TOC (wt%) and HI (mg HC/ g TOC) for the Triassic cases of study.

Elements not related to the organic matter: Th, Zr, Al, Mn

NI2 show Th values between 0 and ~10 ppm with an average of ~0.6 ppm. NI2 shows Th concentrations between 0 and ~5.5 ppm and an average of ~0.8 ppm. Both NI1 and NI2 show contents of Th lower than the UCC (10.7 ppm; McLennan, 2001), mostly this elements is zero. Due to the low contents no correlations between Th and other parameters (both organic and inorganic) have been observed.

Zr shows values between ~4 and ~200 ppm with an average of ~32 ppm in NI2. In NI2, Zr concentrations are between ~7.5 and ~180 ppm, with an average of ~91 ppm. In NI1, Al shows values between ~1.7 x 10^3 ppm and ~ 60.3 x 10^3 ppm with an average ~17.5 x 10^3 ppm; in NI2 it shows values between ~8.5 x 10^3 ppm and ~80 x 10^3 ppm, with an average value of149.4 x 10^3 ppm.

Zr and Al show similar behaviors (figures 8.2.3A-F). Both show positive linear correlations with TOC and total clays + micas and negative (non-linear) correlation with total carbonates. In turn, clays and micas show a linear positive correlation with TOC, whereas total carbonates show a negative non-linear correlation with TOC. In the Triassic cases of study, Zr and Al show values always lower than the UCC value (190 ppm; McLennan, 2001).

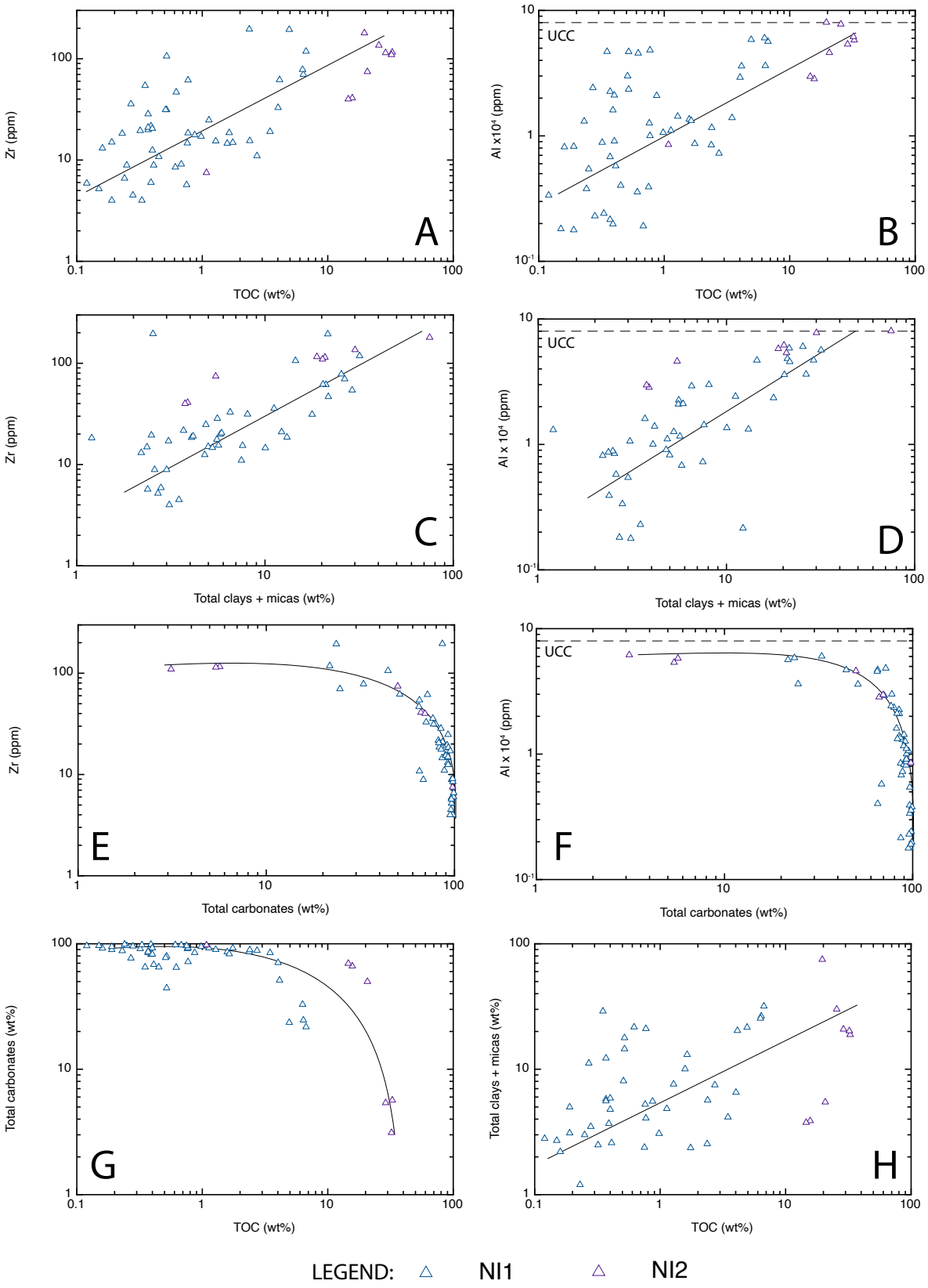

Figure 8.2.3: (A, B, C, D, F) cross plots of Zr and Al (ppm) with TOC (wt%), total carbonates (wt%) and total clays + micas (wt%). (G, H) Cross plots of TOC (wt%) with total carbonates (wt%) and total clays + micas (wt%) for the Triassic cases of study.

Mn shows values between ~30 and ~410 ppm, with an average value of ~133 ppm in NI1. For NI2, it shows values between ~84 and ~189 ppm with an average of ~151 ppm. In the Triassic cases of study no correlations between Mn and TOC has been observed (figure 8.2.4). In addition, Mn concentrations are always below the UCC value (600 ppm; McLennan et al., 2001).

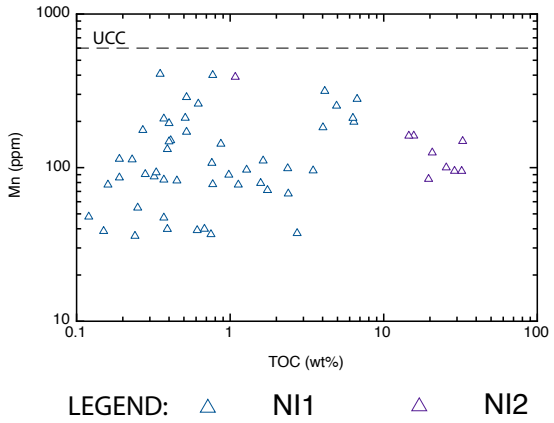

Figure 8.2.4: cross plot of Mn (ppm) with TOC (wt%) for the Triassic cases of study.

Anomalies of trace and Rare Earth Elements (REEs)

The values of trace elements and rare earth elements were obtained only for 15 samples of NI1. The values have been normalized to UCC (McLennan, 2001) to understand how much the composition of the source rocks differs from the average value of the composition of the upper continental crust represented by the horizontal dashed line with value 1 in figure 8.2.5.

The samples have been divided into 3 class divided based on TOC: (i) <1 wt% (7 samples); (ii) 1-2 wt% (1 sample) and (iii) >2 wt% (7 samples). Subsequently the average for each group have been plotted in figure 8.2.5 that shows the values of REEs and TEs. The pattern closer to the UCC value is the one relative to TOC >2 wt%. Gradually more depleted, there is the pattern relative to TOC >1 wt% and finally the pattern of the sample with a TOC value between 1 and 2 wt%. REEs values are depleted compared to the UCC, especially the incompatible ones (on the left side of the graphs in figure 8.2.5A). Trace

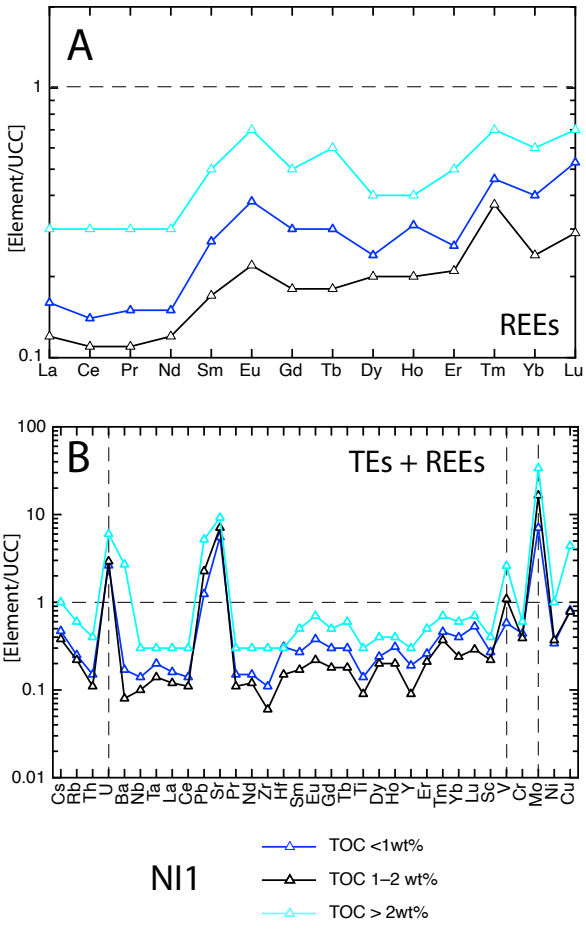

Figure 8.2.5: cross plots of REEs and TEs concentrations (normalized to UCC) for NI1.

elements show strong positive anomalies in U, Pb, Sr, V and Mo, while weaker negative anomalies are observed for Zr, Ti and Y, especially with TOC content lower than 2 wt% (figure 8.2.5B). Finally, high values of barium (~2) have been observed for samples with TOC > 2wt%.

8.2.2 Discussion

Mineralogy and samples observations

The main lithofacies for NI1 are limestones, marlstones and laminated limestones, whereas for NI2 are black shales, marlstones and laminated limestones. Lithofacies and mineralogy (described in detail in chapter 7) indicate that both sections were formed in a shallow environment, probably a carbonate shelf. In particular, laminations suggest that the environment was probably a stagnant basin characterized by restricted circulation and by fluctuations in redox conditions. The latter allowed the preservation of organic matter during reducing periods and correspond to the marlstone and black shales deposition, while during periods of more oxygenated conditions the deposition of carbonate layers occurred.

Elements related to the organic matter: V, Mo, U, Ni and Cu

As for the Cretaceous cases of study, in the Triassic sections the linear positive relationship between V, Mo, U and TOC (figure 8.2.1) suggests that these elements are hosted by the organic matter deposited and preserved under reducing conditions. The linear covariation of these RSEs and TOC suggests a co-enrichment of TOC and RSEs that has started in the same time (i.e. same redox conditions), as suggested by Algeo and Li (2020).

Regarding Ni and Cu, they are positively correlated to both S and TOC indicating that they are hosted mainly by sulphides (e.g. pyrite) and indicating high OM fluxes towards the sediments and reducing conditions that allowed Ni and Cu fixation within the sediments (Tribovillard et al., 2006). In this case, Cu and Ni can be used also as redox proxies even if they are hosted by sulphides and not by organic matter. This is due to the tendency of organic matter fluxes to correlate positively with S; indeed under reducing conditions, especially euxinia, sulfate reducing bacteria (BSR) generates H_2S that react with reduced species of Ni and Cu, forming sulphides.

In addition, in NI1, V, Ni and Cu can show concentrations below the UCC values as shown in figure 8.2.6. This might be due to the fact that (i) V can be fixed in clayey fraction (Tribovillard et al., 2006), (ii) Ni and Cu can be retained within the sediments (e.g. clays and micas), being hosted most frequently by pyrite (or they can form their own sulfides) if sulfate reducing

conditions prevail (Pedersen et al., 1986; Tribovillard et al., 2006). The fraction constituted by clays and micas is low in NI1, especially in the ones poorer in TOC (total clays and micas varies mainly between ~2 and ~30 wt%), suggesting that a depletion of these elements can be also related to low contents of clays and micas. This is visible in figure 8.2.6, where positive correlations between V, Ni, Cu with Al are shown, suggesting that these elements concentrate in the aluminosilicate fraction. In addition, pyrite content is low in NI1 (average of ~0.26 wt%), indicating that there is a lack of one of the main host phases for Cu and Ni, leading to a depletion in these elements.

In NI1 probably Cu and Ni form their own sulphides due to the general absence of pyrite, or more likely, they are bounded to the organic matter or to clays minerals, as suggested by the positive correlation of Ni and Cu with TOC (figures 8.2.2A and 8.2.2B) and Al (figures 8.2.6B and 8.2.6C). Instead, in NI2 a positive correlation is observed between pyrite and trace metals, indicating that pyrite may host both Ni and Cu.

Importantly, in NI1 the samples with TOC >6 wt% (circled in figures 8.2.2A, 8.2.2B, 8.2.2E and 8.2.2F) probably experienced a higher organic matter flux due to the fact that they show Ni and Cu values that are shifted upwards compared to the general trend that link NI1 to NI2 (black lines in figures 8.2.2A and 8.2.2B). Therefore, in this case a higher organic matter content is not due to the development of more reducing conditions (i.e. sulphidic

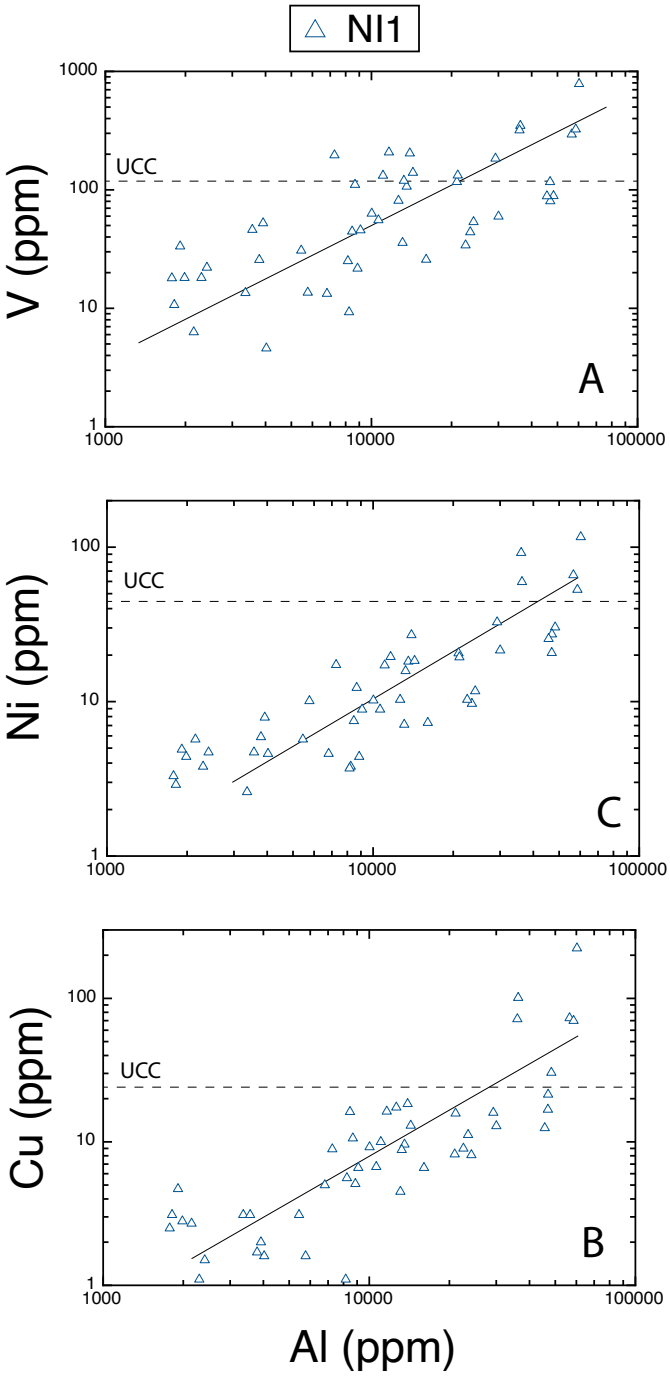

Figure 8.2.6: cross plots of V, Ni and Cu (ppm) with Al (ppm) for NA1.

conditions) that led to a better preservation but to an increase of the OM flux toward the sediments. This is also in agreement with the fact that in figure 8.2.2C and 8.2.2D, Ni and Cu started to increase faster than S for these samples leading to a positive non-linear correlation, contrary to NI2 that is still aligned to the linear trend and that show higher S values (S indicates the presence of H_2S in the depositional environments).

Moreover, the lack of relationship between RSEs (V, Mo, U, NI and Cu) and HI for NI1 could be related to the low TOC content for most of the samples. Indeed, the organic matter represents one of the host phases of the RSEs. In addition, the lithology, mostly rich in carbonates and depleted in clays and micas, determines the lack of another host phase for V, Ni, Cu that result depleted compared to the UCC values. In addition, HI is not mainly determined by the organic matter content or by redox conditions but by the organic matter typology. In fact, the equation to calculate HI is defined as HI = S2/TOC*100, where S2 represents the residual petroleum potential produced by thermal degradation of kerogen (S2) and that depends by the organic matter typology.

Instead, for NI2, a negative relationship is observed between the RSEs and HI (figures 8.2.1B, 8.2.1D, 8.2.1 F, 8.2.2C and 8.2.2D). This is mostly related to the fact that the typology of hydrocarbon generated moves toward the gas typology with the increasing of the organic matter, as indicated in figure 8.2.7, in which a negative correlation is also observed between TOC and HI for NI2.

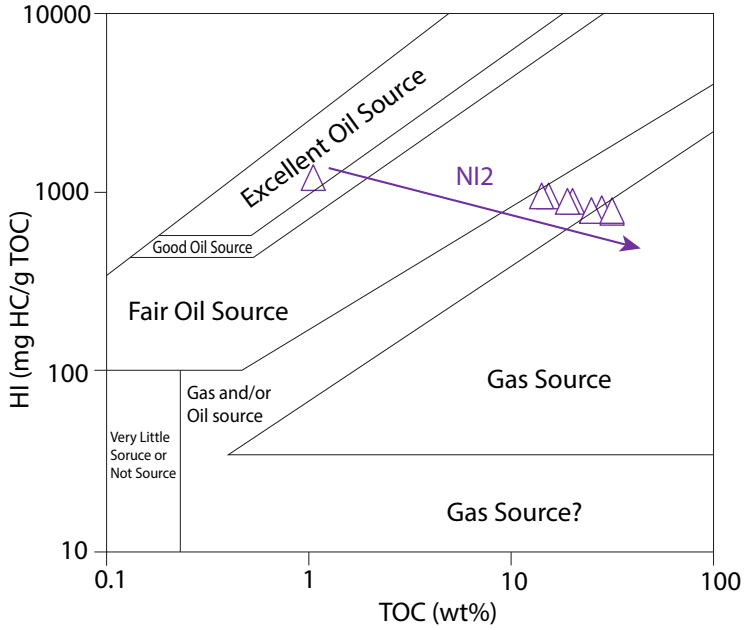

Figure 8.2.7: Source rock characterization (after Jackson et al., 1985) using the cross plots of TOC (wt%) and HI (mg HC/g TOC) for NI2.

Therefore, due to the high RSEs, TOC (up to ~40 wt%) and HI values (between ~300 and ~450 mg HC/g TOC) concentrations, together with a high presence of S, we can infer euxinic conditions for NI2. This hypothesis is also in agreement with the presence of black shales in this section. Instead, we can infer anoxic conditions for NI1 due to the good enrichments of RSEs and organic matter (up to ~8 wt%). In agreement with this idea is the presence of organic matter in marlstones and in the black laminae into limestones.

In turn, for the Triassic immature cases of study V, Mo and U allow to trace the redox conditions at the depositional time and the organic matter content. In fact, V, Mo and U increases with TOC indicating that the redox conditions have become gradually more reducing until reaching euxinia in NI2, leading to the preservation of high amount of organic matter (up to ~40 wt% in NI2). In addition, the linear relationship with TOC means that to a given content of OM, always the same RSEs concentration is recorded by the sediments, allowing to use these elements to trace the original content of OM. Also, Ni and Cu can give information about the depositional environment, on both redox conditions (indirectly) and on the organic matter flux toward the sediments given their relationship with TOC and S.

Elements not related to the organic matter: Th, Zr, Al, Mn

The positive correlation observed between Zr, Al and total clays + micas indicates that these phases are the main host for these elements. In NI1, the clays and micas fraction is composed mainly by illite type (figure 8.2.8), while in NI2 is composed mainly by muscovite (except for the sample NI2/0 that contains illite type up to ~73 wt%; figure 8.2.9). In turn, Al and Zr can be used as an equivalent of the phyllosilicate fraction. Both NI1 and NI2 show a general presence of carbonates, that can reach ~98 wt%.

A linear positive relationship of Al, Zr and total clays and micas with TOC has been observed (figure 8.2.3A and 8.2.3B). Contrarily, total carbonates show negative non-linear correlation with TOC, Zr, Al and clays and micas. This indicate the development of reducing conditions where the deposition of silicates is favored compared to carbonates sedimentation. This relationship is very common in source rocks (Novelli et al., 2004) because clays are characterized by very fine grain size and do not easily allow fluids to pass through them. Indeed, the oxygen contained in the water present in the very small spaces between grains is rapidly

used up during the initial oxidation of any organic matter contained and as they do not allow replacement with other water, a highly anoxic environment is created inside these sediments and the remaining organic matter can be preserved against further alteration.

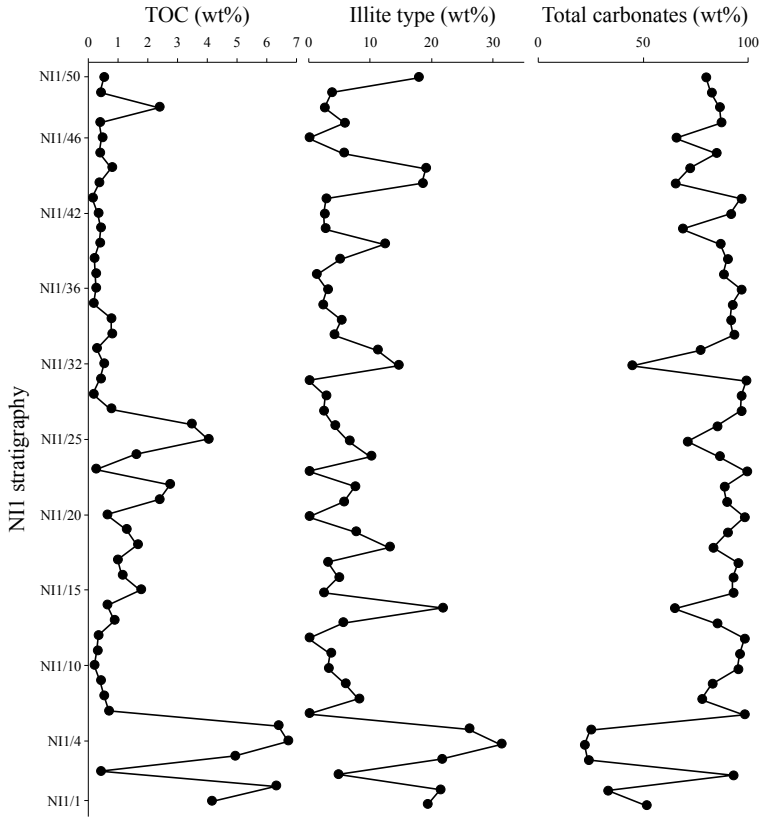

Figure 8.2.8: variation of TOC, illite type and carbonates content (wt%) with stratigraphy in NI1.

Contrary to the Cretaceous cases, in NI1 and NI2 the positive relationship between TOC and clays is not an indicator of enhanced terrigenous input but it indicates the development of a reducing environments in which only silicates can deposit. However, carbonates are rarely zero, especially in NI1, indicating that the environment was shallow with fluctuations in the redox condition which may have led to a temporary increase of the oxygen in the water column.

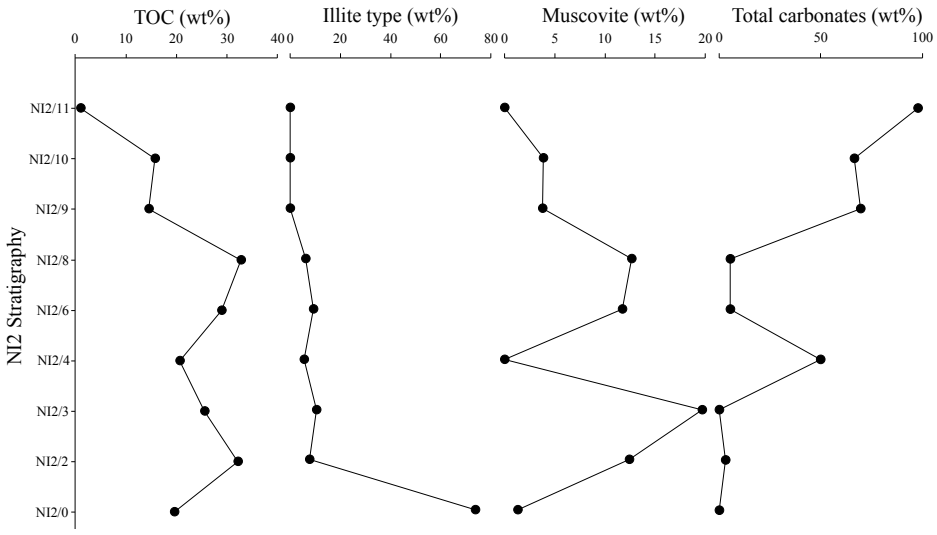

Figure 8.2.9: variations of TOC, illite type, muscovite and carbonates content (wt%) with stratigraphy in NI2.

The depletion of Zr, Al and Th compared to the UCC may indicate that the terrigenous supply from the land was low, in agreement with the idea that these sections have formed in an intraplatform basin with restricted circulation. This is also testified by the sedimentations of fine-grained clays minerals as illite (NI1) and micas as muscovite (NI2).
Finally, low content of Mn both sections point toward the idea that all the samples experienced reducing conditions. However, the lack of a negative correlation may be due to the fact that Mn is not a reliable redox proxy (Tribovillard et al., 2006).

Anomalies of trace and Rare Earth Elements (REEs)

Anomalies in V, Mo, U, Pb, Sr and Ba have been calculated and are defined as described in chapter 3.3. The shape of REEs in figure 8.2.5A has been interpreted as dependent on the provenance of the sediments and to the mineralogical content. In particular, NI1 show a depletion in incompatible elements. In addition, the TEs and REEs (figure 8.2.5) patterns are more depleted compared to 1 (i.e. the value of UCC) compared to the Cretaceous cases of study (CA5 and CA1, figure 8.1.9), indicating that the composition of these rock are farer compared to the composition of the UCC. In fact, NI1 is composed mainly by carbonates (figure 8.2.8), while the UCC values have been calculated on terrigenous sediments (McLennan, 2001).

while anomalies in redox sensitive elements (V and Mo) and Pb are generally related to the presence of organic matter and its preservation under anoxic conditions. This is in agreement with the positive relationship between the anomalies and TOC (figure 8.2.10A, 8.2.10B,

8.2.10C). Mo* shows weak positive relationships with TOC (figure 8.2.10B) and S (figure 8.2.11D) because it has affinity with both organic matter and sulphides.

Contrarily, U shows a weak negative correlation with TOC and a positive correlation with carbonates (figures 8.2.10C and 8.2.11A). This is due the fact that U can co – precipitates with carbonates. Particularly in oxidizing environments, uranium is preferentially incorporated and sequestered by aragonite over calcite. In the long term, uranium can be sequestered by calcite. In particular, U(IV) (insoluble) ion can replace Ca^{2+} in calcite deposited under anoxic conditions.

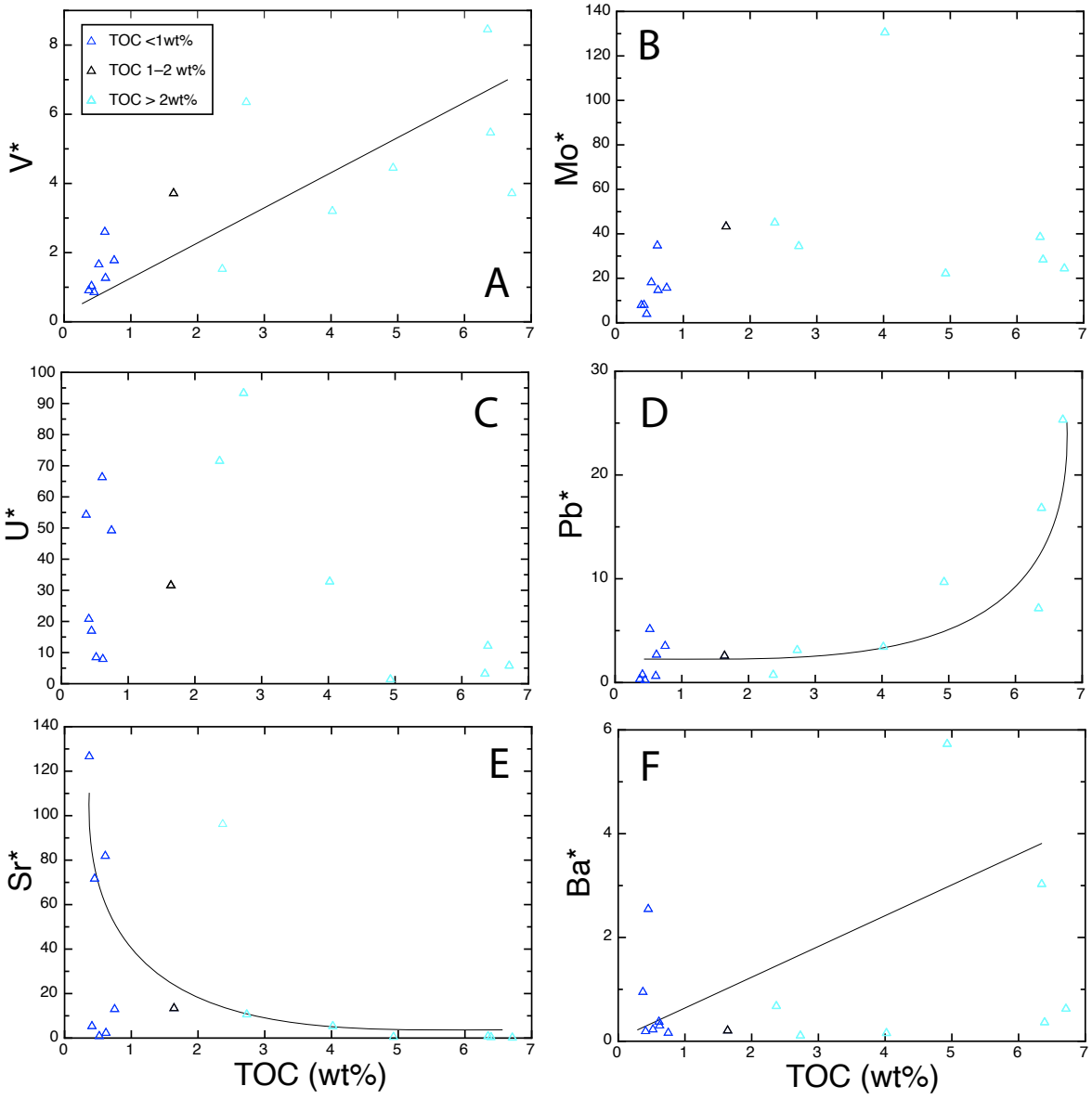

Figure 8.2.10: cross plots of the anomalies of V*, Mo*, U*, Pb*, Sr* and Ba* with TOC (wt%) for NI1. * indicates the anomaly as explained in chapter 3.3.

In addition, Pb is an indirect proxy for the organic matter content: under oxidizing conditions, Pb exists as a cation (Pb^{+}) or as a soluble carbonate compound ($PbCO_3$). In anoxic environments, it is rapidly removed as PbS (insoluble), usually as an independent phase rather than in solid solution with pyrite. Usually, under anoxic and euxinic conditions, it is present in the sulphidic fraction, correlating positively with Mo, V and S. Since it does not reside in the organic fraction, Pb may not show strong correlations with TOC (much weaker than in Mo and V). However, in NI1, Pb correlates positively with TOC (figure 8.2.10D) and total clays + micas (figure 8.2.11B).

Positive anomalies in Sr are related to the carbonate content. In fact, Sr* correlates positively with the carbonate content (figure 8.2.11C) and negatively with TOC (figure 8.2.10E).

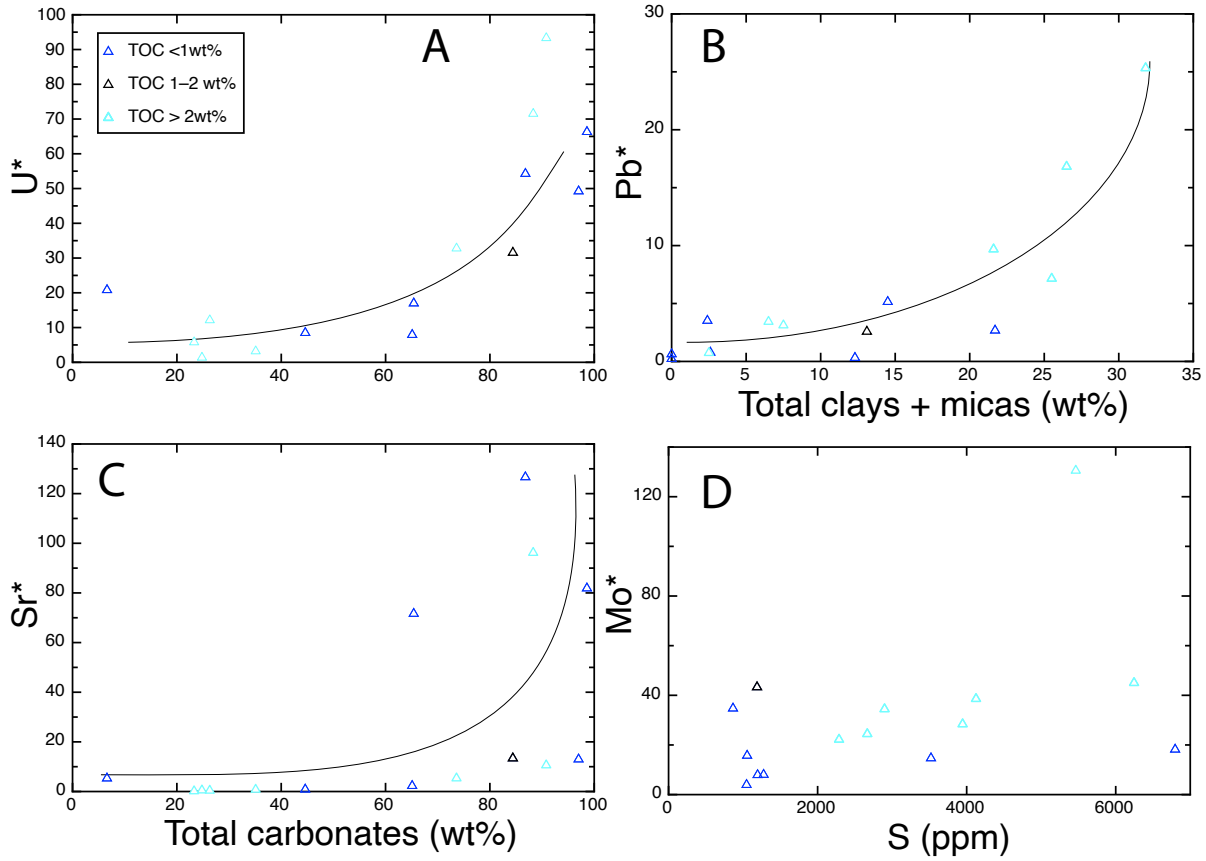

Figure 8.2.11: cross plots of (A) U* with total carbonates content(wt%); (B) Pb* with total clays + micas content (wt%), Sr* and Mo* with total carbonates, total clays + micas and S. * indicates the anomaly as explained in chapter 3.3.

Negative anomalies in Zr, Ti and Y are related to the detrital fraction. In fact, Ti is related, as Al, to the aluminosilicate fraction while Y, as Zr, resides mainly in the in igneous rocks or clastic sediments (Bau, 1996; Pašava et al., 2017). The depositional environment of NI1 is

represented by a shallow basin characterized by a restricted circulation (e.g. intraplatform basin). Negative anomalies in these elements indicate that the terrigenous input was low and that the depositional environment was characterized by stagnant conditions where the deposition occurred for decantation.

Finally, high values of Ba have been also observed in the pattern relative to samples with TOC >2 wt% in figure 8.2.5B. However, the meaning of this anomaly is not well sure due to Ba behavior in presence of high amounts of organic matter. In particular, Tribovillard et al. (2006) propose Ba as a paleoproductivity proxy but with some limitations. Especially, live phytoplankton incorporates Ba (actively or passively, i.e. metabolic uptake or adsorption) that can be released during the decay of phytoplankton necromass and precipitate as a barite in microenvironments where Ba sulfate reaches supersaturation. However, in OM-rich sediments intense reduction of sulfate can occur, leading to the dissolution of barite or the migration of Ba into pore waters. In fact, Ba may be delivered to the sediments with a high organic matter flux, but it can migrate during early diagenesis and precipitate in sediment deposited in absence of high productivity. Such conditions of sulfate reduction usually develop rapidly in OM-rich sediments; consequently, the abundance of Ba cannot be used confidently as a proxy of paleoproductivity in organic-rich sediments, typically present in a high productivity platform. Rather, the effective use of Ba as a paleoproductivity marker may be limited to marine sediments deposited in portions of the ocean with low to moderate productivity (Tribovillard et al., 2006).

In our case, barite has not been detected by XRD, however it can be present as microcrystalline phase. However, Ba anomaly is present in the OM-rich sediments (TOC > 2 wt%; figure 8.2.5B) and Ba* correlates positively with TOC (figure 8.2.10F), maybe indicating an increasing in the organic matter content in agreement with the others RSEs.

8.3 DEVONIAN MATURE SOURCE ROCKS

In this chapter the results and discussion about the Devonian Mature Source Rocks are presented. NA1 is divided in two groups of samples: the first (NA1F) is represented by the 11 OM-rich Frasnian samples, while the second (NA1G) is represented by the 4 sterile Givetian samples. NA2 is of Frasnian age. TOC and HI values for both the cases of study are discussed in the previous chapter 7 about the cases of study.

8.3.1 Results

Elements related to the organic matter: V, Mo, U, Ni and Cu

Vanadium shows concentrations between ~389 and ~297 ppm in NA1F, with an average of ~326 ppm. In NA1G, it shows concentrations between ~211 and ~201 ppm, with an average of ~204 ppm. Finally, in NA2, V values are between ~554 and ~94 ppm, with an average of ~265 ppm. The values are mostly very close or higher than the UCC value for V (107 ppm; McLennan, 2001).

Mo values are always higher that the UCC value of 1.5 ppm (McLennan, 2001) in all the Frasnian cases of study. In NAF, Mo varies between a maximum of ~137 and a minimum of ~62 ppm, with an average of ~95 ppm. In NA1G, Mo concentration is always ~3 ppm. Finally, in NA2, Mo shows values between ~194 and ~9 ppm, with an average of ~70 ppm.

Uranium shows concentrations between ~ 25 and ~15 ppm in NA1F, with an average value of ~21 ppm. In NA1G, U shows an average of ~1 ppm and varied between ~1 and ~2 ppm. Finally, in NA2, U varies between ~43 and ~3 ppm, with an average of ~16 ppm. Except for NA1G, the values are always higher than the UCC concentration for U (2.8 ppm; McLennan, 2001).

These three elements show very different relationships with TOC. All the samples (NA1 and NA2) present a very well-marked positive correlation between U, Mo and TOC, as shown by the black trend lines in figures 8.3.1B and 8.3.1C. Differently, V shows two different trends for NA1 and NA2. Both show a positive relationship between V and TOC, but NA2 show a higher slope than NA1 (figure 8.3.1A). NA1F shows similar V, Mo and U concentrations for similar TOC values to NA2.

Regarding the correlations between the TEs and HI, NA1 and NA2 show always a positive correlation but two different trends. Generally, NA2 shows a higher slope compared to NA1, especially for V and Mo (figures 8.3.1B and 8.3.1D) while is less visible for U (figure 8.3.1F). In addition, NA2 shows HI values lower than NA2F and closer to NA1G.

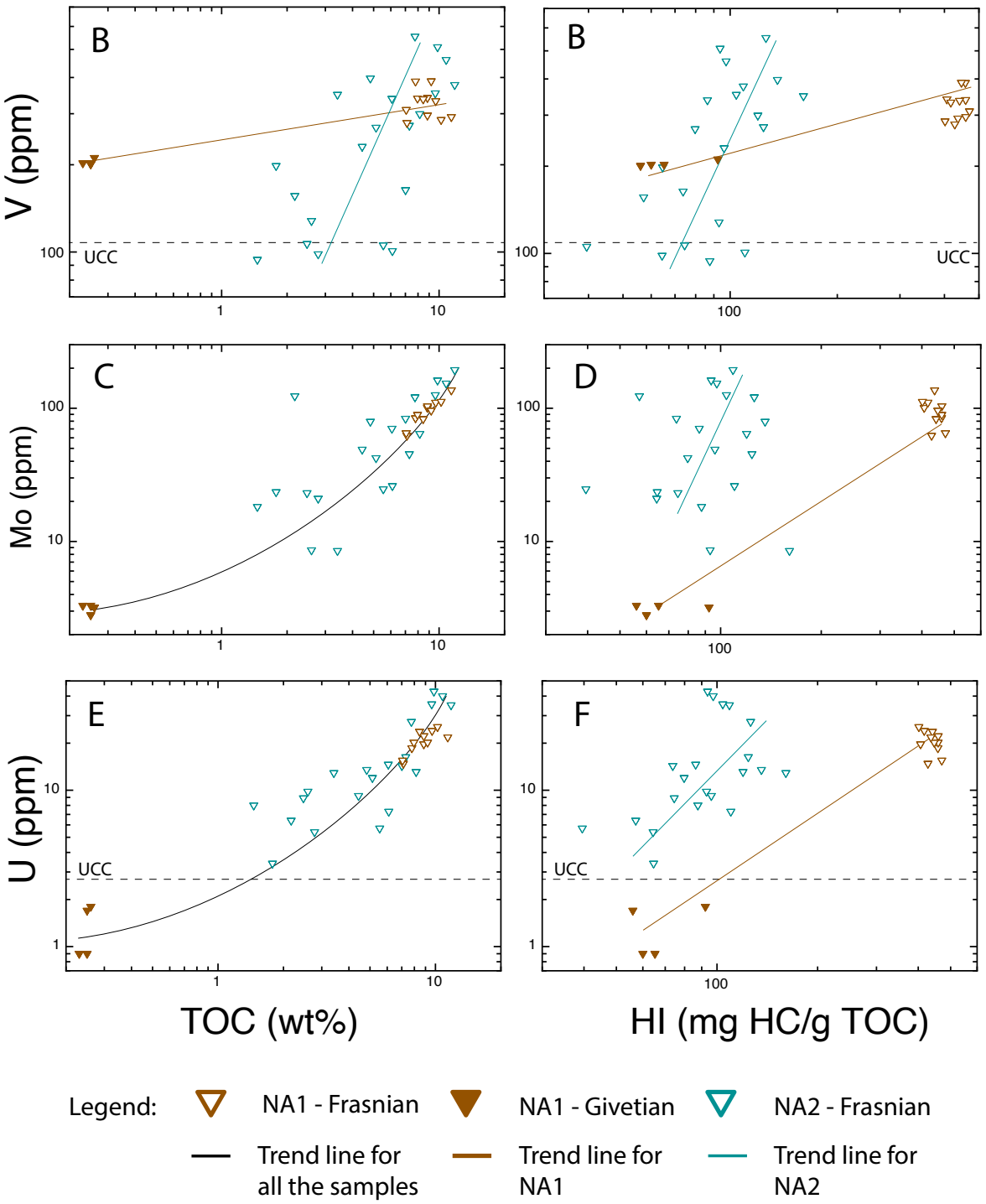

Figure 8.3.1: cross plots of V, Mo and U (ppm) with TOC (wt%) and HI (mg HC/ g TOC) for the Devonian cases of study.

In NA1F, Ni shows concentrations between ~183 and ~120 ppm, with an average of ~145 ppm. It varies between ~67 and ~50 ppm in NA1G, with an average value of ~56 ppm. Finally, in NA2, Ni shows values between ~225 and ~27 ppm, with an average of ~99 ppm. Ni's concentrations are generally very close of above the UCC values (44 ppm; McLennan, 2001) for both NA1 and NA2. Copper shows concentrations between ~124 and ~71 ppm in NA1F,

with an average of ~89 ppm. In NA1G, it shows concentrations between ~17 and ~12 ppm, with an average of ~14 ppm. Finally, in NA2, Cu values are between ~171 and ~16 ppm, with an average of ~78 ppm. NA1F shows Cu values always above the UCC value for Cu (25 ppm; McLennan, 2001), while for NA1G the concentrations are always lower than the UCC. Finally, NA2 shows concentrations generally higher or very close to the UCC value.

Pyrite show an average of ~8wt% in NA1F, while it is very close to zero in NA1G. Finally, in NA2 it shows concentrations between ~52 and ~2 wt%, with an average of ~13 wt%.

Ni and Ci show positive correlations with TOC, HI and pyrite content (figure 8.3.2). However, the two cases of study present two different trends in figure 2, except for the cross plot between Cu and TOC (figure 8.3.2D) in which NA1 and NA2 show a single trend. Especially, NA2 shows a slope of the trend lines in figure 8.3.2 that is always higher than in NA1. Finally, NA1F shows similar Ni and Cu concentrations for similar TOC values to NA2.

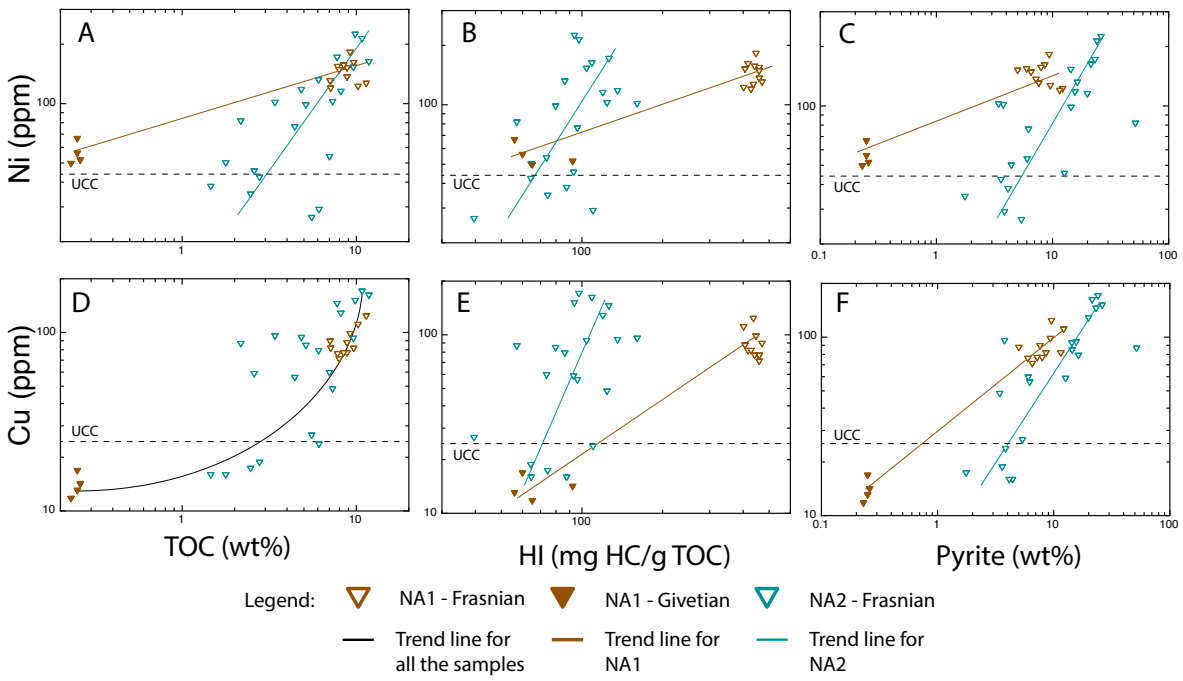

Figure 8.3.2: cross plots of Ni and Cu (ppm) with TOC (wt%), HI (mg HC/ g TOC) and pyrite (wt%) for the Devonian cases of study.

Elements not related to the organic matter: Th, Zr, Al, Mn

NA1F shows Th concentrations between ~8 and ~5 ppm, with an average of ~6 ppm. NA1G shows Th average of ~12 ppm. Finally, in NA2, Th varies between ~14 ppm and zero, with an average of ~5 ppm. Generally, the Th concentrations are lower or very close to the UCC value (10.7 ppm; McLennan, 2001), except of NA1G that shows values slightly higher than the UCC concentration.

Zr shows concentrations between ~141 and ~96 ppm in NA1F, with an average value of ~110 ppm. In NA1G, it varies between ~199 an ~153 ppm and show and average of ~167 ppm. Finally, in NA2, Zr varies between ~131 and ~11 ppm (average of ~67 ppm). Zr concentrations in the Frasnian cases of study are generally lower or very close to the UCC value (190 ppm; McLennan, 2001).

Total clays and micas are very variable in the cases of study: in NA1F and NA1G they show an average of ~54 and ~75 wt%, respectively, whereas in NA2 they varies between ~1 and ~68 wt%, with an average of ~27 wt%.

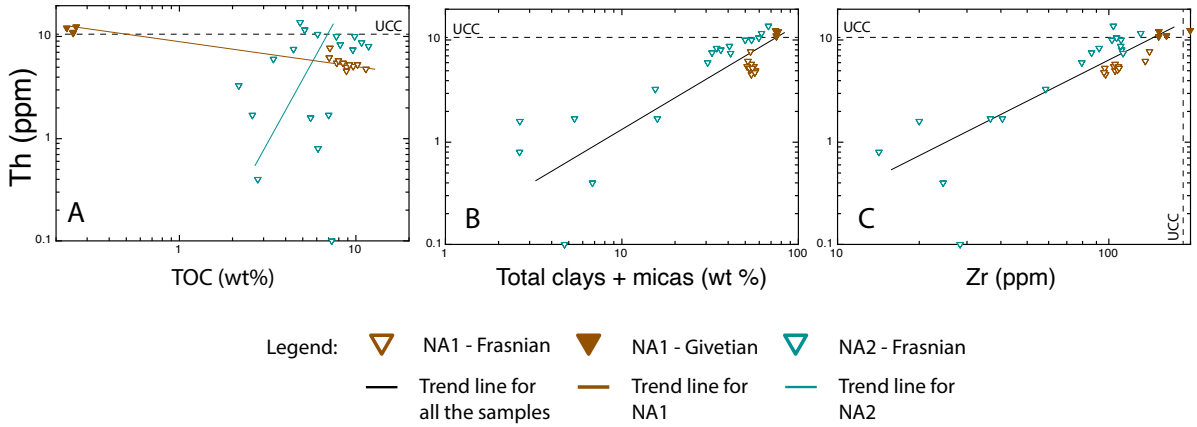

Figure 8.3.3: cross plots of Th (ppm) with TOC (wt%), total clays + micas (wt%) and Zr (ppm) for the Devonian cases of study.

Th and Zr do not show a univocal correlation with TOC (figures 8.3.3A and 8.3.4A); indeed, NA1 shows a weak negative correlation, while NA2 shows a well-marked positive correlation. Instead, Th and Zr show well-marked positive correlations with total clays and micas; moreover, all the Frasnian samples draw a single trend as indicated by the black trend lines in figures 8.3.3B and 3.35B. Finally, Zr and Th show a well-marked positive correlation in which all the samples are aligned a single trend (black trend line in figure 8.3.3C).

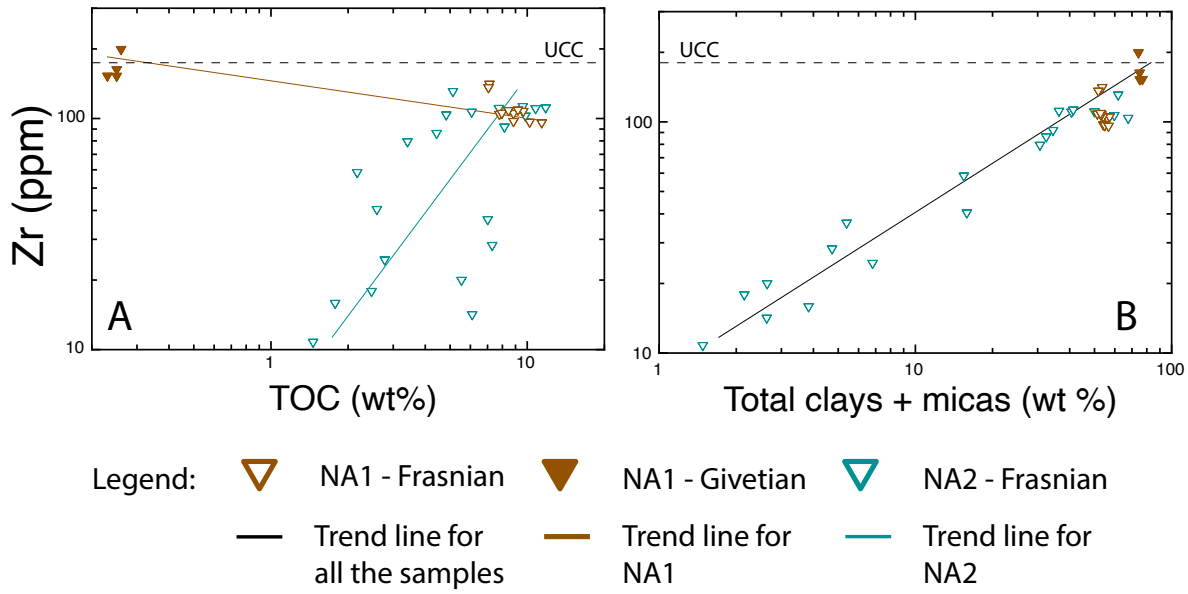

Figure 8.3.4: cross plots of Zr (ppm) with TOC (wt%) and total clays + micas (wt%) for the Devonian cases of study.

Aluminum shows values between ~13.2 x10^4 and ~12.0 x10^4 ppm in NA1F, with an average of ~12.5 x10^4 ppm. In NA1G, it shows an average of ~13.1 ppm. Finally, in NA2, it varies between ~15.8 x10^4 and ~1.6 x10^4 ppm (average of ~8.2 x10^4 ppm). For NA1, Al values are always above the UCC concentration (8.0 x10^4 ppm; McLennan, 2001), while for NA2 it shows values above the UCC only when the total clays and micas content is above 20 wt% (figure 8.3.5B). As for Zr and Th, Al does not show a univocal correlation with TOC (figure 8.3.5A); indeed, NA1 does not show correlations between Al and TOC, whereas NA2 show a positive correlation with TOC. Al show a well-marked positive correlation with total clays and micas and Zr; indeed all the samples are aligned along a single trend line (figure 8.3.5B).

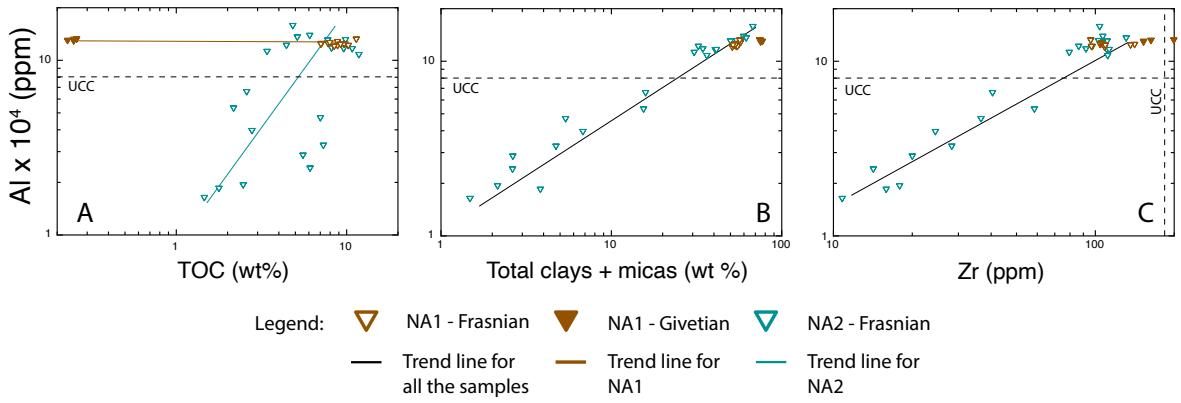

Figure 8.3.5: cross plots of Al (ppm) with TOC (wt%), total clays + micas (wt%) and Zr (ppm) for the Devonian cases of study.

Mn shows values between ~196 and ~101 ppm for NA1F, with an average of ~249 ppm. In NA1G, Mn varies between ~982 and ~160 ppm, with an average of ~593 ppm. Finally, in NA2, Mn concentrations are between ~749 and ~60 ppm (average ~274 ppm). Generally, the Mn concentrations are lower or slightly higher than the UCC value (600 ppm; McLennan, 2001). Mn shows a weak negative relationship with TOC, marked mostly by NA1G (figure 8.3.6).

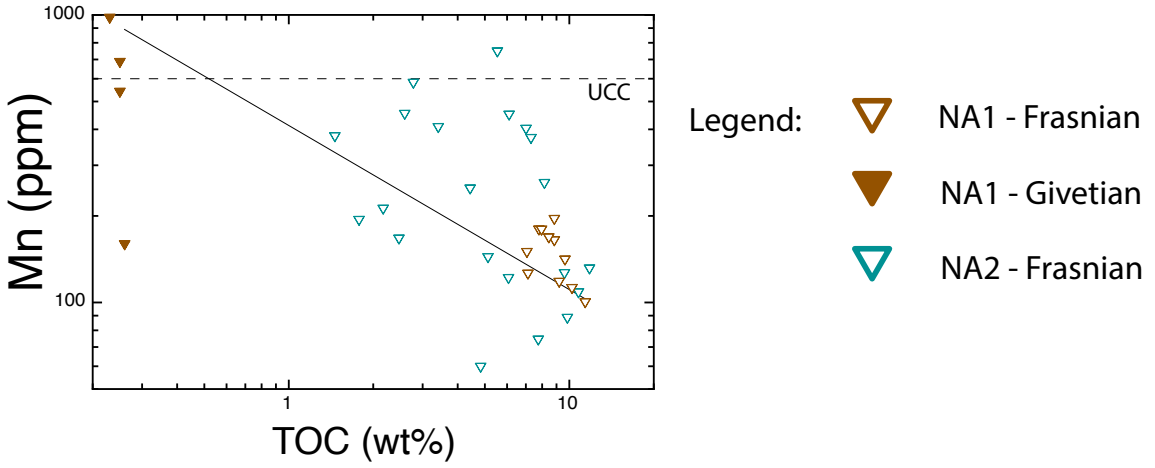

Figure 8.3.6: cross plot of Mn (ppm) and TOC (wt%) for the Devonian cases of study.

8.3.2 Discussions

Elements related to the organic matter: V, Mo, U, Ni and Cu

As for the Cretaceous and Triassic cases of study, in the Frasnian wells positive relationships between V, Mo, U, Ni and Cu and TOC (figure 8.3.1) suggesting that these elements are hosted by the organic matter deposited and preserved under reducing conditions.

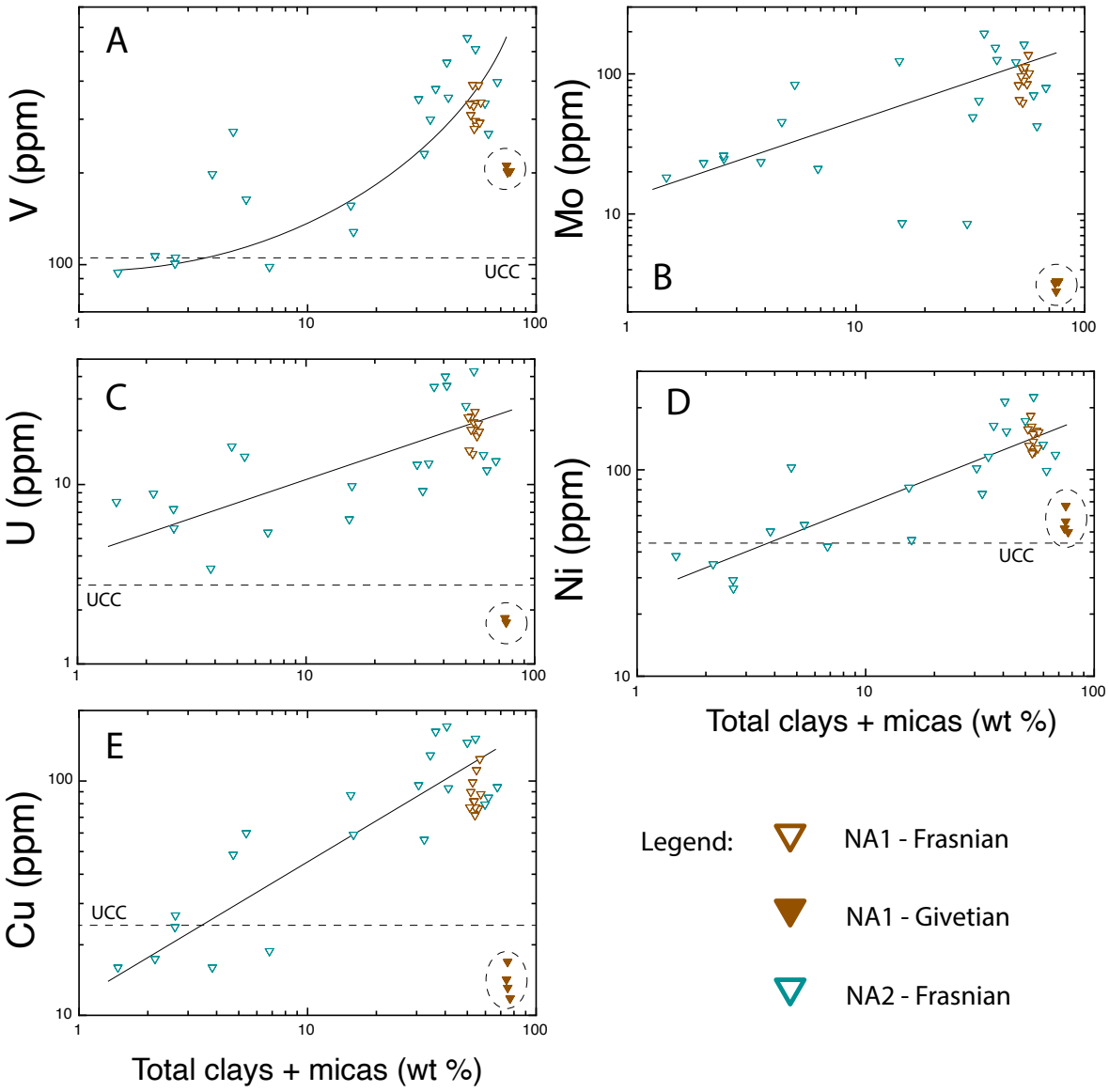

Figure 8.3.7: cross plots of V, Mo, U, Ni and Cu (ppm) with total clays + micas (wt%) for the Devonian cases of study.

However, for V and Ni, NA1 and NA2 show two different trends. Especially, the Givetian samples of NA1 show higher V and Ni contents (~200 ppm and ~60 ppm, respectively) than the UCC, even if they are sterile, and compared to the samples of NA2 richer in TOC (between 1 and 6 wt%) and with V and Ni concentrations below ~200 ppm and ~60 ppm, respectively. This is due to the fact that V and Ni are strongly related to the organic matter (V and Ni can be taken up by tetrapyrrole complexes produced by decay of chlorophyll; Lewan and Maynard, 1982; Lewan, 1984; Breit and Wanty, 1991; Grosjean et al., 2004; Tribovillrd et al., 2006), but also to clays (V) (Breit and Wanty, 1991) or Ni can be retained within the sediments (clays and micas), being hosted most frequently by pyrite under reducing conditions (Tribovillard et al., 2006).

In figure 8.3.7, the relationships between RSEs and total clays + micas are shown. Importantly, the trend lines are in a good agreement for the samples of NA1F and NA2 while the samples NA1G are arranged out of the general trend for Mo, U and Cu (figures 8.3.7B, 8.3.7C, 8.3.7E). This indicates that these elements do not depends on the clay content. Thus, the positive relationship between these elements and total clays + micas is related to the fact that TOC and total clays and micas co-vary positively (figure 8.3.8A). This is likely due to the fact that usually the reducing conditions under which the OM is preserved are the results of stagnant conditions and greenhouse conditions that are associated to the rising of the CCD and seawater acidification, which, in turn, lead to the deposition of mainly silicates and fine grained sediments (e.g. illite). This idea is also confirmed by the negative correlation of total carbonates content and TOC (figure 8.3.8B) for NA2. NA1G samples differ from the trend of NA2 because they are sterile samples in figures 8.3.8A and 8.3.8B. Contrarily, NA1F sample are overlapped to the trend of NA2 because they are more likely related to similar depositional conditions to NA2.

Differently, NA1G samples are very close to the general trend of V, minor of Ni, and total clays + micas (figures 8.3.7A and 8.3.7D), suggesting that V and Ni are likely related to the clay content. The high content of V and Ni of NA1G samples is thereby due to the enrichment in clays and micas of these samples (figure 8.3.8A).

In addition, pyrite shows positive relationships with TOC (figure 8.3.8C), suggesting reducing conditions. In these samples, pyrite contents are very high (up to ~10 wt% in NA1F and to ~50 wt% in NA2), except for the NA1 Givetian samples that shows pyrite contents lower than 0.5 wt%. Except for NA1G samples, the high amount of pyrite is likely related to an environment with high amount of H_2S (strongly euxinic) that allowed sulfurs formation.

Thus, RSEs concentrations together with the presence of OM and high amounts of pyrite point toward strongly reducing conditions. In particular, we can infer strongly euxinic condition when pyrite content is high (e.g. above 10 wt%). Contrarily, the NA1 Givetian samples show low contents of RSEs, TOC and pyrite indicating that oxygen was likely more present in the depositional environment.

In addition, Ni and Cu are used as OM flux tracers. In particular, these elements are mainly delivered to the sediments in association with OM (organometallic complexes) and after its decay, they can be trapped by pyrite if sulfate-reducing conditions prevail (Tribovillard et al., 2006). Thus, if Ni and Cu are not scavenged by settling organic particles, they are not observed to be significantly enriched in sediments even if reducing conditions develop rapidly. Consequently, a high content in Ni and Cu indicates (1) that a high OM flux brought these

elements to the sediments in great abundance and (2) that reducing conditions were met, allowing Ni and Cu fixation within the sediments (Tribovillard et al., 2006). So, while Ni and Cu can be used to trace the OM fluxes toward the sediments, V, Mo and U can be used to assess the redox conditions in the depositional environment.

Excluding the NA1G samples that are sterile and probably related to oxic/suboxic conditions, NA1F and NA2 sample show positive correlations between V, Mo, U and TOC indicating the development of reducing conditions in association with OM preservation. Also positive relationship between Cu, Ni and TOC are observed, indicating that reducing conditions developed rapidly together with high amounts of OM delivered to the sediments (preserved under reducing conditions). In addition, the positive relationship of Cu and Ni with pyrite indicates the development of euxinic conditions.

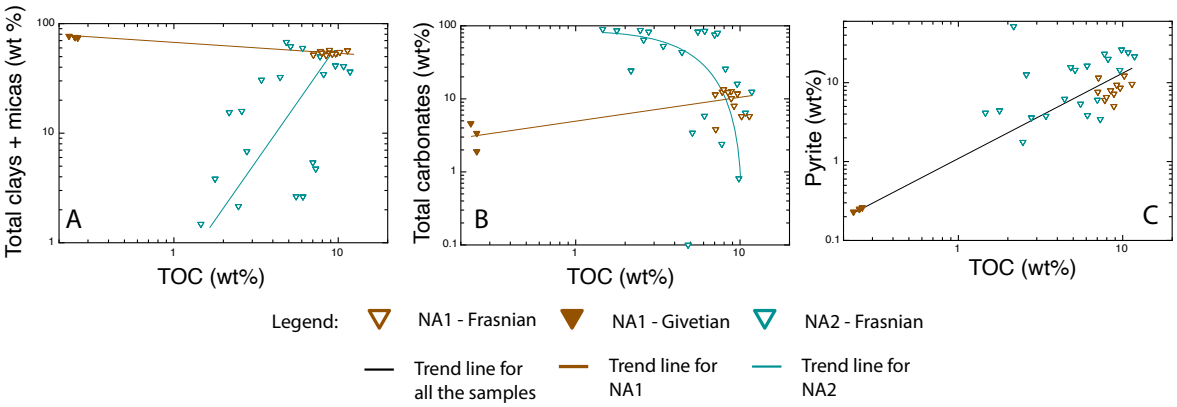

Figure 8.3.8: cross plots of TOC (wt%) with total clays + micas, total carbonates and pyrite (wt%) for the Devonian cases of study.

In addition, all the RSEs show positive relationships with HI, confirming that these elements are hosted by the organic matter and can give information about the redox conditions of the depositional environment. However, different trends are observed for NA1 and NA2. In particular, NA2 shows more vertical trend lines than NA1.

NA1G samples show low HI (<100 mgHC/g TOC) values as a consequence of low TOC contents (<0.2 wt%). NA1F samples show HI contents between ~400 and ~500 mgHC/g TOC for a TOC between ~7 and ~12 wt%, that is much higher than NA2's HI (between ~20 and ~180 mgHC/g TOC) for a TOC between ~1.5 and ~12 wt%. Indeed, NA2 show HI values similar to NA1G than NA1F.

The difference in HI between NA1F and NA2 may be related to two factors: (i) different typology of organic matter or (ii) generation of hydrocarbons and their migration leading to a

depletion in HI (and minor in TOC). The latter hypothesis is more probable, due to the fact that these cases of study are from weakly mature (NA1) to mature (NA2), leading to a depletion in HI, and minor in TOC, compared to the original values that is higher increasing the maturity. In particular, when TOC is constituted by two fraction, the generative organic carbon (GOC) and the non-generative organic carbon (NGOC). The first represents the organic carbon that is converted in hydrocarbons while the second does not contribute toward the hydrocarbons' generation due to its low hydrogen content (Jarvie, 2014). In turn, in a mature source rock GOC would be lower than the equivalent immature source rock, while NGOC would not change. To understand if the maturity level of a rock, S1 (free hydrocarbons already generated by the source rock and not yet expelled), S2 (residual petroleum potential produced by thermal degradation of kerogen) are necessary. They are both analyzed thought the Rock-Eval technique and together they represent the GOC. Both these values are low in mature rock compared to the equivalent immature. In particular, HI consider S2 and TOC (HI=S2/TOC x 100), so it results that the depletion in organic matter due to the hydrocarbon expulsion is more visible in HI than in TOC.

The maturity of the Frasnian cases of study have been estimated by Eni through several thermal maturity parameters om OM, kerogen and generated hydrocarbons (i.e. vitrinite reflectance, thermal alteration index, Tmax from Rock-Eval pyrolysis, fluorescence, spore color index, conodont alteration, biomarkers ratios and correlations between organic maturity parameters) and they suggest a thermal maturity higher for NA2 than NA1. This means that lower HI of NA2 is more likely due to its higher maturity rather than the different OM typology.

We can infer that the maturity for both the cases of study is not very high because although the HI is very different for NA1F and NA2 for similar RSEs values, the TOC does not vary much when RSEs content is similar between the two wells, so the hydrocarbon expelled did not affected much the TOC value. However, due to the fact that the HI looks more depleted in NA2, we can infer higher maturity than NA1.

Elements not related to the organic matter: Th, Zr, Al, Mn

Th, Zr and Al show a well-marked positive correlation with total clays and micas (figures 8.3.3B, 8.3.4B, 8.3.5B), indicating that these elements are hosted mainly by this group of minerals. This is also confirmed by the covariation of Th and Al with Zr (figures 8.3.4C and 8.3.5C).

These elements show a positive correlation with TOC only for NA2 (figures 8.3.3A, 8.3.4A and 8.3.5A), while NA1 shows negative (figures 8.3.3A and 8.3.4A) or no correlations (figure

8.3.5A). In the first case, the positive relationship is not due to the fact that Th, Zr and Al are hosted by the organic fraction but by the fact that the clays and micas portion increase with the TOC content (figure 8.3.8A). In fact, as discussed above, the increase in silicates is mostly due to the fact that the deposition of these minerals is favored under reducing conditions, which are the results of a combination of stagnant and greenhouse conditions, the rising of the CCD and seawater acidification. In addition, many source rocks are constituted of coherent shales because they are characterized by very fine grain size and do not easily allow fluids to pass through them. Indeed, the oxygen contained in the water present in the very small spaces between grains is rapidly used up during the initial oxidation of any organic matter contained and as they do not allow replacement with other water, a highly anoxic environment is created inside these sediments and the remaining organic matter can be preserved against further alteration (Novelli et al., 2004).
Differently, NA1 show a different trend marked by the presence of the sterile samples of Givetian age. The latter are enriched in clays and micas (mainly illite up to ~55 wt% and kaolinite up to ~17 wt%) resulting in enrichments in Th, Zr and Al in concentrations close or higher than the UCC values. Contrarily, NA1F samples show similar (Al) or slightly lower (Th and Zr) values and lower contents in clays and micas (mainly illite up to ~35 wt% and kaolinite up to ~18 wt%) than the NA1G samples.Thus, Th, Zr and Al concentrations in NA1 and NA2 mirror the clays and micas contents and are not dependents on the organic fraction.

Finally, Mn shows a negative correlation with TOC (figure 8.3.6) indicating that for low TOC contents high amount of Mn is deposited as Mn oxy-hydroxides (oxic conditions) while for high TOC contents low Mn contents are due to the dissolution of the Mn oxy-hydroxides under reducing condition. Thus, oxic conditions can be inferred for NA1G samples, while reducing conditions can be inferred for NA1F and NA2.

Summarizing:

- V, Mo and U indicate the development of reducing conditions together with OM preservation since their positive relationship with TOC;
- Ni and Cu indicate the development of reducing conditions (euxinic with the increase of pyrite) and testify high fluxes of organic matter delivered to the sediments. Both these elements are hosted by pyrite;
- V and Ni depends also by the clays and micas contents;

- The higher maturity of NA2 over NA1 is testified by lower HI values for similar TOC and RSEs contents;
- Th, Zr and Al are hosted by clays and micas fraction and are not dependent on the OM contents.

Again, a multi-proxy approach (trace elements, mineralogy and organic parameters) looks successful in the data processing of different rocks, in order to evaluate the main features of the source rocks.

CHAPTER 9

Comparing immature and mature cases of study

In this chapter, we seek to highlight the differences between immature and mature source rocks discussed in the previous chapters. In particular, due to the fact that the thermal degradation do not affect the mineralogical content significantly, we focus on the elements dependent on the organic matter (V, Mo, U, Ni and Cu). Moreover, the elements that do not depend on the OM (Th, Zr, Al) mirror the lithological type of the rock and do not give information about the organic matter content, making them useful to trace the environmental typology of the rock but not the OM content. In addition, some differences between each group of cases of study (Cretaceous, Triassic and Devonian) have been identified. These differences are mainly dependent on the lithology and not on the age or environmental typology.

The comparison we present is qualitative; importantly, we seek to underline the differences between the organic and the inorganic parameters. Specifically, the idea at the base is that the inorganic portion of the rock does not change with maturity. Thus, the inorganic parameters that depends on the organic matter can give us information about the original values of HI and TOC, that are depauperated with the thermal alteration compared to the original ones.

In the following pages, the cases of study are generally represented divided by ages (Cretaceous, Triassic and Devonian) and, where it is possible, by environment typology.

9.1 VANADIUM, MOLYBDENUM AND URANIUM

In figure 9.1 the relationships between the redox sensitive elements (V, Mo and U) and the organic parameters (TOC and HI) for all the cases of study are represented.

The first thing to note is that V shows two different trends for the Cretaceous and Triassic cases of study when TOC < 1wt% (figure 9.1A). This difference is visible also for HI (figure 9.1.B): Cretaceous samples draw a almost horizontal trend that tends to the UCC value (107 ppm; McLennan, 2001), whereas the Triassic samples draw a more vertical trend with a wider range of V that reaches values much above the UCC value. This is due to the fact that V can be hosted by both the organic fraction but also by the clayey fraction that in the Triassic samples (especially in NI1) is low with low organic content (see details in chapter 8.2). Thus, the weak relationship of V with HI is due to the fact that V depends also on the clayey fraction.

A similar consideration can be made for U that can be hosted by the carbonates. That is why in figure 9.1E, with TOC<1wt%, U values are higher for Triassic cases of study than for the Cretaceous ones. Indeed, the first have a carbonate content up to 98wt%.

Another peculiarity we can note is the one related to the HI values of NI2. These samples differ from the general trend drawn by the immature samples in figures 9.1B, 9.1D and 9.1E (this not happen with TOC), because above a certain value of TOC, HI does not increase linearly. This is due to how HI is calculated. HI is the result of S2/TOC*100; N2 shows S2 values between ~63 and ~105 mg HC/g rock with TOC between ~15 and ~32 wt% (there is just a sample with TOC of ~1 wt% and S2 of ~6.5 wt%). Both S2 and TOC fall into the excellent range following Peters (1986). Being TOC very high, the result is that HI fall into a range between ~320 and ~435 mg HC/g TOC (except for the sample with TOC that show a HI of 590 mg HC/g TOC), indicating a kerogen type of II S (the samples are S rich as shown in chapter 8.2) and related to intraplate basins formed on a carbonate shelf.

Looking at the correlations with TOC, it is clear that all the samples arrange along a single trend drawn by the black lines in figures 9.1A, 9.1C and 9.1E. In particular, a good correlation is observed between TOC and Mo (figure 9.1C) that is maintained also with TOC < 1wt%. Instead, for U and V the correlation wane when TOC is <1 wt% (figures 9.1A, 9.1E). This is probably due to the fact that Mo is mainly related to the OM content, while V and U present other host phases besides OM (e.g. clays and micas, sulfides, carbonates or authigenic phases), as has been discussed for each cases of study in chapter 8. This is aspect is visible mainly with low contents of organic matter, because missing the organic matter as a host phase these elements (V and U) needs to concentrates in other mineralogical phases.

Differently, looking at the correlations between the metals and HI, the mature cases of study show a different trend. In particular, NA2 does not arrange along the black trend lines (in figures 9.1B, 9.1D and 9.1E) that characterize the immature cases of study. Indeed, it is arranged vertically, drawing its own trend. This is likely due to the maturity of these samples that led to a depletion of HI respect to the original one. Notably, it is possible to see this difference compared to the immature cases because we assume that the inorganic parameters (V, Mo and U) do not change with thermal degradation. Thus, trace metals enrichments do not disappear, tracking the HI original values, while HI decreases indicating the residual values.

However, NA1 Frasnian (NA1F) samples (except for the Givetian samples that are sterile) show a similar behavior, even if it is less marked. This is likely due to the fact that this case of study is less mature. Thereby, the HI is less depauperated compared to NA2, that show a higher maturity. Thus, it is probable that NA1F has an original HI value slightly higher than the observed. (residual).
Finally, the depletion in HI is not mirrored by an equal depletion in TOC. This is due to how HI is calculated. HI depends on TOC and S2. Also the latter decreases with maturity because in a mature sample hydrocarbons have been already generated and the residual ones are low. So HI mirrors a double decrease, from TOC and from S2.

So, it is possible to trace the original HI content using the these metals content. However, due to the fact that V and U correlates with organic matter and with clays and carbonates, respectively, attention needs to be paid in using these two metals. A way to overcome the problem is to compare only samples with the same lithology. Contrarily, Mo do not change with lithology, making this metal the more reliable in order to track the original HI values.
Generally, assuming that the V, Mo and U contents vary with the organic content following the black line in figures 9.1B, 9.1D and 9.1E, and keeping in mind of the lithology differences, it is probable that the original Hydrogen Index of NA2 and NA1F was higher (around 600) than current one measured on the samples.
Probably the measured values of HI should be shift horizontally until it reaches the immature samples that have the same V, Mo or U value and around to the black trend lines. In addition, the same consideration can be made for TOC, but the difference between the original and the residual values is smaller than for HI. So, the organic carbon content varies a little.

It is important to note that the Devonian samples show high pyrite and S contents, compatible with euxinic conditions in the depositional environment. This is in agreement in the estimated HI values for both NA1 and NA2 that is characteristic of marine environments, with a kerogen type IIS (sulphur rich) typical of euxinic environments.

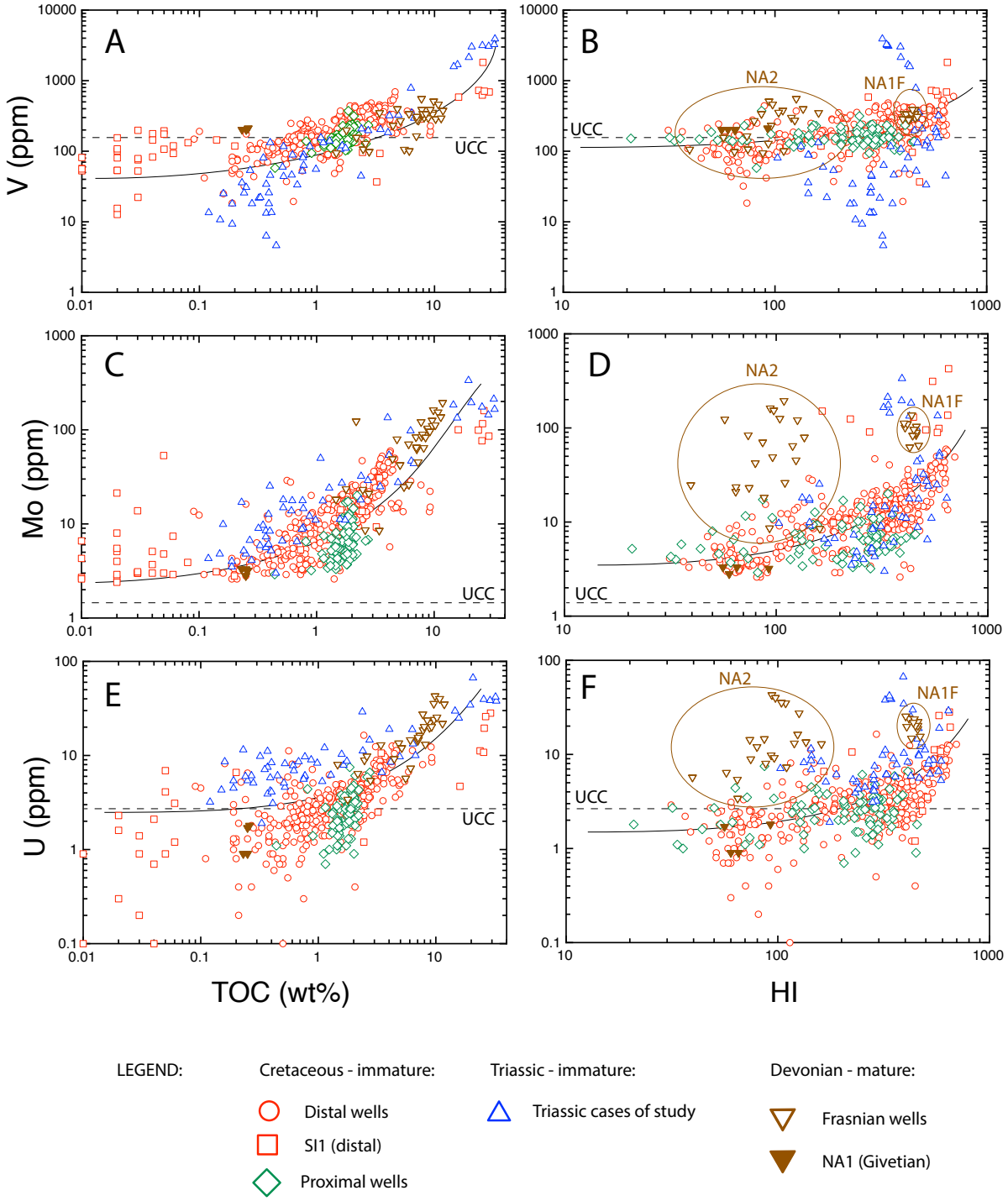

Figure 9.1: V, Mo, U vs TOC and HI for all the cases of study

9.2 NICKEL AND COPPER

The same is visible in figure 9.2, where the relationships between Ni, Cu and the naphtogenic parameters (TOC and HI) are represented.

The low values of Ni and Cu, below the UCC values of 44 ppm and 25 ppm (McLennan, 2001) for the Triassic samples (NI1) are related to low contents is clay minerals (mainly aluminosilicates), as explained in chapter 8.2. Contrarily, the samples of SI1 with TOC<1wt%

show values in Ni and Cu higher than the UCC values due to high clays and micas content that are host phases for these metals. The Devonian-mature cases of study, except for the Givetian ones, show higher values of Ni and Cu as a consequence of higher pyrite and S values. Indeed, Ni and Cu are hosted mainly by pyrite or they can for their own sulphides.

Regarding the relationship with TOC (figures 9.2A and 9.2C), the samples of the mature cases of study are arranged along the black line that represents the trend of the immature cases of study.
Regarding the relationship with HI (figures 9.2B and 9.2D), there are no univocal relationships but in general no significant relationships are observed. In fact, the Cretaceous cases of study show an horizontal trend, whereas Triassic cases of study show a more vertical trend, with a greater range of Ni and Cu compared to the Cretaceous cases. As for the Cretaceous cases of study, the Devonian samples show a horizontal trend, with a narrow range of Ni and Cu and a wide range of HI. Again, the NA2 samples show low HI values compared to the immature cases with similar Cu, Ni and TOC content; moreover, the TOC values do not look much depauperated compared to the immature cases of study represented by the black trend lines in figures 9.2A and 9.2C.

However, because Ni and Cu are not directly related to the organic fraction (details is chapter 3.1), but they are mainly related to pyrite, sediments (clays and micas) and authigenic phases (sulphides), the weak correlation with TOC and the lack of a relationship between Ni, Cu and HI are not surprising. In fact, it looks like the mineralogical content is the main factor that affect Ni and Cu concentrations in a great way.

Thus, because the maturity affect mainly the organic fraction, and because Ni and Cu are affected by the mineralogical composition of the rock, they are not reliable in tracking the original organic matter content. In particular, they are not reliable in tracking the original HI values due to the no univocal relationship between these metals and HI for the immature cases of study.

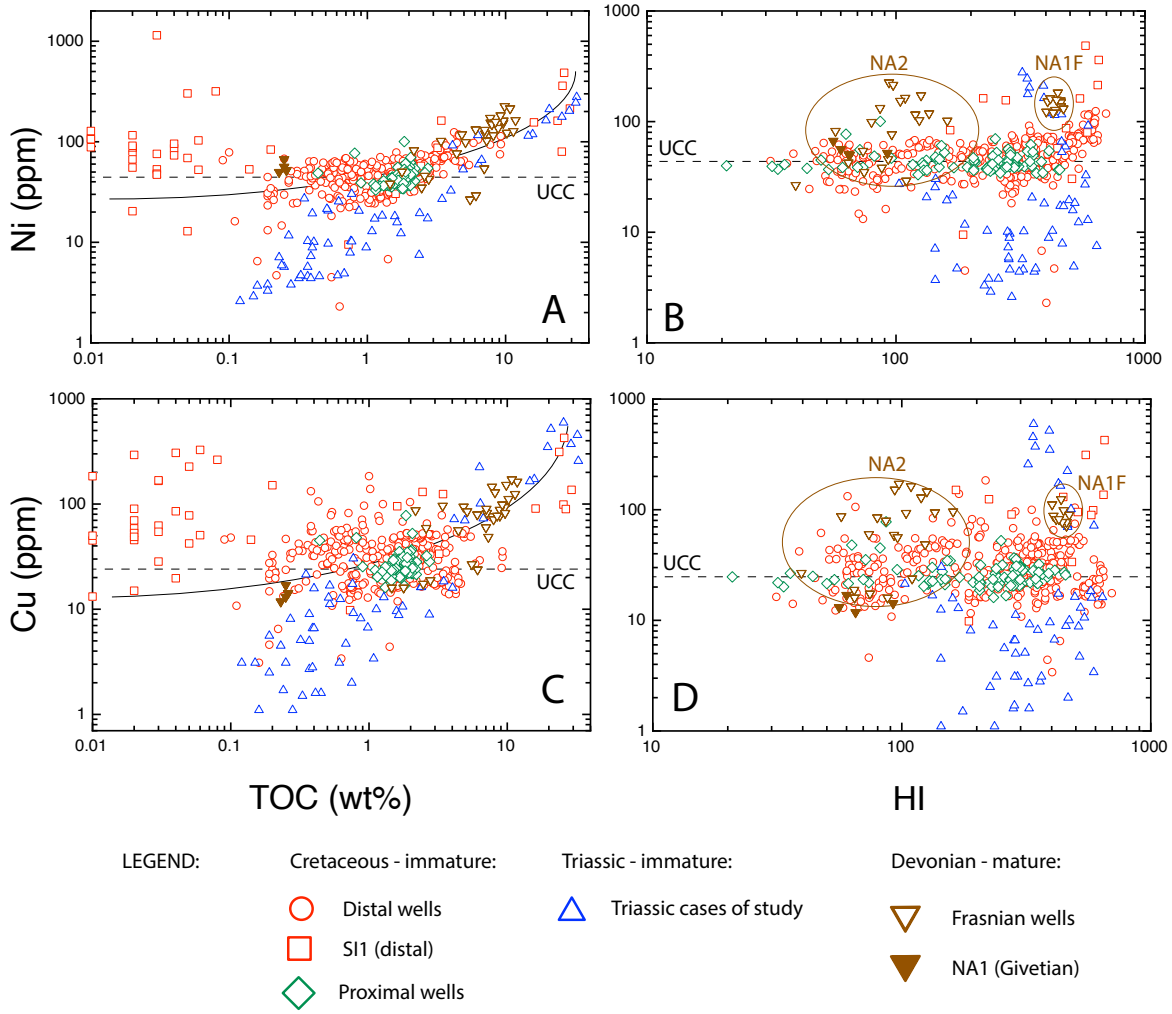

Figure 9.2: Ni and Cu vs TOC and HI for all the cases of study

CHAPTER 10

Conclusions

In chapter 8 the results and discussion on our cases of study are presented. Here, we seek to summarize the characteristics of each group of cases of study (Cretaceous, Triassic and Devonian) and highlight similarities and differences, also according to their maturity degree.

Cretaceous immature cases of study

The positive relationship between the organic parameters (TOC and HI) and V, Mo and U can be used to trace both redox conditions and organic matter content into a sedimentary marine rock. In addition, the relationships between TOC and TEs can give information about the detrital supply in a depositional environment that can led to lower enrichments in trace metals for similar TOC values. Indeed, proximal environments show a dilution of the TEs caused by the higher detrital supply compared to the distal environments.

Ni and Cu can give information about the organic matter flux in the Cretaceous cases of study, whereas are less reliable as redox proxies. Indeed, while the proximal environments are characterized by dilution of a high amount of organic matter by the detrital fraction, the distal cases are characterized by a lower organic matter flux toward the sediments coupled with a limited dilution.

Th, Zr and Al are related to the detrital fraction, indeed they concentrates in clays and micas. In addition, proximal environments show concentrations of these elements that are closer to the UCC values indicating that a higher detrital influx could obfuscates the enrichments in organic matter and RSEs thank to a dilution process.

No univocal correlations have been found between mineralogy and organic matter content. Indeed, proximal cases of study show no correlations between the mineralogical phases and TOC, whereas the distal cases of study shows different relationships between total carbonates and TOC or between total clays + micas and TOC depending on the foraminifera shell production (increasing carbonates) or on the development of reducing and stagnant conditions (increasing clays and micas).

Mn is not always a reliable redox proxy unless it is compared with other more reliable elements as RSEs.

The study of the anomalies has allowed to confirm that V, Mo and U are reliable elements to trace the OM content. In particular, TOC is not a fundamental data to calculate the anomalies; this means that TOC does not result as a necessary data because anomalies in RSEs alone can provide the evidence that in the rocks OM is present and preserved under reducing conditions. In addition, some elements can give another type of information: Sr is positively related to the carbonate content, Zr and Ti to the detrital supply. In addition, the patterns of the TEs and REEs normalized to the UCC values allow to trace the provenance of the sediments and the depositional environment.

Triassic immature cases of study

Also for the Triassic cases of study, V, Mo and U allow to trace the redox conditions at the depositional time and the organic matter content. In fact, V, Mo and U increases with TOC indicating that the redox conditions have become gradually more reducing.

Ni and Cu can give information about the depositional environment, on both redox conditions (indirectly) and on the organic matter flux toward the sediments given their relationship with TOC and S.

A peculiarity of these samples is that V and Ni show a positive correlation with clays and micas content, indicating that a low content of these mineralogical phases can affect the concentrations of V and Ni, especially with low content of organic matter.

Zr and Al can be used as an equivalent of the phyllosilicate fraction because they concentrate mainly in the clays and micas fraction.

The Triassic cases of study show a positive relationship between TOC and clays and micas indicating the development of a reducing environment. These cases of study are likely related to an intraplatform basin with restricted circulation and low terrigenous supply.

Again, Mn shows no correlations with TOC indicating that it is not a reliable redox proxy. However, in agreement with reducing conditions, its concentrations are low.

The study of the anomalies and TEs and REEs patterns of NI1 has led to the following results:

- Positive anomalies in V, Mo, Pb and Ba are generally related to the presence of organic matter;
- Positive anomalies in U and Sr are related to the carbonates content;
- Negative anomalies in Zr, Ti and Y are related to low detrital input in association with a restricted circulation environment. In particular Ti is related to the aluminosilicate fraction, while Y and Zr to the clastic sediments.
- REEs and TEs pattern can give information about the provenance of the sediments. In particular, the depletion compared to the UCC values indicates that the composition of the samples are far compared the UCC. This indicates that the lithology of these samples is different compared to the UCC one.

Devonian mature cases of study

These cases of study are mature, in particular the higher maturity of NA2 over NA1 is testified by lower HI values for similar TOC and RSEs contents.

Again, V, Mo and U show positive relationships with TOC indicating the development of reducing conditions and the OM accumulation and preservation.

Ni and Cu are hosted mainly by pyrite that shows very high contents (it can reach ~50 wt%), thus they testify both the development of reducing conditions and high fluxes of OM toward the sediment – water interface.

As for the Triassic cases of study, V and Ni show a positive relationship with clays and micas contents, indicating that when these mineralogical phases are low, their content decrease.
The peculiarity of the Devonian cases of study are the high pyrite contents that show a positive relationship with TOC indicating the development of euxinia in the samples with high pyrite concentrations.

Again, Th, Zr and Al are hosted by clays and micas and do not show relationship with OM. Finally, Mn shows a negative correlation with TOC, indicating that in this case in can be useful to trace the redox conditions.

Finally, these cases of study show negative correlations between TOC and carbonates content whereas positive correlations between TOC and clays and micas content indicating the development of reducing conditions associated to the rising of the CCD leading to the deposition of mainly silicates and fine-grained sediments.

Comparing immature and mature cases of study

In chapter 9, immature (Cretaceous and Triassic) and mature (Devonian) cases of study have been compared. Specifically, only the proxies related to the organic matter have been considered (V, Mo, U, Ni, Cu). Follow the main results:

- Maturity leads to a decrease in the naphtogenic parameters (TOC and HI), although the depletion is more visible for HI than TOC;
- The degree of maturity determines how much TOC and HI are depauperated compared to the original values;
- Mo allow to track the original TOC and HI values for the mature source rock because, regardless from the mineralogical content, the environment and the age, for the immature source rock, Mo draw a single trend (black lines in figures 9.1C and 9.1D);
- V and U show a dependence on mineralogy (clays and carbonates, respectively) as well as on the organic matter. That is why V and U can be consider reliable metals to track the original values of the naphtogenic parameters only if samples with a similar lithology are considered;
- Ni and Cu do not depend only on the organic matter content, but also by the pyrite and clays and micas contents; thus, the weak covariation with TOC allow to trace the original TOC values but the lack of a relationship with HI makes them not reliable to trace these parameters.

Conclusions and outlooks

The strength of this PhD lies in the high number of cases of study and samples analyzed during the three years. This has been possible thanks to Eni, that firstly has provided the samples and secondly owns a very fast but successful analytical procedure to acquire so many reliable data in a so short time. In addition, despite the analysis have been mostly carried out in Eni laboratories by technicians, each step of the analytical procedure have been followed actively leading to an improvement of the knowledge on classical analytical techniques (i.e. XRD, XRF, TOC-Rock Eval) and sample preparation procedures. Also, the possibility to apply

unconventional analytical techniques and proxies (i.e. LA-ICP-MS, iron speciation, thallium isotopes, etc.) has allowed to acquire new skills on laboratory procedures (e.g. sample preparation) and analysis.
Another very important point that has been crucial to the success of the PhD was the long time spent during the first year on the bibliographic research. In fact, without the knowledge on the geochemistry of low temperature (sedimentary) environments, it would have been impossible to reach these conclusions.

The results of this thesis are very successful and significant. In fact, to our knowledge, this is the first work in which so many data have been analyzed, compared and studied all together from both inorganic and organic point of view. Indeed, in literature there is a lack of comparison of rocks considering age, depositional environment and maturity all together.
Unfortunately, we were not able to analyze other mature cases of study to compare with the immature ones because of the pandemic SARS-CoV-2. Indeed, the last year of PhD was dedicated to the mature cases of study but due to the lockdown, the analysis were completed partially. However, the comparison with the Devonian mature cases of study has led to important results that better results can be achieved by adding even more samples to our data processing. In particular, the results obtained and discussed in chapter 8 and 9 highlight that:

- A multi-proxy approach (trace elements, mineralogy and organic parameters) in necessary and successful in the data processing of different rocks, in order to reconstruct the depositional conditions of a source rock;
- Maturity is firstly observed in a depletion in the HI values, whereas TOC does not show significant impoverishments. In addition, the degree of maturity determines the degree of depletion of TOC and HI;
- Redox Sensitive Elements (V, Mo and U) always show positive correlations with the organic matter content and are not dependent on the age and maturity of the source rocks studied. This allow to use their concentrations to reconstruct the original naphtogenic parameters (TOC_0 and HI_0) when they are depleted because of maturity;
- Lithology can affect the distribution of some elements. For instance, V and U can show some relationships with the mineralogical content (clays and carbonates, respectively) leading to the idea that these elements can be reliable only if rocks with the same lithology are compared. Differently, Mo depends only on the OM, allowing to use this element to compare also very different rocks in terms of lithology;

- Ni and Cu are not always reliable redox proxies, but they can give information about the OM flux toward the sediments;
- Th, Zr and Al reflect the detrital fraction of the rock (aluminosilicates and clastic sediments) and are not related to the OM content. However, these elements can give information about the depositional environment, and in particular about the dilution degree of the OM and RSEs when rocks of different depositional environments (e.g. distal and proximal) are compared;
- Mn concentrations can give information about the redox conditions. However, it is not reliable due to its high mobility after diagenesis. Thus, its use as redox proxy needs to be coupled with other more reliable elements as V, Mo and U;
- Anomalies allow to trace the presence of the organic matter even if the organic data is not present. In fact, as explained for the Cretaceous and Triassic cases of study, V and Mo (and with a lesser extent U) are always enriched in presence of OM, allowing to use them to trace the TOC content or to understand that organic matter was present, even if its concentration in the rock is depleted due to a maturation process. In addition, the shape of TEs and REEs patterns is related to the provenance of the sediments and to the composition and depositional environment of the rock. For instance, a pattern very close to 1 (i.e. UCC value) can be related to a composition that is very similar to the sediments used by McLennan (2001) to calculate the UCC values, whereas a pattern that show depletion/enrichments compared to the UCC values can be related to different compositions (e.g. carbonates rich as NI1). However, just three immature cases of study have been analyzed with laser ablation in order to obtain the TEs and REEs values. A future outlook could be to analyze more samples (also mature) with the laser ablation in order to understand if the anomalies changes with other lithologies and maturity degrees.

These conclusions are very promising, and from an industrial point of view, these results are very useful to evaluate immature source rocks. In particular, using the inorganic geochemistry coupled with the organic parameters allowed us to trace in a qualitative way the redox conditions and the amount of organic matter deposited and preserved. From the first comparisons with the Devonian mature rocks, it is clear that the inorganic fraction of the rock preserves its characteristics with maturity allowing to trace the redox conditions and the original naphtogenic parameters using inorganic geochemistry. This is an important result in order to

evaluate the source rocks. In particular, a better characterization and evaluation of a source rock allow to reduce the exploration risk.

In addition, we have to keep in mind that all the considerations and discussions presented in chapter 8 and 9 are mostly qualitative. In fact, by using RSEs in many cases it is possible to distinguish between oxidizing and reducing conditions, but it is more difficult distinguish between suboxic, anoxic and euxinic. In literature, for many proxies the calibrations have been made on the analysis of suited of samples from modern sedimentary environments with known redox characteristics. However, even for such relatively well calibrated proxies, it is clear that they do not always respond to redox variation in the same way and thus do not necessarily yield the same quantitative values in all paleo-depositional system. In Jones and Manning (1994), an attempt to quantify the redox threshold for trace metals proxies has been made. Their results have been widely applied on other cases of studies even if the authors did not advocate for general applications of their redox proxies.
Thus, in literature there's a lack of general applications for the trace metals proxies. Considering the large suite of samples we have, a possible future step could be to assess thresholds for the RSEs in order to classify the redox conditions. For instance, this is possible with the iron speciation that allow to distinguish between oxic and anoxic conditions and between ferruginous and euxinic conditions (figure 3.2) trough thresholds in the Fe_{HR}/Fe_T and Fe_{PY}/Fe_{HR} ratios (see chapters 3.4 and 12).

CHAPTER 11

Constraining local redox conditions in an equivalent Bonarelli Level in the Fontana Valloneto section (Southern Italy)

In summer 2019, a field trip in Basilicata (Southern Italy) has been carried out to collect samples from a sedimentary section intersecting an equivalent of the Bonarelli Level. The section is called Fontana Valloneto section and is located close to Vaglio di Basilicata. During this PhD, a paper has been published regarding this section using the samples from the collection of Sabato et al. (2007). The paper is entitled "Geochemical evidence for local variability in redox and depositional conditions in a deep-water Bonarelli equivalent section from Southern Tethys (Fontana Valloneto Section, Southern Italy)" and it has been published in 2020 on Ofioliti (vol. 46, No.1). Whereas the new samples collected in 2019 constitute the main subject of Simone Zana's master's degree (December 2020).

11.1 Geological setting

The study area (figure 11.1.1) is located between Vaglio di Basilicata and Cancellara villages, NE of Potenza, on the easternmost thrust edge of the Southern Apennines. In the study area, from top to bottom, three different tectonic units have been identified (ISPRA, 2017; in press; Pieri et al., 2017; Pescatore et al., in press): Groppa d'Anzi, Vaglio di Basilicata and San Chirico tectonic units (figure 11.1.1).

The Groppa d'Anzi Tectonic Unit represents the inner margin of the middle Miocene Southern Apennines foredeep system (the allochthonous units of the early-middle Miocene thrust edge of the Southern Apennines and the overlying wedge-top deposits; Pescatore et al., 1999). The Vaglio di Basilicata Tectonic Unit is constituted by the Cretaceous-Miocene succession of the Lagonegro–Molise Basin sensu Mostardini and Merlini (1986) and is represented from the bottom to the top by Flysch Galestrino, Flysch Rosso and Flysch Numidico formations; the Flysch Galestrino is poorly represented while the Flysch Rosso outcrops widely. The San Chirico Tectonic Unit is made up of three formations: Flysch Rosso, Flysch Numidico and Serra Palazzo Formation. Its Cretaceous – middle Miocene sedimentary succession is mainly represented by Serra Palazzo Formation belonging to the middle Miocene Southern Apennines Foredeep (e.g. Pescatore and Senatore, 1986; Gallicchio and Maiorano, 1999).

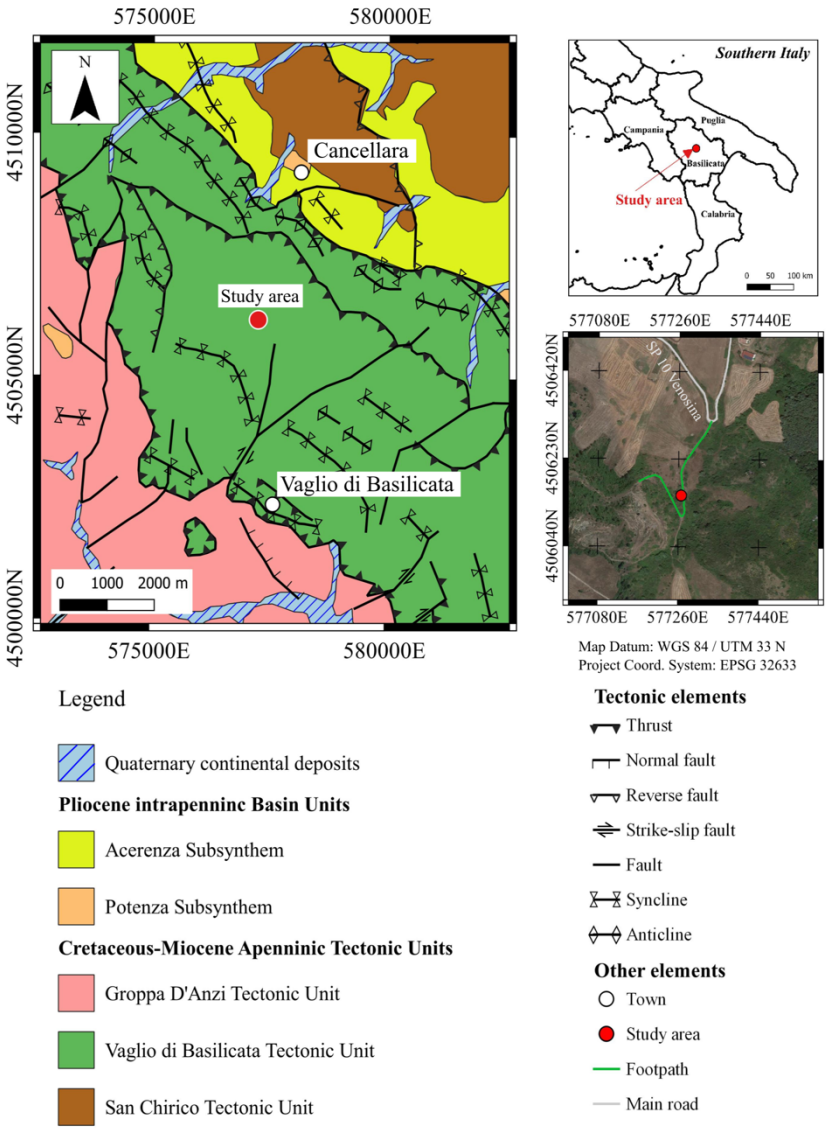

Figure 11.1.1: Tectonic setting of the study area (modified from ISPRA, in press) and outcrop location.

The studied succession crops out close to Vaglio di Basilicata (figure 11.1.1) and constitutes the detachment layer of the Vaglio di Basilicata Tectonic Unit. Locally, the Flysch Galestrino is not represented and this tectonic unit can be subdivided, from the bottom, into three stratigraphic units: lower, intermediate and upper units.

- The lower unit, is represented by varicoloured shale deposits interbedded with radiolarian-rich mudstones and black shale ("argilliti e radiolariti di Campomaggiore" sensu Sabato et al., 2007, lower part of Flysch Rosso, auctt.), includes the "argilliti varicolori" and the "diaspri" (sensu Centamore et al., 1971a and 1971b), and contains Bonarelli Horizon-equivalent (Gallicchio et al., 1996; Sabato et al., 2007) which is

related to the late Cretaceous worldwide Oceanic Anoxic Events OAE 2 (Schlanger and Jenkyns, 1976; Arthur et al., 1990).

- The intermediate unit consists of hemipelagic and clastic resedimented limestones with interbedded Cretaceous-early Miocene red marls and clays; this unit comprises the "calcareniti e argilliti rosse di Fontana Valloneto" sensu Centamore et al. (1971a; b) and corresponds to the middle and upper part of Flysch Rosso (Sabato et al., 2007).
- The upper unit corresponds to the Burdigalian-early Langhian Flysch Numidico Formation (e.g. Ogniben, 1969; Ciaranfi and Loiacono, 1983; Patacca et al., 1992; Gallicchio et al., 1996; Guerrera et al., 2012). This formation is represented by yellowish quartz-rich arenites with interbedded brownish grey clays, exclusively fed by the African Craton (e.g. Fornelli et al., 2019; Butler et al., 2020), and represents the first siliciclastic input in the Lagonegro-Molise Basin.

The lower unit, well represented in the Fontana Valloneto section, was firstly attributed to the Cretaceous–Eocene Sicilidi Units ("Argille Variegate" sensu Ogniben, 1969) and then to more outer units belonging to the Lagonegro–Molise Basin (late Cretaceous– early Miocene; "argilliti varicolori" sensu Mostardini and Merlini, 1986; "Fysch Rosso esterno" sensu Pescatore et al., 1988; "argilliti e radiolariti di Campomaggiore", sensu Sabato et al., 2007). Successively, the "argilliti e radiolariti di Campomaggiore" and the intermediate unit of the Vaglio di Basilicata Tectonic Unit were formally grouped in a single formation (Flysch Rosso) subdivided, from bottom, in two members: "membro diasprigno" and "membro calcareo" (APAT, 2006).

11.2 The outcrop

The Fontana Valloneto stratigraphic section is located along a slope on the north-eastern limb of a syncline with a NW-SE striking axial plane (figures 11.1.1 and 11.2.1). Generally, the section consists of reddish shale, laminated and fissile, interbedded with greenish shale (Fig. 2) indicating that the depositional environment was located in a deep-sea basin for the entire interval represented by the section. The biostratigraphic micropaleontological assemblage has allowed to Sabato et al. (2007) to attribute to the Fontana Valloneto sedimentary succession an age spanning from lower Albian to Turonian (~100 – 90 Ma).

Specifically, this section, as described by Sabato et al. (2007), can be divided into two portions separated by an about 15m-thick zone covered by vegetation. The lower 37 m-thick part, early-middle Albian in age, is mainly made up of reddish siliceous claystone/clayshales with minor

green and grey interbedded layers. Their beds are some centimeters up to a few decimeters thick and show dense parallel- and ripple laminations. Some very thin layers (a few centimeters) of black shales highlight due to the presence of Fe–Mn oxy-hydroxides; in particular, one of this layer, also thanks to its TOC content (~3.5 wt%) was referred by the authors to an organic enriched event called "Valloneto Albian Event 1" (VAE1, sample V13A, in figure 11.2.1). Sabato et al. (2007) show that in this part of the section (samples V0A-V16B in figure 11.2.1), radiolarians (such as: *Dictyomitra montisserei, Dictyomitra gracilis, Dictyomitra pulchra* and *Thanarla brouweri*) are present in the green claystones/clayshales, where they are well preserved. Conversely, in the red shales and black shales, radiolarians and other microfossils are absent.

The upper part of the section, of Cenomanian-Turonian in age, is about 6 m-thick, and is divisible in three packages. The lowermost package (~1,3 m thick; samples V16D-V20A in figure 11.2.1) is mainly represented by thinly bedded red radiolarian-rich mudstone and claystones/clayshales. The age of this part of the section has been attributed to the Cenomanian thanks to the radiolarian assemblages constituted mainly by *Dactyliosphaera silviae, Pseudodictyomitra tiara, Thanarla pulchra, Thanarla veneta, Novixitus mclaughlini, Rhopalosyringium majourensis, Rhopalosyringium petilum* and *Guttacapsa gutta* (lower radiolarian assemblage samples V17 – V25, Sabato et al., 2007). The intermediate package is about 2,3 m-thick (samples V21-V37A in figures 11.2.1 and 11.2.3) and is mainly made of centimeters layers of grey and green dark siliceous mudstones (figure 11.2.3C) with interbedded green siliceous clayshales and black shales (figure 11.2.3B) and very rare limestones (figure 11.2.1). This package shows a very high amount of organic matter with a TOC value spanning from 30 wt% to 41,9 wt%. All the analyzed features allowed the authors to identify the Bonarelli Horizon-equivalent (BH-e) for this part of the section (figures 11.2.1 and 11.2.3), worldwide corresponding to the Oceanic Anoxic Event 2 (OAE 2 sensu Schlanger and Jenkins, 1976). Several micropaleontological assemblage changes moving into the BH-e: the Cenomanian species disappear above the samples V25, while the samples V33 – V37 yield typical Turonian radiolarian species (Sabato et al., 2007).

Finally, the upper package, about 2,7 m-thick and Turonian in age (samples V39B-V47B in figure 11.2.1), represents a continuous sedimentary record, constituted by an alternance of red claystones/clayshales and radiolarian rich-mudstones. Sabato et al. (2007) show a Turonian radiolarian assemblages into this package, constituted by *Crucella cachensis, Hemicryptocapsa polyhedra, Acanthocircus hueyi* and *Alievium superbum*.

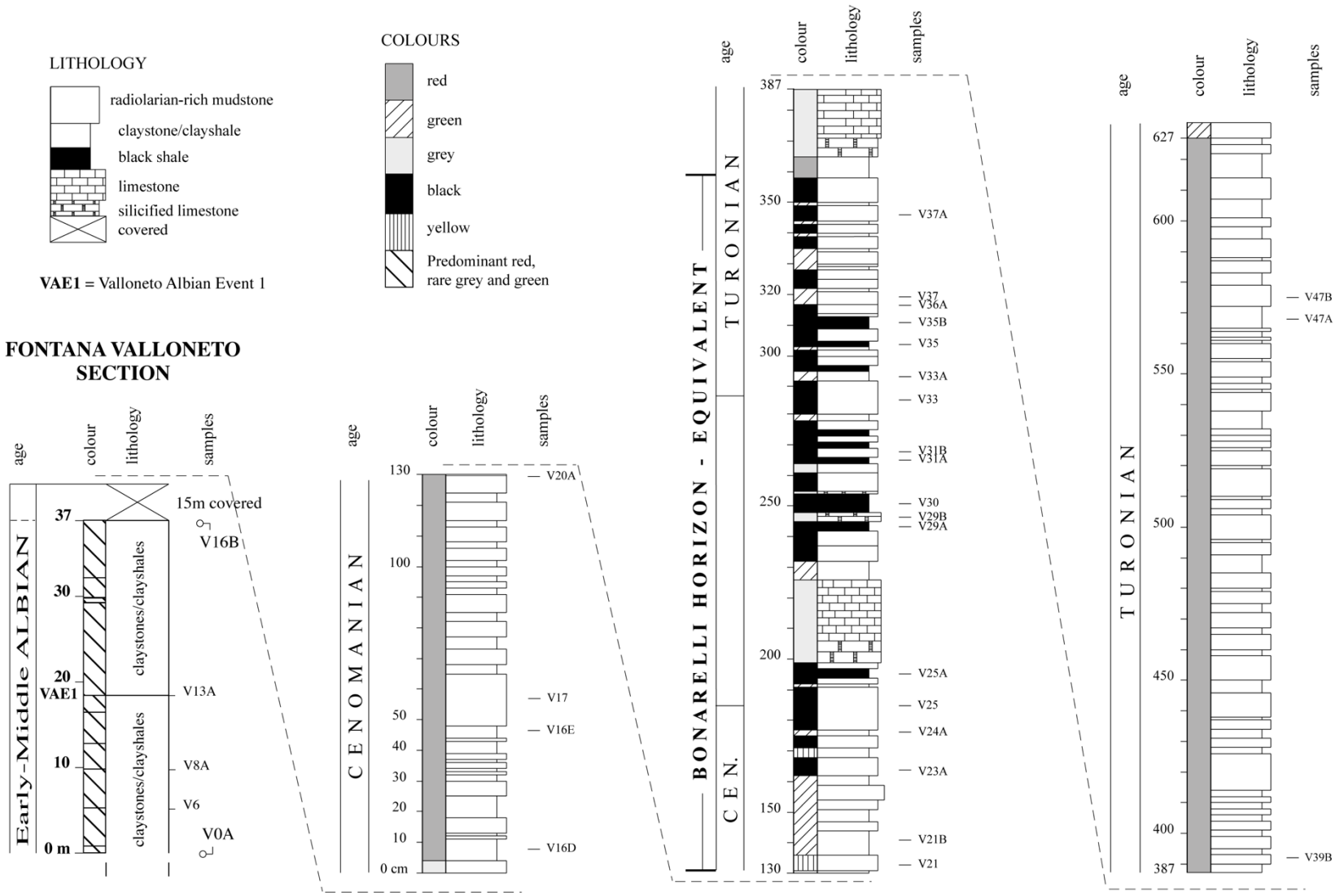

Figure 11.2.1: Stratigraphy of the Bonarelli Horizon-equivalent along the Fontana Valloneto section (modified from Sabato et al., 2007). Take into consideration the different used scales in the two parts of the section.

However, during this PhD a new field work has been made in collaboration with Dott. Alberto Bosino (PhD student at the university of Pavia) and Simone Zana (master's degree student at the University of Pavia).

44 samples have been collected from the section and a new stratigraphic column resulted (figure 11.2.2). The outcrop is ~3.3 m thick and is divisible in three packages. The lowermost package (~20 cm thick) is mainly represented by thinly bedded red radiolarian-rich mudstone and claystones/clayshale in centimeters and millimeters layers. The intermediate package is about 2 m-thick (figures 11.1.1.3) and is mainly made of centimeters layers of grey and green dark siliceous mudstones with interbedded green siliceous clayshales and black shales and very rare limestones. In this package high amount of organic matter can be supposed due to the presence of black radiolarites and black shales (figure 11.2.2) and in agreement with Sabato et al. (2007). It is likely that this package may correspond to the Bonarelli Horizon identified by Sabato et al. (2007) (figures 11.2.1), worldwide corresponding to the oceanic Anoxic Event 2 (OAE 2 sensu Schlanger and Jenkyns, 1976). Finally, the upper package, about 1 m-thick and Turonian in age, represent a sedimentary record of red, yellow and grey radiolarian-rich mudstone and claystones/clayshale in centimeters layers. At times, the radiolarites show impregnations of Mn-Fe oxides (figure 11.2.4).

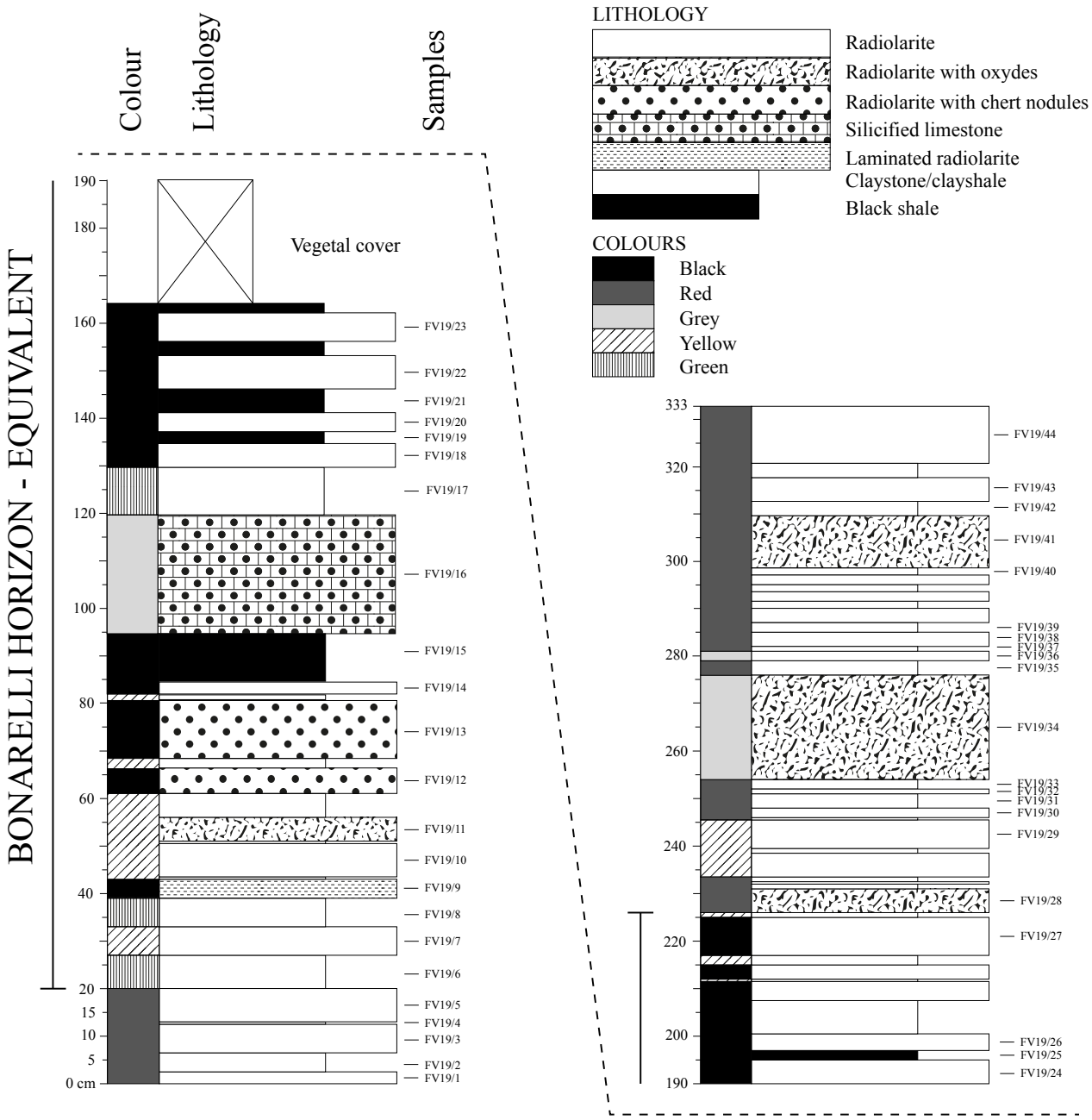

Figure 11.2.2: Stratigraphy of the Bonarelli Horizon-equivalent along the Fontana Valloneto section after the field trip in 2019.

Our field trip shows a stratigraphy in agreement with the one showed by Sabato et al. (2007), indicating that the same section has been samples. In particular, the new stratigraphic section (figure 11.2.2) should correspond to the central part of the section from Sabato et al. (2007) represented in figure 11.2.1, Cenomanian – Turonian in age. However, the poor field exposure prevented to collect samples along the entire section showed in figure 11.2.1.

The Fontana Valloneto section mainly consists of reddish shale, laminated and fissile, interbedded with greenish shale (figures 11.2.1 and 11.2.2) indicating that the depositional

environment was located in a deep-sea basin for the entire interval represented by the section. The thickness of the layers varies from some centimeters up to a few decimeters. The Bonarelli Horizon-equivalent crops out in the central part of the section, in a portion of ~2m-thick in both sections (figures 11.2.3 and 11.2.3). It is constituted mainly by grey and greenish siltstone, black shale, and radiolarites (figures 11.2.1, 11.2.2 and 11.2.3). The section of Fontana Valloneto spans from Lower Albian to Turonian (~100 – 90 Ma) (Sabato et al., 2007), thus representing a continuous sedimentary record intercepting the Anoxic Event 2, equivalent to the Bonarelli Level.

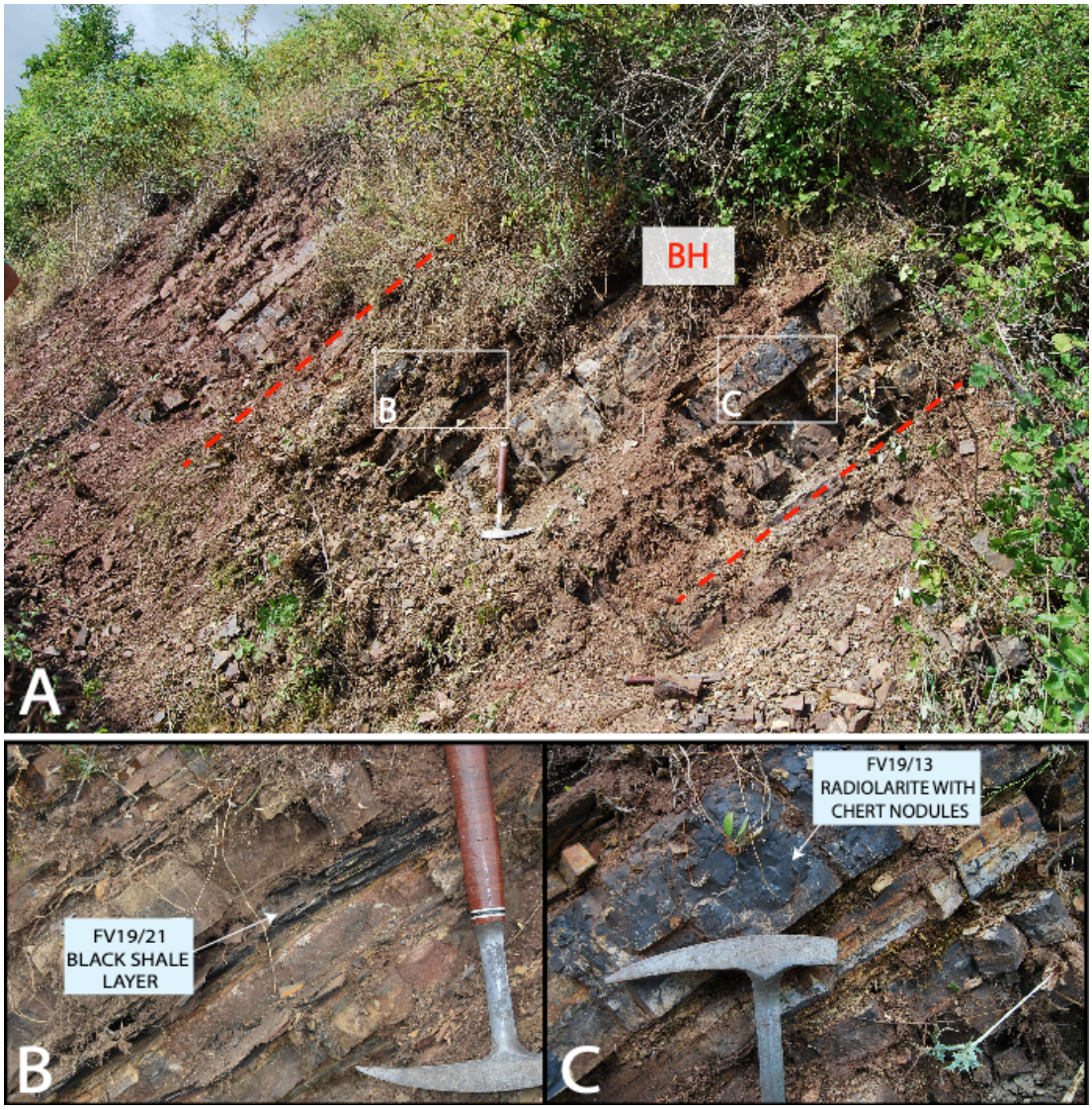

Figure 11.2.3: (A) Outcrop of the upper part of the Fontana Valloneto section containing the Bonarelli Horizon – equivalent (figure 11.2.2); (B) layer of black shales in the Bonarelli Horizon – equivalent; (C) dark siliceous mudstone in the Bonarelli Horizon - equivalent.

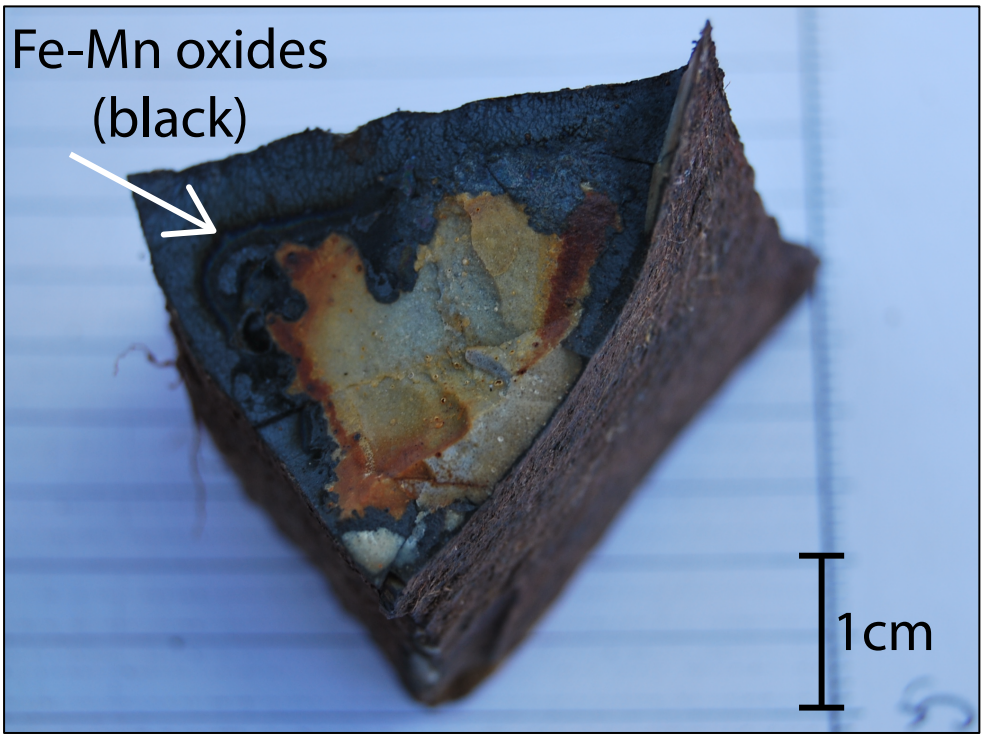

Figure 11.2.4: Detail of Fe-Mn oxides in a yellow radiolarite in Fontana Valloneto Section (FV9/11).

11.3 Materials and methods

Sampling

Thirty-nine surface samples have been selected for the mineralogical and chemical characterization from the collection of Sabato et al., (2007) (figure 11.2.1) spanning the entire section. 17 samples (from V0A to V16B) have been collected in the lower part of the section, Early-Middle Albian in age. 3 samples (from V16D to V20A) have been collected in the middle part of the interval. These samples are of Cenomanian age and are older than the BH. Owning to the BH along the Cenomanian-Turonian boundary, 16 samples (from V21 to V37A) have been selected. Finally, in the upper part of the succession 3 samples (from V39B to V47B) of Turonian age have been selected. The lithology and color of each sample are represented in figure 11.2.1. We must note, however, that the poor field exposure prevented to collect representative samples from Late Albian to Early Cenomanian (~15m; see figure 11.2.1).

Analytical methodologies and techniques

Organic geochemical (TOC and HI) data are from Sabato et al. (2007). Mineralogical and chemical analyses were performed at the Geolab of Eni S.p.a. in San Donato Milanese (Italy). Selected samples were disaggregated and finely grinded with W-Cr mortar. Fused beams using a $Li_2B_4O_7$ flux and pressed pellets were obtained from each pulverized sample. Major and trace

element compositions were obtained by X-ray fluorescence (XRF) on fused beams and pressed pellets, respectively. Mineralogy was acquired by X-ray diffraction (XRD) on X-ray Powder Diffraction (XRPD).

Mineralogical composition was determined by X-ray Powder Diffraction (XRD) using a Panalytical Cubi'X instrument equipped with a CuKα (λ =1.54178 Å) radiation source and a Fast detector. The data have been collected in the spectral interval $3° \leq 2\theta \leq 70°$ with steps of 0.02° 2θ and accumulation times of 10s/step. The quantitative bulk analysis was carried out by means of a full-profile fitting procedure based on the Rietveld method. The high accuracy of the spectra at low 2θ angle (the spectra starts from 2° 2θ) has allowed to distinguish between the clayey phases (especially between kaolinite and chlorite) without any pre-treatments of the samples.

Major and trace element concentrations were determined using a Wavelength Dispersive X-Ray Fluorescence System (Panalytical Magix Pro). The chemical data have been used to check the quality of the mineralogical data by XRD.

11.4 Results

Mineralogy

Table 11.4 shows the mineralogical composition of selected samples, which also include the TOC values from Sabato et al (2007) normalized to 100 wt%. The section is composed mainly by quartz, micas and clays (illite type, kaolinite, vermiculite and chlorite) and other minor phases (goethite, gypsum, fluorapatite, pyrite, plagioclase). Importantly, quartz increases from the bottom to the top of the section with and initial average of ~55 wt% prior to, ~63 wt% during and ~75 wt% after the BH. On the contrary, micas and clays decrease along the section from an average of ~37 wt% before the BH to ~18 wt% after the anoxic event. In particular, illite type increases upward from an average of ~3 wt% before the BH to ~6 wt% during the anoxic event, while after the event it decreases until zero. On the contrary, kaolinite shows an average of ~10 wt% prior to the BH, ~1 wt% during and ~2 wt% after the anoxic event. Also, muscovite shows a similar behavior to kaolinite, varying between ~12 and 10 wt% along the section. Chlorite contents are mostly close to zero, however some sample randomly scattered in the section show contents up to ~21 wt%. In the BH, a little amount of fluorapatite is present (up to ~7.5 wt%). Phases related to surface alteration are present in a good amount (vermiculite, gypsum, goethite, hematite). In particular vermiculite is present in a good amount prior to the BH (~9 wt%) and decreases upward (it reaches ~2 wt% after the BH).

Sample name	(m)	TOC (wt%)	Cal (wt%)	Qz (wt%)	Pl (wt%)	Ilt type (wt%)	Kln (w%)	Ms (wt%)	Vrm (wt%)	Chl (wt%)	Py (wt%)	Hem (wt%)	Gth (wt%)	Gp (wt%)	Hl (wt%)	FAp (wt%)
V47B	57.8	0.03	-	89.1	-	-	1.7	4.5	0.7	-	-	4.2	-	-	-	-
V47A	57.7	0.02	-	55.1	5.5	6.4	4.8	12.7	5.4	3.7	1.3	5.2	-	-	-	-
V39B	55.9	0.02	-	83.6	-	-	-	14.8	0.4	-	-	1.0	-	-	-	-
V37A	55.5	0.02	-	93.6	-	6.4	-	-	-	-	-	-	-	-	-	-
V36A	55.2	2.44	-	88.4	-	9.2	-	-	-	-	-	-	-	-	-	-
V35B	55.1	25.81	-	35.3	4.2	15.1	-	10.7	7.9	0.1	-	-	0.9	-	-	-
V35	55.1	29.19	-	33.2	2.0	-	-	5.8	23.9	0.7	3.1	-	-	2.3	-	-
V33A	54.9	0.05	-	66.2	5.4	7.1	2.0	16.0	1.5	1.9	-	-	-	-	-	-
V31B	54.7	0.73	-	85.1	-	10.9	-	-	3.2	-	0.3	-	-	-	-	-
V31A	54.7	23.77	-	22.4	0.8	2.4	-	6.6	10.1	14.8	-	-	19.2	-	-	-
V30	54.5	25.50	-	43.2	4.9	4.6	5.0	6.8	1.3	4.6	0.2	0.4	-	2.8	0.1	0.8
V29B	54.5	1.60	-	90.7	-	6.6	-	-	-	-	0.9	-	-	-	-	-
V29A	54.4	16.03	-	61.0	3.9	6.0	0.4	-	10.5	2.1	-	-	-	-	-	-
V25A	54.0	26.52	-	41.3	3.3	10.5	6.9	7.4	0.4	1.5	1.0	0.9	-	-	-	0.7
V24A	53.8	0.05	-	41.9	6.0	12.9	2.8	8.4	17.3	2.0	-	1.3	-	-	-	7.5
V23A (dark)	53.7	3.22	-	78.4	-	-	-	15.2	-	-	-	0.1	-	-	-	3.1
V23A (light)	53.6	0.01	-	95.7	-	-	-	4.1	0.2	-	-	-	-	-	-	-
V21B	53.4	0.08	-	47.5	5.8	7.3	-	12.9	21.1	4.1	-	1.3	-	-	-	-
V21	53.4	0.01	-	84.8	-	-	-	-	4.5	-	-	-	10.7	-	-	-
V20A	53.3	0.02	6.9	73.8	3.9	2.4	3.4	7.9	1.2	-	-	-	-	0.3	-	-
V16E	52.5	0.01	3.1	54.4	1.7	-	-	20.7	10.5	0.6	-	6.9	-	1.9	-	-
V16D	52.1	0.01	-	46.7	4.5	2.8	9.7	25.3	5.1	0.2	-	5.5	-	-	-	-
V16B	37.0	0.02	-	56.8	6.0	10.1	0.4	12.0	13.7	1.1	-	-	-	-	-	-
V16A	32.0	0.04	-	42.7	1.2	3.3	28.1	5.3	-	19.5	-	-	-	-	-	-
V15F	31.0	0.02	-	62.8	3.3	2.3	9.3	4.0	18.1	-	-	-	-	-	-	-
V15D	28.0	0.03	-	45.8	5.4	4.3	8.8	16.1	13.1	-	-	6.5	-	-	-	-
V15C	24.0	0.14	-	65.2	3.7	-	8.6	19.8	2.6	-	-	-	-	-	-	-
V15B	22.0	0.02	-	53.1	1.5	-	6.1	14.8	7.3	-	-	-	17.2	-	-	-
V13A	18.0	3.43	-	71.8	3.3	-	7.4	11.0	3.1	-	-	-	-	-	-	-
V12B	15.0	0.05	-	56.1	4.0	4.3	17.0	7.7	11.0	-	-	-	-	-	-	-
V10B	13.0	0.04	-	46.3	0.8	1.1	10.8	8.8	25.8	-	-	6.2	-	-	-	-
V10A	12.0	0.06	-	44.9	4.1	2.3	5.6	14.8	28.4	-	-	-	-	-	-	-
V10	11.0	0.20	-	51.5	3.6	-	9.3	14.6	20.9	-	-	-	-	-	-	-
V8A	10.0	0.04	-	48.5	4.9	5.5	29.6	9.8	0.7	1.0	-	-	-	-	-	-
V6	5.0	0.03	-	47.0	6.2	18.5	6.4	0.3	-	21.1	-	0.6	-	-	-	-
V4A	3.0	0.03	-	66.5	1.1	1.5	14.5	6.3	8.4	1.5	-	-	-	-	-	-
V1	2.0	0.02	-	43.0	-	6.9	16.5	17.0	-	15.7	-	0.9	-	-	-	-
V0B	1.0	0.03	-	53.9	3.1	-	5.0	11.2	16.1	-	-	10.7	-	-	-	-
V0A	0.0	0.06	-	73.5	4.7	-	3.7	15.1	2.8	-	-	-	-	-	-	-

Table 11.4.1 - Mineralogical content of the section normalized to TOC (wt%). Pyrite contents are underestimated (see discussion in chapter 5.1). The grey area represents the BH-e interval. Mineral names are represented in the abbreviated form (Whitney and Evans, 2010): (Cal) calcite, (Qz) quartz, (Pl) plagioclase, (Ilt type) illite type, (Kln) kaolinite, (Ms) muscovite, (Vrm) vermiculite, (Chl) chlorite, (Py) pyrite, (Hem) hematite, (Gth) geothite, (Gp) gypsum, (Hl) halite and (FAp) fluorapatite.

Organic geochemistry

The organic characteristics of the Fontana Valloneto section have been already discussed by Sabato et al. (2007), where can be found an in-depth discussion of the data. Here, we used the TOC values collected by Sabato et al. (2007). The black shales in the BH have high TOC content (>10 wt%) and the values from Rock – Eval pyrolysis suggest that these rocks are "immature", therefore they have Petroleum Potential, TOC and Hydrogen Index (HI) comparable to the original values. Some samples from other lithofacies (i.e., dark siliceous claystone and black siliceous mudstone – samples V23A, V29B, V31B and V36A) from the

Bonarelli Horizon have high organic matter content (TOC between 1 and 10 wt%). The Bonarelli Horizon – equivalent is characterized by a large amount of organic matter for the black shales (the maximum is 29.19 wt%). Finally, optical analyses on kerogen highlight very high amount (>80%) of AOM (Amorphous Organic Matter), and values of HI for samples with TOC > 10 wt% are always above 500 mg HC/g TOC (Sabato et al., 2007), indicating the main presence of algal marine organic matter in these layers.

Elements sensitive to redox conditions (RSEs) and Mn

The RSEs (e.g. V, Mo, U) and Mn (concentrations in table 11.4.2) are used as indicators for redox conditions (see discussions below). In particular, in figure 11.4.1, RSEs and Mn are represented using the enrichment factor (EF), in order to smooth the dilution effect by biogenic silica. The EF is defined as $X_{EF}=[(X/Al)_{sample}/(X/Al)_{UCC}]$ (Algeo and Li, 2020), where X and Al stand for the weight concentrations of element X and Al, respectively. Samples were normalized using the Upper Continental Crust (UCC) compositions of McLennan (2001). If X_{EF} is greater than 1, then element X is enriched relative to average shales and, if X_{EF} is less than 1, it is depleted (Tribovillard et al., 2006).

In our section, values of V, Mo and U are mirrored by increase in TOC (figure 11.4.1). In detail, during the BH, these three elements in sediments are higher than the reference values of the upper continental crust (UCC; McLennan, 2001). The general increase in V, Mo and U with TOC is also observed in the Albian sample V13A (VAE1 in figure 11.4.1). On the contrary, Mn shows an opposite trend (figure 11.4.1), decreasing at increasing TOC, and likely due to the Mn oxides dissolution under reducing conditions (Tribovillard et al., 2006).

Sample name	(m)	V (ppm)	Mn (ppm)	Rb (ppm)	Y (ppm)	Zr (ppm)	Mo (ppm)	U (ppm)	K (wt%)	Ti (wt%)	Al (wt%)	Si (wt%)	TOC (wt%)	Mo/TOC (ppm/wt%)
V47B	57.8	22	14462	17	12	27	3	-	0.45	0.09	2.14	1.00	0.03	N. C.
V47A	57.7	53	2686	83	48	99	3	-	1.82	0.42	6.39	2.99	0.02	N. C.
V39B	55.9	13	482	22	5	23	2	-	0.48	0.07	2.06	0.96	0.02	N. C.
V37A	55.5	16	804	5	2	11	5	-	0.13	0.02	0.62	0.29	0.02	N. C.
V36A	55.2	96	106	10	5	18	14	1	0.24	0.04	0.96	0.45	2.44	5.6
V35B	55.1	1818	148	60	30	76	116	20	2.97	0.55	6.56	3.07	25.81	4.5
V35	55.1	691	346	38	59	58	86	28	1.74	0.36	4.56	2.13	29.19	2.9
V33A	54.9	195	125	102	18	110	5	4	2.18	0.43	6.47	3.02	0.05	N. C.
V31B	54.7	162	207	18	3	35	5	-	0.45	0.09	1.78	0.83	0.73	N. C.
V31A	54.7	726	580	39	23	56	99	11	1.60	0.70	5.51	2.58	23.77	4.2
V30	54.5	624	240	43	18	51	77	11	1.75	0.35	4.83	2.26	25.50	3.0
V29B	54.5	131	5349	19	20	39	14	4	0.52	0.11	2.29	1.07	1.60	8.8
V29A	54.4	584	173	28	12	34	100	5	0.98	0.30	3.45	1.61	16.03	6.2
V25A	54.0	709	327	48	20	66	160	26	2.21	0.49	5.52	2.58	26.52	6.0
V24A	53.8	175	755	108	97	143	53	7	2.55	0.56	7.43	3.47	0.05	N. C.
V23A (dark)	53.7	37	444	18	54	34	9	3	0.43	0.08	1.73	0.81	3.22	2.9
V23A (light)	53.6	53	251	10	9	22	7	-	0.25	0.05	0.95	0.44	0.01	N. C.
V21B	53.4	132	3599	99	35	108	4	-	2.39	0.51	7.53	3.52	0.08	N. C.
V21	53.4	57	4130	10	7	48	4	-	0.38	0.07	1.71	0.80	0.01	N. C.
V20A	53.3	54	59626	27	18	38	6	-	0.84	0.21	3.04	1.42	0.02	N. C.
V16E	52.5	56	59064	68	48	83	3	-	1.57	0.33	5.33	2.49	0.01	N. C.
V16D	52.1	81	13272	86	41	93	3	1	2.04	0.41	6.68	3.12	0.01	N. C.
V16B	37.0	101	3044	64	28	117	3	-	1.60	0.52	6.98	3.26	0.02	N. C.
V16A	32.0	177	541211	33	34	50	5	-	0.76	0.19	3.28	1.53	0.04	N. C.
V15F	31.0	108	242284	29	33	53	4	2	0.69	0.18	3.15	1.47	0.02	N. C.
V15D	28.0	75	226	87	30	123	3	-	1.93	0.53	7.99	3.74	0.03	N. C.
V15C	24.0	145	1756	57	18	105	3	-	1.37	0.41	5.53	2.59	0.14	N. C.
V15B	22.0	80	1069	51	21	89	21	-	1.04	0.27	4.33	2.02	0.02	N. C.
V13A	18.0	93	1836	35	15	87	31	11	0.89	0.32	4.16	1.94	3.43	9.0
V12B	15.0	107	45363	64	20	101	3	1	1.35	0.46	6.80	3.18	0.05	N. C.
V10B	13.0	83	187	82	36	145	3	1	1.72	0.63	8.73	4.08	0.04	N. C.
V10A	12.0	93	490	81	24	128	3	3	1.82	0.58	8.88	4.15	0.06	N. C.
V10	11.0	119	1520	75	21	136	3	7	1.73	0.57	8.47	3.96	0.20	N. C.
V8A	10.0	144	222945	67	47	91	4	2	1.39	0.36	6.40	2.99	0.04	N. C.
V6	5.0	198	486900	44	64	52	14	1	0.68	0.21	4.06	1.90	0.03	N. C.
V4A	3.0	53	1131	52	18	90	3	-	1.03	0.35	5.82	2.72	0.03	N. C.
V1	2.0	155	326109	55	54	85	8	2	1.11	0.33	5.74	2.68	0.02	N. C.
V0B	1.0	79	157	85	30	126	3	1	1.85	0.58	8.58	4.01	0.03	N. C.
V0A	0.0	119	107	74	24	121	7	1	1.68	0.49	7.09	3.31	0.06	N. C.

Table 11.4.2 - RSEs (V, Mo, U), Mn, Y, Zr, Al, Si and Mo/TOC content of the section. The grey area represents the BH-e interval.

Vanadium

In the Fontana Valloneto section, before the BH, V is enriched compared to the UCC (V_{UCC} = 107 ppm; McLennan, 2001) as shown by the EF with an average of ~$1.5x10^4$. During the anoxic event, V_{EF} shows very strong enrichments, with an average value of ~$6.7x10^4$ and a maximum value of ~$2.0x10^5$. In the upper part of the section, after the BH, V_{EF} shows an average of ~$6.2x10^3$.

Molybdenum

In the Fontana Valloneto section, before the BH, molybdenum enrichment factor shows average values of ~7.5 ppm, very close to 1. In the BH, Mo shows enrichments, indeed, the Mo_{EF}

reaches values of ~155 ppm (figure 11.4.1). After the anoxic event, Mo_{EF} shows an average of ~5.3.

Uranium

In the lower part of the Fontana Valloneto section, U results depleted compared to the UCC (U_{UCC} = 2.8 ppm; McLennan, 2001) as U_{EF} shows an average lower than 1. During the anoxic event, U_{EF} increases reaching a maximum of ~17.7 as shown in figure 11.4.1. In the samples after the BH, U is absent.

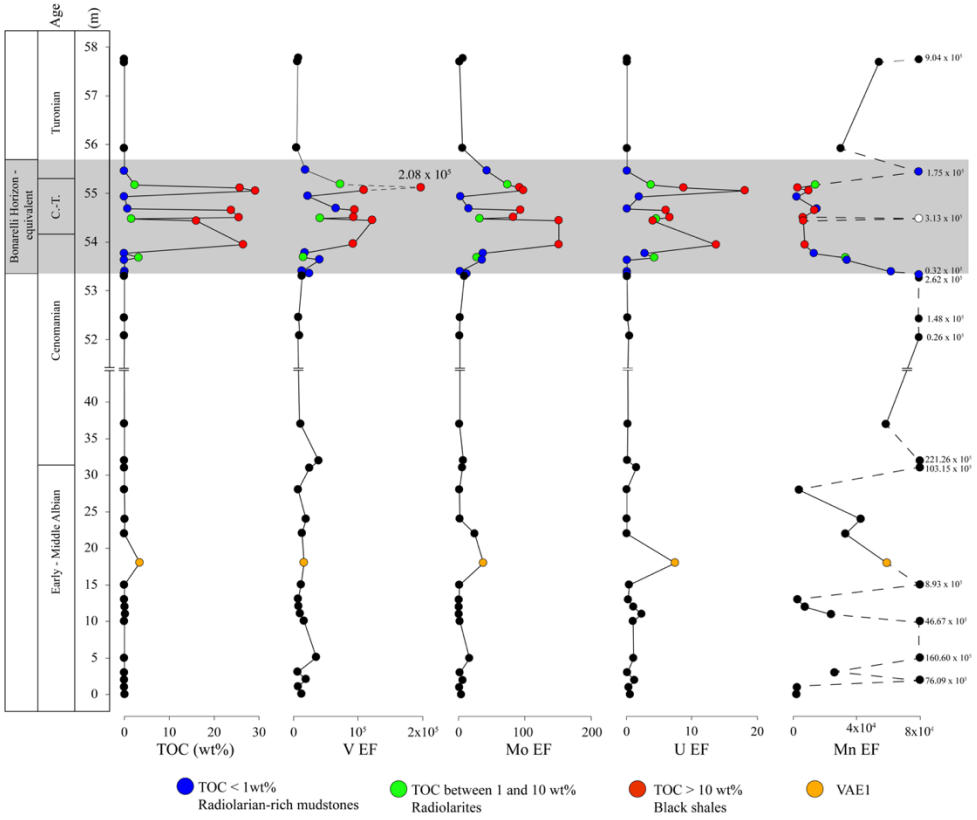

Figure 11.4.1 - Total Organic Carbon (TOC) (values from Sabato et al., 2007) and the enrichment factors of the redox – sensitive elements (V, Mo, U) and Mn. VAE1 stands for "Valloneto Albian Event 1". The white point in the MnEF graph represents an altered sample with anomalous value of Mn.

Manganese

Mn_{EF} in sediments deposited prior to the Bonarelli Horizon – equivalent (Late Albian - Cenomanian) is variable between a minimum of ~$2.0x10^3$ and a maximum of ~$221.2x10^5$ (figure 11.4.1). In the latter case, Mn forms microcrystalline or amorphous phases (e.g. oxy – hydroxides) not detected by XRD but visible in the samples by hand (figure 11.2.4). These phases (e.g. Rancieite, from Sabato et al., 2007) form black or brown crusts, probably incrustations formed during oxygenation events, as confirmed by Fiore et al. (2000) in a similar section from Campomaggiore (Basilicata, Potenza). In the BH, the Mn_{EF} values are lower than in the rest of the section, even if the samples at the onset and at the end of the BH can show

moderate Mn_{EF} values (up to ~$1.7x10^5$). The Valloneto Albian Event 1 is characterized by Mn_{EF} value of ~$5.9x10^4$.

Detrital proxies

Yttrium, zirconium and aluminum are usually used to represent the terrigenous fraction of black shales assuming that: (i) Y and Zr are immobile elements located mainly in igneous rocks or clastic sediments (Bau, 1996; Pašava et al., 2017) and (ii) Zr and Al are contributed by and are located entirely in the siliciclastic/aluminosilicate phases (Calvert and Pedersen, 1993; Tribovillard et al., 2006). All elements show a rough but progressive decrease upsection (figure 11.4.2 and table 11.4.2). Average zirconium and aluminum concentrations are of 72 ppm and 0.49 wt%, respectively. These values are substantially lower than UCC values of 190 ppm and 80400 ppm, respectively (McLennan, 2001). Yttrium concentrations range from 31 to 15 ppm, being thereby closer to the UCC value of 22 ppm (McLennan, 2001). Notably, samples within the BH show highly variable Zr, Al and Y contents, spanning the variability of the entire section. As a whole, there is no correlation between the detrital input and the TOC, as selected samples show variable Zr, Al and Y contents independently on their TOC content.

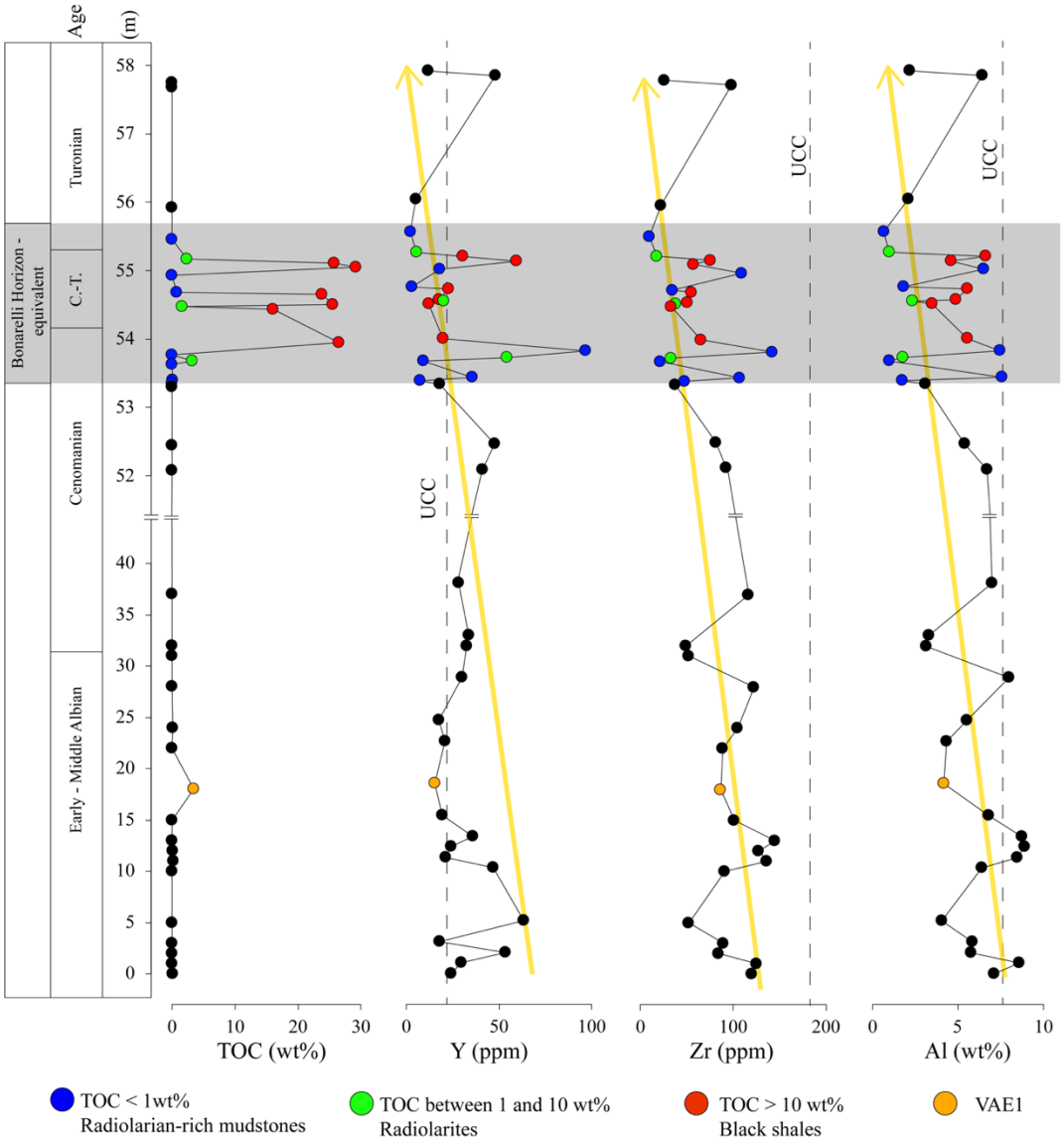

Figure 11.4.2 - Total Organic Carbon (TOC), Y, Zr and Al values along the Fontana Valloneto Section. Vertical dashed lines represent UCC values (McLennan, 2001). VAE1 stands for "Valloneto Albian Event 1". Yellow arrows represent the decreasing trend of Y, Zr and Al.

11.5 Discussion

Mineralogical variability

The almost complete absence of carbonates and widespread presence of quartz (table 11.4.1) indicates that the depositional environment was most likely located below the Calcite Compensation Depth (CCD). This is sustained by the occurrence of radiolarites, as widely documented by the biostratigraphic micropaleontological data collected by Sabato et al. (2007). The low Y, Zr and Al concentrations in the sediments throughout the section, substantially below UCC values (figure 11.4.2), further indicate an overall dilution of terrigenous material with organic matter and/or siliceous radiolarian cherts, pointing to distal deep waters.

Nonetheless, we note that carbonaceous laminae locally characterize the sedimentary section deposited before (i.e., samples V16E and V20A in table 11.4.1) and during the BH, although the latter were not analyzed for chemistry and mineralogy. The local presence of carbonate levels is due to the occurrence of fine-grained turbiditic events (often totally or partially silicified) interrupting the normal pelagic sedimentation (Sabato et al., 2007) rather than fluctuations of the CCD.

The mineralogical variability of clay minerals (figure 11.5.1) shows that illite type clay is mainly present in the Bonarelli Horizon, whereas kaolinite and muscovite occur mostly in the lower portion of the section, before the BH. This variability in clay distribution can be related to changes in the depositional environment at the onset of OAE 2 and, in particular, to the triggering of a slowdown of the oceanic circulation (Scopelliti et al., 2004; Scopelliti et al., 2006; Viaggi et al., 2019). This process, coupled with a distal environment under the CCD, may have caused the sedimentation for decantation of fine clays (i.e. illite type), together with the deposition of high amount of quartz (mainly biogenic) and may have prevented the sedimentation of continental-derived material (i.e. kaolinite and muscovite).

Finally, in table 11.4.1 low contents of pyrite are observed. Especially, pyrite is often absent or close to zero in the black shales related to euxinic conditions (see discussion below). This aspect is likely due to the alteration of pyrite forming not stochiometric and less crystalline phases or Fe oxides (e.g. goethite).

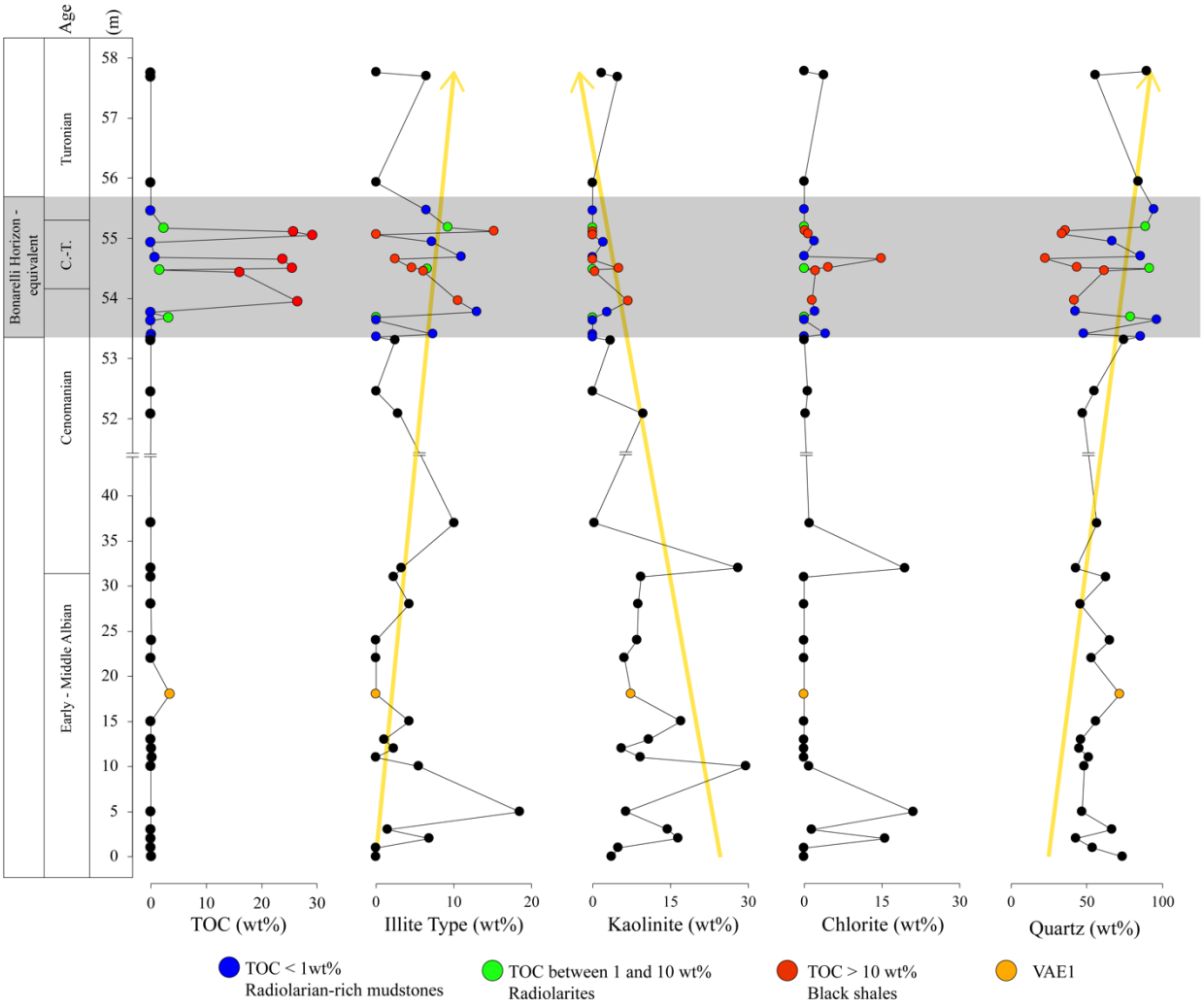

Figure 11.5.1 – Illite type, kaolinite, chlorite, quartz contents along the section. VAE1 stands for "Valloneto Albian Event 1". Yellow arrows represent the decreasing/increasing trend for illite type, kaolinite and quartz.

Some inference on redox conditions and primary productivity

Several authors showed that shale trace metals geochemistry is a powerful tool to assess redox conditions (Tribovillard et al., 2006 and referenced therein). In particular, the gradual variability in concentrations of Redox Sensitive elements (RSEs) (i.e., V, U, Mo) in marine sediments can be used to define oxic (>2.0 ml O_2/l H_2O), suboxic (0.2-2.0 ml O_2/l H_2O), anoxic (<0.2 ml O_2/l H_2O) and euxinic (absence O_2 of presence of free H_2S) conditions. This is possible because under reducing conditions and in laminated and organic-rich facies, RSEs show enrichments compared to global shale or Upper Continental Crust values (hereafter UCC from McLennan, 2001). Contrary, in bioturbated, organic – poor facies deposited under oxygenated conditions, RSEs show little or no enrichments compared to the concentrations in UCC. However, Viaggi et al. (2019) by studying a Late Aptian-Early Campanian immature well

sequence of OAEs (OAE1c, OAE1d, OAE2, OAE3) from Central Atlantic, find a covariance relationship among TOC, HI, U, S, pyrite (redox-related preservation signal), along with V, Mo, Ni, Zn, Se and P interpreted as nutrient-related bioproductivity signal from marine phytoplankton. This covariance pattern between nutrient-related elements complexed to kerogen and redox proxies, suggests the trace metals uptake in deep-sea organic sediments during anoxic events.

An exception is represented by Mn that results enriched under oxidizing conditions forming insoluble Mn oxides and depleted under reducing conditions.

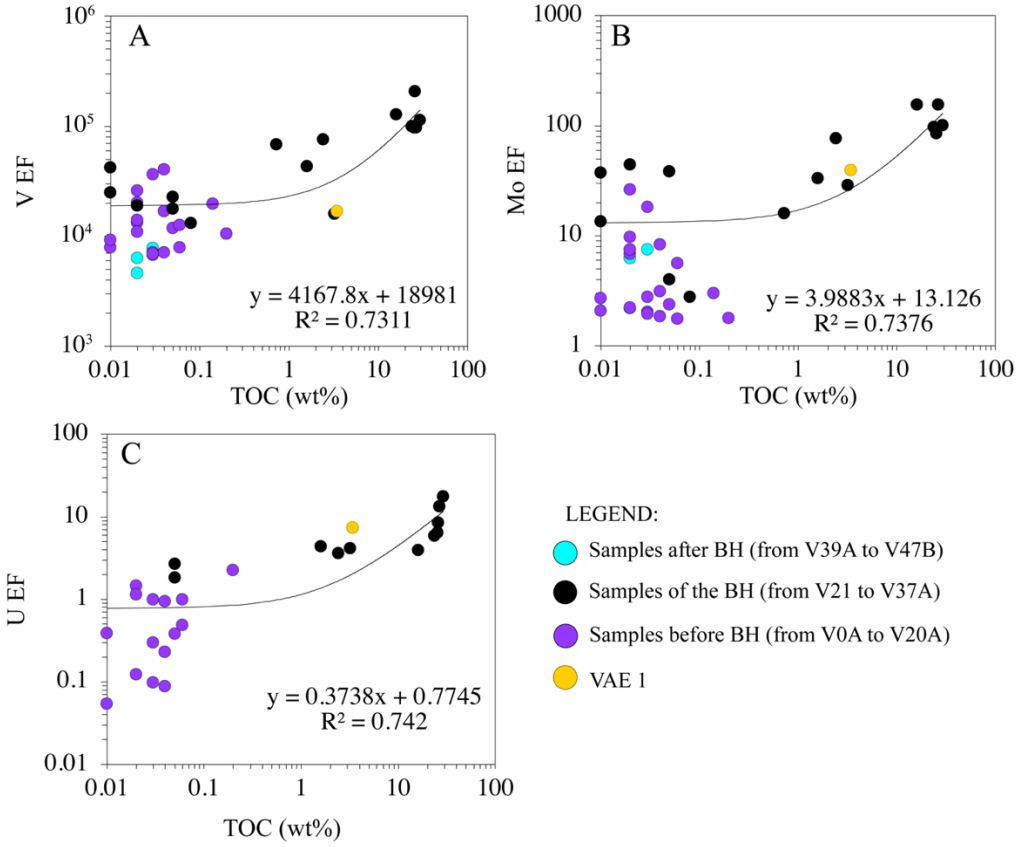

Figure 11.5.2 - Correlation between Total Organic Carbon (TOC) (values from Sabato et al., 2007) and redox – sensitive elements (A) V_{EF}; (B) Mo_{EF}; (C) U_{EF}. VAE1 stands for "Valloneto Albian Event 1".

Vanadium, molybdenum and uranium enrichment factors show positive correlations with TOC. At negligible TOC concentrations, all three elements show values close to those of the UCC (McLennan, 2001), while at high values of TOC, these elements are strongly enriched (figure 11.5.2).

These correlations are particularly well defined in the sediments within the BH, which extend towards very high TOC (> 10 wt%). These TOC-rich black shales (red points in figure 11.5.3) are characterized by strong RSEs enrichments, confirming that reducing conditions

allow both organic matter and trace metals to be preserved and fixed into the sediments (Algeo and Maynard, 2004; Tribovillard et al., 2006; Viaggi et al., 2019). In particular, Mo concentrations always higher than 25 ppm (table 11.4.2) indicate strong euxinic conditions (Scott and Lyons, 2012).

The black radiolarites with TOC between 1 and 10 wt% (green points in figure 11.5.3) show moderate Mo enrichments and Mo values between the UCC value (1.5 ppm; McLennan, 2001) and 25 ppm (table 11.4.2) pointing toward anoxia with limited uptake of Mo (Scott and Lyons, 2012). Also, in the same levels, V and U enrichment factors show values close to or slightly higher than 1 (figure 11.5.3). Regarding Mn_{EF}, V29B show very high Mn, likely related to alteration of the samples, whereas samples V36A and $V23A_{light}$ have Mn values of ~$14x10^3$ and ~$34x10^3$ ppm, respectively (figure 11.5.3). For the latter, the MnEF are high, however, they are placed in a contest of decreasing for the sample $V23A_{light}$ and increasing for the sample V36A, indicating the development of anoxic conditions at the beginning of the Bonarelli Horizon and the ending of the anoxic event, respectively.

Finally, levels with TOC <1 wt% also occur within the BH (blue points in figure 11.5.3). In agreement with low contents of organic matter, these levels consist mainly of grey/yellow/red radiolarian-rich mudstones and have RSEs enrichment factors that approach 1 (blue points in figure 11.5.3). Also, Mn in these samples shows enrichment factors close to 1 during the BH or higher than 1 at the onset and at the end of the anoxic event. It is thereby probable that the Mn concentrations mark the development of the reducing conditions at the beginning of the BH and the return to oxic conditions moving out of the BH. In addition, Gambacorta et al. (2016), describing Albian-Turonian sections containing BH and belonging to the Umbria-Marche Basin and the Belluno Basin (Italy), sustain that during the BH deposition radiolarian-rich layers can deposit during oxic-suboxic conditions possibly associated to a process of winnowing of the seafloor by relatively active bottom currents. Thus, it is possible that the deposition of these layers was temporarily characterized by “less reducing” (probably suboxic) periods in which the organic matter was degraded before being incorporated within the sediments.

Hence, changes in concentration of RSEs and nutrient-related elements suggest for the Bonarelli Horizon fluctuations in redox conditions (ranging between suboxic to euxinic) and in the primary OM productivity. Several authors relate these fluctuations to a strong orbital climatic forcing in which the main high productivity event was caused by a cyclicity of periods characterized by eccentricity-controlled humidity fluctuations. These events induced an increase in riverine influxes (high Rb/Al) and water stratification and, possibly, high aeolian

input (high Ti/Al). Specifically, Rb is known to be present in several common minerals including mica and clay minerals and generally related to the continental weathering of granitic rocks and fluvial discharge (Rachold and Brumsack, 2001; Scopelliti et al., 2004, 2006; Kylander et al., 2011; Tanaka and Watanabe, 2015). The wind, instead, might have favored a mixing of the shallow seawater and an increase of the nutrient supply (Scopelliti et al., 2004; Scopelliti et al., 2006; Galeotti et al., 2009).

In the rest of the section the RSEs enrichment factors gradually decreases towards 1, while Mn slowly increases showing high values of enrichment factor (figure 11.4.1), in agreement with oxigenated conditions and low TOC.

It is worth noting that the sample V13A located at 18 m from the bottom of the section (VAE1; orange point in figure 11.4.1) shows high TOC (~ 3.43 wt%) and enrichments in RSEs (except for V) compared to the neighboring deposits (figure 11.4.1), pointing toward anoxic conditions. Contrarily, Mn is enriched compared to the UCC (Mn_{EF} = ~$59x10^3$) and HI is low (~220 mg HC/g TOC; Sabato et al., 2007), indicating a possible weathering of the sample that led to a decrease in HI (and probably of TOC too) and an increase of Mn compared to the original values. Due to these considerations, we can infer local anoxic conditions during the deposition of the Valloneto Albian Event 1.

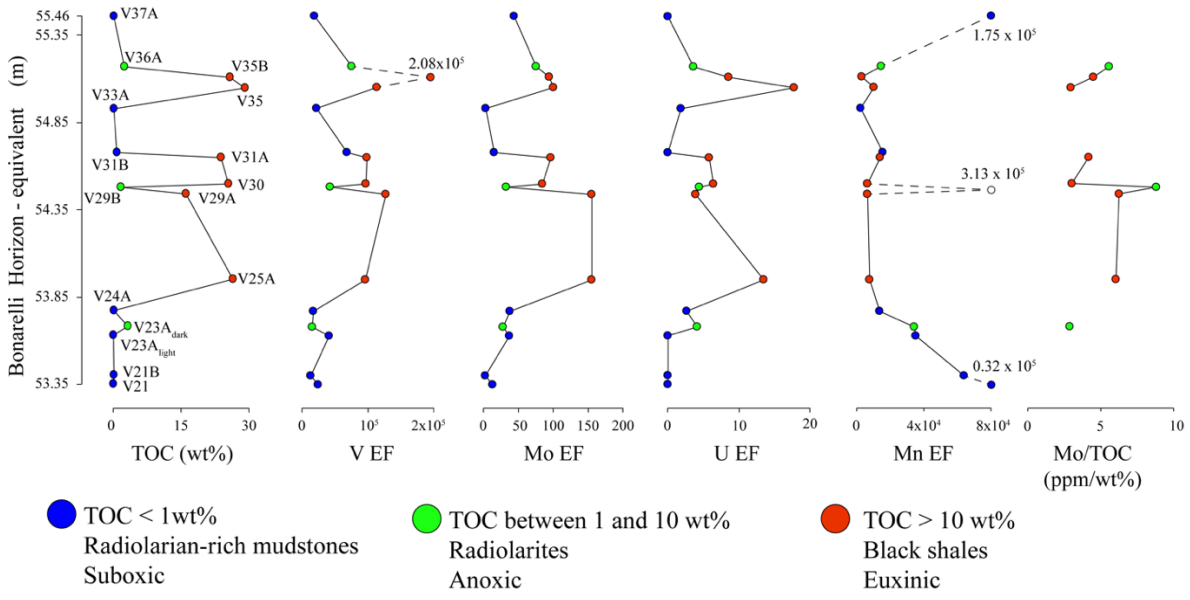

Figure 11.5.3 - Total Organic Carbon (TOC) (data from Sabato et al., 2007), V_{EF}, Mo_{EF}, U_{EF}, Mn_{EF}, Mo/TOC (only for samples with TOC > 1wt%) values along the Bonarelli Horizon – equivalent. The white point in the Mn_{EF} graph represents an altered sample with anomalous value of Mn.

Depositional environment

TOC and RSEs concentrations in the BH level of Fontana Valloneto section suggest that OAE2 was characterized by periods with high productivity and high preservation with redox conditions fluctuating between suboxic to strongly euxinic. Reducing conditions were recorded by other Italian sections that intersect the Bonarelli Level, although related to different mechanisms. For instance, at Bottaccione section (Umbria-Marche, Scopelliti et al., 2006), anoxic-euxinic conditions during OAE 2 were associated to high productivity and high riverine runoff, coupled with a "sluggish" oceanic circulation. Differently, at the Calabianca section (Sicily, Southern Italy) the strong OM productivity is mainly related to an efficient upwelling present along the African passive margin that, in turn, caused euxinic conditions in the entire water column (Scopelliti et al., 2004; Scopelliti et al., 2006; Tribovillard et al., 2012). This difference may be related to the depositional environments that at the Bottaccione section was mid-deep pelagic (1500 – 2500m) and located in a complex basin along the continental margin of the Apulian block (Scopelliti et al., 2006); whereas at the Calabianca section was shallow (1000 – 1500m) and located in the Southern continental margin of the Mesozoic Thethys (Scopelliti et al., 2006; 2008). In addition, during the deposition of the Bonarelli Level in the Bottaccione section, the low carbonates suggest a temporary rise of the CCD linked to increased water acidity as a consequence of enhanced oxidation of organic matter., whereas in the Calabianca section, carbonates contents are always high (~16 wt%; Scopelliti et al., 2004) indicating a shallow depositional environment (Scopelliti et al., 2006).

Based on what inferred before, the Fontana Valloneto section could have recorded redox conditions similar to those of the Bottaccione section during the Bonarelli Horizon, but in a different depositional environment. The lack of carbonates prior to, during and after the BH (table 11.4.2) in fact suggests that the depositional environment was always under the CCD, and that that the entire Fontana Valloneto section was deposited in a more distal and pelagic environment compared to Bottaccione and Calabianca sections. In addition, the Fontana Valloneto BH contains higher TOC contents (> 10 wt%), which indicate (i) higher organic matter productivity, (ii) higher preservation and (iii) lower dilution of OM (and lower sedimentation rates) compared to the Umbrian and Sicilian basins. A combination of the three conditions seems reasonable, and sustained by high OM concentrations, enrichments of nutrient-related trace metals and RSEs (figure 11.5.3) and by the sedimentation of illite type clays over kaolinite and muscovite (figure 11.5.1), likely triggered by a slowdown of the

oceanic circulation (Scopelliti et al., 2004; 2006) through a Cretaceous global long-term eustatic climax (+250 m) during OAE 2 time (Viaggi et al., 2019).

In agreement, a series of proxies (i.e. Ti/Al, K/Al and Rb/Al) is here analyzed, in order to study in more detail the detrital input of the depositional environment during the deposition of the BH.

Specifically, Rachold and Brumsack (2001) suggested that high Ti/Al values can be related to high contribution from fine-grained aeolian input, which is generally Ti-enriched. Fontana Valloneto shows Ti/Al average (figure 11.5.4) values of 0.06 prior to, 0.07 during and 0.05 after the BH that are very close to the UCC values (Ti/Al_{UCC} = 0.05; calculated after McLennan, 2001), indicating that an increase of the influx from aeolian dust occurred during the Bonarelli Horizon.

Own to the high affinity of K compared to Al into illite, the K/Al ratio is considered as another clastic influx proxy and gives information on the detrital input deriving from the fine-grained sediments (Wehausen and Brumsack, 1999; Rachold and Brumsack, 2001; Brumsack, 2006; Soua, 2013). Although in the Fontana Valloneto, K/Al ratios are generally lower than the UCC value (K/Al_{UCC} = 0.35; calculated after McLennan, 2001) (figure 11.5.4) thereby indicating that the fine sedimentation was limited along the entire section, these ratio increase to ~0.30 during the BH, implying a temporarily increase of the fine grained supply. Finally, Rb/Al, that represents the riverine input (Scopelliti et al., 2004, 2006), show an average of ~0.10 along the entire section (figure 11.5.4), that is below the UCC concentration (Rb/Al_{UCC} = 0.13; calculated after McLennan, 2001) indicating that the terrigenous flux related to the rivers was low along the entire section.

Concluding, the detrital proxies aforementioned suggest that the entire section is characterized by a fine-grained sedimentation, in agreement with the idea that the depositional environment of Fontana Valloneto was likely located in a distal deep basin with low riverine influxes from the continent.

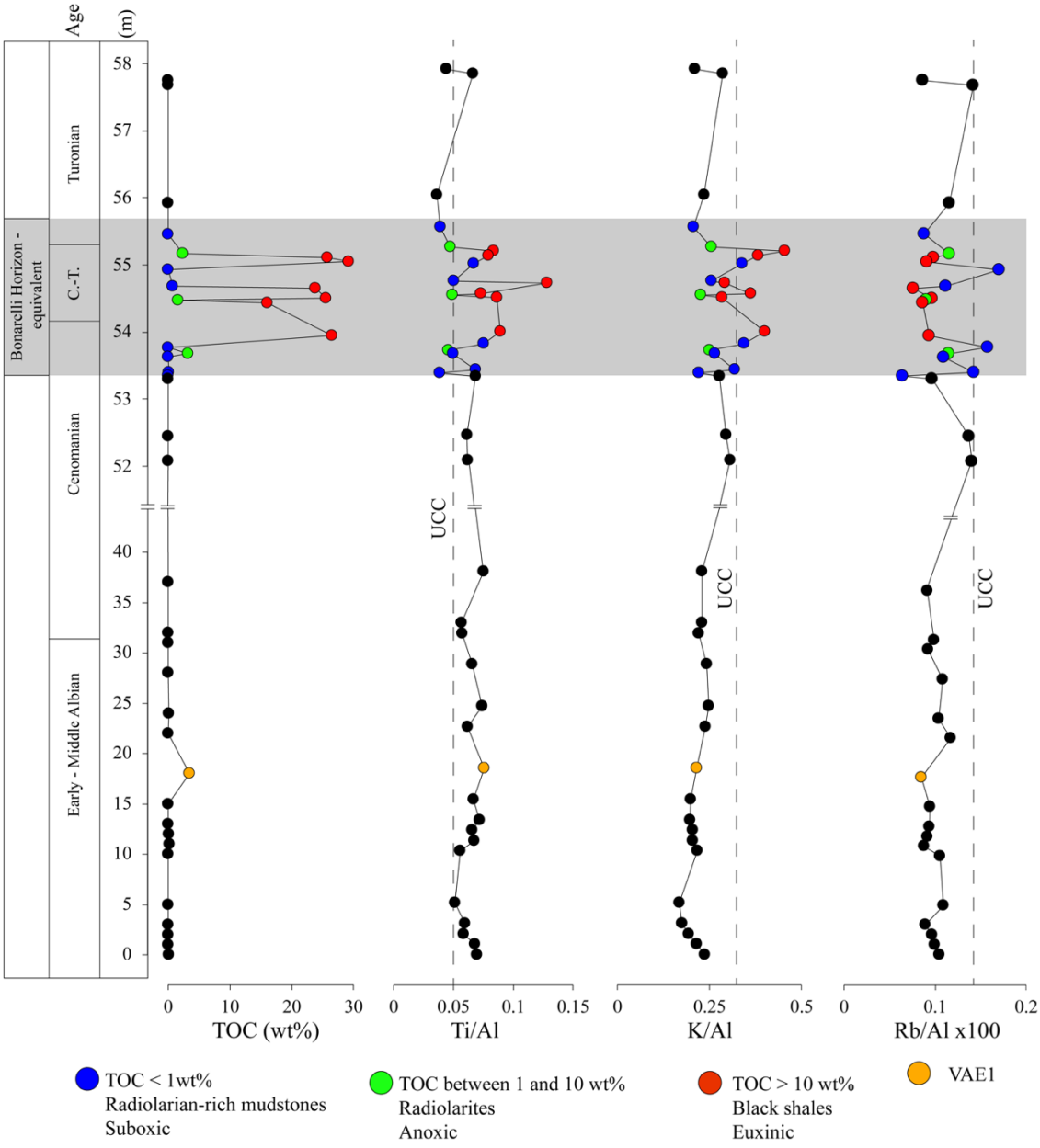

Figure 11.5.4 - Total Organic Carbon (TOC), Ti/Al, K/Al and Rb/Al (x100) along the Fontana Valloneto Section. Vertical dashed lines represent UCC values (McLennan, 2001). VAE1 stands for "Valloneto Albian Event 1".

Causes of variability in redox conditions during OAE 2

Looking in detail at the Bonarelli Horizon, some differences can be noted between the black shales (TOC > 10 wt%) and radiolarites/radiolarian-rich mudstones (TOC < 10 wt%). Black shales (red points in figure 11.5.4) are generally characterized by high peaks in Ti/Al and K/Al compared to the radiolarites (green and blue points in figure 11.5.4) pointing toward the idea that their deposition was associated to fine grained sedimentation. It is probable that the black shales are the results of high bioproductivity and high preservation of the OM under

euxinic conditions, as testified by high TOC values and enrichments in RSEs and nutrient-related metals. This probably occurred in a moment of stagnant conditions where OM deposited together with fine grained sediments (illite and aeolian dust) for decantation. Euxinic conditions may have been promoted by degradation of high amount of OM, produced also thanks to the aeolian input that may have added additional nutrients in surface waters. Finally, the black shales are characterized by low Rb/Al, indicating a low detrital input from rivers during their deposition. This is also in agreement with the hypothesis of Viaggi et al. (2019) in which OAE 2 was associated to a global long-term eustatic climax compatible with starved conditions.

Contrarily, the radiolarian-rich mudstones levels in the BH (green and blue points in figure 11.5.4) are not associated to high TOC, Ti/Al and K/Al values (figure 11.5.4) but to peaks in Rb/Al (figure 11.5.4), Zr, less Al and Y (figure 11.4.2), to minor enrichments in RSEs and to TOC < 10 wt%. These characteristics suggest that the decreasing of OM content is related to the deposition of these layers under less reducing conditions than the black shales, during periods of enhanced riverine supply recorded by peaks in Rb/Al (figure 11.5.4) that may have obfuscated the aeolian signal. In agreement, Gambacorta et al. (2016) sustain that radiolarian layers, belonging to the entire Albian-Turonian section, can be related to oxic-suboxic moments in which the bottom currents might be relatively active. A different situation has been observed in Bottaccione and Calabianca sections (Scopelliti et al., 2006) where the deposition of black shales during the Bonarelli Level has been related to high organic matter productivity in the photic zone in a moment of intense rivers contribution that diluted the aeolian input compared to older and younger times, as suggested by high Rb/Al and low Ti/Al values (Scopelliti et al., 2004, 2006). Conversely, and similar to the Fontana Valloneto section, enhanced siliceous biogenic production (i.e. radiolarites deposition) is related to period of renewal of circulation resulting in a recycling of nutrients. Contemporaneously, an increase of oxygen to deep waters induced OM degradation as suggested by low values in Cr/Al and V/(V+Ni) ratios (Scopelliti et al., 2006).

Global implications

Based on RSEs concentrations discussed above, we showed that the OAE 2 in Fontana Valloneto section, Bottaccione and Contessa (see below) sections are characterized by suboxic – euxinic conditions (figure 11.5.5). A different situation is represented by other localities of the proto-Atlantic Ocean and Western Tethys during OAE 2: i.e. Calabianca section (figure 11.5.5; Scopelliti et al., 2004; 2006), i.e., Furlo section (Umbria - Marche, Central Italy; figure 11.5.5; Owens et al., 2017a), Demerara Rise (Hetzel et al., 2009; Wang et al., 2016; Ostrander

et al., 2017) and Cape Verde (Site 367; Westermann et al., 2014) in which strong euxinia was observed.

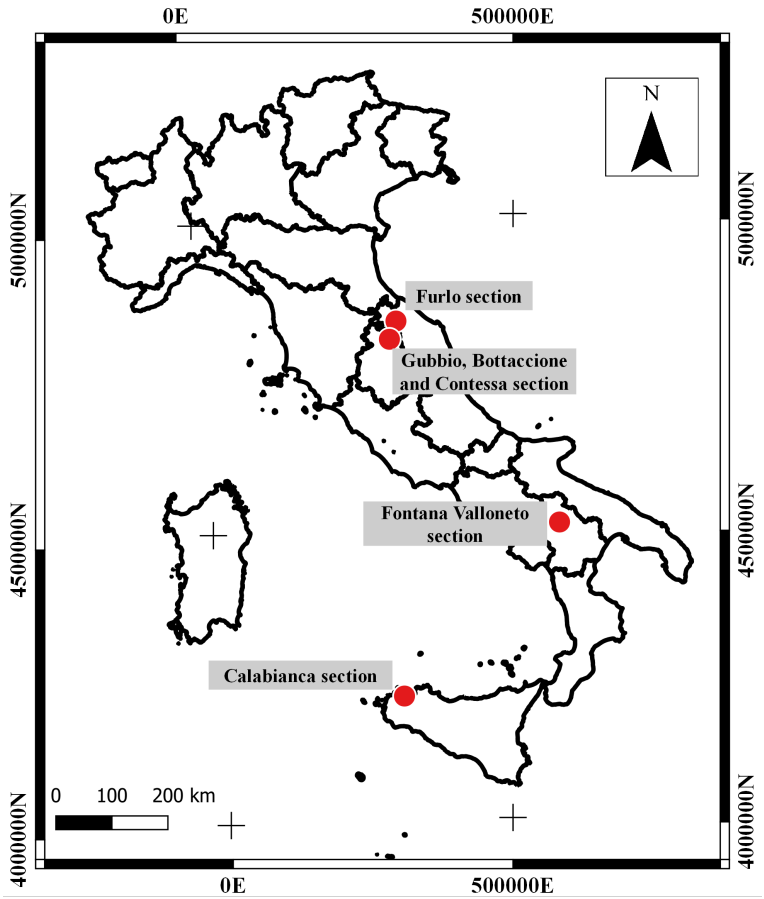

Figure 11.5.5 – Locations of some Italian sections (Furlo, Bottaccione, Contessa, Fontana Valloneto and Calabianca sections).

Here, iron speciation and molybdenum isotopes suggest strongly euxinic conditions throughout the entire OAE 2. These conditions were accompanied by depletions in Mo, V and U concentrations, likely due to the global expansion of euxinia (Hetzel et al., 2009; Westermann et al., 2014; Wang et al., 2016; Ostrander et al., 2017; Owens et al., 2017b). In particular, Owens et al. (2017b) suggested that section marginal marine sediments do not show strong trace-metal enrichments compared to the UCC values during OAE 2 because there was an overabundance of sinks (i.e., anoxic waters and sediments) in many areas of the ocean compared to the relatively small supply (of the ocean inventory). This is in agreement with Viaggi et al. (2019) observation of an OAE 2 depletion of nutrient-related elements (Mo, V), interpreted as temporary seawater "nutrient crisis" induced by starved and stagnant conditions of central Atlantic basin during the Cenomanian-Turonian eustatic climax. This trend, observed in the localities cited above (Furlo section, Demerara Rise, Tarfaya Basin, Cape Verde) and well documented in literature (e.g., Algeo and Maynard, 2004; Reinhard et al., 2013; Goldberg et

al., 2016; Owens et al., 2016; Ostrander et al., 2017a), suggests a drawdown of the global inventory of Mo in the ocean.

	Site	Mo/TOC (ppm/wt%)	References
Proto - North Atlantic	Demerara Rise	2.0	Hetzel et al. (2009)
	Cape Verde (site 367)	5.0	Westermann et al. (2014)
Tethys Ocean	Fontana Valloneto section	4.9	This study
	Calabianca section	2.0	Tribovillard et al. (2012)
	Bottaccione section	4.0	Tribovillard et al. (2012)
	Furlo Section	3.2	Owens et al. (2017)
	Contessa section	3.0	Westermann et al. (2014)

Table 11.5.1 - Overview of Mo/TOC (ppm/wt%) average values within OAE 2. Mo/TOC average values from this study are calculated only for the samples with TOC > 1wt%.

In addition, the Mo/TOC ratio point toward a depleted marine Mo reservoir in all these localities. Algeo and Lyons (2006) show that different Mo/TOC ratios reflect the size of Mo inventory as related to global or local factors. So, normalizing Mo to TOC allow to see relationships that do not depends on organic matter control but only on the reservoir. In table 11.5.1 are represented the Mo/TOC ratios from different the OAE 2 localities, compared to those of the Fontana Valloneto section (figure 11.5.3). The case study presented here, during the BH, shows a Mo/TOC average value of 4.9 (table 11.5.1), which is slightly higher than the others cases of study and the Black Sea values (Mo/TOC average (ppm/wt%) = 4.5 ± 1; Algeo and Lyons, 2006) that is considered the modern analogue of black shales formation during OAEs (except for Cape Verde – Site 367; see below).

Also, Algeo and Lyons (2006) showed that the Mo/TOC values in modern basins are controlled by the restriction of the basin. So, the ratio depends on the renewal time of deep waters relative to the rates of Mo uptake and the H_2S spreading into the water column. For instance, the data from Furlo section (Owens et al., 2017a) reflect the sequestration of Mo by sediments under euxinic conditions that is faster than the water renewal.

Also, Pearce et al. (2008) and Algeo (2004) relate this inventory process to a massive uptake of Mo, but also of V and U, by OM-rich deposits during periods of strong euxinia. This has been observed by the authors not only during OAE 2, but also during others OAEs (e.g. Toarcian – Oceanic Anoxic Event and the Upper Devonian–Lower Mississippian black shale succession of the Central Appalachian Basin).

High Mo values observed in Cape Verde (Site 367) have been linked by the authors (Scott and Lyons, 2012; Tribovillard et al., 2012; Westermann et al., 2014) to the operation of Mn shuttling: variable redox conditions cause Mo to be captured and released by Mn oxides several times within the euxinic layer, accelerating its transport to the seafloor with the particulate and its fixation into the euxinic sediments. This process has been inferred also for the Bottaccione section (Scopelliti et al., 2006) and Contessa section (Westermann et al., 2014). In particular, the latter case records fluctuating conditions between anoxia and euxinia along the Bonarelli Level and in the second part of the OAE 2, δ^{98}Mo shift towards lighter values indicating a non-quantitative removal of Mo from the water column and/or the operation of a Mn shuttling. Thus, Fontana Valloneto shows very similar Mo/TOC concentrations to Cape Verde (site 367) and Bottaccione section (table 11.5.1), pointing toward the idea that a Mn particulate shuttling may have played an important role leading to Mo enrichments. In fact, the enrichment factors of Mo and U (Mo_{EF} and U_{EF}, respectively) calculated for the Fontana Valloneto section are compatible with the particulate shuttling process, accordingly to Algeo and Tribovillard (2009), as shown in figure 11.5.6.

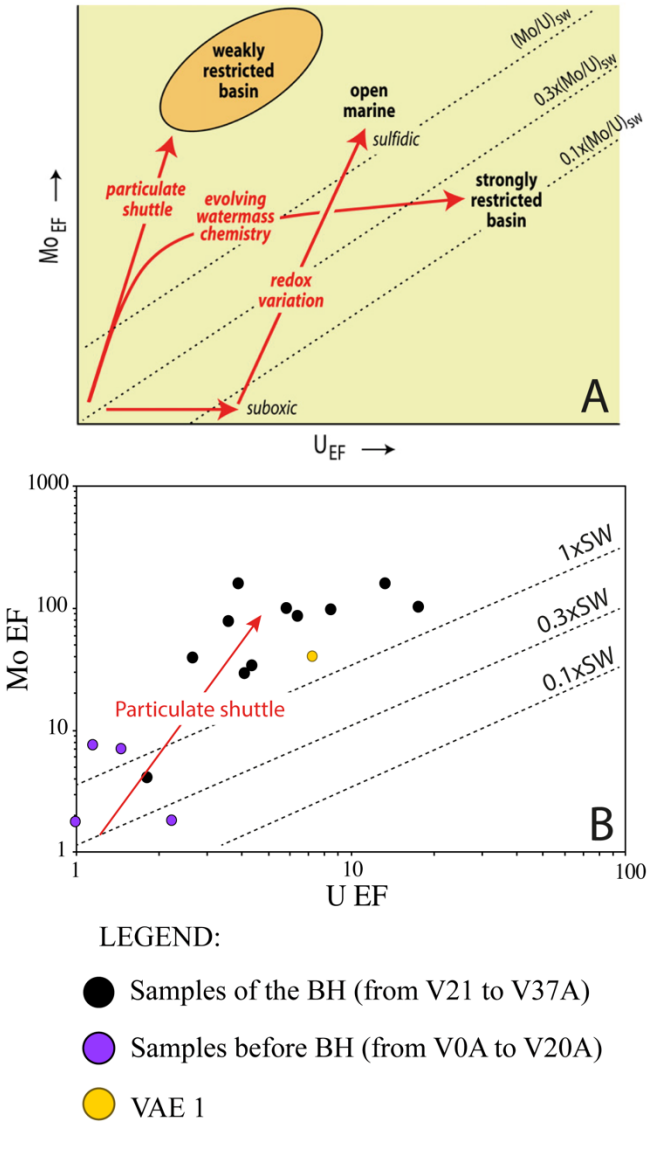

Figure 11.5.6 – (A) Model of enrichment patterns and changes in $(Mo/U)_{auth}$ ratios (from Algeo and Tribovillard, 2009). (B) Cross plot of Mo and U enrichment factors for the Fontana Valloneto section (only EFs > 1 are plotted). The diagonal dotted lines represent the seawater (SW) Mo/U molar ratio of ~7.5–7.9 and fractions thereof.

In combination, data shown in table 11.5.1, especially the Mo/TOC values now available suggest that deep-water Mo concentrations were low in both, the proto-North Atlantic and the Tethys Oceans, and constantly close to (Fontana Valloneto section) or lower than the modern euxinic restricted basin (i.e. Black Sea). Thus, the Mo and RSEs concentrations cannot be explained solely with a local depletion due to "sluggish" circulation in restricted basins. Rather, Nd isotopes from Demerara Rise (Martin et al., 2012) suggest that there was an active water exchange between the Tethys and Central and North Atlantic in the Late Cretaceous. Hence, the comparison between several OEA 2 sections around the world implies that the low Mo/TOC values – in our case associated probably also to depletion in V and U – are due to a global perturbation in redox conditions of the ocean, and the subsequent sink effect within OM-rich sediments.

11.6 Conclusions

The combination of mineralogy, TOC and geochemical data allowed to reconstruct the depositional history of Fontana Valloneto. In particular, the lack of carbonates indicates that the Fontana Valloneto section was located in a deep distal basin (under the CCD) during the entire deposition of the section. In addition, our geochemical data (V, Mo, U, Mn and TOC) suggest a sudden change in the redox conditions at the onset of the BH, which was characterized by fluctuating reducing conditions. These are suggested by three different trends:

(i) Suboxic conditions are characterized by radiolarian-rich mudstones associated to TOC < 1 wt%, RSEs concentrations close to UCC values, variable Mn enrichments;

(ii) Anoxic conditions are characterized by radiolarites associated to TOC between 1 and 10 wt% and little or no enrichments in RSEs and Mn;

(iii) Euxinic conditions are characterized by black shales associated to TOC > 10 wt%, enrichments in RSEs and Mn values close to UCC.

Finally, comparison with other sections intercepting the OAE 2 in the Tethys and in the proto-Atlantic oceans allowed to discuss two implications:

(i) The local variability within the BH in Fontana Valloneto indicate that black shales are associated to high TOC, Ti/Al, K/Al and enrichments in RSEs indicating high bioproductivity, stagnant conditions, fine-grained sedimentation (illite and aeolian dust) and euxinic conditions, while radiolarites/radiolarian-rich mudstones are associated to low TOC, high Rb/Al and low RSEs enrichments indicating an increase of the oceanic circulation and riverine input leading to less reducing conditions;

(ii) Mo/TOC ratio during the BH in the Fontana Valloneto section is consistent with the values of the same ratio from other sections from the proto – Atlantic Ocean and the Mesozoic Tethys, confirming the idea that global reducing conditions during OAE 2 led to a depletion of the global inventory of Mo (but also V and U likely) due to the sink effect of euxinic waters and temporary seawater "nutrient crisis" induced by basin starved conditions associated to the Cenomanian-Turonian global long-term eustatic climax. We favor the idea that Mo depletion was a global process, instead of a consequence of a restriction of the marine basin.

With this work, we define another Italian section intersecting the OAE 2 and located in the Southern Tethys, providing a new case of study to understand the global significance of the geochemical parameters characterizing the sediments formed during these periods of strongly reducing conditions.

CHAPTER 12

Progressive long-term de-oxygenation throughout the mid-Cretaceous: local and global implications

During the third year of PhD (from November 2019 to the beginning of February 2020) a collaboration with the University of California, Riverside (UCR) and the MagLab (Tallahasse) has been carried out. In particular, unconventional analytical techniques have been applied to CA1. Specifically, at the UCR, iron speciation and sulfur isotopes were analyzed, while at the MagLan thallium concentrations and thallium isotopes have been analyzed. 70 samples spanning the entire section of CA1, although the sampling were denser in the interval containing the OAEs, have been selected for the iron speciation and sulfur isotopes analysis. In addition, 40 of these samples have been selected for thallium analysis.

Iron speciation, sulfur isotopes and thallium isotopes are very reliable proxies for redox conditions in the depositional environment. However, they requires a particular procedure in order to prepare the samples for the analysis and, therefore, a very specialized laboratory is necessary. That is why these analytical techniques cannot be added to the daily routine of Eni, but in a research project it was possible to investigate these techniques.

The proxies are described in chapter 3.4, whereas the methodologies are described below, together with the results obtained for CA1. The result of this collaboration is a paper that is going to be published after the end of the PhD.

This chapter is articulated as follow:

1. Introduction to the problem: state of art;
2. Aim of the collaboration with the UCR and MagLab: open questions and the importance of this study;
3. Geological settings and samples: a brief geological review about CA1;
4. Methodologies: iron speciation, sulfur isotopes and thallium isotopes;
5. Results:
6. Discussion.
7. Outlook and future steps

12.1 Introduction to the problem

The section of CA1 intersect four Cretaceous “Oceanic Anoxic Events” (OAEs) (Schlanger and Jenkyns, 1976) as shown in chapter 7.1 and 8.1. Those events are climatic perturbations

associated with excursions in the carbon isotopes ($\delta^{13}C$) (Scholle and Arthur, 1980; Arthur et al., 1990). OAEs are often related to the following phenomena: global warming and high atmospheric CO_2 (Huber et al., 2002; Berner, 2006; Takashima et al., 2006; Barclay et al., 2010; Jarvis et al., 2011), weathering (Pogge von Strandmann et al., 2013; Blumenberg and Wiese, 2012) and increased nutrient fluxes (Trabucho Alexandre et al., 2010), increased hydrothermal activity (Jones and Jenkyns, 2001; Adams et al., 2010, Percival et al., 2018), high sea level (Arthur et al., 1987; Jarvis et al., 2011) and changes in oceanic circulation (Martin et al., 2012; Zheng et al., 2013). These periods are often marked by a strong increase in primary productivity and preservation of marine and terrestrial organic matter (Jenkyns, 2010; Owens et al., 2018; Jin et al., 2020), resulting in the formation of several synchronous series of organic-rich black shales (Schlanger and Jenkyns, 1976; Takashima et al., 2006; Jenkyns, 2010) deposited during phases of expansion of anoxia in deep seawater (Meyer and Kump, 2008; Jenkyns, 2010; Dickson, 2017). Nonetheless, the main trigger mechanism that led to the enhanced burial of organic carbon at different times along the Cretaceous can be different for each OAE. In addition, only some Cretaceous OAEs are known to be global (e.g. OAE2), while others are more localized in certain areas of the ocean (e.g. OAE 1c, 1d and 3) (Takashima et al., 2006). OAE 1c (Late Albian) and OAE 1d (101 – 99.5 Ma; Albian – Turonian; Leckie et al., 2002; Ogg and Hinnov, 2012) are marked by thin organic-rich black shales with irregular distribution (e.g., Coccioni and Galeotti, 1993; Erbacher et al., 1996; Galeotti et al. 2003; Robinson et al., 2004; Navarro-Ramirez et al., 2015). Specifically, OAE 1c has been studied mostly in Central Italy (Amadeus segment; Coccioni and Galeotti, 1993; Erbacher et al., 1996; Galeotti et al. 2003) and in NE Australia (Toolebuc Formation; Haig and Lynch, 1993), in the Morroco Basin (DSDP Site 370), in the Indian Ocean (Site 258 in the Naturaliste Plateau) and in the Bay of Biscay (Site 400; Bralower et al., 1993). OAE 1d was likely restricted to the Tethys and sporadically in South Atlantic, southern Indian, and eastern Pacific Ocean (Leckie et al., 2002). During these two regional events the greenhouse conditions led to an acceleration of the hydrological and atmospheric cycles and in increase in continental weathering and riverine runoff (Galeotti et al. 2003; Bornemann et al., 2005; Giorgioni et al., 2012, 2015). These created the conditions for enhanced fluxes and preservation of organic matter in the oceans. Moreover, an orbital forcing may have played an important role in a strong seasonal contrast with the result of climate changings and unstable circulation that favored the expansion of deep water anoxia (Bornemann et al., 2005; Giorgioni et al., 2012, 2015). In particular, OAE 1c occurred during a1maximum sea-level fall (Haq et al., 1987), with no changes in primary productivity in

seawater but with an increase of the riverine runoff that brought continental organic matter in the oceans (Coccioni and Galeotti, 1993; Erbacher et al., 1996; Galeotti et al. 2003).

In addition, another regional event that has been related to regional reducing conditions is OAE 3 (88.6 – 83.5 Ma; Coniacian – Santonian; Arthur et al., 1990). This occurred during a major cooling trend in Earth's history from greenhouse to more temperate conditions (e.g. Norris et al., 2002; Friedrich et al., 2012). Several studies (Jenkyns, 1980; Wagner et al., 2004; Wagreich, 2009; Wang et al., 2009; Hofmann and Wagner, 2011; Wang et al., 2011; Wagreich, 2012) recognized shallow waters black shales related to OAE 3 in the Atlantic and Caribbean regions only, leading to the idea that this anoxic event is restricted to the low- to mid- latitudinal part of the Atlantic and some adjacent epicontinental basins (Maracaibo Basin and Western Interior Basin), whereas most of the other ocean basins were largely characterized by oxic conditions in deep water.

On the other hand, OAE 2 (94 Ma ca., Cenomanian – Turonian boundary) has been recognized as a global anoxic event in which 40 - 50% by volume of the global ocean was anoxic (Monteiro et al., 2012; Ostrander et al., 2017) while euxinia was restricted to a maximum of 7% of the seafloor (Owens et al., 2013; Owenset al., 2018; Dickson et al., 2016 a, b). The most plausible model that explain the environmental changes during this event is the expansion of the oxygen – minimum zone (OMZ) in the water column due to the enhanced shallow organic matter (OM) productivity (e.g. Moroccan and Peruvian margins; Takashima et al., 2006).

12.2 Aim of the collaboration with UCR and MagLab

Understanding the development of anoxia (<0.2 ml O_2/l H_2O) and euxinia (presence of free H_2S) before, during and after the OAEs as a response to several environmental perturbations allows us to better understand and predict future climate consequences as related to current global change. An increase in oceanic de-oxygenation is already detectable in the modern ocean with the loss of 2% in the last several decades (Keeling et al., 2010; Schmidtko et al., 2017; Long et al., 2016) and it will increase in the next thousand years. What will be the effect of the anthropogenic carbon emissions on marine anoxia it is still debated but it is not yet the development of conditions similar to those of OAEs. Importantly, CA1 is and unique case in which the combination of these analysis allows for a long-term reconstruction of the the paleoredox and paleo environmental conditions during deposition from a local and global record along the Cretaceous, together with the oceanic geochemistry and circulation. These are the results of secular fluctuations in the climate, elements abundance in the oceans (e.g. nutrients) and life development. In addition, the presence of four OAEs allows to trace the redox

conditions, both local and global, at the onset, during and after each OAE in order to understand the paleoenvironmental changes between each anoxic event.

12.3 Geological setting and samples

CA1 is a ~1.8 km-long sedimentary section spanning from Early Aptian to Early Campanian (~115-80 Ma) drilled within a postrift sedimentary succession in the South-Eastern margin of the Central Atlantic. The continuous recovery intersected four anoxic events, namely OAE1c, OAE1d, OAE2 and OAE3. 194 cutting samples (representing 5 meters of drilling) were selected for X-ray diffraction (XRD), X-ray fluorescence (XRF) and TOC-Rock Eval, 70 were available for iron speciation analyses and sulfur analyses, finally 40 samples were available for thallium isotopes analysis. Lithological reconstructions provided by Eni show that the upper part of the sedimentary record consists mainly of shales, predominantly micas and illite, interbedded with thin layers of carbonates, mostly calcite. The central part of the section is formed by an intercalation of shales and sandstones. Moving in towards the older part of the section, the carbonaceous content increases with an intercalation of argillaceous limestones, shales and sandstones (figure 7.1.2). Most of the sediments show TOC values lower than 2 wt%, several enrichments occur mostly in correspondence of each OAE. In particular, OAE 1c is characterized by a TOC average of ~2 wt% and HI between 350 and 450 mgHC/grTOC; OAE 1d shows TOC values between 2 and 4 wt%, while HI is between 500 and 650 mgHC/grTOC. The most prominent enrichment in TOC (up to 9 wt%) and HI (up to 600 mgHC/grTOC) occurs in a ~28m-thick layer at 474 m, corresponding to OAE 2 (~93 Ma; Cenomanian-Turonian). Finally, OAE 3 is characterized by TOC between 2 and 4 wt%, while the average of HI is ~400 mgHC/grTOC.

12.4 Methodologies

Iron speciation and sulfur isotopes($\delta^{34}S$)

Fe speciation and sulphur isotopes analyses were carried out at the Department of Earth Sciences, University of California, Riverside. The speciation of highly reactive iron (Fe_{HR}), which comprises pyrite iron and other iron phases (carbonates, oxides and magnetite) that will react with sulphide to form pyrite in the water column or during early diagenesis, was obtained using a calibrated sequential extraction protocol.

Roughly 100 mg of sample powder was first treated with a buffered sodium acetate solution (pH: 4.5), which extracts carbonate-associated Fe (either siderite, ferroan calcite or dolomite-

ankerite solid-solution series). This fraction is here referred to as Fe_{CARB}. Samples were then treated with a sodium dithionite solution (50 g l^{-1}) buffered to pH=4.8 with acetic acid and sodium citrate. Fe obtained from this extraction step, here referred to as Fe_{OX}, consists of `reducible' iron oxide phases, or iron oxides such as goethite and hematite that are reactive to hydrogen sulphide on early diagenetic timescales. Magnetite (Fe_{MAG}), a mixed-valence iron oxide that does not react with dithionite, was extracted with a 0.2M ammonium oxalate and 0.17M oxalic acid solution (pH=3.2). All the reactions have been carried out in 15ml tubes containing 100 mg of sample (figure 12.4.1). Sequential extracts were analysed on an Agilent 7500ce inductively coupled plasma mass spectrometer after 100-fold dilution of extracts in trace-metal grade 2% HNO_3.

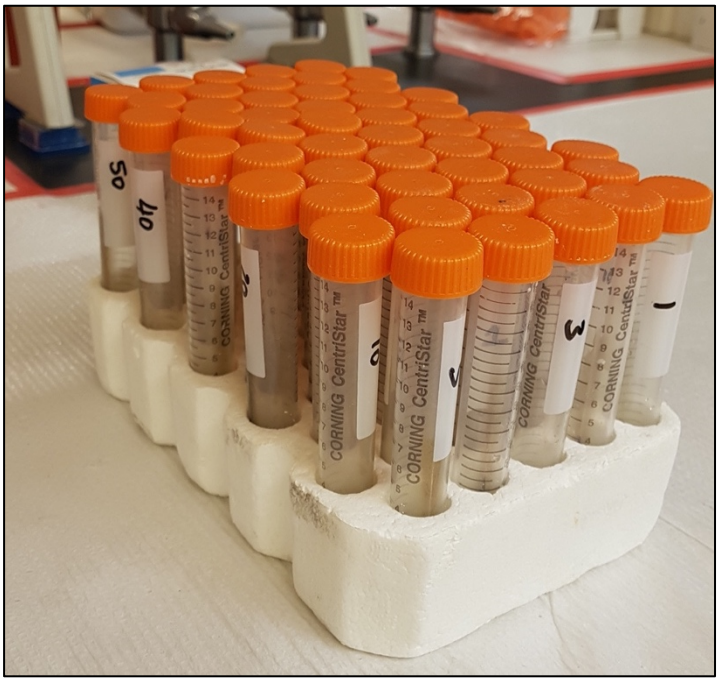

Figure 12.4.1: 15ml tubes to carry out the multi-step reactions of the samples with the acids in oder to obtain Fe_{CARB}, Fe_{OX} and Fe_{MAG}.

Pyrite iron (Fe_{PY}) was calculated (assuming a stichometry of FeS_2) based on wt% sulphur extracted during a 2 h hot chromium chloride distillation followed by iodometric titration. Highly reactive iron is defined as Fe_{HR}= Fe_{CARB} + Fe_{OX} + Fe_{MAG} + Fe_{PY}. On the sulfur extacted was measured also the sulfur isotopic composition on the Thermo Finnigan Delta V Plus continuous-flow stable isotope ratio mass spectrometer following the preparation sample protocol from Canfield et al., (1986) (figure 12.4.2).

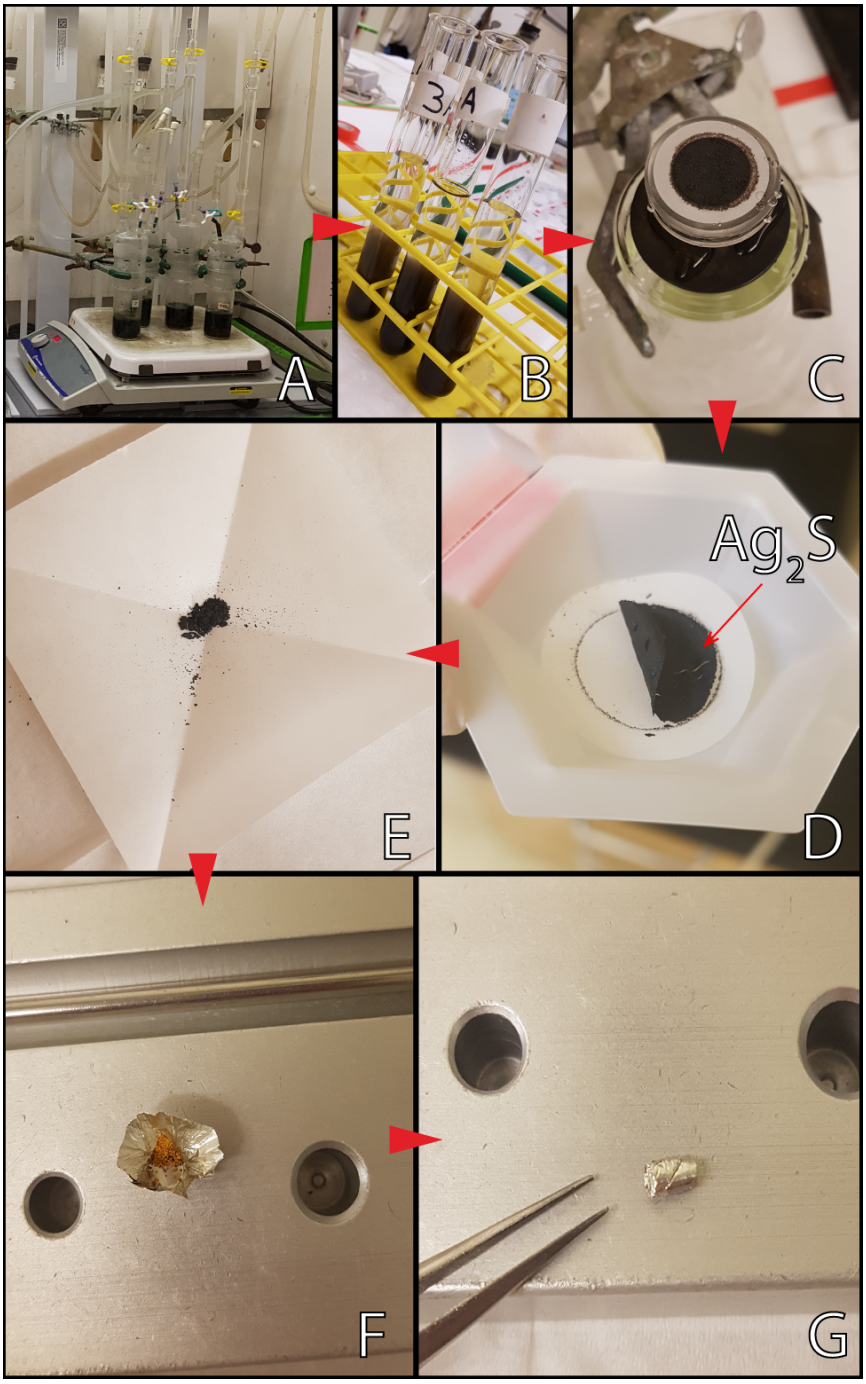

Figure 12.4.2: preparation samples procedure in order to analyze the sulfur isotopes. (A) reaction of the samples with chromium chloride ($CrCl_2$) and HCl as shown in figure 12.4.3; (B) tubes containing Ag_2S; (C) filtered Ag_2S; (D) dry Ag_2S; (E) grounded Ag_2S; (F) Sn capsule containing Ag_2S and a low melting (V_2O_5); (G) sample ready for the sulfur isotope analysis.

The procedure is resumed and consists in several steps listed below:

1. Weight ~150 mg of powdered sample into a digestion flask and add ~10 ml of ethanol in order to concentrate the sample at the bottom of the flask;

2. Attach the trapping vessels (containing 30 ml of $AgNO_3$ NOOH) and the digestion flask to the gas line (figure 12.4.3);
3. Flush the system with N_2 and with a join a solution of ~30 ml of 1M $CrCl_2$ and ~15 ml of HCl with a syringe to each digestion flask;
4. Heat the digestion flask at a temperature of ~200°C and let react for 90 minutes (figure 12.4.2A). During the reaction H_2S is generated carrying the S isotopic signature of the sample. The long-time interval required is necessary to have a complete reaction of the pyrite grains of the samples with the digestion fluids (Canfield et al., 1986). H_2S is carried by the carried gas (N_2) to the trapping vessel and reacts with the $AgNO_3$ NOOH solution leading to the precipitation of Ag_2S;
5. Disconnect the trapping vessel form the gas lines and close the N_2 flux (figure 12.4.2B);
6. Filter the liquids contained in the trapping vessel in order to capiture the Ag2S in a filter (figure 12.4.2C);
7. Dry the filter with Ag_2S in an oven for 24 hours at 50°C;
8. Remove Ag_2S from the filter and break it up (figure 12.4.2E);
9. Weight ~0.35 mg of Ag_2S and ~2.0 mg of vanadium pentoxide (V_2O_5) that act as a low melting in a Sn capsule (figure 12.4.2F);
10. Close the capsule (figure 12.4.2G). The sample is ready for the analysis using the Thermo Finnigan Delta V Plus continuous-flow stable isotope ratio mass spectrometer.

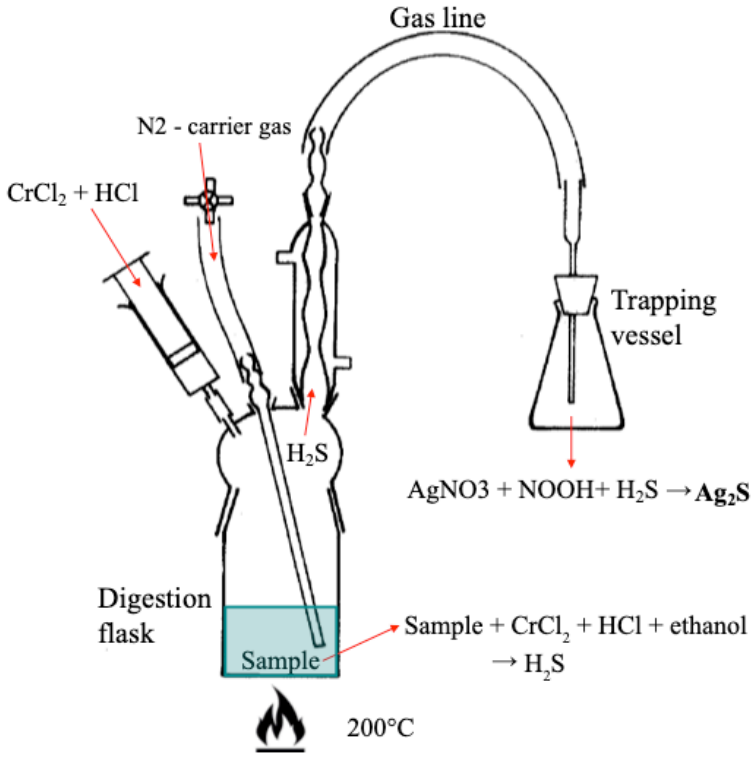

Figure 12.4.3 (modified after Canfield et al., 1986): scheme of the reaction of the sample with chromium chloride ($CrCl_2$) and HCl, resuting in the precipitation of Ag_2S.

Thallium isotopes ($\varepsilon^{205}Tl$)

Thallium isotopes analyses were carried out at the MagLab, Florida State University, Tallahassee. The analysis follows three steps: (i) sample digestion, (ii) Tl purification and (iii) sample analysis.

Previously powdered samples were digested using the following procedure: (i) samples were leached in 2M HNO_3 for 12 hours and centrifuged to retrieve the supernatent, containing the leached fraction (primarily pyrites and organic matter). These were then dried down and redissolved in conc. HNO_3-HCl to remove organic matter (plus a follow-up with 50% HNO_3 + H_2O_2). These were dried down and rehydrated in 1M HCl, and brominated water was added; (ii) samples were then processed using established column procedures (you should just cite one of the other papers, probably Ostrander 2017). This involves two runs through micro-columns filled with Bio-Rad AG1-X8 anion exchange resin to remove Pb; (iii) samples were run on an Agilent 7500cs quadrupole ICP-MS for Tl concentration (figure 12.4.4).

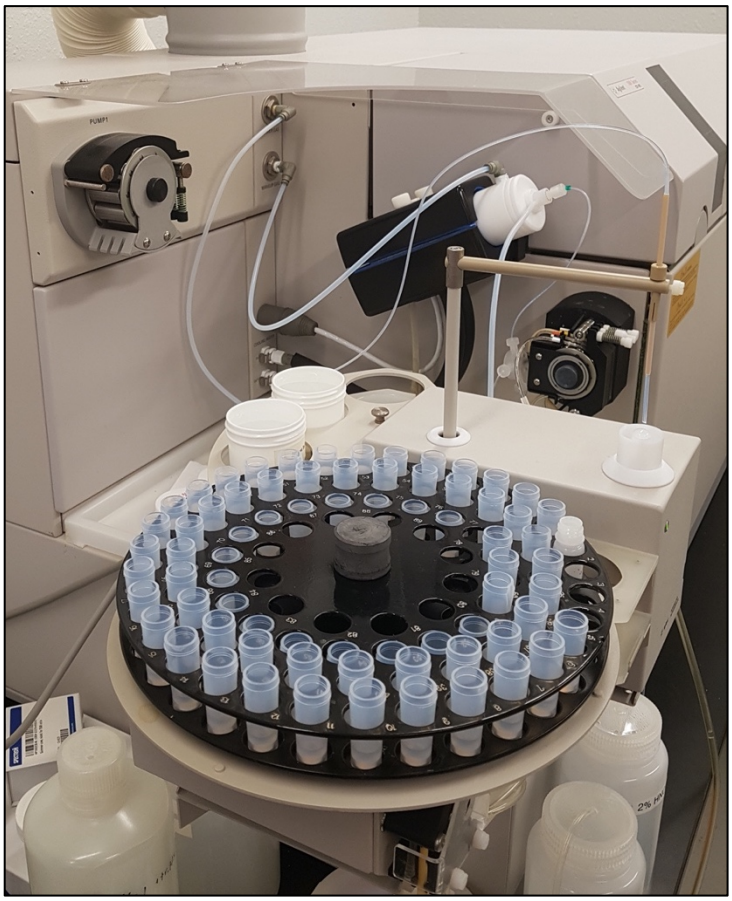

Figure 12.4.4: thallium concentrations analysis with Agilent 7500cs quadrupole ICP-MS.

Samples are spiked with NIST-SRM-981 Pb and run on a Thermo Finnigan Neptune Multi-Collector ICP-MS with connected Aridus II autosampler. (If needed, values were compared to the USGS shale reference material SCo-1, with long-term precision of $\varepsilon^{205}Tl = -3.00 \pm 0.3$. Thallium was isolated from a sample matrix using previously described anion exchange chromatography techniques. Only one column was used during Tl purification. The Tl isotope compositions were determined using a Thermo Finnigan Neptunemultiple collector inductively coupled plasma mass spectrometer.

12.5 Results

The results are shown in figure 12.5.1. The samples have Fe_T between 1.12 and 5.95 wt% that being normalized to Al may indicate enrichments beyond the detrital average (0.51%; Raiswell et al., 2008), thereby suggesting anoxic conditions along the entire section (Lyons and Severmann, 2006). The ratio of highly reactive Fe (Fe_{HR}) to Fe_T is also indicative of anoxia in the depositional environment (Raiswell and Canfield, 1998; Lyons et al., 2009). In our section Fe_{HR} is composed mainly by Fe_{PY}, especially in the central part of the section containing the

OAEs (from 956 to 145m). Accordingly, in the lower part (from the bottom to 956 m) and in the upper part (from 145m to the top of the section) of the sedimentary interval have Fe_{HR}/Fe_T relatively low showing an average of 0.44 and 0.45, respectively, and a single exception at 0.32. At the onset of OAE 1c and until OAE 3 the Fe_{HR}/Fe_T increases towards a peak value of 0.90 reached during the euxinic conditions of OAE 2. Similar to Fe_{HR}/Fe_T, the ratio of pyrite Fe (Fe_{PY}) to Fe_{HR} measures the fraction of the reactive Fe pool that has been pyritized in presence of hydrogen sulphide (Lyons et al., 2009). The lower part and in the upper part section have values ranging between 0.21-0.58 and 0.24-0.45. The Fe_{PY}/Fe_{HR} ratios increase gradually in the central part of the section (average value 0.63), where it reaches a peak value of 0.87 during the OAE2.

Given the local occurrence of carbonates (see supplementary material) the trace metal values are normalized to the total carbonate content. Molybdenum contents are highly variable and on a first sight tend to increase at increasing TOC. The most severe perturbations of Mo values are observed in correspondence of the OAEs and between them, especially right before OAE 1d, where a strong increase is observed and Mo reach the peak value of 138ppm during the event at 629 m. From OAE 1d to OAE 2 there is a gradual decrease in the Mo concentrations that reach values as low as 13 ppm during OAE 2. Vanadium and uranium have a variabilities very similar to Mo from the bottom of the section until OAE 1c and from the end of OAE 3 to the top, showing values comparable to the average shales value of 130 ppm and 2 ppm, respectively (Turekian and Wedepohl, 1961), whereas in the central part of the section (956 – 145m)1a sharp increases is observed, as response to increase in TOC. Similarly to Mo, V and U decreases (169 ppm and 8 ppm, respectively) within OAE 2, and then quickly recover until peak values (2417 ppm and 43 ppm) immediately after the event. Manganese concentrations are generally highly variable from the bottom of the section to the onset of OAE1d (1885-657 m) where they show a sharp decrease to an average ~300 ppm until the top of the section.

From the bottom of the section to 956m, Tl isotope compositions are relatively scattered but constantly heavier that the modern seawater value ($\varepsilon^{205}Tl = -6$; Owens et al., 2017a), with an average $\varepsilon^{205}Tl = -4.5$. The $\varepsilon^{205}Tl$ does not change throughout the OAE1c and OAE1d, although a decrease towards negative $\varepsilon^{205}Tl$ can be observed at the onset of OAE1d where it decreases gradually towards more negative values ($\varepsilon^{205}Tl = -5.8$). A positive shift is seen immediately before the beginning of OAE2 and during OAE2 the Tl isotopes increase sharply towards $\varepsilon^{205}Tl \sim -2.9$. After the OAE2 event, the values decrease gradually to an plateau value of $\varepsilon^{205}Tl = -4.9$. A negative trend is observed during OAE3 with $\varepsilon^{205}Tl$ values as low as -6.6. Finally, from 145m to the top of the section, the isotopic composition decrease reaching values close to the modern

seawater value. The average pyrite contents increase from 2.2 wt% in the lower part of the section is 2.2 wt% to 4.3 wt% in the central part, with a maximum value of 7.1 wt% during the OAE1d. The average between 956 and 145m is relatively high at 5.0 wt%. The lower part of the section has sulfur isotopes highly variable, with a negative peak at 1775 m having $\delta^{34}S$ = 26.7‰, and an average -9.6‰. From OAE1c to OAE2, the average $\delta^{34}S$ becomes rather constant, with an average of -14.1‰. The $\delta^{34}S$ values start to increase after OAE2 towards the end of OAE3, when the average $\delta^{34}S$ values reached -6.4‰. The interval between OAE1d and OAE2 shows some variability between a maximum -9.6 ‰ value of and a minimum value of -17.3‰. Finally, upward, the section shows a strong decrease to extremely negative values of -22.3 ‰.

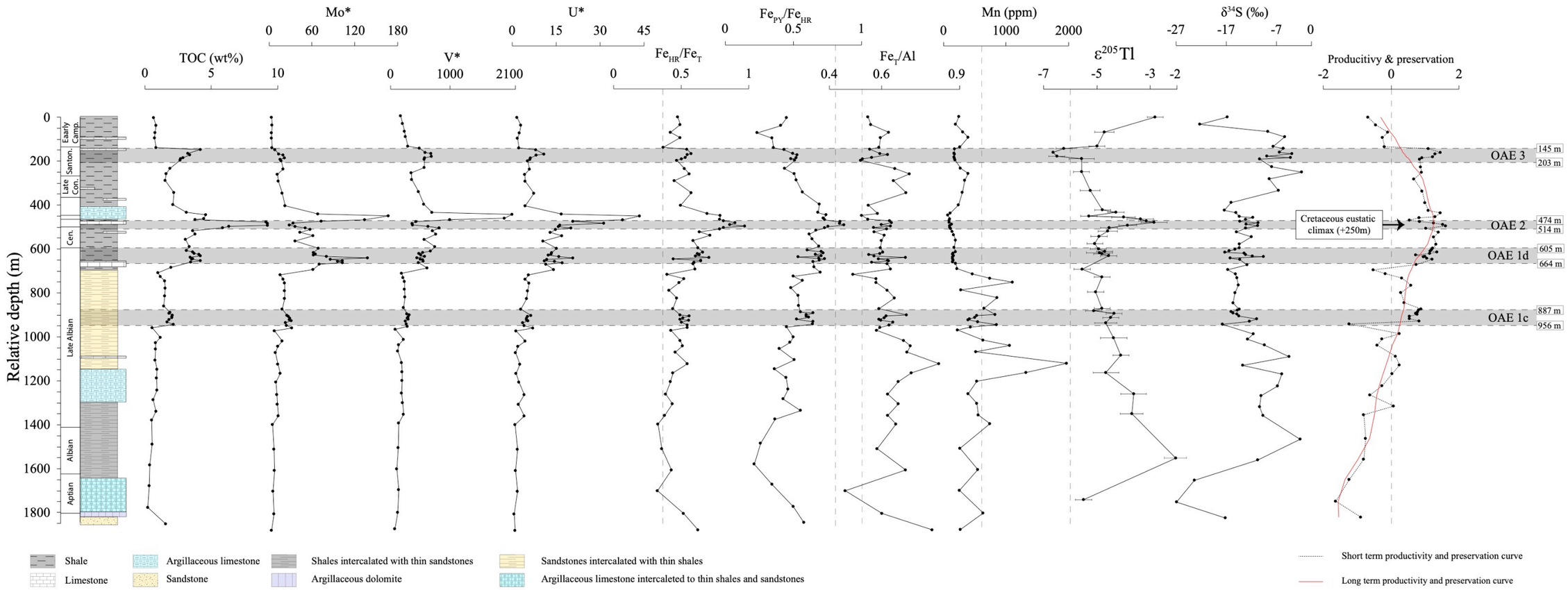

Figure 12.5.1: straigraphic column and logs of TOC, Mo, V, U (* indicates normalization to total carbonate content), iron speciation (Fe_{HR}/Fe_T, FeP_Y/Fe_{HR} and Fe_T/Al), Mn, Tl isotopes, S isotopes and productivity & preservation factors (from Viaggi et al., 2019).

12.6 Discussion

Our analyses show that Fe speciation values are often exceeding the threshold of local anoxia and indicates that the redox conditions along the section were moderately anoxic throughout most of the investigated period (figure 12.5.1). The section spans ~35Ma, so an important aspect to take in account is the development of the depositional environment. This deepens progressively with the opening of the central portion Atlantic Ocean (data provided by Eni).

Notable deviations of the Fe_{HR}/Fe_T and Fe_{PY}/Fe_{HR} ratios from those of the modern seawater (0.38 and 0.43, respectively; Raiswell and Canfield, 1998; Poulton and Canfield, 2011) characterize the section from the onset of OAE 1c (Late Albian) towards the end of OAE 3 (Santonian). This suggests that the deposition of the sediments occurred within bottom water under reducing conditions for an extremely long time span (~ 20 Ma). On a closer inspection, during OAE 1c locally anoxic-ferruginous conditions developed in a shallow water depositional environment, as testified by high Fe_T concentrations (figure 12.5.1). During this period anoxia is related to a stagnant shallow basin where depletion of oxygen is a result of dense vertical water stratification. After this event a slight decrease in the Fe_{HR}/Fe_T values is observed, pointing toward more oxygenated conditions (figure 12.5.1). From the onset of OAE 1d, progressively more euxinic conditions are recorded. The paleophysiography see the section in a deeper part of the basin, in a context of upwelling and OMZ that is gradually starting to develop. At the time of OAE2, Fe_{PY}/Fe_{HR} values suggest strong widespread euxinic conditions (figure 12.5.1). This evolution is confirmed by the variations of other redox-sensitive elements, such as Mo, V and U which in the same period consistently show strong enrichments (figure 12.5.1). In particular, the trend of the Fe_{HR}/Fe_T and Fe_{PY}/Fe_{HR} ratios is very similar to that of the redox & bioproductivity factor, the latter expressing organometallic complexes from the covariance of a redox-sensitive preservation (TOC, HI, U, S, pyrite) and a nutrient-related bioproductivity (V, Ni, Mo, Zn, Se, P) terms (Viaggi et al., 2019). This result is striking because it demonstrates the effectiveness of the Fe_{HR}/Fe_T and Fe_{PY}/Fe_{HR} ratios as redox proxy and links the development of reducing conditions in the central Atlantic to the Cretaceous long-term eustatic curve (Viaggi et al., 2019). We note, however, that after a first period of uptake of these elements within the sediments, the onset of OAE 1d led to a drawdown in V and Mo contents that culminated during OAE 2. Here, in contrast with the very high OM content in sediments, the contents of V and Mo approximate crustal values, while U does not record a decrease but the increase is not strong how we expected. This peculiar depletion of the nutrient – related trace metals has been interpreted by Viaggi et al. (2019) as a temporary seawater “nutrient

crisis" induced by starved and stagnant conditions of Central Atlantic basin during the Cenomanian - Turonian long-term eustatic climax (figure 12.5.1). The section before OAE 2 is located in the OMZ at ~ 200m depth. In fact, it is plausible that during this period there was a shutdown of the global oceanic circulation, leading to a lack of nutrients supply and a consequent depletion of the trace metals inventory in the oceans. OAE 2 was a period of high OM production and preservation as testified by high TOC and HI values; a combination of the lack of nutrients supply and eutrophication has led to the depletion of bio-essential metals in the basin (Viaggi et al., 2019). OM plays a fundamental role in the transport of the metals from the water column to the sediment – water interface and their fixation into the sediments (e.g. organometallic complexes). This was associated to an expansion of the OMZ and its euxinic portion. There was a great deposition of OM – rich black shales that contributed to the trace metals removing from seawater (Algeo, 2004; Pearce et al., 2008). After OAE 2 a recovery of the trace metals inventory is recorded (figure 12.5.1), even if the iron speciation suggests that the conditions were still locally euxinic. Fe_{PY}/Fe_{HR} values point toward a reduction of the areal extension of euxinia until reaching OAE 3 where a last pulse of local euxinia is recorded. Nevertheless, Manganese shows a different trend (figure 12.5.1): high values are observed from the bottom of the section to the onset of OAE 1d, pointing apparently towards oxic conditions. From OAE 1d, Mn values decreases. Between OAE 2 and OAE 3, a little increase is observed and it might indicate a return to locally oxic conditions before a new local1peak (OAE 3), maybe affected by more global conditions.

The decrease of V, Mo and U values is observed in other sedimentary section in the Atlantic Ocean intersecting OAE 2 (e.g., ODP Site 1258 at Demerara Rise, eastern equatorial Atlantic; Tarfaya Basin) (Algeo and Rowe, 2012; Goldberg et al., 2016; Owens et al., 2016; Dickson, 2017; Ostrander et al., 2017). In these localities, data suggest a global expansion of reducing conditions during the event that caused a drawdown of the marine inventories of redox-sensitive metals. Immediately after this event, Mo, V and U promptly recover and reached peak values at almost 30, 5 and 4, respectively, times the typical shale contents. The decrease in Mo and V inventories during the main phase of OAE 2 is well documented in literature and related to a global collapse in the oceanic reservoir (Hetzel et al., 2009; Goldberg et al., 2016; Owens et al., 2017b; Ostrander et al., 2017). However, our data show that the drawdown towards crustal values in global Mo reservoirs becomes evident since the onset of OAE 1d and culminated during the OAE 2. It seems thereby obvious that locally euxinic conditions developed starting from OAE 1d and then they progressively expanded until the end of OAE 2. So, the progressive expansion of euxinia in the studied section started with OAE1d, ~ 10 Ma before the OAE 2.

Based on trace elements concentrations and iron speciation, we can argue that our section shows a progressive continuity in the de-oxygenation starting from OAE 1d to OAE 2.
However, Tl recorded a different global situation (figure 12.5.1). Tl tends to be incorporated within Mn-oxides with a large positive isotope fractionation factor, and during periods of well oxygenated bottom water, global $\varepsilon^{205}Tl_{seawater}$ are isotopically light. Despite the drawdown in V and Mo started during OAE1d, our data show that the positive shift in $\varepsilon^{205}Tl_{seawater}$ is limited to OAE2. The isotopic composition suggests that the values along the mid-Cretaceous were more positive than the modern ocean. Until the onset of OAE 1d, it is clear that the values trend toward more oxygenated conditions. Along the Cretaceous, the Atlantic Ocean was progressively opening: the northern part of the Atlantic Ocean was already open and the OMZ was limited to the slope, where, probably, a relatively large amount of nutrients provided by upwelling and riverine inputs led to an intense primary OM production and a consequent degradation and sedimentation of some organic matter in the sediments. While the central part of the Atlantic were more similar to shelf basin with shallow water. A well-developed paleophysiography with upwelling and an associated OMZ evolved starting from the interval between OAE 1d and OAE 2 (figure 12.6.1 modified from Sewal et al., 2007).

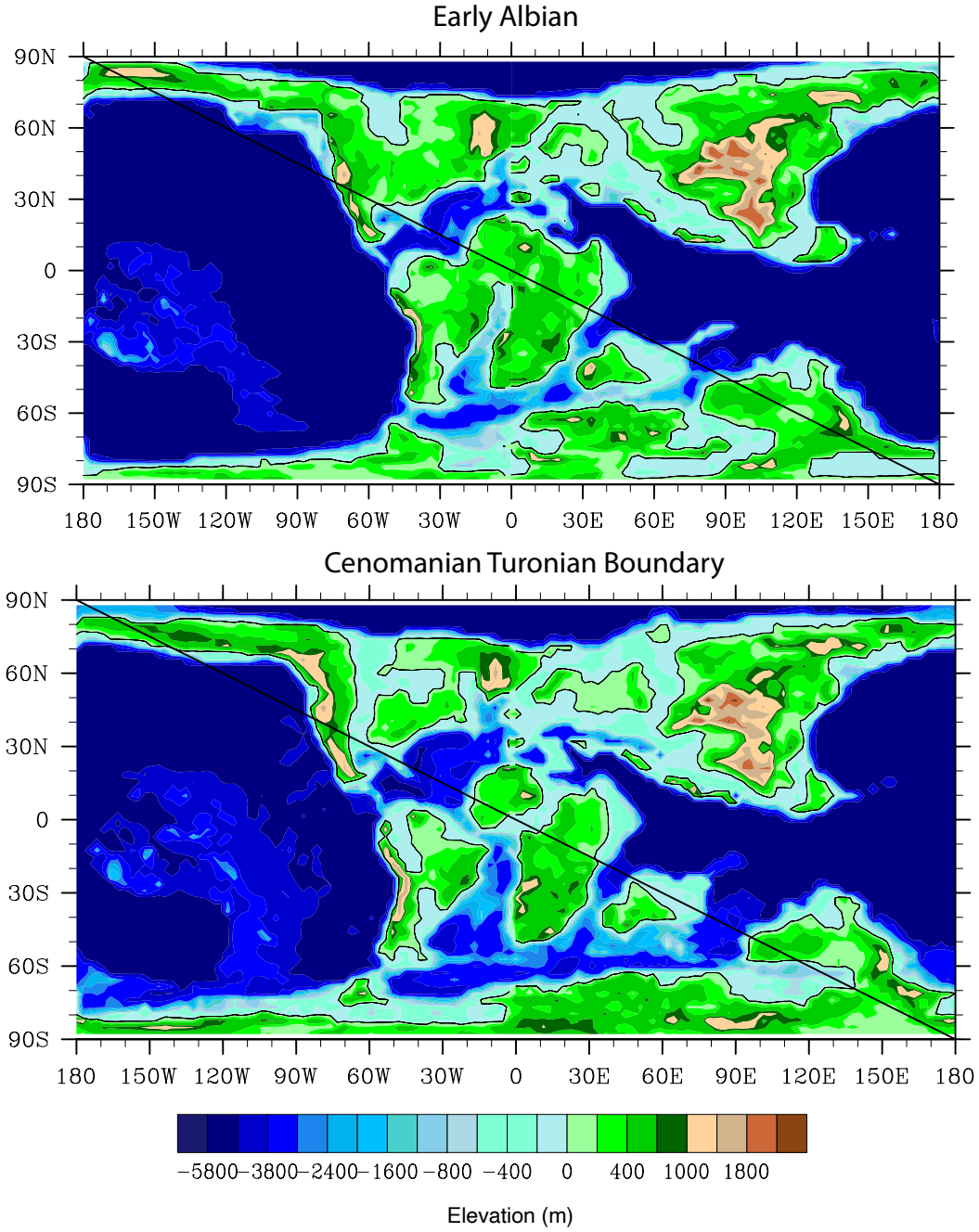

Figure 12.6.1: representation of the Atlantic Ocean opening from Early Albian to the Cenomanian – Turonian Boundary (from Sewal et al., 2007).

A recent study showed that Demerara Rise (in the western margin of the Atlantic Ocean) departures of the Tl isotopes toward less negative values (up to -2.5) commenced ~43 ± 11 thousand years before the globally known perturbation of the C-isotopes defining the OAE2 (Ostrander et al., 2017). This observation suggests that the deoxygenation of the sediment-water interface at Demerara Rise slightly anticipated the expansion of global euxinia, most likely due to the onset of the main activity of the Caribbean LIP (Adams et al., 2010; Du Vivier et al., 2014; Percival et al., 2018) formed ~200 thousand years before OAE2. The addition of nutrients

might have increased the primary OM productivity and provoked a cascade of environmental changes (i.e., local anoxia, changes in seawater chemistry) that ultimately led to the perturbation of the global C-isotope cycle (Schlanger and Jenkyns, 1976). Following this idea, the primary OM productivity was the main trigger mechanism of the OAE2. Interestingly, these authors show that the drawdown slightly anticipated the efficient removal of oxygen depicted by the Tl isotopes (by ~ 59 kyr). As explained before, decreases in nutrients such as V, Mo and U are indicative of expansion of the global anoxia (Emerson and Huested, 1991; Algeo, 2004; Tribovillard et al., 2006; Gordon et al., 2009). Our section shows that V, Mo and U start to decrease much earlier than the onset of OAE 2 how have been previously reported and ~10 million years before that the de - oxygenation of water started to affect the Tl isotope and, ultimately, the C cycle leading to the onset of OAE 2.

In addition, Tl provides fundamental data to constrain global anoxia along the section, recording how Mn burial flux changes. The isotopic composition suggests that the values along the mid-Cretaceous were more positive than the modern ocean. Until the onset of OAE 1d it is clear that the values tend toward oxic conditions. At the onset of OAE 1d the section recorded a change of the redox conditions. A portion of the anoxic seafloor became progressively sulphidic and the relatively anoxic portion decrease until the onset of OAE 2. From here, an expansion of the OMZ and by consequence of the overall euxinic area is recorded. This process, together with a global shutdown of the oceanic circulation, caused a gradual decrease of Mo and V concentrations in the sediments deposited between OAE 1d and OAE 2. The euxinic area of the ocean started to retrieve immediately after OAE 2 mirrored by an increase of Mo and a decrease of Tl isotopes values. This process was probably driven by a recovery of the oceanic circulation and upwelling that supply nutrients back to the photic zone, following the long-term eustatic decrease after the Cenomanian-Turonian climax (Viaggi et al., 2019). The global trend tend toward oxic conditions. In particular, during OAE 3, Tl isotopic composition became lighter, suggesting a local increase of the global Mn oxide burial, and implying that the global conditions were oxic. Tl values during this interval are more negative even than the modern seawater values ($\varepsilon^{205}Tl_{seawater}$ = -6; Owens et al., 2017), implying that there was a high amount of Mn available in the water column. This can be related to high weathering degrees, that introduce high amounts of Mn in the oceans, allowing more to be buried, while a relatively oxic seafloor is maintained.

12.7 Outlooks

The work realized so far in collaboration with UCR and MagLab is very promising. In particular, CA1 is a unique case that provide a long-term record of the Cretaceous. However, the part of the discussion about the sufur isotopes is still missing due to the difficulties in the data interpretation. It will be the goal of the months after the end of the PhD to complete this work and realize a publication. Hopefully, we will be able to publish on a scientific journal with a impact factor. Indeed, this section represents the first case of long-term record of the Cretaceous from the Central Atlantic. This area is only accessible to oil companies due to the richness in hydrocarbons. The possibility to drill for research purposes is excluded to the risk to have a contamination of the cores by hydrocarbons and organic materials. Thereby, the possibility to have a complete section, intersecting four anoxic events and free of any pollution/contaminants is more unique and rare, giving to this work the possibility to be one of the first in this field. In addition, the collaboration with the professors Timothy Lyons (UCR) and Jeremy Owens (MagLab), which are top expert in this field, give more prominence to our work and give us the possibility to improve our knowledge on how to apply inorganic geochemistry on OM-rich sedimentary rocks.

REFERENCES

Achterberg E.P., Van den Berg C.M.G., Colombo C., 2003. High resolution monitoring of dissolved Cu and Co in coastal surface waters of the western North Sea. Contin. Shelf Res. 23, 611–623.

Adams D. D., Hurtgen M. T. and Sageman B. B., 2010. Volcanic triggering of a biogeochemical cascade during Oceanic Anoxic Event 2. Nature geoscience, 3(3), 201-204.

Adegoke A. K., Abdullah W. H., Hakimi M. H., and Yandoka B. M. S., 2014. Geochemical characterization of Fika Formation in the Chad (Bornu) Basin, northeastern Nigeria: implications for depositional environment and tectonic setting. Applied geochemistry, 43, 1-12.

Adelson J.M., Helz G.R. and Miller C.V., 2001. Reconstructing the rise of recent coastal anoxia; molybdenum in Chesapeake Bay sediments. Geochim. Cosmochim. Acta 65, 237–252.

Alberdi-Genolet M. and Tocco R., 1999. Trace metals and organic geochemistry of the Machiques Member (Aptian–Albian) and La Luna Formation (Cenomanian–Campanian), Venezuela. Chemical Geology, 160(1-2), 19-38.

Algeo T.J., 2004. Can marine anoxic events draw down the trace element inventory of seawater? Geology, 32, 1057-1060, https://doi.org/10.1130/G20896.1

Algeo T. J. and Maynard J.B., 2004. Trace-element behavior and redox facies in core shales of Upper Pennsylvanian Kansas-type cyclothems. Chem. Geol., 206, 289–318, https://doi.org/10.1016/j.chemgeo.2003.12.009

Algeo T.J. and Lyons T.W., 2006. Mo–total organic carbon covariation in modern anoxic marine environments: implications for analysis of paleoredox and paleohydrographic conditions. Paleoceanography, 21, PA1016, https://doi.org/10.1029/2004PA001112

Algeo T. J. and Maynard J. B., 2008. Trace-metal covariation as a guide to water-mass conditions in ancient anoxic marine environments. Geosphere, 4(5), 872-887.

Algeo T. J. and Tribovillard N., 2009. Environmental analysis of paleoceanographic systems based on molybdenum–uranium covariation. Chemical Geology, 268(3-4), 211-225. https://doi.org/10.1016/j.chemgeo.2009.09.001

Algeo T. J. and Rowe H., 2012. Paleoceanographic applications of trace-metal concentration data. Chemical Geology, 324, 6-18.

Algeo T. J. and Li C., 2020. Redox classification and calibration of redox thresholds in sedimentary systems. Geochimica et Cosmochimica Acta.

Algeo T. J. and Liu J., 2020. A re-assessment of elemental proxies for paleoredox analysis. Chemical Geology, 119549.

APAT, 2006. Carta Geologica d'Italia 1:50,000 - Catalogo delle Formazioni - Unità tradizionali (2). Quad. Serv. Geol. d'Italia, S.EL.CA., Firenze, serie III, 7(VII), pp. 382.

Arthur M., Brisson-Noël A. and Courvalin P., 1987. Origin and evolution of genes specifying resistance to macrolide, lincosamide and streptogramin antibiotics: data and hypotheses. Journal of antimicrobial chemotherapy, 20(6), 783-802.

Arthur A., Jenkyns H.C., Brumsack H.J. and Schlanger S.O., 1990. Stratigraphy, geochemistry, and paleoceanography of organic carbon-rich Cretaceous sequences. Cretaceous Resources Events and Rhythms (Eds R.N. Ginsburg and B. Beaudoin), NATO ASI Series C, Kluwer Academic Publishers, 304, 75–119.

Baioumy H. and Lehmann B., 2017. Anomalous enrichment of redox-sensitive trace elements in the marine black shales from the Duwi Formation, Egypt: evidence for the late Cretaceous Tethys anoxia. Journal of African Earth Sciences, 133, 7-14.

Barclay R. S., McElwain J. C. and Sageman, B. B., 2010. Carbon sequestration activated by a volcanic CO 2 pulse during Ocean Anoxic Event 2. Nature geoscience, 3(3), 205-208.

Bau M., 1996. Controls on the fractionation of isovalent trace elements in magmatic and aqueous systems: evidence from Y/Ho, Zr/Hf, and lanthanide tetrad effect. Contributions to Mineralogy and Petrology, 123(3), 323-333.

Berner R.A., 2006. GEOCARBSULF: a combined model for Phanerozoic atmospheric O_2 and CO_2. Geochim. Cosmochim. Acta, 70, 5653–5664.

Berrang P. G. and Gril, E. V., 1974. The effect of manganese oxide scavenging on molybdenum in Saanich Inlet, British Columbia. Marine Chemistry, 2(2), 125-148.

Bertine K. K. and Turekian K. K., 1973. Molybdenum in marine deposits. Geochimica et Cosmochimica Acta, 37(6), 1415-1434.

Blumenberg M. and Wiese F., 2012. Imbalanced nutrients as triggers for black shale formation in a shallow shelf setting during the OAE 2 (Wunstorf, Germany). Biogeosciences, 9, 4139–4153, https://doi.org/10.5194/bg-9-4139-2012

Bonacina G., Sanfilippo A., Zana S., Bosino A., Previde Massara E., Viaggi P., Sabato L., Gallicchio S., Scotti P., (2020). Geochemical evidence for local variability in redox and depositional conditions in a deep-water Bonarelli equivalent section from Southern Tethys (Fontana Valloneto section, southern Italy), Ofioliti, vol. 46 (1).

Bornemann A., Pross J., Reichelt K., Herrle J. O., Hemleben C. and Mutterlose J., 2005. Reconstruction of short-term palaeoceanographic changes during the formation of the

Late Albian 'Niveau Breistroffer'black shales (Oceanic Anoxic Event 1d, SE France). Journal of the Geological Society, 162(4), 623-639.

Bralower T.J., Sliter W.V., Arthur M.A., Leckie R.M., Allard D. and Schlanger S.O., 1993. Dysoxic/anoxic episodes in the Aptian–Albian (Early Cretaceous). In: Pringle, M., Sager, W.W., Sliter, W.V., Stein, S. (Eds.), The Mesozoic Pacific: Tectonics, and Volcanism. American Geophysical Union, Washington, DC, Monograph, pp. 5–37 (77).

Breit, G. N. and Wanty R. B., 1991. Vanadium accumulation in carbonaceous rocks: a review of geochemical controls during deposition and diagenesis. Chemical Geology, 91(2), 83-97.

Broecker W. S. and Peng T. H., 1982. Tracers in the Sea.

Brumsack H. J., 1986. The inorganic geochemistry of Cretaceous black shales (DSDP Leg 41) in comparison to modern upwelling sediments from the Gulf of California. Geological Society, London, Special Publications, 21(1), 447-462.

Brumsack H. J., 1989. Geochemistry of recent TOC-rich sediments from the Gulf of California and the Black Sea. Geologische Rundschau, 78(3), 851-882.

Brumsack H.J., 2006. The trace metal content of recent organic carbon-rich sediments: implications for Cretaceous black shale formation. Palaeogeogr. Palaeoclimatol. Palaeoecol., 232, 344–361, https://doi.org/10.1016/j.palaeo.2005.05.011

Butler R.W.H., Pinter P.R., Maniscalco R., Hartley A.J., 2020. Deep-water sand fairway mapping as a tool for tectonic restoration: decoding Miocene central Mediterranean paleogeography using the Numidian turbidites of southern Italy. Journal of the Geological Society, 117, 766-783, https://doi.org/10.1144/jgs2020-008

Calvert S. E. and Piper D. Z., 1984. Geochemistry of ferromanganese nodules from DOMES Site A, Northern Equatorial Pacific: Multiple diagenetic metal sources in the deep sea. Geochimica et Cosmochimica Acta, 48(10), 1913-1928.

Calvert S.E. and Pedersen T.F., 1993. Geochemistry of recent oxic and anoxic marine sediments: implications for the geological record. Marine geology, 113(1-2), 67-88.

Calvert S. E. and Pedersen T. F., 1996. Sedimentary geochemistry of manganese; implications for the environment of formation of manganiferous black shales. Economic Geology, 91(1), 36-47.

Canfield D. E., Raiswell R., Westrich J. T., Reaves C. M. and Berner R. A., 1986. The use of chromium reduction in the analysis of reduced inorganic sulfur in sediments and shales. Chemical geology, 54(1-2), 149-155.

Canfield D. E., Thamdrup B. and Hansen J. W., 1993. The anaerobic degradation of organic matter in Danish coastal sediments: iron reduction, manganese reduction, and sulfate reduction. Geochimica et Cosmochimica Acta, 57(16), 3867-3883.

Caplan M. L. and Bustin R. M., 1999. Devonian–Carboniferous Hangenberg mass extinction event, widespread organic-rich mudrock and anoxia: causes and consequences. Palaeogeography, Palaeoclimatology, Palaeoecology, 148(4), 187-207.

Caplan M. L. and Bustin R. M., 2001. Palaeoenvironmental and palaeoceanographic controls on black, laminated mudrock deposition: example from Devonian–Carboniferous strata, Alberta, Canada. Sedimentary Geology, 145(1-2), 45-72.

Centamore E., Chiocchini U., Jacobacci A., Lanari G. and Santagati G., 1971a. Geologia della zona nord-occidentale del F° 187 "Melfi" (Lucania). Boll. Serv. Geol. It., 91: 113-148.

Centamore E., Chiocchini U., Jacobacci A., Lanari G. and Santagati G., 1971b. Geologia della zona tra Acerenza e Avigliano (prov. Di Potenza). Studi Geol. Camerti, I: 97-12.

Chaillou G., Anschutz P., Lavaux G., Schäfer J. and Blanc G., 2002. The distribution of Mo, U, and Cd in relation to major redox species in muddy sediments of the Bay of Biscay. Marine Chemistry, 80(1), 41-59.

Ciaranfi N. and Loiacono F., 1983. Il Flysh Numidico nel quadro dell'evoluzione tettonico-sedimentaria infraoceanica dell'Appennino meridionale. Studi Geol. e Geof. regioni pugliese e lucana, 16, 43pp.

Coccioni R. and Galeotti S., 1993. Orbitally induced cycles in benthonic foraminiferal morphogroups and trophic structure distribution patterns from the Late Albian "Amadeus Segment"(Central Italy). Journal of Micropalaeontology, 12(2), 227-239.

Cruse A. M. and Lyons T. W., 2004. Trace metal records of regional paleoenvironmental variability in Pennsylvanian (Upper Carboniferous) black shales. Chemical Geology, 206(3-4), 319-345.

Crusius J., Calvert S., Pedersen T. and Sage D., 1996. Rhenium and molybdenum enrichments in sediments as indicators of oxic, suboxic and sulfidic conditions of deposition. Earth and Planetary Science Letters, 145(1-4), 65-78.

Crusius J. and Thomson J., 2000. Comparative behavior of authigenic Re, U, and Mo during reoxidation and subsequent long-term burial in marine sediments. Geochimica et Cosmochimica Acta, 64(13), 2233-2242.

Demaison G. J. and Moore G. T., 1980. Anoxic environments and oil source bed genesis. AApG Bulletin, 64(8), 1179-1209.

Dickson A. J., Jenkyns H. C., Porcelli D., Van den Boorn S. and Idiz E., 2016a. Basin-scale controls on the molybdenum-isotope composition of seawater during Oceanic Anoxic Event 2 (Late Cretaceous). Geochimica et Cosmochimica Acta, 178, 291-306, https://doi.org/10.1016/j.gca.2015.12.036

Dickson A.J., Jenkyns H.C., Porcelli D., Van Den Boorn S., Idiz E. and Owens, J.D., 2016b. Corrigendum to "Basinscale controls on the molybdenum-isotope composition of seawater during Oceanic Anoxic Event 2 (Late Cretaceous)". Geochim. Cosmochim. Acta, 189, 404–405, https://doi.org/10.1016/j.gca.2016.06.025

Dickson A. J., 2017. A molybdenum-isotope perspective on Phanerozoic deoxygenation events. Nature Geoscience, 10(10), 721-726.

Du Vivier A.D.C., Selby D., Sageman B.B., Jarvis I., Gröcke D.R. and Voigt S. 2014. Marine $^{187}Os/^{188}Os$ isotope stratigraphy reveals the interaction of volcanism and ocean circulation during Oceanic Anoxic Event 2. Earth Planet. Sci. Lett., 389, 23–33, https://doi.org/10.1016/j.epsl.2013.12.024

Eggins S. M., 2003. Laser ablation ICP-MS analysis of geological materials prepared as lithium borate glasses. Geostandards Newsletter, 27(2), 147-162.

Emerson S. R. and Huested S. S., 1991. Ocean anoxia and the concentrations of molybdenum and vanadium in seawater. Marine Chemistry, 34(3-4), 177-196.

Erbacher J., Thurow J. and Littke R., 1996. Evolution patterns of radiolaria and organic matter variations: a new approach to identify sea-level changes in mid-Cretaceous pelagic environments. Geology, 24(6), 499-502.

Erickson B. E. and Helz G. R., 2000. Molybdenum (VI) speciation in sulfidic waters:: stability and lability of thiomolybdates. Geochimica et Cosmochimica Acta, 64(7), 1149-1158.

Espitaliè J., La Porte J. L., Madec M., Marquis F., Le Plat P., Paulet J. and Boutefeu, 1977. Méthode rapide de caractérisation des roches mères de leur potential petrolier et de leur degré d'evolution. Rev. l'Inst. Français Petrole, 32 (1), p. 23-42.

Fernex F., Février G., Bénaïm J. and Arnoux A., 1992. Copper, lead and zinc trapping in Mediterranean deep-sea sediments: probable coprecipitation with Mn and Fe. Chemical Geology, 98(3-4), 293-306.

Fiore S., Piccarreta G., Santaloia F., Santarcangelo R. and Tateo F., 2000. The Flysch Rosso shales from the Southern Apennines, Italy. 1. Mineralogy and geochemistry. Periodico di Mineralogia, 69(1), 63-78.

Fornelli A., Gallicchio S. andj Micheletti F., 2019. U-Pb detrital zircon ages and compositional features of Bifurto quartz-rich sandstones from Southern Apennines (Southern Italy):

comparison with Numidian Flysch sandstones to infer source area. Italian Journal of Geosciences 138(2), 216-230, https://doi.org/10.3301/IJG.2019.02

François R., 1988. A study on the regulation of the concentrations of some trace metals (Rb, Sr, Zn, Pb, Cu, V, Cr, Ni, Mn and Mo) in Saanich Inlet sediments, British Columbia, Canada. Mar. Geol. 83, 285–308.

Friedrich O., Norris R.D. and Erbacher J., 2012. Evolution of middle to Late Cretaceous oceans – A 55 m.y. record of Earth's temperature and carbon cycle. Geology, 40, 107–110, https://doi.org/10.1130/G32701.1

Galeotti S., Sprovieri M., Coccioni R., Bellanca A. and Neri R., 2003. Orbitally modulated black shale deposition in the upper Albian Amadeus Segment (central Italy): a multi-proxy reconstruction. Palaeogeography, Palaeoclimatology, Palaeoecology, 190, 441-458.

Galeotti S., Rusciadelli G., Sprovieri M., Lanci L., Gaudio A. and Pekar S., 2009. Sea-level control on facies architecture in the Cenomanian-Coniacian Apulian margin (Western Tethys): a record of glacio-eustatic fluctuations during the Cretaceous greenhouse? Palaeogeogr. Palaeoclimatol. Palaeoecol., 276, 196–205, https://doi.org/10.1016/j.palaeo.2009.03.011

Gallego-Torres D., Martínez-Ruiz F., Paytan A., Jiménez-Espejo F. J. and Ortega-Huertas M., 2007. Pliocene–Holocene evolution of depositional conditions in the eastern Mediterranean: role of anoxia vs. productivity at time of sapropel deposition. Palaeogeography, Palaeoclimatology, Palaeoecology, 246(2-4), 424-439.

Gallicchio S., Marcucci M., Pieri P., Premoli Silva I., Sabato L., Salvini G., 1996. Stratigraphical data from a Cretaceous claystones sequence of the" Argille varicolori" in the Southern Apennines (Basilicata, Italy). Palaeopelagos, 6, 261-272.

Gallicchio S. and Maiorano P., 1999. Revised stratigraphy of the Serra Palazzo formation, a Miocene foredeep turbidite succession of the Southern Apennines (Italy). Rivista Italiana di Paleontologia e Stratigrafia 105, 287-302.

Gambacorta G., Jenkyns H.C., Russo F., Tsikos H., Wilson P.A., Faucher G. and Erba, E., 2015. Carbon- and oxygen-isotope records of mid-Cretaceous Tethyan pelagic sequences from the Umbria Marche and Belluno Basins (Italy). Newsl. Stratigr., 48, 299–323.

Gambacorta, G., Bersezio, R., Weissert, H. and Erba, E., 2016. Onset and demise of Cretaceous oceanic anoxic events: The coupling of surface and bottom oceanic processes in two

pelagic basins of the western Tethys. Paleoceanography, 31(6), 732-757, https://doi.org/10.1002/2015PA002922

Giorgioni M., Weissert H., Bernasconi S. M., Hochuli P. A. Coccioni R. and Keller C. E., 2012. Orbital control on carbon cycle and oceanography in the mid-Cretaceous greenhouse. Paleoceanography, 27(1).

Giorgioni M., Weissert H., Bernasconi S. M., Hochuli P. A., Keller C. E., Coccioni, R., Petrizzo M. R., Lukenedere A. and Garcia T. I., 2015. Paleoceanographic changes during the Albian–Cenomanian in the Tethys and North Atlantic and the onset of the Cretaceous chalk. Global and Planetary Change, 126, 46-61.

Glikson M., Chappell B. W., Freeman R. S. and Webber E., 1985. Trace elements in oil shales, their source and organic association with particular reference to Australian deposits. Chemical Geology, 53(1-2), 155-174.

Goldberg S., Su C. and Forster H. S., 1998. Sorption of molybdenum on oxides, clay minerals, and soils. Adsorption of Metals by Geomedia. Academic Press, San Diego, 401-426

Goldberg T., Poulton S.W., Wagner T., Kolonic S.F. and RehkÄmper, M., 2016. Molybdenum drawdown during Cretaceous Oceanic Anoxic Event 2. Earth Planet. Sci. Lett., 440, 81–91, https://doi.org/10.1016/j.epsl.2016.02.006

Gordon G. W., Lyons T. W., Arnold,G. L., Roe J., Sageman B. B. and Anbar A. D., 2009. When do black shales tell molybdenum isotope tales?. Geology, 37(6), 535-538.

Grosjean E., Adam P., Connan J. and Albrecht P., 2004. Effects of weathering on nickel and vanadyl porphyrins of a Lower Toarcian shale of the Paris basin. Geochimica et Cosmochimica Acta, 68(4), 789-804.

Guerrera F., Martìn-Algarra A., Martìn-Martìn, M., 2012. Tectono-sedimentary evolution of the ‘Numidian Formation’ and lateral facies (southern branch of the western Tethys): constraints for central–western Mediterranean geodynamics. Terra Nova 24, 34–41. https://doi.org/10.1111/j.1365-3121.2011.01034.x

Haig D. W. and Lynch D. A., 1993. A late early Albian marine transgressive pulse over northeastern Australia, precursor to epeiric basin anoxia: foraminiferal evidence. Marine Micropaleontology, 22(4), 311-362.

Haq B.U., Hardenbol J.A.N. and Vail P.R., 1987. Chronology of fluctuating sea levels since the Triassic. Science, 235, 1156–1167.

Hasegawa T., 1997. Cenomanian-Turonian carbon isotope events recorded in terrestrial organic matter from northern Japan. Palaeogeogr. Palaeoclimatol. Palaeoecol., 130, 251– 273.

Hastings D. W., Emerson S. R. and Mix A. C., 1996. Vanadium in foraminiferal calcite as a tracer for changes in the areal extent of reducing sediments. Paleoceanography, 11(6), 665-678.

Helz G. R., Miller C. V., Charnock J. M., Mosselmans J. F. W., Pattrick R. A. D., Garner C. D. and Vaughan D. J., 1996. Mechanism of molybdenum removal from the sea and its concentration in black shales: EXAFS evidence. Geochimica et Cosmochimica Acta, 60(19), 3631-3642.

Hetzel A., Böttcher M.E., Wortmann U.G. and Brumsack H.J., 2009. Paleo-redox conditions during OAE 2 reflected in Demerara Rise sediment geochemistry (ODP Leg 207). Palaeogeogr. Palaeoclimatol. Palaeoecol., 273, 302–328, https://doi.org/10.1016/j.palaeo.2008.11.005

Hofmann P. and Wagner T., 2011. ITCZ controls on Late Cretaceous black shale sedimentation in the tropical Atlantic Ocean. Paleoceanography, 26(4).

Huber,B. T., Norris R. D. and MacLeod K. G., 2002. Deep-sea paleotemperature record of extreme warmth during the Cretaceous. Geology, 30(2), 123-126.

Huerta-Diaz M. A. and Morse J. W., 1990. A quantitative method for determination of trace metal concentrations in sedimentary pyrite. Marine Chemistry, 29, 119-144.

Huerta-Diaz M. A. and Morse J. W., 1992. Pyritization of trace metals in anoxic marine sediments. Geochim. Cosmochim. Acta, 56(7), 2681-2702.

I.S.P.R.A., 2017. Carta geologica in scala 1:50.000, Foglio Geologico 471 Irsina. ISPRA, Serv. Geol. D'It., Ed. System Cart. ISBN-10: 8893110636. Available online: https://www.isprambiente.gov.it/Media/carg/471_IRSINA/Foglio.html

I.S.P.R.A., in press. Carta geologica in scala 1:50.000, Foglio Geologico 470 Potenza. ISPRA, Serv. Geol. D'It. Available online: https://www.isprambiente.gov.it/Media/carg/470_POTENZA/Foglio.html

Jackson K. S., Hawkins P. J. and Bennett A. J. R. 1985. Regional facies and geochemical, evaluation of southern Denison Trough. APEA J., 20: 143–158.

Jarvie D. M., 2012. Shale resource system for oil and gas: Part 2-shale-oil resource system, in Breyer J.A. (Ed.), Shale reservoirs-Giant resources for the 21st century. AAPG Memoir 97, pp. 89-119.

Jarvie D. M., 2014. Components and processes affecting producibility and commerciality of shale resource systems. Geologica Acta: an international earth science journal, 12(4), 307-325.

Jarvis I.A.N., Murphy A.M. and Gale, A.S., 2001. Geochemistry of pelagic and hemipelagic carbonates: criteria for identifying systems tracts and sea-level change. J. Geol. Soc., 158, 685–696, https://doi.org/10.1144/jgs.158.4.685

Jenkyns H. C., 1980. Cretaceous anoxic events: from continents to oceans. Journal of the Geological Society, 137(2), 171-188.

Jenkyns H.C., 2010. Geochemistry of oceanic anoxic events. Geochem. Geophys. Geosyst., 11, Q03004, https://doi.org/10.1029/2009GC002788

Jin C., Li C., Algeo T. J., Wu S., Cheng M., Zhang Z. and Shi W., 2020. Controls on organic matter accumulation on the early-Cambrian western Yangtze Platform, South China. Marine and Petroleum Geology, 111, 75-87.

Jones B. and Manning D. A., 1994. Comparison of geochemical indices used for the interpretation of palaeoredox conditions in ancient mudstones. Chemical geology, 111(1-4), 111-129.

Jones C.E. and Jenkyns H.C., 2001. Seawater strontium isotopes, oceanic anoxic events, and seafloor hydrothermal activity in the Jurassic and Cretaceous. Am. J. Sci., 301, 112–149, https://doi.org/10.2475/ajs.301.2.112

Keeling R. F., Körtzinger A. and Gruber N., 2010. Ocean deoxygenation in a warming world. Annu. Rev. Mar. Sci. 2, 199–229.

Kelly S. D., Newville M. G., Cheng L., Kemner K. M., Sutton S. R., Fenter P., Sturchio N. C. and Spotl C., 2003. Uranyl incorporation into natural calcite. Environ. Sci. Technol. 37, 1284–1287.

Kelly S. D., Rasbury E. T., Chattopadhyay S., Kropf A. J. and Kemner K. M., 2006. Evidence of a stable uranyl site in ancient organic-rich calcite. Environ. Sci. Technol. 40, 2262–2268.

Klinkhammer G. P. and Palmer M. R., 1991. Uranium in the oceans: where it goes and why. Geochimica et Cosmochimica Acta, 55(7), 1799-1806.

Kylander M. E., Ampel L., Wohlfarth B. and Veres D., 2011. High-resolution X-ray fluorescence core scanning analysis of Les Echets (France) sedimentary sequence: new insights from chemical proxies. Journal of Quaternary Science, 26(1), 109-117. https://doi.org/10.1002/jqs.1438

Lanci L., Muttoni G. and Erba E., 2010. Astronomical tuning of the Cenomanian Scaglia Bianca Formation at Furlo, Italy. Earth Planet. Sci. Lett., 292, 231–237, https://doi.org/10.1016/j.epsl.2010.01.041

Leckie R. M., Bralower T. J. and Cashman R., 2002. Oceanic anoxic events and plankton evolution: Biotic response to tectonic forcing during the mid-Cretaceous. Paleoceanography, 17(3), 13-1.

Lewan M. D. and Maynard J. B., 1982. Factors controlling enrichment of vanadium and nickel in the bitumen of organic sedimentary rocks. Geochimica et Cosmochimica Acta, 46(12), 2547-2560.

Lewan M. D., 1984. Factors controlling the proportionality of vanadium to nickel in crude oils. Geochimica et Cosmochimica Acta, 48(11), 2231-2238.

Leythaeuser D., 2005. Origine, migrazione e accumulo del petrolio. In Enciclopedia degli Idrocarburi. Vol. I, pp. 65-84. Istituto della Enciclopedia Italiana fondata da Giovanni Treccani S.p.a.

Long M. C., Deutsch C. and Ito T., 2016. Finding forced trends in oceanic oxygen. Global Biogeochemical Cycles, 30(2), 381-397.

Lyons T. W., Werne J. P., Hollander D. J. and Murray R. W., 2003. Contrasting sulfur geochemistry and Fe/Al and Mo/Al ratios across the last oxic-to-anoxic transition in the Cariaco Basin, Venezuela. Chemical Geology, 195(1-4), 131-157.

Lyons T. W. and Severmann S., 2006. A critical look at iron paleoredox proxies: New insights from modern euxinic marine basins. Geochimica et Cosmochimica Acta, 70(23), 5698-5722.

Lyons T. W., Anbar A. D., Severmann S., Scott C. and Gill B. C., 2009. Tracking euxinia in the ancient ocean: a multiproxy perspective and Proterozoic case study. Annual Review of Earth and Planetary Sciences, 37, 507-534.

Martin E.E., MacLeod K.G., Jiménez Berrocoso A. and Bourbon E., 2012. Water mass circulation on Demerara Rise during the Late Cretaceous based on Nd isotopes. Earth Planet. Sci. Lett., 327–328, 111–120, https://doi.org/10.1016/j.epsl.2012.01.037

McCarthy K., Rojas K., Niemann M., Palmowski D., Peters K. and Stankiewicz A., 2011. Basic petroleum geochemistry for source rock evaluation. Oilfield Review, 23(2), 32-43.

McLennan S. M., 2001. Relationships between the trace element composition of sedimentary rocks and upper continental crust. Geochemistry, Geophysics, Geosystems, 2(4), https://doi.org/10.1029/2000GC000109

McManus J., Berelson W. M., Klinkhammer G. P., Hammond D. E. and Holm C., 2005. Authigenic uranium: relationship to oxygen penetration depth and organic carbon rain. Geochimica et Cosmochimica Acta, 69(1), 95-108.

Meyer K. M. and Kump L. R., 2008. Oceanic euxinia in Earth history: causes and consequences. Annu. Rev. Earth Planet. Sci., 36, 251-288.

Meyers S. R., Sageman B. B. and Lyons T. W., 2005. Organic carbon burial rate and the molybdenum proxy: Theoretical framework and application to Cenomanian-Turonian oceanic anoxic event 2. Paleoceanography, 20(2).

Middelburg J. J., De Lange G. J. and van Der Weijden C. H., 1987. Manganese solubility control in marine pore waters. Geochimica et Cosmochimica Acta, 51(3), 759-763.

Monteiro F. M., Pancost R. D., Ridgwell A. and Donnadieu Y., 2012. Nutrients as the dominant control on the spread of anoxia and euxinia across the Cenomanian-Turonian oceanic anoxic event (OAE2): Model-data comparison. Paleoceanography, 27(4).

Morford J. L. and Emerson, S., 1999. The geochemistry of redox sensitive trace metals in sediments. Geochimica et Cosmochimica Acta, 63(11-12), 1735-1750.

Morford J. L., Russell A. D. and Emerson S., 2001. Trace metal evidence for changes in the redox environment associated with the transition from terrigenous clay to diatomaceous sediment, Saanich Inlet, BC. Marine Geology, 174(1-4), 355-369.

Morford J. L., Emerson S. R., Breckel E. J. and Kim S. H., 2005. Diagenesis of oxyanions (V, U, Re, and Mo) in pore waters and sediments from a continental margin. Geochimica et Cosmochimica Acta, 69(21), 5021-5032.

Morse J. W. and Luther Iii G. W., 1999. Chemical influences on trace metal-sulfide interactions in anoxic sediments. Geochimica et Cosmochimica Acta, 63(19-20), 3373-3378.

Mostardini F. and Merlini S., 1986. L'Appennino centro – meridionale. Sezioni geologiche e proposta di modello strutturale. Mem. Soc. Geol. It., 35, 177-202.

Naimo D., Adamo P., Imperato M. and Stanzione D., 2005. Mineralogy and geochemistry of a marine sequence, Gulf of Salerno, Italy. Quaternary International, 140, 53-63.

Nameroff T.J., Calvert S.E. and Murray J.W., 2004. Glacial–interglacial variability in the eastern tropical North Pacific oxygen minimum zone recorded by redox-sensitive trace metals. Paleoceanography 19, PA1010. doi:10.1029/2003PA000912.

Navarro-Ramirez J. P., Bodin S., Heimhofer U. and Immenhauser A., 2015. Record of Albian to early Cenomanian environmental perturbation in the eastern sub-equatorial Pacific. Palaeogeography, Palaeoclimatology, Palaeoecology, 423, 122-137.

Norris R. D., Bice K. L., Magno E. A. and Wilson P. A., 2002. Jiggling the tropical thermostat in the Cretaceous hothouse. Geology, 30(4), 299-302.

Novelli L., Sella M., Giacca D., Mazzei R., Croce M. Pulga M., 2004. Hydrocarbons: Origin, exploration and production. Eni Corporate University; Scuola Enrico Mattei.

Ogg J. G. and Hinnov, L. A., 2012. Cretaceous. In The geologic time scale (pp. 793-853). Elsevier.

Ogniben L., 1969. Schema introduttivo alla geologia del confine calabro – lucano. Mem. Soc. Geol. It., 453-763.

Ostrander C. M., Owens J. D. and Nielsen S. G., 2017. Constraining the rate of oceanic deoxygenation leading up to a Cretaceous Oceanic Anoxic Event (OAE 2:~ 94 Ma). Science advances, 3(8), https://doi.org/10.1126/sciadv.1701020

Owens J. D., Gill B. C., Jenkyns H. C., Bates S. M., Severmann S., Kuypers M. M., Woodfine R. G. and Lyons, T. W., 2013. Sulfur isotopes track the global extent and dynamics of euxinia during Cretaceous Oceanic Anoxic Event 2. Proceedings of the National Academy of Sciences, 110(46), 18407-18412.

Owens J.D., Reinhard C.T., Rohrssen M., Love G.D. and Lyons, T.W., 2016. Empirical links between trace metal cycling and marine microbial ecology during a large perturbation to Earth's carbon cycle. Earth Planet. Sci. Lett., 449, 407–417, https://doi.org/10.1016/j.epsl.2016.05.046

Owens J.D., Lyons T.W., Hardisty D.S., Lowery C.M., Lu Z., Lee B. and Jenkyns H.C., 2017a. Patterns of local and global redox variability during the Cenomanian – Turonian Boundary Event (Oceanic Anoxic Event 2) recorded in carbonates and shales from central Italy. Sedimentology, 64, 168-185, https://doi.org/10.1111/sed.12352

Owens J. D., Nielsen S. G., Horner T. J., Ostrander C. M. and Peterson L. C., 2017b. Thallium-isotopic compositions of euxinic sediments as a proxy for global manganese-oxide burial. Geochimica et Cosmochimica Acta, 213, 291-307.

Owens J. D., Lyons T. W. and Lowery C. M., 2018. Quantifying the missing sink for global organic carbon burial during a Cretaceous oceanic anoxic event. Earth and Planetary Science Letters, 499, 83-94.

Owens J. D., 2019. Application of thallium isotopes: tracking marine oxygenation through manganese oxide burial, Geochemical Traces in Earth System Science, doi: 10.1017/9781108688697

Parkinson D. N.,1996. Gamma-ray spectrometry as a tool for stratigraphical interpretation: examples from the western European Lower Jurassic. Geological Society, London, Special Publications, 103(1), 231-255.

Pašava J., Frýda J. and Štorch, P., 2017. Trace element variations as a proxy for reconstruction of palaeoenvironmental changes during the Late Aeronian faunal and carbon isotope

perturbations: new data from the peri-Gondwanan region. Geological Quarterly, 61(1):91–98, https://doi.org/10.7306/gq.1313

Patacca E., Scandone, P., Bellatalla M., Perilli N. and Santini U., 1992. The Numidian-sand event in the Southern Apennines. Mem. Sci. Geol. Padova, 43, 297-337.

Pattan J. N. and Pearce, N. J. G., 2009. Bottom water oxygenation history in southeastern Arabian Sea during the past 140 ka: results from redox-sensitive elements. Palaeogeography, Palaeoclimatology, Palaeoecology, 280(3-4), 396-405.

Pearce C. R., Cohen A. S., Coe A. L. and Burton K. W., 2008. Molybdenum isotope evidence for global ocean anoxia coupled with perturbations to the carbon cycle during the Early Jurassic. Geology, 36(3), 231-234, https://doi.org/10.1130/G24446A.1

Pedersen T. F. and Price N. B., 1982. The geochemistry of manganese carbonate in Panama Basin sediments. Geochimica et Cosmochimica Acta, 46(1), 59-68.

Pedersen T. F., Vogel J. S. and Southon, J. R., 1986. Copper and manganese in hemipelagic sediments at 21 N, East Pacific Rise: Diagenetic contrasts. Geochimica et Cosmochimica Acta, 50(9), 2019-2031.

Percival, L. M., Jenkyns, H. C., Mather, T. A., Dickson, A. J., Batenburg, S. J., Ruhl, M., Stephen P. Hesselbo S. P., Barclay R., Jarvis I., Robinson S. A. and Woelders, L., 2018. Does large igneous province volcanism always perturb the mercury cycle? Comparing the records of Oceanic Anoxic Event 2 and the end-Cretaceous to other Mesozoic events. American Journal of Science, 318(8), 799-860.

Pescatore T.S. and Senatore M., 1986. A comparison between a present-day (Taranto Gulf) and a Miocene (Irpinian Basin) foredeep of the Southern Apennines (Italy). In Foreland Basins (Eds P.A. Allen & P. Homewood), p. 169. Special Publication 8 of the IAS, 36.

Pescatore T., Renda P., Tramutoli M. and 1988. Rapporti tra le unità lagonegresi e le unità sicilidi nella media valle del Basento, Lucania (Appennino Meridionale). Mem Soc. Geol. It., 41: 353-361.

Pescatore T.S., Renda P., Schiattarella M. and Tramutoli M., 1999. Stratigraphic and structural relationships between Meso-Cenozoic Lagonegro basin and coeval carbonate platforms in southern Apennines, Italy. Tectonophysics 315, 269–286.

Pescatore T., Di Nocera S and Matano, F.1with the contributions of1Ciampo G, Di Donato V., Esposito P. and Riviello A., in press. Note illustrative della Carta Geologica d'Italia alla scala 1:50.000, F° 470 Potenza. ISPRA, Serv. Geol. d'It., 140 pp. Available online: https://www.isprambiente.gov.it/Media/carg/note_illustrative/470_Potenza.pdf

Peters K. E., 1986. Guidelines for evaluating petroleum source rock using programmed pyrolysis. AAPG bulletin, 70(3), 318-329.

Pi D. H., Jiang S. Y., Luo L., Yang J. H. and Ling H. F., 2014. Depositional environments for stratiform witherite deposits in the Lower Cambrian black shale sequence of the Yangtze Platform, southern Qinling region, SW China: Evidence from redox-sensitive trace element geochemistry. Palaeogeography, Palaeoclimatology, Palaeoecology, 398, 125-131.

Pieri P., Gallicchio S., Sabato L., and Tropeano M. with the contribution of Boenzi F., Lazzari M., Marino M. and Vitale G, 2017. Note illustrative della Carta Geologica d'Italia alla scala 1:50.000, F° 471 Irsina. ISPRA, Serv. Geol. d'It., Ed. System Cart, 112 pp. ISBN-10: 8893110636. Available online: https://www.isprambiente.gov.it/Media/carg/note_illustrative/471_Irsina.pdf.

Piper D. Z. and Perkins R. B., 2004. A modern vs. Permian black shale—the hydrography, primary productivity, and water-column chemistry of deposition. Chemical geology, 206(3-4), 177-197.

Pogge Von Strandmann P.A.E., Jenkyns H.C. and Woodfine R.G., 2013. Lithium isotope evidence for enhanced weathering during Oceanic Anoxic Event 2. Nat. Geosci., 6, 668–672, https://doi.org/10.1038/ngeo1875

Poulton S. W. and Canfield D. E., 2011. Ferruginous conditions: a dominant feature of the ocean through Earth's history. Elements, 7(2), 107-112.

Rachold V. and Brumsack H. J., 2001. Inorganic geochemistry of Albian sediments from the Lower Saxony Basin NW Germany: palaeoenvironmental constraints and orbital cycles. Palaeogeography, Palaeoclimatology, Palaeoecology, 174 (1-3), 121-143, https://doi.org/10.1016/S0031-0182(01)00290-5

Raiswell R. and Berner R. A., 1985. Pyrite formation in euxinic and semi-euxinic sediments. American Journal of Science, 285(8), 710-724.

Raiswell R. and Canfield D. E., 1998. Sources of iron for pyrite formation in marine sediments. American Journal of Science, 298(3), 219-245.

Raiswell R., Newton R., Bottrell S. H., Coburn P. M., Briggs D. E., Bond D. P. and Poulton S. W., 2008. Turbidite depositional influences on the diagenesis of Beecher's Trilobite Bed and the Hunsrück Slate; sites of soft tissue pyritization. American Journal of Science, 308(2), 105-129.

Rajendran A., Kumar M. D. and Bakker J. F., 1992. Control of manganese and iron in Skagerrak sediments (northeastern North Sea). Chemical geology, 98(1-2), 111-129.

Reeder R. J., Nugent M., Lamble G. M., Tait C. D. and Morris D. E., 2000. Uranyl incorporation into calcite and aragonite: XAFS and luminescence studies. Environmental Science & Technology, 34(4), 638-644.

Reeder R. J., Nugent M., Tait C. D., Morris D. E., Heald S. M., Beck K. M., Wayne P. H. and Lanzirotti A., 2001. Coprecipitation of uranium (VI) with calcite: XAFS, micro-XAS, and luminescence characterization. Geochimica et Cosmochimica Acta, 65(20), 3491-3503.

Reinhard C.T., Planavsky N.J., Robbins L.J., Partin C.A., Gill B.C., Lalonde S.V., Bekker A., Konhauser K.O. and Lyons T.W., 2013. Proterozoic ocean redox and biogeochemical stasis. Proc. Natl Acad. Sci., 110, 5357– 5362, https://doi.org/10.1073/pnas.1208622110

Rimmer S. M., 2004. Geochemical paleoredox indicators in Devonian–Mississippian black shales, central Appalachian Basin (USA). Chemical Geology, 206(3-4), 373-391.

Robinson S. A., Williams T. and Bown P. R., 2004. Fluctuations in biosiliceous production and the generation of Early Cretaceous oceanic anoxic events in the Pacific Ocean (Shatsky Rise, Ocean Drilling Program Leg 198). Paleoceanography, 19(4).

Sabato L., Gallicchio S., Pieri P., Salvini G. and Scotti P., 2007. Cretaceous anoxic events in the argilliti e radiolariti di Campomaggiore unit (Lagonegro-Molise basin, southern Italy). Boll. Soc. Geol. It., Spec. Issue No. 7, 57-74.

Schlanger S.O. and Jenkyns H.C., 1976. Cretaceous oceanic anoxic events: causes and consequences. Geol. Mijnbouw, 55, 179–184.

Schmidtko S., Stramma L. and Visbeck M., 2017. Decline in global oceanic oxygen content during the past five decades. Nature, 542(7641), 335-339.

Scholle P.A. and Arthur M.A., 1980. Carbon isotope fluctuations in Cretaceous pelagic limestones; potential stratigraphic and petroleum exploration tool. AAPG Bull., 64, 67–87.

Scopelliti G., Bellanca A., Coccioni R., Luciani V., Neri R., Baudin F., Chiari M. and Marcucci M., 2004. High-resolution geochemical and biotic records of the Tethyan “Bonarelli Level” (OAE 2, Latest Cenomanian) from the Calabianca–Guidaloca composite section, nortwestern Sicily, Italy. Palaeogeogr. Palaeoclimatol. Palaeoecol. 208, 293–317, https://doi.org/10.1016/j.palaeo.2004.03.012

Scopelliti G., Bellanca A., Neri R., Baudin F. and Coccioni R., 2006. Comparative high-resolution chemostratigraphy of the Bonarelli Level from the reference Bottaccione section (Umbria–Marche Apennines) and from an equivalent section in NW Sicily:

Consistent and contrasting responses to the OAE2. Chemical Geology, 228(4), 266-285, https://doi.org/10.1016/j.chemgeo.2005.10.010

Scopelliti G., Bellanca A., Erba E., Jenkyns H. C., Neri R., Tamagnini P., Luciani V. and Masetti D., 2008. Cenomanian–Turonian carbonate and organic-carbon isotope records, biostratigraphy and provenance of a key section in NE Sicily, Italy: Palaeoceanographic and palaeogeographic implications. Palaeogeography, Palaeoclimatology, Palaeoecology, 265(1-2), 59-77, https://doi.org/10.1016/j.palaeo.2008.04.022

Scott C. and Lyons T. W., 2012. Contrasting molybdenum cycling and isotopic properties in euxinic versus non-euxinic sediments and sedimentary rocks: Refining the paleoproxies. Chemical Geology, 324, 19-27, https://doi.org/10.1016/j.chemgeo.2012.05.012

Soua M., 2011. Productivity and bottom water redox conditions at the Cenomanian-Turonian Oceanic Anoxic Event in the southern Tethyan margin, Tunisia.

Soua M., 2013. Siliceous and organic-rich sedimentation during the Cenomanian–Turonian Oceanic Anoxic Event (OAE 2) on the northern margin of Africa: an evidence from the Bargou area, Tunisia. Arabian Journal of Geosciences, 6(5), 1537-1557, https://doi.org/10.1007/s12517-011-0434-0

Sun Y. Z. and Püttmann W., 2000. The role of organic matter during copper enrichment in Kupferschiefer from the Sangerhausen basin, Germany. Organic Geochemistry, 31(11), 1143-1161.

Sundby B., Martinez P. and Gobeil C., 2004. Comparative geochemistry of cadmium, rhenium, uranium, and molybdenum in continental margin sediments. Geochimica et Cosmochimica Acta, 68(11), 2485-2493.

Takashima R., Nishi H., Huber B.T. and Leckie M., 2006. Greenhouse world and the Mesozoic Ocean. Oceanography, 19, 82–92.

Tanaka K. and Watanabe N., 2015. Size distribution of alkali elements in riverbed sediment and its relevance to fractionation of alkali elements during chemical weathering. Chemical Geology, 411, 12-18. https://doi.org/10.1016/j.chemgeo.2015.05.025

Taylor S. R. and McLennan S. M., 1985. The continental crust: its composition and evolution. nited States: N. p., 1985. Web.

Them T. R., Gill B. C., Caruthers A. H., Gerhardt A. M., Gröcke D. R., Lyons T. W., Marroquínc S. M., Nielsenh S. G., Trabucho Alexandre J. P. and Owens J. D., 2018. Thallium isotopes reveal protracted anoxia during the Toarcian (Early Jurassic)

associated with volcanism, carbon burial, and mass extinction. Proceedings of the National Academy of Sciences, 115(26), 6596-6601.

Trabucho Alexandre J., Tuenter E., Henstra G. A., van der Zwan K. J., van de Wal R. S., Dijkstra H. A. and de Boer P. L., 2010. The mid-Cretaceous North Atlantic nutrient trap: black shales and OAEs. Paleoceanography, 25(4).

Tribovillard N., Averbuch O., Devleeschouwer X., Racki G. and Riboulleau A., 2004a. Deep-water anoxia over the Frasnian–Famennian boundary (La Serre, France): a tectonically induced oceanic anoxic event?. Terra Nova, 16(5), 288-295.

Tribovillard N., Riboulleau A., Lyons T. W. and Baudin F., 2004b. Enhanced trapping of molybdenum by sulfurized marine organic matter of marine origin in Mesozoic limestones and shales. Chemical Geology, 213(4), 385-401.

Tribovillard N., Ramdani A. and Trentesaux A., 2005. Controls on organic accumulation in Upper Jurassic shales of northwestern Europe as inferred from trace-metal geochemistry.

Tribovillard N., Algeo T. J., Lyons T. W. and Riboulleau A., 2006. Trace metals as paleoredox and paleoproductivity proxies: an update. Chemical geology, 232(1-2), 12-32, https://doi.org/10.1016/j.chemgeo.2006.02.012

Tribovillard N., Algeo T. J., Baudin F. and Riboulleau A., 2012. Analysis of marine environmental conditions based onmolybdenum–uranium covariation—Applications to Mesozoic paleoceanography. Chemical Geology, 324, 46-58, https://doi.org/10.1016/j.chemgeo.2011.09.009

Turekian K. K. and Wedepohl K. H., 1961. Distribution of the elements in some major units of the earth's crust. Geological Society of America Bulletin, 72(2), 175-192.

Tyson R. V. and Pearson T. H., 1991. Modern and ancient continental shelf anoxia: an overview. Geological Society, London, Special Publications, 58(1), 1-24.

Tyson R. V., 2001. Sedimentation rate, dilution, preservation and total organic carbon: some results of a modelling study. Organic Geochemistry, 32(2), 333-339.

Viaggi P., Scotti P., Previde Massara E., Knezaurek G., Menichetti E., Piva A., Torricelli St. and Gambacorta G., 2019. Paleoceanographic Evolution of mid-Cretaceous Paleobioproductivity and Paleoredox Chemometric Signals. Conference abstract and presentation. 3rd International Congress on Stratigraphy STRATI 2019 (2-5 July 2019, Milan), https://doi.org/10.13140/RG.2.2.32655.94886

Vorlicek T. P. and Helz G. R., 2002. Catalysis by mineral surfaces: implications for Mo geochemistry in anoxic environments. Geochimica et Cosmochimica Acta, 66(21), 3679-3692.

Vorlicek T. P., Kahn M. D., Kasuya Y. and Helz G. R., 2004. Capture of molybdenum in pyrite-forming sediments: role of ligand-induced reduction by polysulfides. Geochimica et Cosmochimica Acta, 68(3), 547-556.

Wagner T., Sinninghe Damsté J. S., Hofmann P. and Beckmann B. (2004). Euxinia and primary production in Late Cretaceous eastern equatorial Atlantic surface waters fostered orbitally driven formation of marine black shales. Paleoceanography, 19(3).

Wagreich, M., 2009. Coniacian-Santonian oceanic red beds and their link to Oceanic Anoxic Event 3. Cretaceous Oceanic Red Beds: Stratigraphy, Composition, Origins, and Paleoceanographic and Paleoclimatic Significance, 91, 235-242.

Wagreich M., 2012. "OAE 3"-regional Atlantic organic carbon burial during the Coniacian-Santonian. Climate of the Past, 8(5), 1447.

Wang C. S., Hu X. M., Huang Y. J., Scott R. W. and Wagreich M., 2009. Overview of Cretaceous Oceanic Red Beds (CORBs): a window on global oceanic and climate change. Cretaceous Oceanic Red Beds: Stratigraphy, Composition, Origins and Paleoceanographic and Paleoclimatic Significance: SEPM Special Publication, 91, 13-33.

Wang C. S., Hu X., Huang Y., Wagreich M., Scott R., and Hay W., 2011.Cretaceous oceanic red beds as possible consequence of oceanic anoxic events, Sediment. Geol., 235, 27–37.

Wang X., Reinhard C. T., Planavsky N. J., Owens J. D., Lyons T. W. and Johnson T. M., 2016. Sedimentary chromium isotopic compositions across the Cretaceous OAE2 at Demerara Rise Site 1258. Chemical Geology, 429, 85-92, https://doi.org/10.1016/j.chemgeo.2016.03.006

Wanty R. B. and Goldhaber M. B., 1992. Thermodynamics and kinetics of reactions involving vanadium in natural systems: Accumulation of vanadium in sedimentary rocks. Geochimica et Cosmochimica Acta, 56(4), 1471-1483.

Wedepohl K. H., 1971. Environmental influences on the chemical composition of shales and clays. Physics and Chemistry of the Earth, 8, 307-333.

Wedepohl K. H., 1991. Chemical composition and fractionation of the continental crust. Geologische Rundschau, 80(2), 207-223.

Wehrly B. and Stumm W., 1989. Vanadyl in natural waters: adsorption, and hydrolysis promote oxygenation. Geochim. Cosmochim. Acta 53, 69–77.

Westermann S., Vance, D., Cameron, V., Archer, C. and Robinson, S.A., 2014. Heterogeneous oxygenation states in the Atlantic and Tethys oceans during Oceanic Anoxic Event 2. Earth Planet. Sci. Lett., 404, 178–189, https://doi.org/10.1016/j.epsl.2014.07.018

Whitfield M., 2002. Interactions between phytoplankton and trace metals in the ocean. Adv. Mar. Biol. 41, 3–120.

Zheng Y., Anderson R.F., van Geen A., Kuwabara J., 2000. Authigenic molybdenum formation in marine sediments: a link to pore water sulfide in the Santa Barbara Basin. Geochim. Cosmochim. Acta 64, 4165–4178.

Zheng Y., Anderson R.F., van Geen A., Fleisheir M.Q., 2002a. Preservation of non-lithogenic particulate uranium in marine sediments. Geochim. Cosmochim. Acta 66, 3085–3092.

Zheng Y., Anderson R.F., van Geen A., Fleisheir M.Q., 2002b. Remobilization of authigenic uranium in marine sediments by bioturbation. Geochim. Cosmochim. Acta 66, 1759–1772.

Zheng Y., Jenkyns H. C., Gale A. S., Ward D. J. and Henderson G. M., 2013. Changing ocean circulation and hydrothermal inputs during Ocean Anoxic Event 2 (Cenomanian–Turonian): evidence from Nd-isotopes in the European shelf sea. Earth and Planetary Science Letters, 375, 338-348.